Synthesis and processing of MAX phases by Powder Injection Moulding and Additive Manufacturing

by

Eduardo Tabares Lorenzo

A dissertation submitted by in partial fulfilment of the requirements for the degree of Doctor of Philosophy in

Materials Science and Engineering

Universidad Carlos III de Madrid

Advisor(s):

Sophia A. Tsipas
Antonia Jiménez Morales

Tutor:

Sophia A. Tsipas

March 2022

A Miguel,
Isabel
y Daviana

Preface

This PhD Thesis has been carried out at the Group of Powder Technology (GTP), of the Department of Materials Science and engineering and Chemical Engineering on the Carlos III University of Madrid (UC3M).

In order to improve the quality of the work, part of this work has been performed at an international research stay at RHP Technology GmbH in Seibersdorf (Austria) under the supervision of Dr. Erich Neubauer and Dr. Michael Kitzmantel. The 4-month research stay was financially supported by the Carlos III University, through a competitive research grant, and by the Institute of Chemistry and Material Álvaro Alonso Barba (IAAB).

During the course of this work, two grants have been awarded to the candidate to assist to the International Conference and Expo on Advance Ceramics and Composites (ICACC). The first one celebrated in Daytona Beach, FL, USA in January 2019 (Contract No. 2016124-25) and the second one held as an on-line congress in January 2021.

This PhD Thesis complies with the requirements for its mention as International PhD that has been established in article 15 of the Real Decreto 99/2011 in the “Ordenación de la Enseñanza Universitaria Oficial” (B.O.E. Nº 35 of January 28, 2011, pp 13909 - 13926) as is described in the Rules and Regulations for PhD studies at the Carlos III University of Madrid.

Agradecimientos

Aunque no me caracterizo por ser una persona de muchas palabras, quiero aprovechar estas líneas para agradecer a todas las personas que me han acompañado a lo largo de estos años. Nos hemos divertido mucho pero también hemos sufrido un poco. Aunque seguramente las palabras se queden cortas mi agradecimiento es enorme con todos ustedes.

En primer lugar, me gustaría dar las gracias a mis directoras, Toñi y Sophia. Gracias por darme la oportunidad de realizar este trabajo y por la confianza y libertad que me han brindado. Por todo el apoyo recibido durante estos años. Por la paciencia y comprensión cuando las cosas no salían del todo bien o había algún deadline al que no llegaba. Gracias por todas las palabras de ánimo.

En segundo lugar, a todas las personas que siguen o han pasado por el grupo de investigación de tecnología de polvos. Gracias por hacerme un hueco, por la ayuda y el cariño que he recibido durante estos años. Mónica, Paula, Juan, José Manuel, Maru, Carlos, Nerea, Elisa, Eva, Christian gracias por recibirme siempre con una sonrisa. A Sandra quiero agradecerte toda la ayuda que me has dado en los inicios de mi tesis, esa ayuda sin duda está reflejada en este trabajo. A Elena que, junto con Toñi en el grado y Sophia en el máster, me han dado ese empujón necesario para meterme de lleno en el mundo de los materiales y en el de la investigación. Si más adelante me arrepiento ya sé a quienes culpar.

A todas las personas del departamento que siempre han estado dispuestas a ayudar o dar una palabra amable. Gracias Luis y Juan Carlos por responder a todas las preguntas raras y solucionar los problemas que tenemos en el día a día. Gracias Cristina por todas las horas de microscopio y de enseñanza con los equipos.

I would like to thank Erich Neubauer and Michael Kitzmantel for the opportunity of working with you at RHP. It was an incredible experience both personal and professional. Also, my gratitude to Lilla, Tamas and Fabian for all your time and wonderful welcome.

A todos los doctorandos con lo que he tenido la oportunidad de compartir esta etapa y días largos en el laboratorio Bea, Julia, Estela, Paula, Raquel, Lucía, Javi, Gleydis, Morena, Pedro, Guille, Marta, Sara, Andrés, Betty, Edu, Irene, Jose, Tamara, Nacho, Facu, Alex, Víctor, Raúl, Sydonne, Miguel Ángel…. a todos, gracias. A María Fernández por su sonrisa, a Nieves por los pistachos y a Segundo y Marcos por hacerme los días más amenos, también por las cervezas.

A María y Alberto por los grandes momentos durante todos estos años, Fernando Poo no es lo mismo, el barrio les echa de menos. Natalia, gracias por enseñarme a ver las cosas de otra manera, a veces con la mirada perdida. Jorge, yubro gracias por tu apoyo y carcajadas contagiosas. Andrea, gracias por sacarme siempre una sonrisa, la mejor compañera de pádel que se puede tener. Carmen, gracias por tu ayuda y apoyo en absolutamente todo. Esta última etapa ha sido más llevadera gracias a ti. Meu, gracias por todo tu tiempo, en las buenas y en las malas. Aunque lejos, todavía nos quedan muchas cosas por hacer. Cate, sin duda este doctorado no hubiera sido lo mismo sin ti. Gracias por transmitirme tu alegría e incansable energía. Sin ustedes este camino hubiera sido mucho más complicado.

A mis amigos de siempre que estarán enfriando las cervezas para cuando acabe. Sergio, Jaime, Pope, Guille, Cuti, Jonay, Yeray, Carla algún día les explicaré de qué iba todo esto.

He tenido la suerte de haberme encontrado con la mejor persona posible durante estos años. Amaya, gracias por tu constante apoyo cerca y lejos. Gracias por aguantarme y gracias por estar siempre ahí.

Todo el esfuerzo, trabajo y cariño no puede ser lo suficientemente agradecido, aún así, un enorme agradecimiento a mis padres por el apoyo incondicional y la enorme confianza. He llegado y es gracias a ustedes. Por último, a mi hermana Daviana. Gracias por tu ánimo constante y tu entusiasmo absoluto en cada paso del camino. Has sido una parte muy importante de este trabajo durante todos estos años y qué mejor que lleve tu portada.

.

Published and submitted content

This thesis has been done as a compendium of different works published in scientific journals. A list of the scientific publications that encompass this work are listed below:

- E. Tabares, A. Jiménez-Morales, S.A. Tsipas, “Study of the synthesis of MAX phase Ti_3SiC_2 powders by pressureless sintering”, Bol. La Soc. Esp. Ceram. y Vidr. 60 (**2020**) 41-52. Publisher: ELSEVIER; ISSN: 0366-3175; Category: Materials Science, Ceramics Position: 7 of 29 (Q1) IMPACT FACTOR: 2.383 (JCR 2020)

  https://doi.org/10.1016/j.bsecv.2020.01.004.

- E. Tabares, S.C. Cifuentes, A. Jiménez-Morales, S.A. Tsipas, “Injection moulding of porous MAX phase Ti_3SiC_2 without using space-holder”, Powder Technol. 380 (**2021**) 96-105. Publisher: ELSEVIER; ISSN: 032-5810; Category: Engineering, Chemical: 30 of 143 (Q1); IMPACT FACTOR: 5.134 (JCR 2020)

  https://doi.org/10.1016/j.powtec.2020.11.022.

- E. Tabares, M. Kitzmantel, E. Neubauer, A. Jiménez-Morales, S.A. Tsipas, “Extrusion-based Additive Manufacturing of Ti_3SiC_2 and Cr_2AlC MAX phases as candidates for High Temperature Heat Exchangers”, J. Eur. Ceram. Soc. 42 (**2021**) 841-849. Publisher: ELSEVIER; ISSN: 0955-2219; Category: Materials Science, Ceramics Position: 1 of 29 (Q1) IMPACT FACTOR: 5.302 (JCR 2020)

  https://doi.org/https://doi.org/10.1016/j.jeurceramsoc.2021.10.042.

- E. Tabares, M. Kitzmantel, E. Neubauer, A. Jiménez-Morales, S.A. Tsipas, “Sinterability, Mechanical Properties and Wear Behavior of Ti_3SiC_2 and Cr_2AlC MAX Phases”, Ceramics 5 (**2022**) 55–74. Publisher: MDPI; ISSN: 2571-6131; Category: Materials Science, Multidisciplinary | Materials Science.

  https://doi.org/10.3390/ ceramics5010006.

In addition, two different congress papers have been published and are part of this work:

- E. Tabares, S.C. Cifuentes, A. Jiménez-Morales, S.A. Tsipas, “Powder injection moulding of MAX phase Ti_3SiC_2”, in: Euro PM 2019 Congr. Exhib., **2019**. ISBN: 978-189907251-4.

- E. Tabares, G. Mazón-Ortíz, S.C. Cifuentes, M. Kitzmantel, E. Neubauer, A. Jiménez-Morales, S. Tsipas, “Mechanical properties of 3D printed MAX phases”, in Euro PM 2021 Congr. Exhib., **2021**.

Other research merits

Complementary to the work performed during the PhD thesis a separate study resulted in a congress paper. This work was also included in a scientific publication, listed below:

- E. Tabares, B. Velasco, E. Gordo, A. Jiménez-Morales, S.A. Tsipas, "Oxidation behavior of porous Ti_2AlC and Ti_3SiC_2 produced by powder metallurgy", in: Euro PM 2018 Congr. Exhib., **2018**. ISBN: 978-189907250-7.

- S.A. Tsipas, E. Tabares, T. Weissgaerber, T. Hutsch, F. Sket, B. Velasco, "Thermophysical properties of porous Ti_2AlC and Ti_3SiC_2 produced by powder metallurgy", J. Alloys Compd. 857 (**2021**). Publisher: ELSEVIER; ISSN: 0925-8388; Category: Metallurgy and Metallurgical Engineering Position: 6 of 80 (Q1) IMPACT FACTOR: 4.631 (JCR 2020).

  https://doi.org/10.1016/j.jallcom.2020.158145.

In addition, during the completion of this thesis various aspects that encompass this work have been presented at national and international conferences. (* denotes presenting author):

- E. Tabares*, S.A. Tsipas, A. Jiménez-Morales. "Synthesis of Ti_3SiC_2 MAX phase by powder metallurgy". **Oral communication**. Congreso Nacional de Materiales 2018, Salamanca, Spain (**2018**).

- E. Tabares*, B. Velasco, E. Gordo, A. Jiménez-Morales, S.A. Tsipas. "Oxidation behaviour of porous Ti_2AlC and Ti_3SiC_2 produced by powder metallurgy". **Oral communication**. EUROPM 2018, Bilbao, Spain (**2018**).

- E. Tabares*, S.C. Cifuentes, S.A. Tsipas, E. Gordo, A. Jiménez-Morales. "Novel processing of MAX Phase Ti_3SiC_2 by Powder Injection Molding". **Oral communication**. ICACC 19, Daytona Beach, Florida, USA (**2019**).

- E. Tabares*, S.C. Cifuentes, S.A. Tsipas, A. Jiménez-Morales. "Moldeo por inyección de polvos de fase MAX Ti_3SiC_2". **Oral communication**. CEIPM 2019, Madrid, Spain (**2019**).

- E. Tabares*, S.C. Cifuentes, A. Jiménez-Morales, S.A. Tsipas. "Powder injection moulding of MAX phase Ti_3SiC_2". **Oral communication**. EUROPM 2019, Maastricht, Netherlands (**2019**).

- E. Tabares*, G. Mazón-Ortiz, S. C. Cifuentes, A. Jiménez-Morales, S.A. Tsipas. “Fases MAX: Síntesis, producción y procesado”. **Oral communication**. VIII Jornada de Jóvenes Investigadores, Madrid, Spain (**2019**).

- E. Tabares*, S. C. Cifuentes, A. Jiménez-Morales, S.A. Tsipas. “Propiedades mecánicas de fase MAX Ti_3SiC_2 porosa producida por moldeo por inyección de polvos (PIM)”. **Oral communication** On-line. LVII Congreso Nacional de la Sociedad Española de Cerámica y Vidrio, Catellón, Spain (**2020**).

- E. Tabares*, A. Jiménez-Morales, M. Kitzmantel, E. Neubauer, S.A. Tsipas. “Additive Manufacturing of MAX phase feedstocks”. **Oral communication** On-line. ICACC 21 (**2021**).

- E. Tabares, S.C. Cifuentes, A. Jiménez-Morales, S.A. Tsipas*. “Rheological behavior of printable MAX phase feedstocks”. **Oral communication** On-line. ICACC 21 (**2021**).

- E. Tabares, G. Mazón-Ortiz, S.C. Cifuentes, M. Kitzmantel, E. Neubauer, S.A. Tsipas*, A. Jiménez-Morales. “Mechanical properties of 3D printed MAX Phases”. **Oral communication** On-line. EUROPM 2021 (**2021**).

- E. Tabares*, M. Kitzmantel, E. Neubauer, A. Jiménez-Morales, S.A. Tsipas. “Impresión 3D de fases MAX mediante Composite Extrusion Modelling”. **Oral communication**. IX Jornada de Jóvenes Investigadores, Madrid, Spain (**2021**).

- E. Tabares*, M. Kitzmantel, E. Neubauer, S.A. Tsipas, A. Jiménez-Morales. “Wear behaviour of Hot-pressed Ti_3SiC_2 and Cr_2AlC MAX phases”. **Oral communication** On-line. ICACC 22 (**2022**).

Contents

Abstract **1**

Resumen **3**

1. Introduction **5**

1.1 Historical background and introduction to MAX Phases 9

1.2 Powder Injection Moulding 26

1.3 Additive Manufacturing 42

References 49

2. Motivation and objectives **69**

2.1 Motivation 73

2.2 Objectives 75

References 77

3. Thematic unit, materials and methods **79**

3.1 Scheme of the experimental work 83

3.2 Initial materials and MAX phase synthesis characterisation 83

3.3 Conventional powder metallurgy consolidation 94

3.4 Powder injection moulding 98

3.6 Composite Extrusion Modelling 113

References 117

4. Synthesis of MAX phases **121**

4.1 Study of the synthesis of MAX phase Ti_3SiC_2 powders by pressureless sintering 125

5. Conventional processing of MAX phases **139**

5.1 Sinterability, mechanical properties and wear behaviour of Ti_3SiC_2 and Cr_2AlC MAX phases 143

6. Powder Injection Moulding of MAX phases **165**

6.1 Powder injection moulding of MAX phase Ti_3SiC_2 169

6.2 Injection moulding of porous MAX phase Ti_3SiC_2 without using space-holder 177

7. CEM study of MAX phases feedstocks **189**

7.1 Extrusion-based additive manufacturing of Ti_3SiC_2 and Cr_2AlC MAX phases as candidates for high temperature heat exchangers 193

7.2 Mechanical properties of 3D printed MAX phases 205

8. Conclusions **213**

9 Future lines and perspectives **221**

Abstract

MAX phases are a family of ternary materials with a fixed stoichiometry and a general formula of $M_{n+1}AX_n$, where M is a transition metal, A is generally an element of groups IIIA and IVA of the periodic table, X is either carbon or nitrogen and n a value between 1 and 3. Their nano-laminated structure gives these materials an unusual combination of (1) metallic properties, such as, good electrical and thermal conductivity, machinability, high damage tolerance; and (2) ceramic properties such as high rigidity, resistance to corrosion and oxidation and good mechanical properties at high temperatures. This unique combination of properties makes these materials very promising candidates for industrial applications with demanding conditions, which has prompted the study, design and development of these family of materials. Some of the conventional consolidation routes for MAX phases are pressureless sintering, hot pressing or spark plasma sintering, however they have limitation in the production of parts with complex shapes.

In this work, the design and optimisation of the synthesis route was performed for different MAX phases with the aim of obtaining high purity powders studying the reaction mechanism during the synthesis. Ti_3SiC_2 and Cr_2AlC MAX phases were selected for this work. The synthesis of these MAX phases was successfully carried out from different elemental powders (Ti, SiC, C, Cr and Al). In addition, the scalability of the powder production was achieved maintaining high phase purity while controlling the particle size distribution of the powders. To assess the quality of the powders produced, various conventional powder metallurgy processing routes were studied, such as pressureless sintering and hot pressing. For these samples, porosity measurements, mechanical properties (cyclic compression test) and wear behaviour were analysed, studying the influence of the processing route on the behaviour of the materials.

In this context, the main challenge of this PhD is to demonstrate the viability of non-conventional processing techniques such as Powder Injection Moulding (PIM) and Composite Extrusion Modelling (CEM) for the production of near-net-shape MAX phase samples. These two technologies start from pelletised feedstocks and allow the production of samples with a higher freedom of design, reducing post-processing steps. The objective was to produce complex-shaped parts as well as increasing the application range of MAX phases, their reproducibility and production volume.

For the successful production of MAX phase samples by PIM and CEM the selection of the binder system as well as the optimisation of the solid loading of the feedstocks is necessary and, for this purpose, the rheological properties of the materials were

characterised. Two multicomponent binders were selected for this study, firstly, an environmentally-friendly binder consisting of a combination of a sustainable polymer (polyethylene glycol, PEG) and a biopolymer (cellulose acetate butyrate, CAB), and secondly, a binder composed of the same sustainable polymer (PEG) and polypropylene (PP).

Porous MAX phases with tailored porosity were obtained by PIM processing, avoiding the use of spacer holder. Additive manufactured parts by CEM were also successfully produced, using the same feedstocks. Debinding and sintering processes were optimized in both cases.

In conclusion, it was possible to obtain good quality parts with custom geometries through PIM and CEM for both Ti_3SiC_2 and Cr_2AlC MAX phases, suitable for industrial applications with special requirements, such as catalytic devices, filters or as high temperature heat exchangers.

Resumen

Las fases MAX son una familia de materiales ternarios con una estequiometría fija y una fórmula general $M_{n+1}AX_n$, donde M es un metal de transición, A es generalmente un elemento de los grupos IIIA y IVA de la tabla periódica, X es carbono o nitrógeno y n un valor entre 1 y 3. La estructura nano laminada de estos materiales proporcionan una combinación inusual de propiedades metálicas, tales como, buena conductividad eléctrica y térmica, fácil mecanizado y alta tolerancia al daño, y de propiedades cerámicas como alta rigidez, resistencia a la corrosión y oxidación y buenas propiedades mecánicas a altas temperaturas. Esta exclusiva combinación de propiedades ha hecho que las fases MAX sean considerados para aplicaciones industriales en las que se requieren condiciones exigentes, lo cual ha impulsado el estudio, diseño y desarrollo de esta familia de materiales. Algunas de las rutas convencionales de consolidación para este tipo de materiales son compactación y sinterización, prensado en caliente o spark plasma sintering, pero tienen limitaciones en la producción de piezas con formas complejas.

En este trabajo, el diseño y optimización de las rutas de síntesis para diferentes fases MAX han sido estudiadas con el objetivo de obtener polvo con una alta pureza analizando los mecanismos de reacción durante la síntesis. Las fases MAX seleccionadas han sido Ti_3SiC_2 y Cr_2AlC. La síntesis de estas fases MAX se ha llevado a cabo con éxito a partir de distintos polvos elementales (Ti, SiC, C, Cr y Al). Además, el escalado de la producción del polvo se logró manteniendo la alta pureza de las fases MAX procesadas controlando la distribución de tamaño de partícula. Con el objetivo de evaluar los polvos producidos, diversos procesados convencionales de la pulvimetalurgia fueron estudiados como, por ejemplo, presión y sinterización y hot pressing. Para las muestras consolidadas se estudió la porosidad, las propiedades mecánicas (compresión cíclica) y el comportamiento a desgaste, analizando la influencia de las rutas de procesamiento en el comportamiento de los materiales.

En este contexto, el principal reto de esta Tesis Doctoral es la de demostrar la viabilidad de procesar fases MAX a través de rutas “no convencionales” como son el moldeo por inyección de polvos (PIM) y el Composite Extrusión Modelling (CEM). Todo esto para la fabricación de piezas near-net-shape de fases MAX. Estos dos tipos de procesado parten de feedstocks en forma de pellets permitiendo la producción de piezas con una mayor libertad de diseño, reduciendo posteriores etapas de postprocesado. El objetivo principal es fabricar piezas complejas y de esta manera aumentar los posibles campos

de aplicación para las fases MAX, así como aumentar la reproducibilidad y el volumen de producción para estos materiales.

Para la producción de fases MAX a través de PIM y CEM es necesario la selección adecuada de los polímeros que van a conformar el binder y, además, una optimización de la cantidad de sólido que se va a utilizar para la producción de feedstocks. Es por ello por lo que las propiedades reológicas de estos materiales han sido estudiadas en profundidad. Dos sistemas ligantes multicomponentes han sido utilizados para la producción de feedstocks. Por un lado, un binder respetuoso con el medioambiente compuesto por polietilenglicol (PEG) y un biopolímero (acetato butirato de celulosa, CAB). Por otro lado, se desarrolló otro sistema ligante con el mismo polímero sostenible (PEG) y polipropileno (PP).

A través del procesamiento por PIM, se obtuvieron piezas con una porosidad a medida, evitando el uso de sistemas espaciadores. Por otro lado, se fabricaron con éxito piezas por manufactura aditiva a través de la tecnología CEM. Además, se optimizaron los procesos de debinding y sinterización de las piezas.

Como conclusión, cabe destacar que mediante PIM y CEM fue posible obtener piezas de buena calidad con geometrías a medida tanto para la fase MAX Ti_3SiC_2 como para la fase Cr_2AlC, aptas para aplicaciones industriales con requerimientos especiales como, por ejemplo, dispositivos catalíticos, filtros o como intercambiadores de calor de alta temperatura.

CHAPTER 1

INTRODUCTION

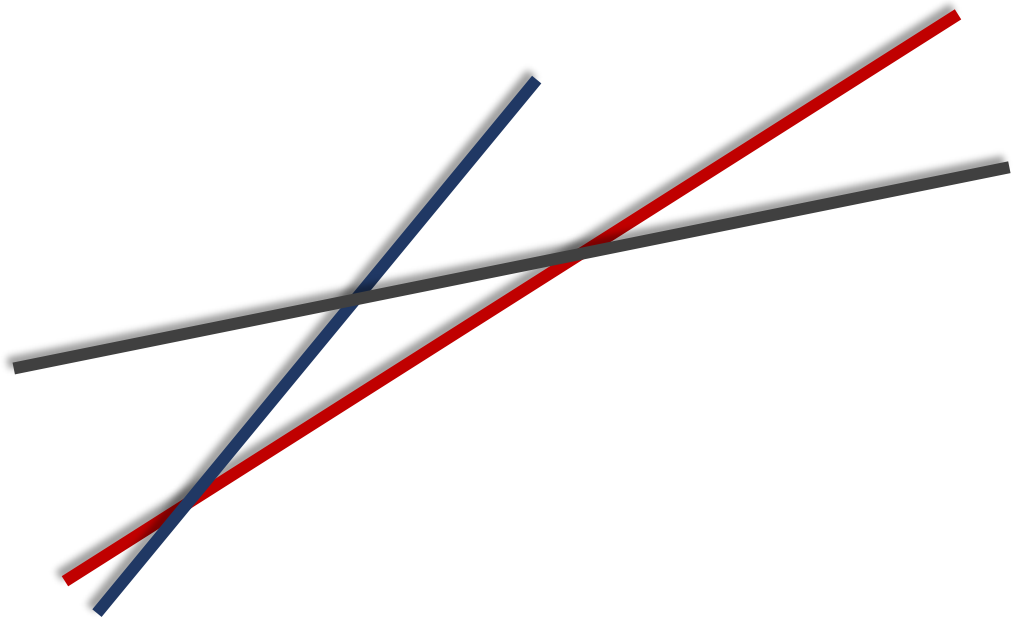

Contents

1.1 Historical background and introduction to MAX Phases 9

1.1.1 Properties of MAX phases 11

1.1.1.1 Mechanical properties 11

1.1.1.2 Oxidation and corrosion resistance 13

1.1.1.3 Thermal conductivity properties 15

1.1.1.4 Electrical properties 15

1.1.1.5 Tribological behaviour 17

1.1.2 Synthesis methods and consolidation techniques 18

1.1.3 Applications 21

1.2 Powder injection moulding 26

1.2.1 Overview of the PIM process 27

1.2.1.1 Initial material selection (Powder and binder system) 27

1.2.1.2 Feedstock production and mixing 30

1.2.1.3 Injection 34

1.2.1.4 Debinding 35

1.2.1.5 Sintering 37

1.2.2 Applications and overview of MAX phases in PIM 39

1.3 Additive Manufacturing 42

1.3.1.1 Direct AM 42

1.3.1.2 Indirect AM 44

1.3.2 Overview of the Composite Extrusion Modelling process 46

1.3.3 Applications and overview of MAX phases in AM 47

References 49

1. Introduction

1.1 Historical background and introduction to MAX Phases

The discovery of the family of MAX phase materials dates back to the 1960s. Nowotny and Jeitschko found a new class of carbides and nitrides with good mechanical properties [1]. These compounds had a similar atomic ratio and followed a common structure with a layered disposition and were called H-type phases.

In 1967, their investigations led up to the discovery of several different ternary phases and, among them, two new compounds with a specific stochiometric arrangement: Ti_3SiC_2 and Ti_3GeC_2, with a similar layer disposition of the Ti-C system and the Si or Ge elements. After this, this H-type phases went overlooked for a long period of time with not much relevant work done for these materials until 1996. In this year, Barsoum studied the characteristics of the Ti_3SiC_2 compound and established the $M_{n+1}AX_n$ formula, giving this family of materials the MAX phase name [2]. In his work, Barsoum described the unusual properties of these materials as compounds with a relatively soft behaviour for a titanium carbide, rigid and with good machinability. Since then, the interest on MAX phases has increased and researchers have focused on the characterisation of the properties and the synthesis routes for obtaining high purity MAX phases [3–6].

MAX phases are a family of materials of more than 60 known compounds, that share a common structure, with different chemical compositions. The chemical elements that encompass the MAX acronym are divided into different groups in the periodic table: being M an early transition metal (highlighted in blue in Figure 1), A an element typically from the IIIA and IVA groups of the periodic table (highlighted in red in Figure 1) and X either carbon or nitrogen (black in Figure 1). This family of materials has a fixed stoichiometry and a general formula of $M_{n+1}AX_n$, where n is a number between 1 and 3 [3,7,8]. MAX phases have a hexagonal nanolaminated crystalline structure (space group P/63/mmc). The laminated structure is composed of layers of the MX elements, where the X elements occupies the centre of the octahedral site formed by the M_6X structure, interleaved by layers of the A element, located in the centre of trigonal prisms. The n value of the $M_{x+1}AX_n$ formula establishes the amount of layers that separate each A group layer. This nanolaminated organisation can be observed in Figure 2, where the three most common classifications of the MAX phases (211, 312 and 413), according to their stoichiometry, are shown [8–10].

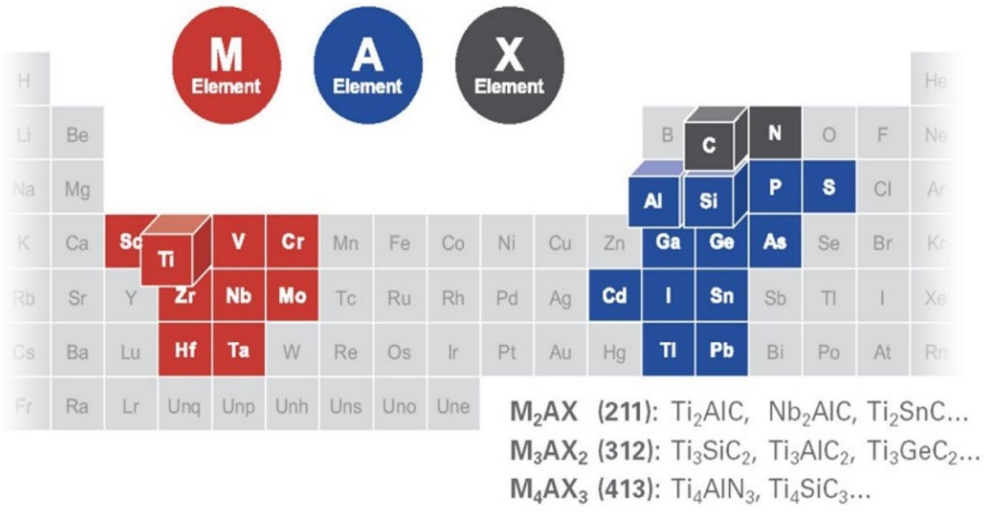

Figure 1. Periodic table highlighting the different elements that create MAX phases [7].

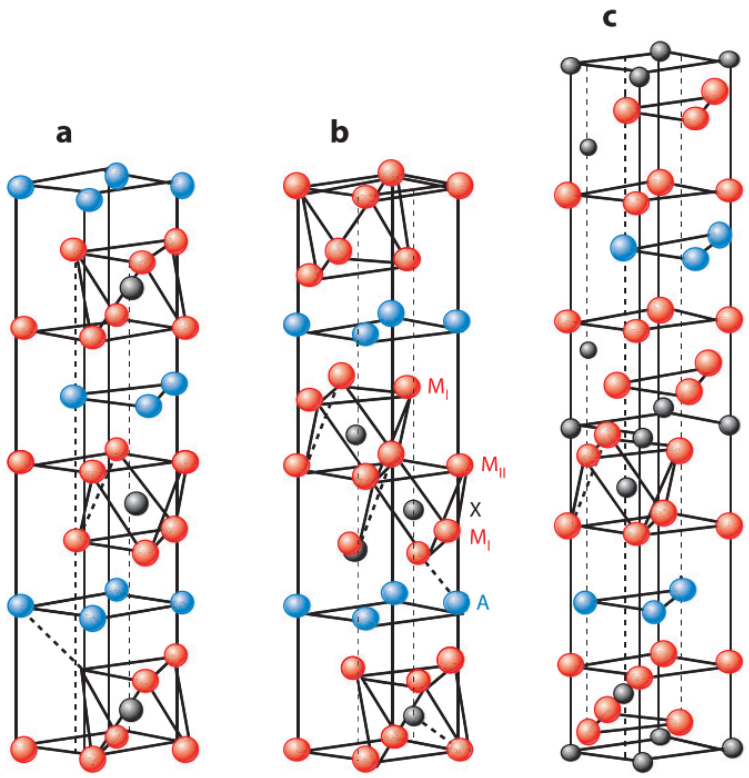

Figure 2. Unit cells representing the crystalline structures of MAX phases for: a) 211 phases, b) 312 phases and c) 413 phases. Elements highlighted in red correspond to M, blue to A and black to X in the $M_{n+1}AX_n$ formula [9].

During the last years, the number of publications related to MAX phases has increased, focused on the search for new MAX phases as it can be seen in Figure 3. Furthermore, the physical and chemical properties of these materials have also been in the scope of researchers, increasing the potential applications of this family of materials. Some of the most studied MAX phases are Ti_3SiC_2, Cr_2AlC, Ti_2AlC and its 312 phase Ti_3AlC_2.

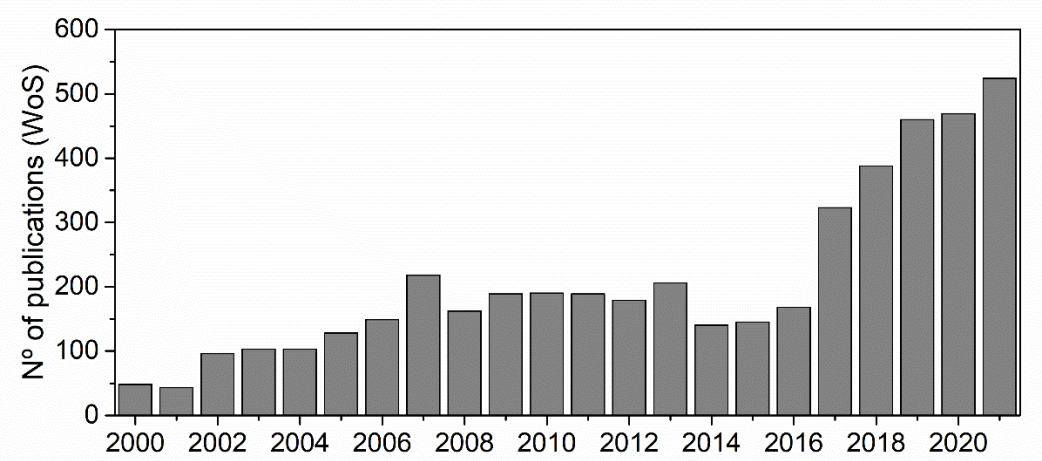

Figure 3. Number of publications per year obtained from the Web of Science searching for key words: MAX phases, Ti_3SiC_2, Cr_2AlC, Ti_2AlC, Ti_3AlC_2, V_2AlC, Ti_4AlN_3 and Ti_2AlN.

1.1.1 Properties of MAX phases

Due to their nanolaminated structure and layer arrangement, MAX phases exhibit a unique and excellent combination of metallic and ceramic-like properties. From the characteristic metallic properties, MAX phases exhibit high electrical conductivity, good thermal conductivity, and ease to be machined. From the ceramic point of view, high stiffness, good mechanical properties at high temperature and good oxidation and corrosion resistance are some of the main MAX phase attributes. Some of the most interesting properties of MAX phases are detailed below:

1.1.1.1 Mechanical properties

MAX phases have the ability to tolerate localised damage preventing the propagation of cracks through the material. This behaviour is related to their laminar structure, that differentiate these materials from the brittle mechanical response of ceramics. The damage tolerance properties of MAX phases is explained by the kink band formation [10]. At room temperature, dislocations move mainly in the basal plane and are able to multiply. This fact is important, since, while the dislocations are restricted to move in the basal planes, they create incipient kink bands (IKB), which is a unique deformation mechanism of MAX phases, amongst other deformation mechanism, allowing the high damage tolerance of these materials. If a crack forms inside the material as a result of delamination, the propagation of the crack will by limited due to the formation of these kink bands.

MAX phases are relatively soft, with a Vickers hardness between 2 and 8 GPa. They exhibit a fracture toughness of 5-20 $MPa \cdot m^{1/2}$, higher than ceramics, and a good machinability. MAX phases are lightweight materials with typical density values between 4 and 6 g/cm^3. Good thermal shock resistance and rigidity are some of the most relevant

properties characteristic for this family of materials. All this, while being easily machinable [7]. In addition, MAX phases have an anisotropic response to nanoindentations [10]. Once an indentation is made, basal planes delaminate and cracks are formed parallel to the basal planes. On the other hand, with these parallel cracks generated by the nanoindentation results in a higher plastic deformation and a lower hardness, which creates a staking of the delamination on the indentation edges.

Regarding elastic properties, MAX phases exhibit a nonlinear elastic behaviour not usual for stiff materials. This behaviour is observed once a cyclical load is applied to the material and commonly observed in compressive loads. Once the cyclic load is applied the behaviour of these materials maintains a hysteresis behaviour, resulting in stress and strain loops. This effect has been studied by Zhou et al [11] for hexagonal closed pack metals and by Barsoum et al.[12] for MAX phases, establishing that the fully reversible stress-strain loop in cyclical loading is caused by the IKB that are generated in the crystallographic arrangement of MAX phases. It has been established that the stress-strain values of the compressive behaviour of the MAX phases has a strong dependence on the size and shape of the grains, as it can be observed in Figure 4, were fine and coursed grained Ti_3SiC_2 samples are tested under compressive loads.

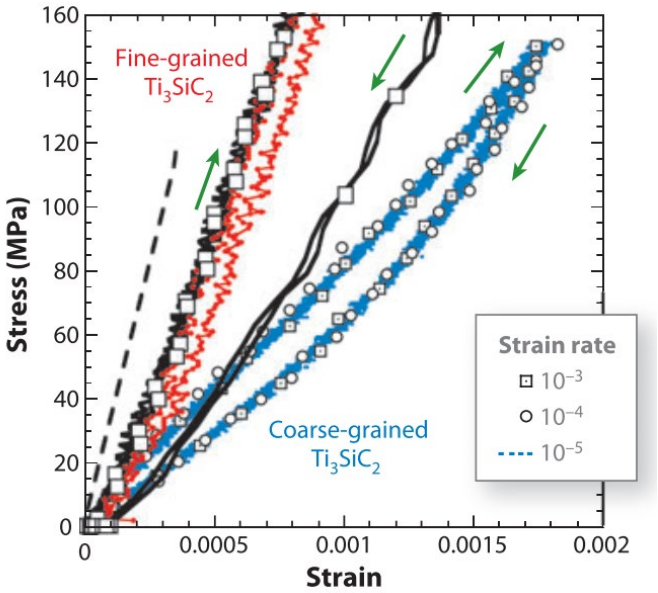

Figure 4. Stress-strain curves of Ti_3SiC_2 samples with fine grains (red) and coarse grains (blue) [9].

Several models have been developed to predict the behaviour of materials as a response to load cycles; among them the Preisach-Mayergoyz model (PM) has been demonstrated to describe accurately the hysteresis in the stress-strain behaviour of MAX phases by Zhou et al. [13]. In their work, they analysed porous Ti_2AlC by cyclic compressive loads and modelled the behaviour by Preisach-Mayergoyz model. In summary, they expose that kinking nonlinear elastic (KNE) materials exhibit a double

effect of, firstly: local stresses maxima wipes out the effect of other lower stresses and secondly: there is a congruency on the hysteresis loops for each loading and unloading cycle. This is due to the nonlinear response of those KNE and thus, the PM model is applicable for MAX phases.

In terms of high temperature mechanical behaviour, the response is different depending on the elements that the MAX phases contain. Nevertheless, all MAX phases experiment a brittle-to-plastic transition temperature causing a decrease of the fracture toughness above that temperature [12]. Hardening occurs after each cycle at high temperatures (1200 ºC) and the stress-strain behaviour depends on the strain rate. Moreover, the good response of MAX phases to thermal shock is another interesting property. Thermal shock resistance of MAX phases has a strong dependence on the grain size. Furthermore the thermal shock resistance of MAX phases has been attributed to the crack healing properties generated by the formation of smaller domains due to thermal residual stresses and, also, the presence of highly protective oxide layers when there is presence of air [14,15].

1.1.1.2 Oxidation and corrosion resistance

Another of the important attributes that gives MAX phases good mechanical behaviour at high temperature is thanks to the oxidation resistance and stability in air. Although the oxidation resistance of the MAX phases varies depending on the elements that is composed from, some of the most resistance MAX phases are Ti_3SiC_2, Cr_2AlC and Ti_2AlC. This is, mainly, due to the formation of a protective oxidation layer of TiO_2 and Al_2O_3 [8]. The oxidation mechanism of MAX phases occurs approximately at 600 ºC and can be described by the reaction seen in Equation 1:

Equation 1 $$M_{n+1}AX_n + bO_2 = M_{n+1}O_x + AO_y + X_nO_{2b-x-y}$$

There are many studies that have focused on the study of the oxidation properties of MAX phases [16–18]. Both dense and porous samples have been characterised studying the oxidation mechanism and protective layer formation at high temperatures. The oxidation mechanism that occurs is not entirely clear with studies proposing parabolic, cubic and logarithmic oxidation behaviours at different test conditions [16,17,19,20]. What has been demonstrated is the oxide layer formation during the test, creating a protective layer.

For Ti_3SiC_2, oxide layers grow through diffusion of oxygen from the outside towards the internal zone, while titanium diffuses to the exterior of the material and silicon oxidises by reaction, without inward or outward diffusion [21]. This leads to the creation of a double layer composed of, TiO_2 as the external layer and an internal layer of a

combination of SiO_2 and TiO_2 (Figure 5-a). TiO_2 usually appears as rutile during the formation of the protective oxide layer, while SiO_2 is mainly amorphous silica at low temperatures, transforming into cristobalite at higher temperatures (above 1200 ºC) [8,21]. Oxide layers are usually dense and resistant to thermal cycling. Moreover, oxide layers formed show a lack of cracks at short times and the oxidation mechanism exhibits a parabolic kinetic at 1000 ºC. It has been demonstrated that the kinetics of Ti_3SiC_2 can change to a linear behaviour with the increase of temperature and increasing the exposure times. Although this transition is not fully understood, this change in the behaviour of Ti_3SiC_2 could be due to a decomposition of the MAX phase at high temperatures, increasing the amount of the TiC phase. The deterioration of the oxidation behaviour influence by the presence of TiC has been indirectly studied analysing the effect of adding SiC and TiC to Ti_3SiC_2. The composites produced were compared to bulk Ti_3SiC_2 and exhibit different behaviours. The addition of SiC generated thinner well-adhered TiO_2 and SiO_2/TiO_2 layers. On the other hand, TiC generated much thicker layers resulting on a lower oxidation resistance [22].

The oxidation behaviour of Cr_2AlC has also been reported, analysing the diffusion mechanism occurring. At temperatures above 800 ºC, Al_2O_3 (corundum) starts to appear, by the diffusion of aluminium elements to the external zone of the material, creating a well-adhered oxide layer. One of the main advantages of Cr_2AlC is the lack of oxide formation with chromium, creating only that Al_2O_3 protective layer, withstanding operating temperatures of up to 1300 ºC in air and cyclic testing, exhibiting cubic oxidation kinetics. Although the formation of this well-adhered and single Al_2O_3 layer is beneficial, the diffusion of the A element to the outer zones of the sample and the reaction with oxygen produces a decomposition of the material into porous chromium carbides (Cr_7C_3) between the oxide layer and the substrate at temperatures above 1150 ºC. This could create a decrease of the stability of the protective layers by crack formation while in service [20].

Ti_2AlC MAX phase forms a well-adhered Al_2O_3 layer on the surface with a secondary layer of TiO_2 (Figure 5-b). This protective oxide layer formed on Ti_2AlC, as well as on Ti_3AlC_2, makes the Ti-Al-C system one of the highest oxidation resistive MAX phases that can withstand thermal cycles of 1300 ºC [7,23]. Apart from the stability and adherence of the protective Al_2O_3 to the surface, one of the reasons for the high resistance of these material to oxidation is the similarity in the thermal expansion coefficient of both the phases that coexist (Al_2O_3 and Ti_2AlC) [24]. This makes this MAX phase a great candidate for their use as thermal barrier coatings (TBC) since it avoids the generation of thermal stresses and reduces the spallation and delamination of the

oxide layer. Nevertheless, the formation of TiO_2 can be a drawback for the oxidation behaviour of Ti_2AlC and Ti_3AlC_2 MAX phases, limiting the formation of the Al_2O_3, since it is this oxide layer that controls the oxidation kinetics of the material with, typically, a cubic kinetic behaviour [3].

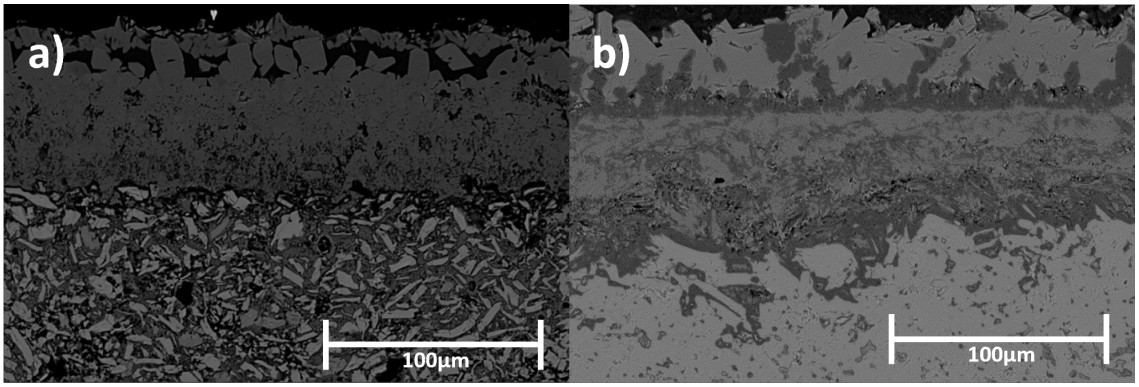

Figure 5. SEM micrographs of the oxidation layers form for a) Ti_2AlC and b) Ti_3SiC_2 after cyclic oxidation tests in air at 1000 ºC and 900 ºC, respectively [16].

1.1.1.3 Thermal conductivity properties

In materials science, the thermal conductivity is determined by the heat transport from the high temperature zones to low temperature areas. It is typically related to the metallic substances since the transmission of the vibrated energy, causing the heat, is eased due to the free electrons in their structure. In this sense, MAX phases behaves as a metallic compound with good thermal conductivity properties [25].

At room temperature, MAX phase conductivities, vary from 12 to 60 W/m·k. Compared to the rest of materials (Figure 6), those conductivity values are more similar to the ones of metallic materials than to those of ceramics. This property is essential particularly for high temperature applications. Within the MAX phase materials, thermal conductivity varies depending on the element that composes each phase. Ti_2AlC has a thermal conductivity of 46 W/m·k at room temperature, being the MAX phase with the highest thermal conductivity. Ti_3SiC_2 has also high thermal conductivity values (37 W/m·k). Furthermore, Cr_2AlC presents a lower thermal conductivity at 18 W/m·k, but still in the metallic range. All of these materials exhibit a linear behaviour with temperature, with a decrease on the thermal conductivity properties as the temperature increases [7,8,10].

1.1.1.4 Electrical properties

In the case of the electrical conductivity properties of MAX phases it is possible to observe a similar behaviour as for the thermal conductivity properties. MAX phases, behave as metallic materials (Figure 7). As reference values displaying those materials studied in this work: Ti_2AlC has an electrical conductivity of $9{,}9 \cdot 10^6$ S/m, Ti_3SiC_2 $3{,}1 \cdot 10^6$ S/m and Cr_2AlC $1{,}4 \cdot 10^6$ S/m [8].

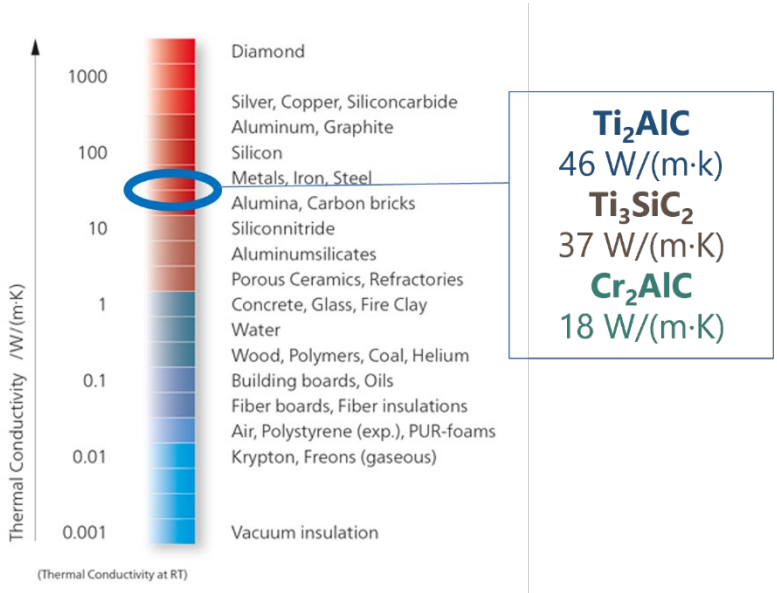

Figure 6. Thermal conductivity properties of different materials compared to those of MAX phases Ti_2AlC, Ti_3SiC_2 and Cr_2AlC [25].

It has been demonstrated that the electrical resistivity of most of the MAX phases varies linearly with temperature, as in metallic materials. At a glance, the electrical conductivities/resistivities of MAX phases depend on the elements that compose the materials. Ti_3SiC_2 has a lower electrical resistivity compared to titanium from temperatures between 0 K and 1000 K. In the case of phases that contain aluminium, the thermal resistivity varies with the temperature depending on the element M, on the $M_{n+1}AX_n$ formula, although the A element has also an impact on the conductivity values [26]. X, being carbon or nitrogen, is the element with the least effect on the variation of electrical resistivity with temperature [7]. Ti_2AlC and Ti_3SiC_2 electrical resistivity increases linearly from room temperature to 1000 K [27].

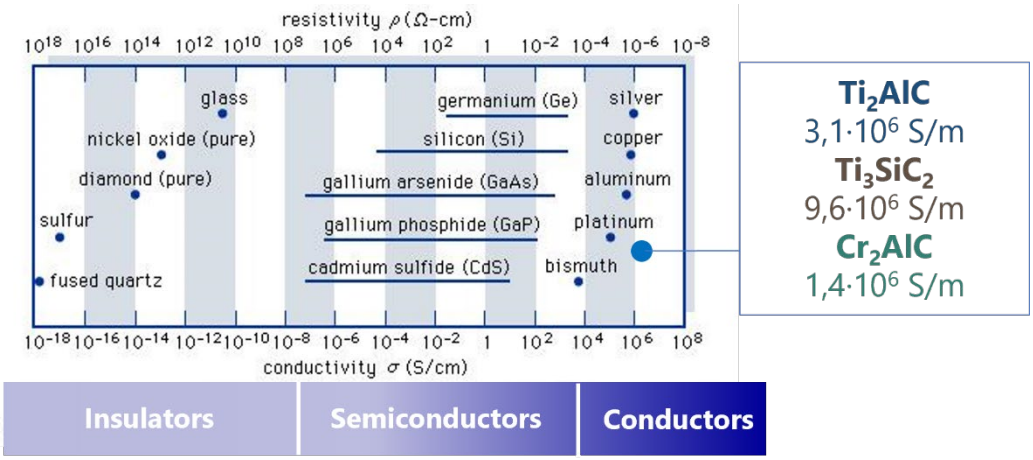

Figure 7. Electrical conductivity properties of different materials compared to those of MAX phases Ti_2AlC, Ti_3SiC_2 and Cr_2AlC [28].

1.1.1.5 Tribological behaviour

The wear behaviour of MAX phases was first studied in the 90´s; researchers observed that the machining properties of Ti_3SiC_2 had a similarity to graphite. The coefficient of friction (μ or COF) was measured on the basal planes of Ti_3SiC_2 using a lateral force microscope. COF measured exhibited exceptionally low values of $2 \cdot 10^{-3}$ [2]. However, studies performed with polycrystalline samples had higher COF values to those reported for the basal planes [29,30], with wear rates relatively high.

Nevertheless, the nanolaminated structure of MAX phases offers good tribological behaviour and this is due to the lubricating effect that the torn material produces under wear conditions. This lubricating effect has been previously reported and it is explained by the delamination of the debris generated, which creates a graphitic-like effect on the surface, reducing the COF during wear and improving the tribological behaviour of MAX phases [31–33]. Furthermore, the tribological properties of MAX phases vary with temperature with a better wear behaviour at high temperatures [34,35].

El-Raghy et al. [29] analysed the wear behaviour of hot-isostatically-pressed (HIP) Ti_3SiC_2 samples and studied how the grain size affected the wear properties of the materials. Their work showed a high difference on the coefficient of friction during the first stages of the wear test, caused by the abrasive conditions of the wear, and a stabilisation of this coefficient reaching similar values at 500 s, due to the effect of the debris acting as a third body. A three-body abrasive wear behaviour was also proposed by Magnus et al. [31] during pin-on-disk tests performed to dual Ti_3AlC_2-Ti_2AlC MAX phase samples.

Wear behaviour of Cr_2AlC has also been studied analysing the influence of the spark plasma sintering (SPS) parameters by Shamsipoor et al. [36]. In their work, different purities of MAX phase were achieved after the consolidation process. Nevertheless, the wear behaviour of the samples improved with the amount of Cr_2AlC phase in the final samples. The wear mechanism observed for this MAX phase was predominantly adhesive wear produced by the delamination of the material.

Due to the good properties of these materials, MAX phases have been studied as a reinforcement to improve the wear response of substrates. Yu et al. [37] used Ti_2AlC as a reinforcement to a magnesium alloy. In their work, spin-on-disk tests were carried out with different amount of MAX phases added and compared to the raw alloy. It was observed that the wear properties of the Ti_2AlC-magnesium alloy compound improved thanks to the self-lubricating effect of the MAX phases.

1.1.2 Synthesis methods and consolidation techniques

MAX phase synthesis processes have been in constant study due to the difficulty of obtaining high purity or single-phase elements of these materials. Researchers are continuously proposing new synthesis routes or adjusting existing ones to develop high purity MAX phases, through the understanding of the synthesis mechanism. For the MAX phases studied in this work, a brief review of the processes is shown in this section. The most studied MAX phases and their synthesis routes are summarised in Table 1. It is possible to observe that most of the works are focused on the in-situ synthesis of the MAX phases. Some of the most common techniques for the production of MAX phase samples are: hot-pressing, hot-isostatic pressing, pressureless sintering and spark plasma sintering. Some of the synthesis routes for these materials are detailed below.

Table 1. Summary of the most common techniques for the synthesis of MAX phases in powder and consolidated form.

MAX Phase	Processing techniques*	
	Powder synthesis	In-situ synthesis
Ti_3SiC_2	S-L [5], PS [6], SHS [4], MS [38]	CVD [39], HP [40], HIP [41], SPS [42]
Ti_2AlC	HP [43]	HP [43], HIP [44], SPS [45]
Ti_3AlC_2	-	PS [46], HP [47], SPS [48]
Cr_2AlC	-	PS [20], SPS [49],
Zr_2AlC	-	PS [50], HP [51]
Ti_4AlN_3	-	HP [52], HIP [53]

*Synthesis techniques abbreviated in the table correspond to: S-L (Solid-Liquid reaction), PS (pressureless sintering), SHS (Self-propagating High temperature Synthesis), CVD (Chemical Vapour Deposition), HP (Hot-pressing), HIP (Hot-Isostatic Pressing), SPS (Spark Plasma Sintering), MS (Molten Salt Shielding)

The production of MAX phase powders usually starts from the elemental powders that conform the specific phase that wants to be obtained. It is also common to combine those elemental powders with carbides or nitrides which also match the MAX phase desired. Molar ratios of the starting materials are commonly designed depending on the stoichiometry of the MAX phase, with some adjustments taken into consideration such as the sublimation properties of the powders. The powder production is frequently performed by routes that allow the later crushing of the synthesised pellets. Thus, processes like pressureless sintering (PS) or Self-propagating High temperature synthesis (SHS) are commonly used. Most recently, a new process route through a

combustion solution synthesis, that is a variation of the sol-gel process, has been used that could allow the production of MAX phase powders [54]. In this work, the MAX phase Cr_2GaC was synthesised using a nitrate (NO_3^-) combined with Cr and Ga, and citric acid ($C_6H_8O_7$) as the carbon source. In addition, Molten salt has also recently been used as shielding agent for the synthesis of Ti_3SiC_2 in air [38]. Dash et al. achieved the production of high purity powders of Ti_3SiC_2 and Ti_2AlN using potassium bromide (KBr) as a protective barrier for a cost-efficient MAX phase production. Nevertheless, the most common powder production routes are detailed bellow.

Ti_3SiC_2, has been investigated through a wide range of techniques. Solid liquid reaction (S-L), for example, was used by Sun et at. [5] introducing fluorite (NaF) to the elemental powers to create the liquid phase. More conventional techniques have been also explored, such as, PS. Cordoba et al [6] proposed this process to analyse the reaction mechanism of this MAX phase for a number of different molar combinations in inert atmospheres. Demonstrating the evaporation of silicon during the process and the need to adjust the A element in the initial molar ratio calculations. Other cost-efficient techniques have been proposed as SHS. El Saeed et al. [4] obtained high purity Ti_3SiC_2 with a strict control of the atmosphere to avoid contamination and oxidation of the elements during the process.

Due to the challenge of producing high purity materials, MAX phases are often synthesised in-situ, while the consolidation step is performed. Through this process it is possible to obtain final samples starting from the raw material and reducing the overall problematic of long synthesis optimisation processes.

Some of the consolidation techniques used for Ti_3SiC_2 synthesising, are described below. Goto et al. [39], proposed chemical vapour deposition (CVD) as a synthesis route, using $TiCl_4$, $SiCl_4$ and CCl_4 as staring gases. At temperatures between 1300 and 1600 ºC an electronic current was applied to promote the deposition and synthesis of the MAX phase. Although this process was very innovative, the use of these gasses for the production of MAX phases creates a low cost-efficiency process were the gasses need to be pressurised and heated for the vapour deposition of the synthesised phases. Hot pressing (HP) and Hot isostatic pressing (HIP) have been one of the most used consolidation methods for most of the MAX phases. Ti_3SiC_2 specifically, has been in-depth studied by Barsoum and El-Raghy, reporting the synthesis mechanism and properties of Ti_3SiC_2 through HP and HIP [2,41,55]. Spark plasma sintering (SPS) has also been studied by Gao et al. obtaining high density samples with a small presence of TiC impurities [42]. As stated earlier, these processes (HP, HIP and SPS) are

undoubtedly the most common consolidation techniques to produce MAX phase samples while performing the synthesis. Nevertheless, and not only for MAX phases but for all powder materials in general, these techniques have a limited geometrical sample production, demanding a post-processing if a specific shape is required.

High purity Cr_2AlC has also been achieved starting from elemental powders and with an almost stoichiometric molar ratio. It is common for this MAX phase to add an excess of aluminium into the initial molar ratio to prevent its loss during the synthesis step. One of the most successful synthesis routes for this MAX phase is starting from elemental powders with a molar ratio of 2:1,1:2 through pressureless sintering [20]. In this work, the PS route was used as a powder production process for the later consolidation of the high purity Cr_2AlC with NH_4HCO_3 (ammonium hydrogen bicarbonate) to produce macroporous samples. SPS has been also used for the synthesis of Cr_2AlC. Zuber et al. [56] produced samples starting from elemental powders with a molar ratio of 2:1.02:0.97 and compared them to HIP-ed samples obtained from Cr, Cr_3C_2 and Al, with a molar ratio of 0.525:0.425:1.2. These two molar ratios and processes were selected to understand the oxidation behaviour of coarse and fine grains samples, reporting the importance of the initial selected powder size and the consolidation process. Other works have studied the deposition abilities of Cr_2AlC powder to be used as protective coating. The powders to be cold sprayed were synthesised starting from chromium carbide (Cr_2C_3) and elemental chromium and aluminium with a molar ratio of 1:1:2,05, respectively, [49]. Go et al. successfully obtained a bonded coating to a stainless-steel substrate avoiding cracks or delamination maintaining high purity levels of the MAX phase.

The synthesis mechanism of Cr_2AlC has been studied starting from elemental powders. Xiao et al. [57] studied MAX phase formation and analysed the temperature influence on Cr/Al powders with a molar ratio of 2:1.2 and observed a formation of single phase $AlCr_2$ at 1100 ºC. After this the $AlCr_2$ powders were mixed with C with a 1:1 molar ratio and obtained high purity Cr_2AlC at 1400 ºC. This model represents the enhanced MAX phase formation for Cr_2AlC. Nevertheless, this synthesis was performed in a two-step process, and the reactivity of the elemental Cr:C powders is not considered. This could explain the formation and final appearance of chromium carbides in the final composition.

The synthesis of Ti_2AlC MAX phase has been extensively studied and, to date, Ti_2AlC and Ti_3SiC_2 MAX phase powders are the only ones to be commercialised. Barsoum et al. [43,44], reported the consolidation of Ti_2AlC polycrystalline samples produced by HP and HIP. In this work, the synthesis started with Ti, Al_4C_3 and graphite powders. SPS

has also been studied for the production of Ti_2AlC obtaining bulk single-phase samples, starting from elemental powders [58]. A study of the reaction mechanism for the formation of Ti_2AlC has been performed by Gauthier-Brunet et al [59], studying the temperature influence on the formation of Ti_2AlC and Ti_3AlC_2 MAX phase starting from Ti, Al_4C_3 and C with a molar ratio of 8:1:1. They observed different reactions occurring at a temperature range between 570 ºC and 800 ºC. After this temperatures Ti and Al_4C_3 is no longer observed, indicating a complete reaction of these powders generating TiC_x, Ti_3Al and Ti_3AlC_x. These three phases and the remaining C are the precursors for the formation Ti_2AlC. In addition, they were able to detect the 312 phase on the Ti-Al-C system at temperatures above 1400 ºC. They suggest that the formation of this MAX phase needs higher temperature to be formed as well as TiC as a secondary phase still present in the mixtures to react with Ti_2AlC.

Several studies have focused on the use of MAX phases to develop Ceramic Matrix Composites (CMC). This is commonly done to improve different aspects of the MAX phases: mechanical properties and oxidation behaviour [60,61]. The influence on the oxidation properties of Cr_2AlC by the addition of ceramic fibres has been studied by Go et al. [62]. In this work, Al_2O_3, SiC and C fibres were used as reinforcement, obtaining promising results in the case of Al_2O_3. Although SiC and C fibres reacted with the core Cr_2AlC phase, the use of Al_2O_3 fibres led to a well-adhered protective oxidation layer. In addition, MAX phases have been used as a reinforcement to improve electrical properties or yield resistance of other materials [63,64]. Wenbo et al. [64] used Ti_3SiC_2 and Ti_2AC to reinforce a magnesium alloy (AZ91D) studying the influence of the MAX phase reinforcement on the mechanical properties of the samples produced. They were able to tailor the yield strength and the ultimate tensile strength of the samples, with the addition of different amount of MAX phase powders (5-20 vol.%). Although some agglomeration of the Ti_2AlC powders and decohesion of the Ti_3SiC -Mg interphase was found, they suggest that the bonding strength of MAX phase-Mg composites can be controlled improving the mechanical properties of the materials.

1.1.3 Applications

With some of the most interesting properties of the MAX phases stated above, it is possible to see the great potential that this family of materials has, especially when an intermediate material between a metal and a ceramic is required. MAX phases studies in the last decade explore the use of these materials as candidates for several potential applications. Some of the most promising fields suggested are detailed below.

The stability of MAX phases at high temperatures between 1100 and 1400 ºC, proposes these family of materials as a great candidate for numerous applications in aggressive high temperature applications. As heating elements, MAX phases have shown good stability under cyclic heating and cooling cycles under different atmospheres (air, argon, hydrogen or vacuum). The protective oxide layer generated in outer zones on the material, well-adhered to the core, makes this material suitable as heating elements. Figure 8 shows a resistance made of Ti_2AlC working at 1450 ºC.

Figure 8. Ti_2AlC heating element produced by Kanthal working at a temperature of 1450 ºC in air [8].

As structural high temperature materials, MAX phases can operate in heated elements in gas turbine engines. Materials used in the aerospace industry require strict performances at aggressive environments. Most importantly, component weight is a special factor that needs to be considered in order to reduce costs. Good behaviour at high temperatures and low density, makes MAX phases a promising material for these applications. As an example, Ti_3SiC_2 has half the density of some of the alloys used in turbine engines and can withstand high temperatures under severe strength conditions [65].

Several studies have proposed MAX phases as a protective coating for metallic and ceramic alloys acting as a thermal barrier coating (TBC) [49]. TBCs are required to be thermally insulating and stable at high temperatures, with low coefficient of thermal expansion (CTE). Not only as coating but as the substrate for TBC, Cr_2AlC has been studied. Gonzalez-Julian et al. [19] analysed the deposition of yttria stabilised zirconia (YSZ) to Cr_2AlC substrates. They observed a formation of an Al_2O_3 layer between the substrate and the YSZ porous coating which improved the adhesion of the coating which was able to withstand 1200 ºC thermal cycles for 500 h. All this makes MAX phases a great candidate for these applications with coefficient of thermal expansion (CTE) values

of 12 x 10^{-6} k^{-1} for Cr_2AlC [66] and 9 x 10^{-6} k^{-1} for Ti_2AlC [7], similar to those commonly used for TBCs, for example YSZ with a CTE of 10,2 x 10^{-6} k^{-1}.

Under oxidation or tribological conditions Ti_2AlC has shown better properties compared to graphite. Other studies suggest the use of Ti_3SiC_2 as coating under highly oxidative environments to produce a protective oxide layer, while increasing the oxidation resistance of substrates [7,8].

In terms of electrical conductivity, one of the earliest use cases of Ti_3SiC_2 was as a sputtering target for electrical contact applications [8].These components are usually the weakest elements in an electronic system and, thus, it is important for new solutions to solve the problems with wear and oxidation resistance and good thermal and electrical conductivities. Other MAX phases such as Cr_2AlC are also used to generate thin films on steels [67] for environmental protection. Furthermore, Ti_3SiC_2 has been also used as an electrical contact for SiC in electronic devices, profiting from the thermodynamic equilibrium of both materials and allowing the components to operate at higher temperatures [10].

In addition, MAX phases are great candidates as catalytic devices or high temperature heat exchangers (HTHXs). Both applications demand oxidation resistance and high temperature stability since they are exposed to harsh conditions while transferring corrosive fluids or hot gases [2]. Ceramic heat exchangers, that are more resistant to high temperatures, oxidation and corrosion, exhibit low thermal shock resistance and, in addition, are difficult to process, having lower thermal conductivity than desired [68–70]. HTHXs are used in gas turbine systems [71], high efficiency power plants [72,73], solar plants [74], hydrogen production [75], and high temperature fuel cell systems [76]. In this topic and as a gas burner, a Ti_2AlC nozzle demonstrator (Figure 9) has been produced and compared under service conditions to steel, exhibiting better thermal and corrosive stability under severe conditions.

For some of the applications stated above, HTHXs, catalytic devices or gas burners, a certain level of porosity is required to operate under harsh conditions. This is why some of the efforts on characterising the oxidation behaviour of MAX phases have been studied to macroporous samples. This is the case of Gonzalez-Julian et al. [20], as mentioned previously, they used NH_4HCO_3 as a temporary pore former that was later removed obtaining Cr_2AlC foams with porosities between 35 and 75 vol.%. They observed an increase on the compressive strength of the foams after oxidating them at 1200 ºC for 1 h. Velasco et al. [77] also produced Ti_3SiC_2 and Ti_2AlC foams starting from commercial MAX phase powders. In their work, saccharose was used as space holder

element to avoid corrosive problems and ease the elimination of the pore former in water. They analysed the influence of the porosity in the thermal and electrical conductivity properties, observing a decrease of this value with the increase of the porosity. Furthermore, the oxidation behaviour of different porous samples (20-60 vol.%) was analysed. They observed the typical oxide formation of these MAX phases, as stated above, with a cubic driven kinetics, under cyclical test in air. With all this and, as an example, Ti_3SiC_2 processed in macroporous form, presents a combination of properties that makes it a potential candidate to be used as substrates for high-efficiency catalytic devices in vehicles. The use of an electrically conductive material such as Ti_3SiC_2 as a catalytic support adds two advantages; first, it allows the catalytic converter to be activated by electrical heating in a very short time and, secondly, allows the deposition of catalytic coatings of high quality on the surface by electrochemical deposition [78]. In addition, Ti_3SiC_2 is also superior in mechanical resistance and has good behaviour against corrosion, which is necessary for this application.

Figure 9. Gas burner nozzles of Ti_2AlC and steels tested in service at 1400 ºC [8].

Nuclear applications has been another focus of the MAX phase researchers due to the good radiation tolerance of these materials. Several studies have been performed in order to characterise different materials under irradiation conditions. Although Ti_3SiC_2 [79], Ti_2AlC [80], Ti_3AlC_2 [81], Cr_2AlC [82] and V_2AlC [83] have been studied for their use as cladding materials for third generation light-water reactors, the Zr_{n+1}-AlC_n MAX phases have shown the best properties and enhanced neutronic properties with relatively low neutron absorption. More specifically, Zr_2AlC due to a combination of the neutron transparency and the formation of an Al_2O_3 protective layer makes this MAX phase a great candidate as a cladding material. One of the main concerns is the poor behaviour

of this material to Loss of Coolant Accident (LOCA) [84]. Nevertheless, the new nuclear reactors design is meant to use lead-based coolants and in this case MAX phases show good compatibility with Pb [85]. All this combined with the good corrosion and oxidation behaviour of MAX phases make this material as a great candidate for nuclear applications.

1.2 Powder injection moulding

Powder injection moulding (PIM) is a powder metallurgy processing method for the production of small parts with complex shapes which starts from the raw material in powder form. The process is based on the mixing of the powders with a polymeric agent, called binder system, that will be responsible for giving the necessary viscosity to the powders to be injected. This powder-binder mixture is often referred as feedstock. Once the feedstocks are prepared, they are heated up in a barrel and pressure is applied to inject them into a mould with the desired final shape of the component to be produced. A green part is obtained after the injection moulding process, and the polymeric agent in the system needs to be removed. This binder removal process is called debinding and it is based on the use of temperature or solvent agents for the degradation of the polymeric system. Once a brown part (sample with no binder) is obtained, a sintering process is carried out for the physicochemical interaction of the powders. In this process diffusion phenomena occurs and the consolidation through densification of the material is done attaining a dense final part with a dimension shrinkage caused by the debinding and sintering process [86,87].

Powder injection moulding is considered a mature technology for a large number of industries; mainly, industrial machinery, medical components and the automotive sector [88–90]. The volume of parts produced per year and the amount of companies that have adopted this processing technique for component production has steadily increased in the last decades. Furthermore, PIM has been implemented in new sectors such as, hand tooling, electronics or aerospace [91,92].

Some of the advantages of the PIM process compared to other production techniques are listed below:

- Wide range of materials. PIM allows to use a broad variety of materials during its process, starting from the powders to be consolidated followed by the binder system to be used. Both ceramic and metals can be used in powder form to obtain final parts. In addition, a wide-range of polymeric binders can be selected depending on the temperature properties of the powders to be injected or the debinding process that is going to be performed depending on the interaction with the raw material [93].
- Shape complexity. Through PIM it is possible to obtain near-net-shape samples, with good final part quality and tolerances, avoiding using post-machining processes to the components. Inserted holes or threads can also be obtained with this technology [94].

- Low production costs. Due to the automatic nature of the process, the production of large-scale batches of parts is highly cost efficient. In addition, the reduction or elimination of post-processing steps due to the great surface finish and dimensional tolerances of the PIM process saves production costs [87,95].

Nevertheless, powder injection moulding presents some limitations in terms of component production. For example, large components cannot be produced through this technology [86]. In addition, to ensure a good final quality of the samples, a specific particle size and morphology of the powders is required increasing the production cost of the process.

1.2.1 Overview of the PIM process

The powder injection moulding technology is an intricate process in which the success of the sample production depends on the optimisation of all the stages of the process. After the selection of the initial materials, PIM process, as stated earlier, can be divided into 4 different main steps: mixing, injection, debinding and sintering (Figure 10). In the following sections each step of the process will be described.

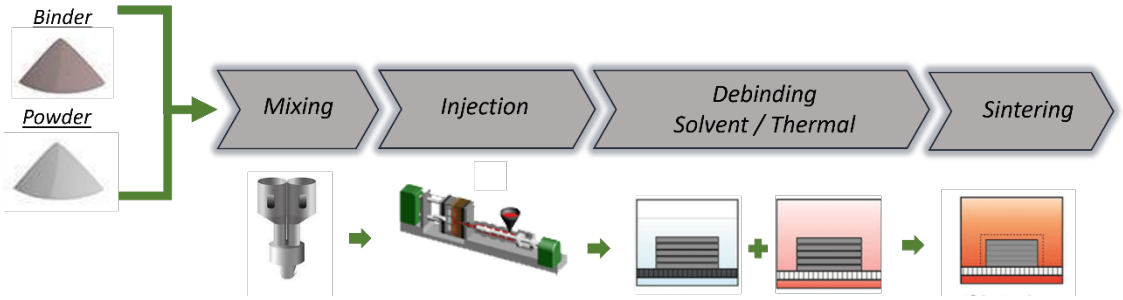

Figure 10. Powder injection moulding process stages.

1.2.1.1 Initial material selection (Powder and binder system)

The selection of powders and polymeric binder for the feedstock production is a critical step on the injection process since the adequacy of the initial materials will determine the viability of the process. In order to ensure the feasibility of the injection process, initial materials should comply certain requirements. The most important characteristics are detailed below:

Powders:

Regarding powders, it is necessary to ensure maximum packing densities in order to obtain highly dense parts. For this purpose, powders need to be tailored in terms of shape and particle size distribution. Although some difference arises for metallic and

ceramic powders, regarding the powder production, the most common characteristics that the powder material should have, are listed below.

- Particle size and size distribution. Powders used for the injection process are recommended to have a maximum size of 22 μm and a broad particle size distribution. This characteristics would ensure the correct packing of the particles and a good sinterability [96].
- Morphology. The powder morphology most used in powder injection moulding is spherical. This particle shape promotes the correct homogenisation of the powders with the binder improving the rheological behaviour of the feedstocks and, therefore, the densification after sintering. Spherical morphology, although recommended, could present some disadvantages after the debinding process, where the particle contact could fail resulting in a collapse of the brown part [87,96].
- Density and other considerations. In terms of tap density, that is related to the packing properties of the powders, values should be above the 50% of the theoretical density. In addition, powder should not create agglomerates to guarantee the correct mixing of the feedstocks and present low risk of toxicity and explosion [86].

The most used ceramics material in this technology are alumina (Al_2O_3) [97], ferrite ceramics (Mn-Zn ferrite, Ni-Zn ferrite or Mg-Zn ferrite) [98,99] and piezoelectric ceramics ($PbZrTiO_3$ or $BaTiO_3$) [100]. The powder production of ceramics for PIM, in general, is usually through mechanical methods (grinding or milling). The problem with the mechanical methods is the difficulty to control the particle size and its distribution, and a later chemical process is commonly used to refine the powder and tailor its physical properties for PIM. Solid-state reactions, liquid solutions or gas reactions are commonly used for the production of high purity small particle powders. Nevertheless, these processes tend to be expensive routes, producing highly agglomerated powder that need to be addressed once the feedstock production is performed [101].

On the other hand, metallic powders are the most used through PIM. Stainless-steels [102,103] or titanium alloys [95] are some of the most commonly used powders. The main advantage of metallic materials is their ability to be melted at relatively low temperatures, compared to ceramics, and produce powders by atomization processes. Although the high reactivity of metallic powders demands a control on the production conditions, processes like gas atomisation have been highly studied to

produce high quality powders with the possibility of tailoring the particle size distribution while obtaining spherical or quasi-spherical powders [104]. In addition, atomisation processes allow to obtain finer powders that can increase the packing density of the feedstocks produced, obtaining highly dense parts.

Binder:

Polymeric binders used for PIM are commonly designed as multicomponent systems. One of those is going to be in charge of giving to the material structural stability, usually referred as backbone. Thermoplastic polymers are generally selected to be used as backbone in feedstock production to take advantage of the possibility to be melted and solidified during the process. Some of the most used are: polypropylene (PP), polyethylene (PE) or ethylene vinyl acetate (EVA) [101]. The secondary element of the multicomponent binder system has two purposes. First, to improve the flowability of the material, that is the capability of the material to move once, in this case, a force is applied to it. Secondly, this material is going to be removed from the injected sample leaving free channels and pores for the backbone to be correctly removed, avoiding the creation of internal defect in the samples. Some of the most used polymers as secondary component are waxes. Moreover, additives are commonly used to improve the properties of the polymeric systems. As an example, stearic acid is used to lower the surface tensions between the powder and the binder and to improve the homogeneity through a correct dispersion of the powders in the binder [101].

The development of binder composition is a never-ending research and new polymeric systems arise to comply with the necessities of the PIM process and solve some of the problems that other binders have. Some of this new polymers that have attracted the attention of researchers are Poliacetal (POM) [105], which eases the degradation properties without adding a secondary polymer, or polyethylene-glycol (PEG) [106] that can act as a backbone with good mechanical properties and as secondary element allowing the removal of the polymer from the feedstock by a solvent debinding process using water. Nevertheless, the polymeric system must be carefully selected and in concordance with the solid loading (powder) that is going to be used for the feedstocks. As an example, water soluble binder are usually not used with highly reactive metals since it could cause the contamination of the material to be sintered.

With all this, some of the most important aspects that a polymeric system should have, are detailed below:

- Interaction with powder. The polymeric binder system should display good wettability and adhesion to the powders. Capillary attraction between the particles

and chemically inert to avoid reaction with the powders. All this should ensure the correct homogenisation of the feedstocks [93,107].

- Fluidity properties. Rheological properties of the binder should have low viscosity at the injection temperature, low viscosity influence on temperature changes and a certain rigidity to ensure the correct extraction of the part from the mould after the injection process [107].
- Degradation. Binders have to be chemically stable during storage. In addition, the degradation temperature has to be above the mixing and injection temperature to ensure the correct fluidity during the process and the reusability after the process. Furthermore, the degradation products of the system should not be toxic or corrosive [87,96].
- Other considerations. Different properties such as high thermal conductivity, low thermal expansion coefficient and other factors as availability and cost of the raw material should be considered upon the binder selection.

1.2.1.2 Feedstock production and mixing

To produce feedstock for the injection moulding process it is necessary to control certain parameters in order to assure the successful injection of the materials. Powder-binder systems have a unique behaviour, depending on the initial materials selected, and the interaction between them needs to be strictly controlled. This is why for the optimisation of the feedstocks, a rheological characterisation is needed to select the ideal composition in terms of amount of powder that the binder can accept and its behaviour with pressure and temperature.

Homogeneity of the feedstocks has to be thoroughly studied for the appropriate injection of the parts and proper sintering of the materials. For this purpose, homogenous feedstocks have to be produced with the optimal amount of solid content (powders) in the mixture. For a proper sintering, feedstocks must contain the maximum possible amount of powders, without compromising the flowability properties of the feedstock by an increase on the viscosity. This optimal solid loading is the state where all powder particles are correctly surrounded by the binder system. With an insufficient amount of solid loading, feedstocks will have good flowability due to the low viscosity, but the excess of binder will create heterogeneities in the feedstocks, resulting in sintering problems. On the other hand, feedstocks with an excess of solid content will increase the viscosity of the mixture resulting in moulding problems and heterogeneities in the injected parts creating air bubbles in the feedstocks [108–110]. Figure 11 shows, as a representation, the different states of a feedstock depending on the solid loading.

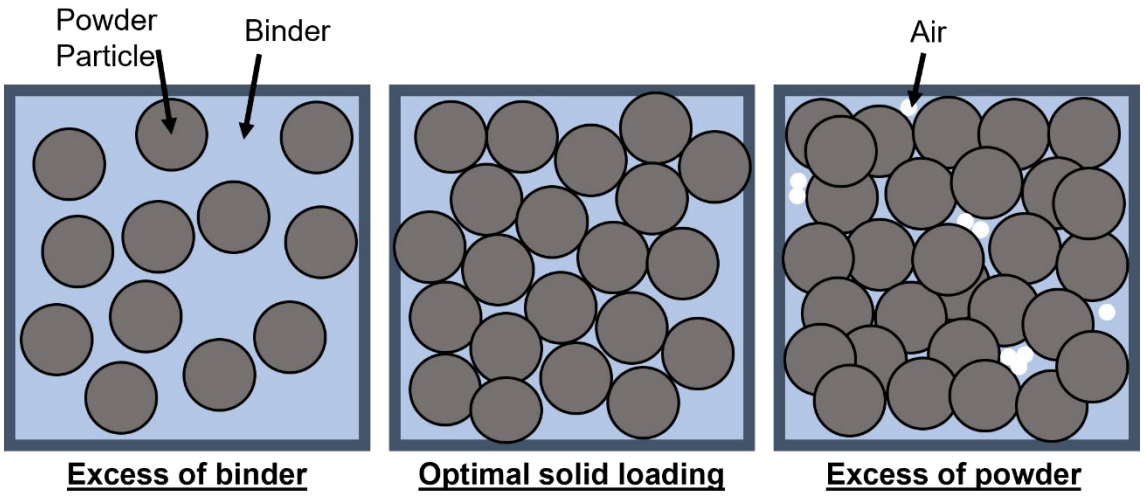

Figure 11. Schematic representation of feedstocks with different solid loadings.

To study the homogeneity and the effect of the amount of solid loading on the flowability of the feedstocks, rheological properties must be analysed. With the rheological analysis, the response to an external force is quantified, and as a consequence, its effect on deformation and flow of a material. To analyse this behaviour and to select an optimal feedstock to be injected, several studies are performed. Some of the most used rheological characterisation techniques are torque rheology or capillary rheology.

Torque rheology is based on the study of the force that the mixing rotors are exerting while mixing the powder-binder system to produce a feedstock. Through this technique it is possible to study the critical and optimal solid loading of feedstocks. The critical solid loading of a feedstocks determines the maximum amount of powders that a binder system is able to accept, while maintaining the homogeneity of the mixture [111]. Usually, while mixing feedstocks with a solid content below the critical solid loading, there is an initial increase on the torque response, due to the friction generated by the powders. Once the mixture starts to homogenise, there is a decrease on the torque, that, with time, reaches a stable value. On the other hand, mixtures with solid contents above that critical point are not able to reach that stable state. Increasing torque value with time is caused due to the lack of homogeneity generated by the powder excess in the mixture. Both effects can be observed in Figure 12 where zircon feedstocks were developed with solid loading between 52.5 and 65% by Hidalgo et al [112]. Torque values start to decrease for lower solid content feedstocks (52.5-62.5 vol.%) and they stabilise at 50 min. When the critical solid loading is surpassed (65 vol.%) the feedstock is not able to homogenise and torque values steadily increase with time.

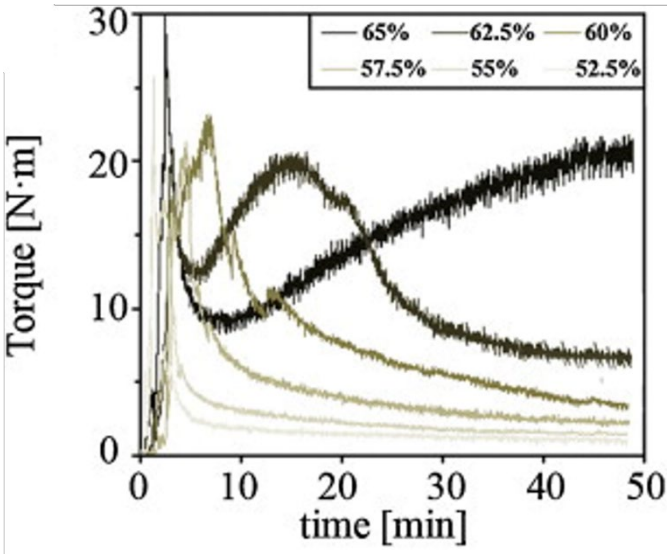

Figure 12. Torque rheology curves of zircon/PEG-CAB feedstocks exhibiting the influence of the solid loading content to their torque behaviour [112].

In addition, multistep torque rheology has been proposed in the last years as an effective route to determine critical solid loadings of feedstocks. This process measures the torque response of a feedstock by increasing the amount of solid loading in the mixture in the same test, thus, different solid loadings can be measured in one trial, as opposed to the conventional torque rheology, where different solid loadings are tested separately [109]. Multistep torque rheology allows to determine the critical solid loading of a feedstock reducing the amount of powders used during the test. This is of extremely importance for expensive powders or for characterisation at a laboratory scale. One of the main drawbacks of this test is that the filled chamber volume varies during the test. This could result in altered measurements if the solid loadings to be analysed are not carefully selected. The basis of torque multistep testing is to fill the chamber with a solid loading and once the torque has stabilised increase the amount of powder to the mixture, until the maximum desired solid content is reached (Figure 13-a). With the stabilised torque plotted as a function of the solid loading it is possible to see a shift on the behaviour of different solid loadings with a change on the slope, determining the critical solid loading of the mixture (Figure 13-b). Optimal solid loadings can be estimated from the torque analysis and selected below the critical point. Nevertheless, capillary rheology tests are commonly performed to further analyse the optimal solid loading of feedstocks.

Capillary rheology is one of the most common rheological tests performed to feedstocks, since it resembles in a smaller scale the injection moulding process. This technique is performed to analyse the response of the feedstocks' viscosity with temperature and shear rates. This test, similar to the injection process, is performed at temperatures above the melting point of the polymeric system and below the degradation temperature [86]. Viscosity (η) is defined as the measure of a fluid´s resistance to flow generated by

the internal friction during the movement of the fluid. Thus, the viscosity is dependent on the shear stress ($\dot{\gamma}$) and shear rate (τ) as shown Equation 2.

Equation 2 $$\tau = \eta \cdot \dot{\gamma}$$

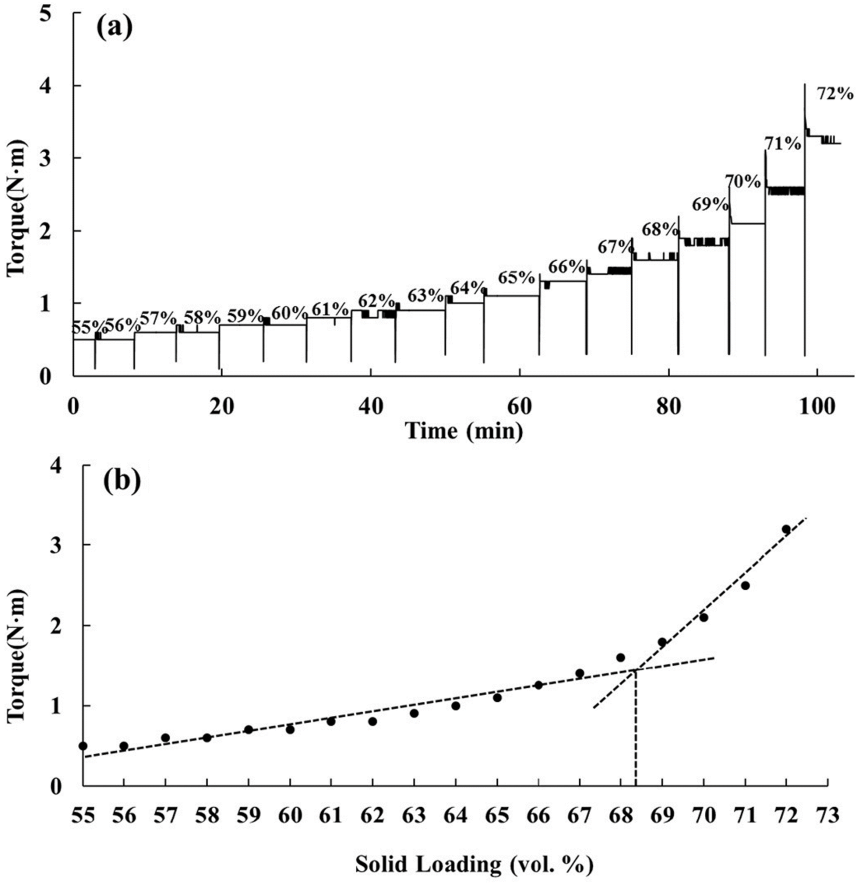

Figure 13. a) Multistep torque analysis as a function of time and b) stabilised torque as a function of solid loading analysing the change of slope of a Ti-6Al-4V/PE-PP-wax feedstock [110].

From the measured viscosity of the feedstocks and their dependence on the shear rate, several behaviours can be observed (Figure 14). Fluids in which the shear stress varies linearly with the shear rate and its viscosity is independent of the shear rate are called Newtonian fluids. From the point of view of the PIM process, it is beneficial that the fluids decrease in viscosity as the shear rate increases, that is, that they show a behaviour called pseudoplastic. Dilatant fluids are not recommended, since they will cause an increase in viscosity during injection, which could result in the separation of the powder-binder system making it difficult to process (Figure 14-a). Furthermore, Ostwald-de-Waele's power-law of fluids [87] allows to evaluate the sensitivity of a feedstock at different shear rates as represented in (Figure 14-b) and follow Equation 3:

Equation 3 $$\tau = k \cdot \gamma^n$$

Where τ is the shear force, k is the consistency index of the fluid, γ is the shear rate and n the fluid index. Thus, values of n>1 represent a dilatant behaviour of the material, n<1

pseudoplastic and n=1 Newtonian. Typically, feedstock with fluid index n<1 are desirable for optimum rheological behaviour. In addition, viscosity values below 1000 Pa·s for shear rates between 100 and 10000 s-1 are necessary for a correct injection process.

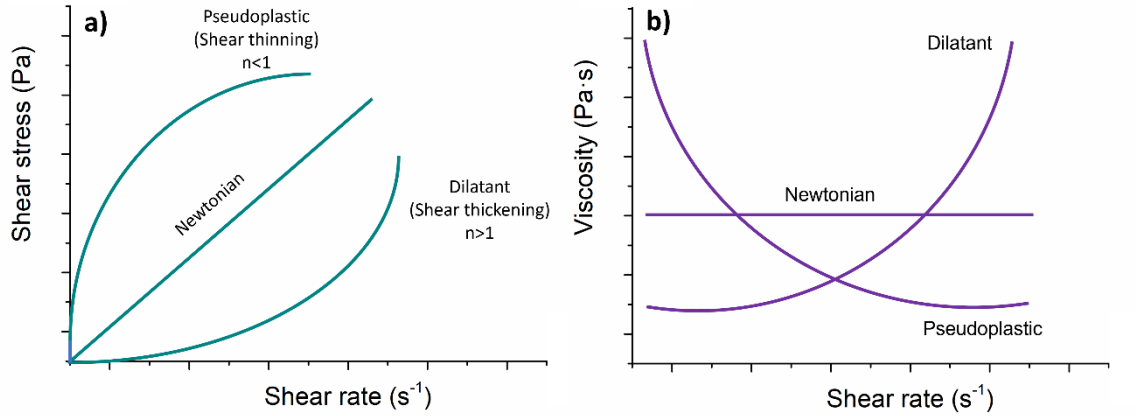

Figure 14. Pseudoplastic, Newtonian and dilatant fluid behaviour example of ideal feedstocks represented as a function of a) shear stress and b) viscosity.

Once the initial materials are chosen and the optimal solid loading of the feedstock is selected, the initial step on the injection moulding process starts by mixing the raw materials to produce the feedstocks. This process is typically carried out in rotatory mixers or extruders. The polymers are melted in a heated chamber and the powders are poured in while the rotors or the extrusion screw rotate for the mixing. Afterwards, feedstocks are pelletised or granulated for the injection process.

1.2.1.3 Injection

After the optimisation of the powder-binder system, the next stage is the injection of the feedstocks into a mould with the desired sample shape. In this process the feedstocks are introduced in pellet form into the heated barrel which will increase the temperature of the material, reducing its viscosity so that it can be injected into the mould. Feedstocks, once injected through the nozzle will start to occupy the zones of the mould, acquiring the desired shape. The success of the injection process depends on the optimisation of the injection parameters, such as, feedstock temperature, mould temperature, injection pressure or holding pressure, amongst others, that will have an effect on the final green part produced [113]. Pressures applied for low pressure PIM range between 0,2 and 50 MPa, while for high pressure PIM are between 50 and 150 MPa [87].

Low-pressure injection moulding (LPPIM) allows to obtain injected parts with low equipment and tooling costs, reducing the energy consumption. Researchers have considered LPIM as an attractive route for small series production and rapid prototyping. Although with lower pressures there is lower packing of the powders, compared to high pressure systems, several studies have focused on this process to obtain highly

densified materials. Furthermore, to solve these challenges, lower viscosity feedstocks need to be prepared for LPIM [86,87]. During the last years there has been an increase on the studies related to modelling and feedstock characterisation regarding LPIM of titanium [114,115] and alumina [116]. This is due to an effort to reduce the cost of the PIM process and a result of the low viscosity values (below 100 Pa·s) that the feedstocks produced exhibit, making them attractive for LPIM. Nevertheless, Moghadam et al. [117] studied the production of rectangular samples using Paraffin wax and LDPE binder with a 53 vol.% solid content of titanium. LPIM was used for the obtention of green samples applying a pressure of 1 MPa. Sintered samples exhibited a 95% relative density, demonstrating the possibility of obtaining good quality samples through LPIM. Moreover, alumina samples have been also obtained by LPIM [116]. Sardarian et al. produced alumina/paraffin wax-based feedstocks with a solid loading of 60 vol.% using pressure between 0,1 and 0,6 MPa. Values of up to 91% relative densities were obtained after the sintering process.

1.2.1.4 Debinding

After obtaining the green part with the chosen geometry, the next step in the injection moulding process is the debinding. In this step an external agent (i.e., heat, solvent) is used for the degradation of the polymeric system. An almost complete elimination of the binder occurs at this stage and the removal needs to be controlled in order to avoid internal defects or damaging the sample. The debinding is one of the most critical steps in the PIM process and therefore, needs to be optimised [108,113,118].

There are different debinding methods that can be performed to green parts in order to remove the polymeric systems depending on the characteristics of the binder. Most typical processes are detailed below:

- Solvent debinding. In this type of debinding a solvent agent is required to remove the binder system. Typically, binders removed by this process are systems containing waxes or oils and for the degradation of this products organic solvents in liquid or gaseous state (alcohol, acetone or hexane) are usually used [119,120]. In addition, water can be used as solvent agent for water-soluble polymers as polyethylene glycol (PEG) [106,121]. Solvent debinding is typically performed for multicomponent binder systems [106]. Although there are some works which use solvent debinding as one step process for the binder removal [121], the intention of this process is to remove the filler binder and create open porosity on the injected samples, for a later thermal debinding of the backbone. Usually, the solvent debinding process is performed to remove the paraffin wax

from the green parts, thanks to their solubility in organic solvents, such as heptane. Heating the solvent agent can increase the degradation kinetics, changing the solubility and diffusion of the binder [122]. Some of the key parameters to control during this process are the surface to volume ratio, which it is crucial for the solvent to be able to penetrate all the samples, and is directly related with the sample´s volume, and temperature. Several studies show the effectiveness of this method for a later removal of backbones such as PP [123] or HDPE [124]. The use of PEG binders has increased during the last years, due to the possibility of avoiding organic solvents for the debinding of the samples. PEG has been used as a filler for a wide range of backbone materials: PP [125], PMMA [126] or PLA [127], among others. The use of water-soluble binder, such as PEG, is particularly relevant for the development of greener processes with minimum environmental impact, since the use of organic solvent implies higher toxicity and a chemical hazard. On the other hand the use of water could also produce contamination of high reactivity powders [104].

Some of the advantages of solvent debinding are that lower temperatures for the debinding usually mean a lower defect and distortions of the samples. Additionally, this process is faster than thermal debinding and the components retain their rigidity after the process.

- Thermal debinding. The degradation of the polymer occurs by the action of heat. Usually, and depending on the material, this process is carried out under protective atmospheres to avoid contamination. This debinding process should be performed at low heating rates to reduce the possibility of defect appearance due to the degradation gases produced. This means that thermal debinding is usually a long process. Since most of the binders used for PIM are PP, PE or EVA, the thermal process is commonly used for the degradation of these binders [104]. Due to the difference on the constitution of these polymers, the temperature and time of the process varies depending in the polymer that is being used. Nevertheless, this process is commonly done between 200 ºC and 600 ºC [128]. Thermal debinding, if not controlled properly, leads to the accumulation of internal gasses in the sample, resulting in the appearance of cracks or the complete destruction of the sample. Yet, this process is still widely used for the complete degradation of the polymeric system in the green samples. This main drawback is one of the reasons why the two-step debinding process has been used. The elimination of the filler by solvent debinding eases the gas movement through the porosity created avoiding the appearance of internal defects. However, thermal debinding is suited for a wide range of binders, the installation

costs are low and the debinding and sintered process can be performed in the same furnace, avoiding the handling of brittle brown samples [86,104].

- Other debinding processes. Supercritical debinding: this is similar to the solvent debinding process but, usually, requires liquid carbon dioxide at temperatures between 50 and 70 ºC to remove typically waxes in the binder system. One of the main problems of the supercritical debinding is the necessity of a special equipment for the use of liquid CO_2. Catalytic debinding: in this case, a catalytic agent is required for the degradation of the binder system. The most conventional is nitric acid. Is it a fast process that achieves the complete elimination of the binder, with good structural integrity of the samples after the process. One of the main drawbacks of this debinding technique is the expensive equipment that is needed for the use of the catalytic agents and the corrosion and health implications that the nitric acid condensation presents.

In brief, to control the appearance of defects and ensure a correct structural integrity of the samples, a multicomponent binder is commonly used as polymeric system. This allows to combine different polymers and use different steps in the debinding process, reducing the possibility of creating defects in the components. The binder composition is usually selected to perform a two-step debinding. Firstly, a solvent debinding, eliminating the majority of the binder system and creating interconnected pores, which will facilitate the removal of the backbone polymers in a secondary stage, usually carried out by thermal debinding [124,129].

After the debinding, an almost free binder part is obtained, this part is commonly referred as brown and is highly fragile due to the fact that is composed by, mainly, powder particles bonded by weak diffusion links [86,87]. Furthermore, the presence of any non-degraded polymer during the sintering stage is a big concern for high reactive powders, specially metals, which can produce carbides resulting in the embrittlement of the material. This is another reason why the debinding process needs to be carefully selected and controlled.

1.2.1.5 Sintering

After obtaining the brown part, it is necessary to densify the sample in order to obtain a solid component. For this purpose and as a final stage of the injection process, sintering of the samples is performed.

The sintering is a mandatory stage for all powder metallurgy processes, in which powders with the desired final geometry are densified through a thermally activated process. During sintering the physicochemical reaction of the powders occurs in different

stages. First, an initial bonding of the particles begins and a “neck” starts to growth between the particles. With time, these necks grow, closing the channels between particles by mass transportation mechanism, while isolated pores appear. Lastly, the densification of the sample is enhanced reducing the amount of porosity in the parts with a total growth of the necks creating the grain boundaries [130].

Some of the parameters that influence the sinterability of the materials are: chemical composition of the powders, powder morphology and particle size distribution. Moreover, process temperature, time, atmosphere, heating and cooling rates or pressure also have an effect on the final microstructure of the material [131]. Nevertheless, the optimal sintering cycle depends on the material processed. Final PIM sintered parts have usually residual porosity and a post-processing hot isostatic pressing (HIP) route is commonly used for the high densification of the material [95].

Throughout the debinding and sintering processes there is a shrinkage of the parts due to the elimination of the polymer system and, most noticeably, due to the densification of the parts. This effect is controlled in the PIM process by the oversizing of the moulds which can compensate the shrinkage effect [132].

Although PIM technology is usually focused on the maximum densification of the materials for structural and functional applications for industries such as automotive, medial or consumer electronics [133], several works have focused in the obtention of porous materials by this technology. There are two strategies for the obtention of porous samples. First, decreasing the amount of solid loading in the mixtures would result in a minor packing of the powders, thus, leaving more open spaces after the debinding process. This approach could lead to the loss of structural integrity of the samples in the brown state if the amount of powder is not enough for the stability of the sample. On the other hand, and in the same manner for common macroporous structure production, a sacrificial element is used to act as a space holder.

Heaney et al. [134] proposed the production of porous stainless-steels (316L) by PIM for applications as surgical implants, filters or self-lubricating bearings. The pore size required for these applications are in the range of 0,5 μm to 500 μm for filters and 100-500 μm in implants. In their work, they used gas and water atomised powders to analyse the difference on the morphology. Feedstocks using paraffin wax were prepared with a solid loading range of 40 to 50 vol.%. Samples were solvent debound in heptane and sintered at 950 ºC under flowing hydrogen gas. The porosity of the sintered samples reached a 40-55% with a pore radius of 4-10 μm. Although no rheology behaviour of the feedstocks is shown in their work, they suggest that both water and gas atomised

powders are useful for porous PIM production. It can be observed from their work that the morphology of the powders has an influence on the final porosity of the samples, since under the same conditions of solid loading and sintering temperatures, final samples exhibit a 1% porosity difference, showing the influence of the initial material selection on the properties of the final sample.

Space holder method has been also used by several authors to produce foams of stainless steels [135], or cooper [136]. Different materials have been used to act as a space holder, nevertheless the most used binder for this purpose has been polymethyl methacrylate (PMMA), due to its good behaviour under thermal debinding. Manonukul et al. [137] reported the addition of PMMA as a space holder to a polyacetal-based binder. The volumetric fraction of the binders was fixed to 40 vol.% and the amount of powders (316L) were varied from 10 to 60 vol.% with PMMA space holder balancing the volume fraction (from 0 to 50 vol.%). With the addition of the space holder they achieved a better control on the morphology and size of the generated porosity after sintering the samples. On the contrary, samples showed an additional shrinkage depending on the amount of PMMA used, obtaining porosities as high as 65%.

1.2.2 Applications and overview of MAX phases in PIM

With the versatility that the PIM technology offers, MAX phases are great candidates for the production of near-net-shape components with complex geometries. Although most of the work in the PIM industry focuses on the production of dense components, it is possible to process samples with a tailored porosity through injection moulding [138,139]. As stated in **Section 1.1.3** some of the interesting applications for MAX phases are orientated to the production of porous components. Taking into advantage that the PIM process boosts the porosity of the samples due to the presence of a binder during the injection step and, on the other hand, the common lack of sinterability of ceramics, the processing of this family of materials through PIM stands as a promising route for the production of porous materials for catalytic devices, heat exchangers or damage tolerance structures.

During the last years, porous MAX phases have been developed, typically by the space holder technique. In this method, the use of a sacrificial element is required to create the porosity in the compacts, which will later be removed from the core of the samples exposing the porosity. Reactive sintering of powders under vacuum has been used to process porous Ti_3SiC_2 with porosity ranging from 28 vol.% up to 42 vol.% [140,141]. This processing method has also been used to produce porous MAX phase composites of Ti_3SiC_2/TiC, Ti_3AlC_2/TiC and Ti_4AlN_3/TiN from different initial powder mixtures,

obtaining porosities ranging from 5 vol.% up to 35 vol.% [142]. In another study, porous composites with 70 vol.% of Ti_3SiC_2 phase and 30 vol.% of TiC phase were produced also by reactive sintering. It was shown that porous materials have higher specific creep resistance compared to the dense material [143]. In recent years, the space holder method using salt (NaCl) [144] has been used to make porous materials of Ti_2AlC, obtaining MAX phase samples with a porosity ranging from 10 vol.% to 71 vol.%. They observed that the thermal conductivity at room temperature decreases with the amount of porosity but wasn´t affected by the pore size. Gonzalez-Julian et al [20] used the replica method technique to create macroporous MAX phases. In their work, NH_4HCO_3 was used as a sacrificial template for the pore formation, controlling the amount of porosity generated in Cr_2AlC samples. Other studies, focused on the production of Ti_2AlC and Ti_3SiC_2 foams using saccharose as the space holder to facilitate the elimination of the space holder material, avoiding the use of organic solvent or corrosion effects in the samples [145,146]. This method allows the production of samples with different degrees of porosity and pore size that can be easily controlled by a simple method.

In addition, MAX phase porous materials have been produced by suspension preparation and the replica method. Ti_2AlC macroporous foams were prepared by Bowen et al. [147] starting from MAX phase powders mixed with an anti-settler agent to suspend the powder in the PEG solution during the replica process. The polyurethane foam, acting as the replica structure, was removed by pyrolysis at 800 ºC, obtaining microporous Ti_2AlC structures. Moreover, Sun et al [148] obtained reticulated Ti_3AlC_2 through colloidal suspension preparation. Following the same method as described before they analysed the rheological properties of the suspensions and produced the reticular MAX phases by calcination of the polyurethane, followed by the sintering of the powders at 1350 ºC for 1 h under argon. The macroporous samples produced exhibit a well-defined and homogenous reticulated structure with 80% of porosity.

The main problematic of the common techniques for porous MAX phase production is the lack of control in the final shape of the samples. In spite of the good machinability of MAX phases, a near-net-shape technique for sample production would lower the production costs and increase the interest of these materials for new applications. In terms of powder injection moulding of MAX phases, to the best of the authors knowledge there are few published works that explore this field. This has been performed by Gonzalez-Julian et al. [149]. In this work, commercially available Ti_3SiC_2 and Ti_2AlC powders were prepared with a 62 vol.% of solid content using paraffin (60 vol.%) as a filler, a Polyolefin (Hostalen GA, 35 vol.%) as the backbone and stearic acid (5 vol.%). Feedstocks exhibited pseudoplastic rheological behaviour for temperatures between 150

ºC and 180 ºC. Gear-wheel-shaped samples were obtained after the injection process. After debinding and sintering, samples showed a density of 81% and 90% for Ti_3SiC_2 and Ti_2AlC, respectively. Moreover, they explored the injection process for MAX phase composites using Ti_2AlC as ceramic matrix and a 10 wt.% of SiC fibres. Although these composites showed good rheological properties, they were not able to densify, due to the reactivity between Ti_2AlC and SiC during the sintering stage. Stumpf et al [150] also studied the injection moulding process for Ti_2AlC MAX phase commercially available powders. In their work, they produced a wall structure with Ti_2AlC acting as the building block and aluminium/polysiloxane as the “mortar” in the structure. The aim of this setup was to study the damage tolerance of the MAX phase and analyse the mechanical properties of the composite compared to monolithic Ti_2AlC. To prepare the feedstocks, they first functionalised the MAX phase with stearic acid to hydrophobize the powders. Then, they prepared the feedstocks using paraffin (15 wt.%) and carnauba wax (2 wt.%) as polymeric system and an 83 wt.% of solid content. After the injection at 120 ºC, Ti_2AlC blocks were placed in a furnace at 300 ºC for 2 h for the thermal debinding of the polymeric system, and at 1350 ºC for 4h for the sintering, all of the process under flowing argon atmosphere. After the preparation of the brick-and-mortar structure, sintering of the building walls was performed at 1100 ºC, enhancing the Al-melt infiltration into the Ti_2AlC; this produced highly dense samples with similar strength and higher toughness compared to the monolithic Ti_2AlC injected sample.

With all this, the production of complex shaped porous MAX phases could broaden the possible applications of these materials and make them a potential candidate for applications like catalytic devices, high temperature heat exchangers or high temperature filters through their processing by PIM.

1.3 Additive Manufacturing

In the last years, Additive Manufacturing (AM) has grown from a technology for the production of prototypes, towards a new processing route to develop near-net-shape parts for various industrial sectors. In the materials community, AM has become a “hot topic” for the design and fabrication of a wide range of materials. From structural purposes of commonly used stainless steels to functional applications of new materials, AM postulates as a promising route for the production of new designs and new materials never before used in the industry [151].

One of the main reasons of the thriving inception of Additive Manufacturing in the materials processing is the amount of technologies that encompasses, allowing to select the ones more suited for a certain material. Besides polymer 3D printing, metals and ceramics materials have been widely studied due to the possibility of using this technology to obtain final parts without posterior machining processes, for a large number of applications, with a freedom of design that distinguishes AM from the rest of processing technologies [152,153].

For metallic and ceramic printing, it is possible to differentiate two main groups in the AM technologies: direct and indirect AM. These two classifications are mainly based on the possibility of obtaining the final part directly after the process or the requirement of a post-processing step. The most relevant techniques that encompasses direct and indirect AM are detailed below.

1.3.1.1 Direct AM

Direct Additive Manufacturing technologies starts from the raw material in powder form or from processed materials in wire or sheet form. Figure 15 shows the most relevant processes encompassed in direct AM.

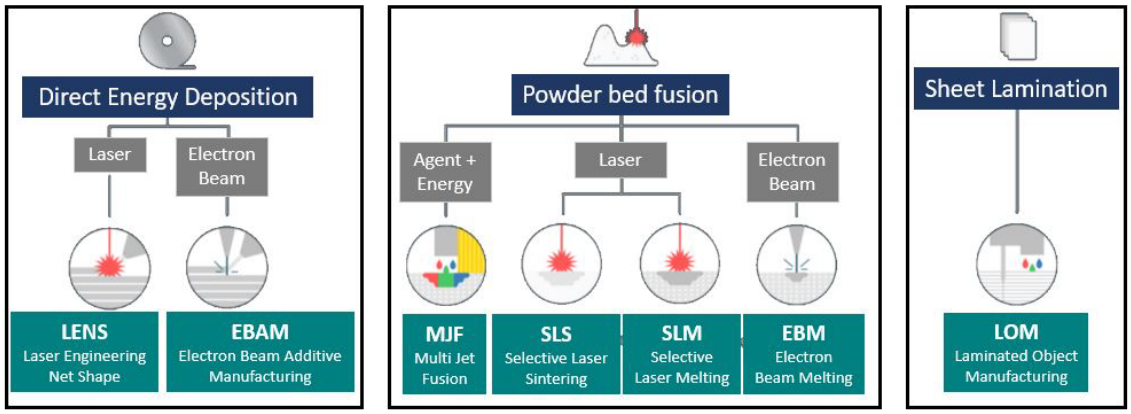

Figure 15. Schematic representation of the most relevant processes in direct AM technology.

Within the direct AM technologies, Direct Energy Deposition (DED) starts from the material to be deposited in wire or powder form. In this technology the material is sintered in-situ using a laser or an electron beam. The consolidation of the final part is performed in a layer-by-layer basis, as all AM techniques, where the material is being deposited at the same time as the energy source is applied [154,155]. DED is commonly used for stainless steels, titanium or aluminium-based alloys, ceramics or composites [156,157]. Some of the advantages of this technique are the broad range of materials that can be used, high deposition rates and the ability of printing full parts or coatings amongst others [158]. On the other hand, due to the local temperature difference produced during printing, residual stress and deformation can occur. In addition, there is a low efficiency when powders are used, with low recyclability and a post machining of the printed samples is usually required [159].

Another of the most common direct AM techniques is Powder Bed Fusion (PBF). In this case, the starting material is in powder form placed in a bed where the energy source is applied to selected zones with the geometry of the layer to be sintered or melted. A new layer of fresh powder is spread in the bed after the consolidation of the previous layer, repeating the process until the final desired samples is obtained. One of the most employed techniques used in this group is Selective laser melting (SLM) [160,161]. Through this techniques metals are predominantly used due to their ease to be melted once the energy source is applied; mainly titanium and aluminium alloys or stainless steels have been the most studied materials through Power Bed Fusion AM [162]. Nevertheless, ceramics materials have been also studied. Due to the high melting point of ceramics, a binder material that melts at a lower temperature is commonly used to create an initial bridging of the particles [152]. PBF techniques allow the use of a wider range of materials in powder form with a higher recyclability of the material compared to DED techniques. However, there are several powder characteristics that need to be addressed in order to obtain successful 3D printed structures. The morphology of the powders is an important aspect; generally, spherical powders are preferred for the correct deposition of the powder bed and the effective sintering of the material once the energy source is applied. In addition, the flowability of the powders is a key factor in PBF techniques, since the deposition of each powder layer on the bed depends on this aspect [162]. To control the flowability, the particle size distribution of the powders must be studied. The excess of fine particles in the powder system reduces the flowability, affecting the deposition of the powder bed, resulting in a failed printed part. In addition, particle size distributions with big D_{90} can create porosity during the consolidation of the parts [163].

As an alternative to the wire or powders starting materials, Sheet Lamination starts from a sheet. In this technique, a laminated sheet is deposited with the desired layered shape and the next layer is sticked above. One of the use cases for Laminated Object Manufacturing (LOM) is the production of composite matrices through a rapid prototyping for metallic and ceramic materials [164]. LOM stands as an interesting route for the production of 3D models from tape-casted parts, allowing the possibility of printing ceramic parts from this technique [165,166]. Some of the advantages of this technique rely on the reduction of internal stress generation, reducing the shrinkage and deformation of the printed parts. In addition, very large parts can be produced by this technique [167]. However, the accuracy of the parts, in terms of the surface quality, is a big drawback when a metal is used, since commercial sheets of 0,2-0,5 mm thickness result in poor quality parts [164].

1.3.1.2 Indirect AM

As stated above, indirect AM techniques require a post-processing method, typically a debinding and sintering process, for the fabrication of the final parts. Some of the most important technologies that are comprised within the indirect AM technologies are described in Figure 16.

VAT photopolymerization starts from the idea of using a resin or a slurry that contains the metal or ceramic powders to be printed. The resin used gives the material the necessary viscosity to be deposited in a layer by layer form and an energy source such as a laser, a projector or a LED light, builds the desired final part through photopolymerization [168]. VAT photopolymerization, processes such as Stereolithography (SLA) or Digital Light Processing (DLP), have been commonly used for the 3D printing of polymers. These techniques showed several benefits compared to other AM processes, such as, high accuracy of the printed parts with low layer heights and cost-efficiency, amongst other [169]. Polymer composites have been also developed through this technique to increase the strength of the printed materials to improve the corrosion or erosion resistance for biomedical application [170]. In recent years, several efforts have been made to apply this technology to metallic and ceramic materials using the polymeric resin as binder. Different companies, as Lithoz GmbH and Incus GmbH, are focused on the technology development of lithography-based solutions for the 3D printing of ceramics and metals, respectively. Nevertheless, this technology lacks on the possibility of printing with high powder concentrations or a strict control on the powder size of the material to be printed [171].

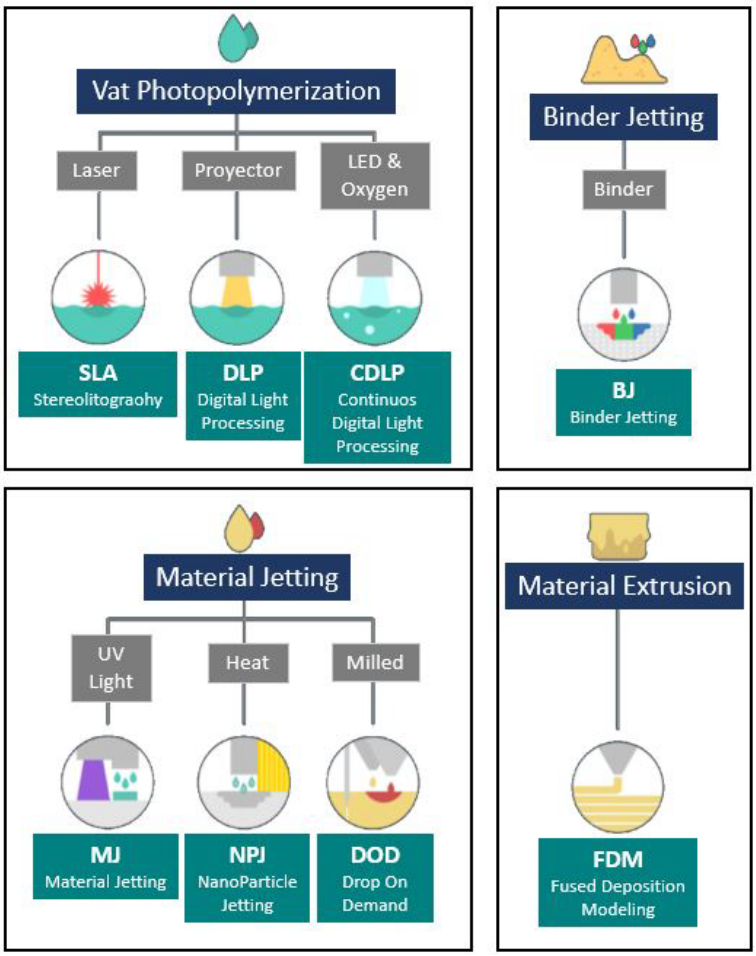

Figure 16. Schematic representation of the most relevant processes in indirect AM technology.

Binder Jetting, as SLM process, requires a powder bed and, in this case, instead of an energy source for the sintering of the materials a binder is jetted into the powder to generate the parts, with a continuous spreading of a new layer of fresh powder after the binder jetting [172,173]. Another indirect technique is the material jetting. In this case, the binder-powders system is jetted while printing the part. This technology also requires an energy source for the consolidation of the sample as, for example, UV light [174]. Due to the porosity typically obtained thought this technique, Binder jetting has been extensively used for the production of casting moulds, allowing the gas evacuation and avoiding defects on the casted parts [175]. With the evolution of this technology and the obtention of higher density samples, Binder jetting stands as a promising processing route for medical applications as denture framework [176] or implants [177].

Lastly, Material Extrusion is one of the most widely used Additive Manufacturing techniques for filament polymer 3D printing and, in the last years, also for metallic and ceramic components. Through Fused deposition modelling (FDM), also referred as Fused Filament Fabrication (FFF), is it possible to obtain high quality final parts using feedstocks in a filament form. This type of processing starts from a filament, which is

extruded and heated through a nozzle to be deposited layer by layer. The polymeric binders used for this technology require specific flexibility properties [152]. As one of the most used printing technologies there are several studies on the optimisation and future prospective of a wide range of materials, most commonly: stainless-steel (17-4 PH [178], 316L [179]) for structural applications, or Titanium alloys (Ti-6Al-4V [180]) and ceramics such as TiO_2 [181] for biomedical applications. Moreover, the homogeneity is a key factor in the case of filament production. Several studies are focused on the correct dispersion of the powder-binder system for the production of good quality parts. In this aspect, a new promising process through colloidal suspension can avoid the heterogeneities generated by the agglomeration of the powders in the feedstocks [182].

1.3.2 Overview of the Composite Extrusion Modelling process

Through the previous section is it clear how for a successful printing the prerequisites of the raw materials are strictly related for the type of processing to be used. In addition, not all materials are suited to comply with these requirements. As seen, powder bed fusion techniques require the use of spherical powders for the correct deposition of the powder bed and the densification of the samples. Ceramics cannot be produced in a filament form without a polymeric binder for Direct Energy Deposition systems, and not all metals are successfully sintered by laser or electron beams. Powder morphology is a huge drawback for powder-bed-based technologies in the indirect AM, since the correct powder wettability of the binders depends on that morphology. Furthermore, not all polymers are suited for the filament production and the flexibility requirements of a feedstock filament limits them to a few number of suitable binder polymers.

Composite Extrusion Modelling (CEM), also described as screw-based AM, stands as an alternative processing route to solve some of the problematics of conventional AM techniques and broadens the range of materials that can be used. This technology combines the fundamental aspects of Powder Injection Moulding and Fused Deposition Modelling [183,184].

With CEM, pelletised feedstocks can be used for the obtention of 3D parts. As for FDM the material is extruded, in this case by a screw, into the heated zone to give the feedstocks the necessary viscosity. Feedstocks are then extruded through a nozzle to be deposited into the bed in a layer-by-layer basis. A schematic representation of the CEM process is shown in Figure 17.

CEM offers the possibility of avoiding the difficult steps of the filament production, while increasing the range of polymeric systems to be used through this technology. As opposed to FDM, there are no specific diameter requirement for the correct extrusion of

the filaments and no flexibility constraints for the pellets. In addition, reusability of the failed printed parts is possible by granulating or pelletising the feedstocks, while the temperatures of the printing are selected correctly avoiding the degradation of the polymeric system [185].

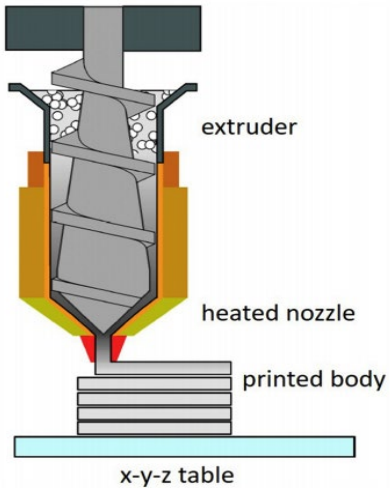

Figure 17. Schematic representation of the screw-based composite extrusion modelling (CEM) process [183].

With all this, CEM stands as a promising processing route, offering the possibility to print materials that do not typically comply with the required morphologies of the powder bed technologies or are not able to be produced as filaments or wires, allowing to print highly charged feedstocks, using novel binder compositions [184]. Initially, the focus on the research of CEM and pellet-extrusion was on the validation of the process comparing the final parts to FDM printed materials. Thus, some of the earlier research was performed with widely used powders such as stainless steel 316L [186] or 17-4 PH [187] starting from PIM feedstocks. Most recently, new materials and polymeric binders have been used, exploring the possibility of using hard metals and cermets for tooling applications [184] or using drugs-loaded polymeric systems for the pharmaceutical industry [188].

1.3.3 Applications and overview of MAX phases in AM

MAX phases have been previously processed by Additive Manufacturing techniques. In 2002 W. Sun et al. [40,189] published a three-stage fabrication process of Ti_3SiC_2 MAX phase. In their work, they printed the samples by rapid prototyping, which is an early development of the binder jetting technique, using water soluble binders. After the 3D printing of the MAX phase powders, cold isostatic pressing of the samples was performed to increase the densification in the later sintering step. Final samples were obtained with a final density of 90%. Years later, Mylena M. M. Carrijo et al. [190] would

study the influence on the post-pressing parameters of rapid prototyping Ti_3SiC_2-based composites, achieving high densification with a 1,7 wt.% of residual porosity.

A different technique was followed by B. Nan et al. [191]. In this case, the synthesis of the MAX phases was performed after printing the samples by Inkjet printing combined with liquid silicon infiltration (LSI). Direct ink writing was employed by H. Elsayed et al. [192] to produce MAX phase Ti_2AlC with porous structures. In this work, after achieving good dispersion of the Ti_2AlC powders in the ink, printed samples were obtained with porosities between 44 and 63 vol.%.

Other MAX phases have also been printed using printable inks. Cr_2AlC was printed using aqueous suspensions to obtain cellular structures. Porosities of up to 60 vol.% were obtained by M. Belmonte et al. [193], who studied the thermal and electrical conductivities of the printed parts.

Additionally, Laminated Object Manufacturing (LOM) was used by Krinitcyn et al. [194] to obtain Ti_3SiC_2 3D printed samples. In their work, LOM was used as an indirect deposition route combining TiC and SiC powders with a slurry. The objective was to produce green laminates by tape casting to conform the shape of the samples, followed by a posterior pyrolysis and a subsequent sintering for the in-situ synthesis of the MAX phase and the consolidation of the sample. To reduce the porosity of the printed samples, a liquid silicon infiltration in vacuum was performed, obtaining a shrinkage of less than 3%.

The possibility that AM offers for the production of solid porous or cellular systems in combination with the excellent properties of MAX phases, makes this type of processing a promising candidate to produce porous MAX phases for high temperature applications. For example, High Temperature Heat Exchangers (HTHXs) materials need high temperature stability. In addition, to increase the efficiency of these components, complex shapes are required and, in this sense, the combination of CEM processing and MAX phases is an interesting use case for these materials.

References

[1] W. Jeitschko, H. Nowotny, Die Kristallstruktur von Ti3SiC2: ein neuer Komplexcarbid-Typ, Monatshefte Für Chemie - Chem. Mon. 98 (1967) 329–337. https://doi.org/10.1007/BF00899949.

[2] M.W. Barsoum, T. El-Raghy, Synthesis and characterization of a remarkable ceramic: Ti3SiC2, J.Am.Ceram.Soc. 79 (1996) 1953–56. https://doi.org/10.1111/j.1151-2916.1996.tb08018.x.

[3] J. Gonzalez-Julian, Processing of MAX phases: From synthesis to applications, J. Am. Ceram. Soc. 104 (2021) 659–690. https://doi.org/10.1111/jace.17544.

[4] M.A. El Saeed, F.A. Deorsola, R.M. Rashad, Optimization of the Ti3SiC2 MAX phase synthesis, Int. J. Refract. Met. Hard Mater. (2012). https://doi.org/10.1016/j.ijrmhm.2012.05.001.

[5] S. Zhimei, Z. Yi, Z. Yanchun, Synthesis of Ti3SiC2 powders by a solid-liquid reaction process, Scr. Mater. 41 (1999) 61–66. https://doi.org/10.1016/S1359-6462(99)00054-8.

[6] J.M. Córdoba, M.J. Sayagués, M.D. Alcalá, F.J. Gotor, Synthesis of Ti3SiC2 powders: Reaction mechanism, J. Am. Ceram. Soc. 90 (2007) 825–830. https://doi.org/10.1111/j.1551-2916.2007.01501.x.

[7] M.W. Barsoum, The Mn+1AXn Phases: A New Class of Solids, Prog. Solid State Chem. 28 (2000) 201–281. https://doi.org/10.1016/S0079-6786(00)00006-6.

[8] M. Barsoum, MAX phases: Properties of machinable ternary carbides and nitrides, John Wiley & Sons, 2013. https://doi.org/10.1002/9783527654581.

[9] M.W. Barsoum, M. Radovic, Elastic and Mechanical Properties of the MAX Phases, Annu. Rev. Mater. Res. 41 (2011) 195–227. https://doi.org/10.1146/annurev-matsci-062910-100448.

[10] M. Barsoum, T. El-Raghy, The MAX phases: unique new carbide and nitride materials, 2001. https://doi.org/10.1511/2001.28.736.

[11] A.G. Zhou, S. Basu, M.W. Barsoum, Kinking nonlinear elasticity, damping and microyielding of hexagonal close-packed metals, Acta Mater. 56 (2008) 60–67. https://doi.org/10.1016/j.actamat.2007.08.050.

[12] M.W. Barsoum, M. Radovic, Elastic and mechanical properties of the MAX

phases, Annu. Rev. Mater. Res. 41 (2011) 195–227. https://doi.org/10.1146/annurev-matsci-062910-100448.

[13] A.G. Zhou, S. Basu, G. Friedman, P. Finkel, O. Yeheskel, M.W. Barsoum, Hysteresis in kinking nonlinear elastic solids and the Preisach-Mayergoyz model, Phys. Rev. B - Condens. Matter Mater. Phys. 82 (2010) 43–45. https://doi.org/10.1103/PhysRevB.82.094105.

[14] G.M. Song, Y.T. Pei, W.G. Sloof, S.B. Li, J.T.M. De Hosson, S. van der Zwaag, Oxidation-induced crack healing in Ti3AlC2 ceramics, Scr. Mater. 58 (2008) 13–16. https://doi.org/10.1016/j.scriptamat.2007.09.006.

[15] H.B. Zhang, Y.C. Zhou, Y.W. Bao, M.S. Li, Abnormal thermal shock behavior of Ti3SiC2 and Ti3AlC2, J. Mater. Res. 21 (2006) 2401–2407. https://doi.org/10.1557/jmr.2006.0289.

[16] S.A. Tsipas, E. Tabares, T. Weissgaerber, T. Hutsch, F. Sket, B. Velasco, Thermophysical properties of porous Ti2AlC and Ti3SiC2 produced by powder metallurgy, J. Alloys Compd. 857 (2021) 158145. https://doi.org/10.1016/j.jallcom.2020.158145.

[17] X.H. Wang, Y.C. Zhou, Oxidation behavior of Ti3AlC2 powders in flowing air, J. Mater. Chem. 12 (2002) 2781–2785. https://doi.org/10.1039/b203644d.

[18] X.K. Qian, X.D. He, Y.B. Li, Y. Sun, H. Li, D.L. Xu, Cyclic oxidation of Ti3AlC2 at 1000–1300 °C in air, Corros. Sci. 53 (2011) 290–295. https://doi.org/10.1016/J.CORSCI.2010.09.033.

[19] J. Gonzalez-Julian, T. Go, D.E. Mack, R. Vaßen, Thermal cycling testing of TBCs on Cr2AlC MAX phase substrates, Surf. Coatings Technol. 340 (2018) 17–24. https://doi.org/10.1016/j.surfcoat.2018.02.035.

[20] J. Gonzalez-Julian, S. Onrubia, M. Bram, C. Broeckmann, R. Vassen, O. Guillon, High-temperature oxidation and compressive strength of Cr2AlC MAX phase foams with controlled porosity, J. Am. Ceram. Soc. 101 (2018) 542–552. https://doi.org/10.1111/jace.15224.

[21] M.W. Barsoum, T. El-Raghy, L.U.J.T. Ogbuji, Oxidation of Ti3SiC2 in air, J. Electrochem. Soc. 144 (1997) 2508–2516. https://doi.org/10.1149/1.1837846.

[22] M.W. Barsoum, Fundamentals of ceramics, Institute of Physiscs Pub., Bristol, UK, ISBN 9780585462608, 2003.

[23] J.W. Byeon, J. Liu, M. Hopkins, W. Fischer, N. Garimella, K.B. Park, M.P. Brady, M. Radovic, T. El-Raghy, Y.H. Sohn, Microstructure and residual stress of alumina scale formed on Ti2AlC at high temperature in air, Oxid. Met. 68 (2007) 97–111. https://doi.org/10.1007/s11085-007-9063-0.

[24] M. Sundberg, G. Malmqvist, A. Magnusson, T. El-Raghy, Alumina forming high temperature silicides and carbides, Ceram. Int. 30 (2004) 1899–1904. https://doi.org/10.1016/j.ceramint.2003.12.046.

[25] C.Y. Ho, R.W. Powell, P.E. Liley, Thermal conductivity of the elements: a comprehensive review, J. Phys. Chem. Ref. Data. 3 (1974) 1–796. https://doi.org/https://doi.org/10.1063/1.3253100.

[26] J.D. Hettinger, S.E. Lofland, P. Finkel, T. Meehan, J. Palma, K. Harrell, S. Gupta, A. Ganguly, T. El-Raghy, M.W. Barsoum, Electrical transport, thermal transport, and elastic properties of M2AlC (M = Ti, Cr, Nb, and V), Phys. Rev. B. 72 (2005) 115120. https://doi.org/10.1103/PhysRevB.72.115120.

[27] T.H. Scabarozi, S. Amini, P. Finkel, O.D. Leaffer, J.E. Spanier, M.W. Barsoum, M. Drulis, H. Drulis, W.M. Tambussi, J.D. Hettinger, S.E. Lofland, Electrical, thermal, and elastic properties of the MAX-phase Ti2SC, J. Appl. Phys. 104 (2008). https://doi.org/10.1063/1.2959738.

[28] S. Sze, Holton, Semiconductor device, Encycl. Br. (2016). https://www.britannica.com/technology/semiconductor-device (accessed November 1, 2021).

[29] T. El-Raghy, P. Blau, M.W. Barsoum, Effect of grain size on friction and wear behavior of Ti3SiC2, Wear. 238 (2000) 125–130. https://doi.org/10.1016/S0043-1648(99)00348-8.

[30] A. Souchet, J. Fontaine, M. Belin, T. Le Mogne, J.L. Loubet, M.W. Barsoum, Tribological duality of Ti3SiC2, Tribol. Lett. 18 (2005) 341–352. https://doi.org/10.1007/s11249-004-2761-8.

[31] C. Magnus, D. Cooper, J. Sharp, W.M. Rainforth, Microstructural evolution and wear mechanism of Ti3AlC2 – Ti2AlC dual MAX phase composite consolidated by spark plasma sintering (SPS), Wear. 438–439 (2019) 203013. https://doi.org/10.1016/j.wear.2019.203013.

[32] D. Davis, A.F. Shah, B.B. Panigrahi, S. Singh, Effect of Cr2AlC nanolamella addition on tribological properties of 5W-30 engine oil, Appl. Surf. Sci. 493 (2019)

1098–1105. https://doi.org/10.1016/j.apsusc.2019.07.097.

[33] H. Yan, K. Liu, P. Zhang, J. Zhao, Y. Qin, Q. Lu, Z. Yu, Fabrication and tribological behaviors of Ti3SiC2/Ti5Si3/TiC/Ni-based composite coatings by laser cladding for self-lubricating applications, Opt. Laser Technol. 126 (2020) 106077. https://doi.org/10.1016/j.optlastec.2020.106077.

[34] Z. Huang, H. Zhai, M. Guan, X. Liu, M. Ai, Y. Zhou, Oxide-film-dependent tribological behaviors of Ti3SiC2, Wear. 262 (2007) 1079–1085. https://doi.org/10.1016/j.wear.2006.11.003.

[35] L. Qu, G. Bei, M. Nijemeisland, D. Cao, S. van der Zwaag, W.G. Sloof, Point contact abrasive wear behavior of MAX phase materials, Ceram. Int. 46 (2020) 1722–1729. https://doi.org/10.1016/j.ceramint.2019.09.145.

[36] A. Shamsipoor, M. Farvizi, M. Razavi, A. Keyvani, Influences of processing parameters on the microstructure and wear performance of Cr2AlC MAX phase prepared by spark plasma sintering method, J. Alloys Compd. 815 (2020) 152345. https://doi.org/10.1016/j.jallcom.2019.152345.

[37] W. Yu, D. Chen, L. Tian, H. Zhao, X. Wang, Self-lubricate and anisotropic wear behavior of AZ91D magnesium alloy reinforced with ternary Ti2AlC MAX phases, J. Mater. Sci. Technol. 35 (2019) 275–284. https://doi.org/10.1016/j.jmst.2018.07.003.

[38] A. Dash, R. Vaßen, O. Guillon, J. Gonzalez-Julian, Molten salt shielded synthesis of oxidation prone materials in air, Nat. Mater. 18 (2019) 465–470. https://doi.org/10.1038/s41563-019-0328-1.

[39] T. Goto, T. Hirai, Chemically vapor deposited Ti3SiC2, Mater. Res. Bull. 22 (1987) 1195–1201. https://doi.org/10.1016/0025-5408(87)90128-0.

[40] W. Sun, D.J. Dcosta, F. Lin, T. El-Raghy, Freeform fabrication of Ti3SiC2 powder-based structures: Part I - Integrated fabrication process, J. Mater. Process. Technol. 127 (2002) 343–351. https://doi.org/10.1016/S0924-0136(02)00284-4.

[41] T. El-raghy, M.W. Barsoum, A. Zavaliangos, S.R. Kalidindi, Processing and mechanical properties of Ti3SiC2: II, Effect of grain size and deformation temperature, J.Am.Ceram.Soc. 82 (1999) 2855–2860. https://doi.org/10.1111/j.1151-2916.1999.tb02167.x.

[42] N.F. Gao, J.T. Li, D. Zhang, Y. Miyamoto, Rapid synthesis of dense Ti3SiC2 by spark plasma sintering, J. Eur. Ceram. Soc. 22 (2002) 2365–2370.

https://doi.org/10.1016/S0955-2219(02)00021-3.

[43] M.W. Barsoum, A progress report on Ti3SiC2, Ti3GeC2, and the H-phases, M2BX, J. Mater. Synth. Process. 5 (1997) 197–216. https://www.scopus.com/inward/record.uri?eid=2-s2.0-0031140611&partnerID=40&md5=324d2a9d7fb9da68e29d0501060ccd38.

[44] M.W. Barsoum, M. Ali, T. El-Raghy, Processing and characterization of Ti2AlC, Ti2AlN, and Ti2AlC0.5N0.5, Metall. Mater. Trans. A Phys. Metall. Mater. Sci. 31 (2000) 1857–1865. https://doi.org/10.1007/s11661-006-0243-3.

[45] P. Wang, B. Mei, X. Hong, J. Zhu, W. Zhou, Fabrication of Ti2AlC by spark plasma sintering from elemental powders and thermodynamics analysis of Ti-Al-C system, J. Wuhan Univ. Technol. Mater. Sci. Ed. 22 (2007) 325–328. https://doi.org/10.1007/s11595-006-2325-x.

[46] L. Gao, T. Han, Z. Guo, X. Zhang, D. Pan, S. Zhou, W. Chen, S. Li, Preparation and performance of MAX phase Ti3AlC2 by in-situ reaction of Ti-Al-C system, Adv. Powder Technol. 31 (2020) 3533–3539. https://doi.org/10.1016/j.apt.2020.06.042.

[47] N. V. Tzenov, M.W. Barsoum, Synthesis and characterization of Ti3AlC2, J. Am. Ceram. Soc. 83 (2000) 825–832. https://doi.org/10.1111/j.1151-2916.2000.tb01281.x.

[48] C. Yang, S.Z. Jin, B.Y. Liang, S.S. Jia, Low-temperature synthesis of high-purity Ti3AlC2 by MA-SPS technique, J. Eur. Ceram. Soc. 29 (2009) 181–185. https://doi.org/10.1016/j.jeurceramsoc.2008.05.035.

[49] T. Go, Y.J. Sohn, G. Mauer, R. Vaßen, J. Gonzalez-Julian, Cold spray deposition of Cr2AlC MAX phase for coatings and bond-coat layers, J. Eur. Ceram. Soc. 39 (2019) 860–867. https://doi.org/10.1016/j.jeurceramsoc.2018.11.035.

[50] B. Tunca, T. Lapauw, O.M. Karakulina, M. Batuk, T. Cabioc'h, J. Hadermann, R. Delville, K. Lambrinou, J. Vleugels, Synthesis of MAX Phases in the Zr-Ti-Al-C System, Inorg. Chem. 56 (2017) 3489–3498. https://doi.org/10.1021/acs.inorgchem.6b03057.

[51] T. Lapauw, K. Lambrinou, T. Cabioc'h, J. Halim, J. Lu, A. Pesach, O. Rivin, O. Ozeri, E.N. Caspi, L. Hultman, P. Eklund, J. Rosén, M.W. Barsoum, J. Vleugels, Synthesis of the new MAX phase Zr2AlC, J. Eur. Ceram. Soc. 36 (2016) 1847–1853. https://doi.org/10.1016/j.jeurceramsoc.2016.02.044.

[52] I.M. Low, W.K. Pang, S.J. Kennedy, R.I. Smith, High-temperature thermal stability of Ti2AlN and Ti4AlN3: A comparative diffraction study, J. Eur. Ceram. Soc. 31 (2011) 159–166. https://doi.org/10.1016/j.jeurceramsoc.2010.09.014.

[53] C.J. Rawn, M.W. Barsoum, T. El-Raghy, A. Procipio, C.M. Hoffmann, C.R. Hubbard, Structure of Ti4AlN3 - a layered Mn+1AXn nitride, Mater. Res. Bull. 35 (2000) 1785–1796. https://doi.org/10.1016/S0025-5408(00)00383-4.

[54] J.P. Siebert, L. Bischoff, M. Lepple, A. Zintler, L. Molina-Luna, U. Wiedwald, C.S. Birkel, Sol-gel based synthesis and enhanced processability of MAX phase Cr2GaC, J. Mater. Chem. C. 7 (2019) 6034–6040. https://doi.org/10.1039/c9tc01416k.

[55] T. El-Raghy, M.W. Barsoum, Processing and mechanical properties of Ti3SiC2: I, Reaction path and microstructure evolution, J. Am. Ceram. Soc. 82 (1999) 2849–2854. https://doi.org/10.1111/j.1151-2916.1999.tb02167.x.

[56] A. Zuber, V. Gauthier-Brunet, J. Roger, J. Gonzalez-Julian, T. Ouisse, S. Dubois, Towards a better understanding of the high-temperature oxidation of MAX phase Cr2AlC, J. Eur. Ceram. Soc. (2021) 1–8. https://doi.org/10.1016/j.jeurceramsoc.2021.12.057.

[57] L.O. Xiao, S.B. Li, G. Song, W.G. Sloof, Synthesis and thermal stability of Cr2AlC, J. Eur. Ceram. Soc. 31 (2011) 1497–1502. https://doi.org/10.1016/j.jeurceramsoc.2011.01.009.

[58] X. Hong, B. Mei, J. Zhu, W. Zhou, Study on the fabrication of Ti2AlC by spark plasma sintering, J. Chinese Ceram. Soc. 31 (2003) 991–993. https://www.scopus.com/inward/record.uri?eid=2-s2.0-1942521185&partnerID=40&md5=52230f4fb33d16bdca43bf7fd7d5d960.

[59] V. Gauthier-Brunet, T. Cabioc'h, P. Chartier, M. Jaouen, S. Dubois, Reaction synthesis of layered ternary Ti2AlC ceramic, J. Eur. Ceram. Soc. 29 (2009) 187–194. https://doi.org/10.1016/j.jeurceramsoc.2008.05.039.

[60] W.B. Tian, Z.M. Sun, H. Hashimoto, Y.L. Du, Synthesis, microstructure and mechanical properties of Ti3SiC2-TiC composites pulse discharge sintered from Ti/Si/TiC powder mixture, Mater. Sci. Eng. A. 526 (2009) 16–21. https://doi.org/10.1016/j.msea.2009.08.029.

[61] J. Zhu, H. Jiang, F. Wang, C. Yang, D. Xiao, Synthesis, microstructure and mechanical properties of Cr2AlC/Al2O3 in situ composites by reactive hot

pressing, J. Eur. Ceram. Soc. 34 (2014) 4137–4144. https://doi.org/10.1016/j.jeurceramsoc.2014.07.021.

[62] T. Go, R. Vaßen, O. Guillon, J. Gonzalez-Julian, Processing and oxidation response of Cr2AlC MAX-phase composites containing ceramic fibers, Open Ceram. 6 (2021). https://doi.org/10.1016/j.oceram.2021.100090.

[63] Y. Zhang, S. Zhimei, Y. Zhou, Cu/Ti3SiC2 composite: A new electrofriction material, Mater. Res. Innov. 3 (1999) 80–84. https://doi.org/10.1007/s100190050129.

[64] W. Yu, X. Pi, W. Chen, M. Vallet, A. Guitton, L. Zhang, Effects of A-site atoms in Ti2AlC and Ti3SiC2 MAX phases reinforced Mg composites: Interfacial structure and mechanical properties, Mater. Sci. Eng. A. 826 (2021) 141961. https://doi.org/10.1016/j.msea.2021.141961.

[65] Y. Du, J.C. Schuster, H.J. Seifert, F. Aldinger, Experimental investigation and thermodynamic calculation of the titanium – silicon – carbon system, J.Am.Ceram.Soc. 203 (2000) 3–9. https://doi.org/10.1111/j.1151-2916.2000.tb01170.x.

[66] J.L. Smialek, J.A. Nesbitt, T.P. Gabb, A. Garg, R.A. Miller, Hot corrosion and low cycle fatigue of a Cr2AlC-coated superalloy, Mater. Sci. Eng. A. 711 (2018) 119–129. https://doi.org/10.1016/j.msea.2017.10.098.

[67] D.E. Hajas, M. to Baben, B. Hallstedt, R. Iskandar, J. Mayer, J.M. Schneider, Oxidation of Cr2AlC coatings in the temperature range of 1230 to 1410°C, Surf. Coat. Technol. 206 (2011) 591–598. https://doi.org/10.1016/j.surfcoat.2011.03.086.

[68] C.A. Lewinsohn, M.A. Wilson, J.R. Fellows, H.S. Anderson, Fabrication and joining of ceramic compact heat exchangers for process integration, Int. J. Appl. Ceram. Technol. 9 (2012) 700–711. https://doi.org/10.1111/j.1744-7402.2012.02788.x.

[69] J. Schmidt, M. Scheiffele, M. Crippa, P.F. Peterson, E. Urquiza, K. Sridharan, L.C. Olson, M.H. Anderson, T.R. Allen, Y. Chen, Design, fabrication, and testing of ceramic plate-type heat exchangers with integrated flow channel design, Int. J. Appl. Ceram. Technol. 8 (2011) 1073–1086. https://doi.org/10.1111/j.1744-7402.2010.02573.x.

[70] C. Schmitt, D.W. Agar, F. Platte, S. Buijssen, B. Pawlowski, M. Duisberg, Ceramic

plate heat exchanger for heterogeneous gas-phase reactions, Chem. Eng. Technol. 28 (2005) 337–343. https://doi.org/10.1002/ceat.200407119.

[71] K.A. Al-attab, Z.A. Zainal, Performance of high-temperature heat exchangers in biomass fuel powered externally fired gas turbine systems, Renew. Energy. 35 (2010) 913–920. https://doi.org/10.1016/j.renene.2009.11.038.

[72] D. Aquaro, M. Pieve, High temperature heat exchangers for power plants: Performance of advanced metallic recuperators, Appl. Therm. Eng. 27 (2007) 389–400. https://doi.org/10.1016/j.applthermaleng.2006.07.030.

[73] C. Luzzatto, A. Morgana, S. Chaudourne, G. Sorbieg, A new concept composite heat exchanger to be applied in high-temperature industrial processes, Science (80-.). 17 (1997) 789–797.

[74] Q. Li, G. Flamant, X. Yuan, P. Neveu, L. Luo, Compact heat exchangers: A review and future applications for a new generation of high temperature solar receivers, Renew. Sustain. Energy Rev. 15 (2011) 4855–4875. https://doi.org/10.1016/j.rser.2011.07.066.

[75] C. Mansilla, J. Sigurvinsson, A. Bontemps, A. Maréchal, F. Werkoff, Heat management for hydrogen production by high temperature steam electrolysis, Energy. 32 (2007) 423–430. https://doi.org/10.1016/j.energy.2006.07.033.

[76] L. Magistri, A. Traverso, A.F. Massardo, R.K. Shah, Heat exchangers for fuel cell and hybrid system applications, J. Fuel Cell Sci. Technol. 3 (2006) 111–118. https://doi.org/10.1115/1.2173665.

[77] B. Velasco, S. Tsipas, B. Ferrari, E. Gordo, MAX phase foams produced via powder metallurgy process using water soluble space holder, Powder Metall. 58 (2015) 95–99. https://doi.org/10.1179/0032589915Z.000000000226.

[78] J. Kašpar, P. Fornasiero, N. Hickey, Automotive: catalytic converters current status, Catal. Today. 77 (2003) 419–449. https://doi.org/https://doi.org/10.1016/S0920-5861(02)00384-X.

[79] H. Zhang, R. Su, I. Szlufarska, L. Shi, H. Wen, Helium effects and bubbles formation in irradiated Ti3SiC2, J. Eur. Ceram. Soc. 41 (2021) 252–258. https://doi.org/10.1016/j.jeurceramsoc.2020.08.015.

[80] F. Wang, Q. Su, M. Nastasi, M.A. Kirk, M. Li, B. Cui, Evolution of irradiation defects in Ti2AlC ceramics during heavy ion irradiation, Ceram. Int. 44 (2018) 14686–14692. https://doi.org/10.1016/j.ceramint.2018.05.095.

[81] J. Ward, D. Bowden, D. Stewart, M.W. Barsoum, P. Frankel, M. Preuss, Influence of proton-irradiation temperature on the damage accumulation in Ti 3 SiC 2 and Ti 3 AlC 2, Scr. Mater. 165 (2019) 98–102. https://doi.org/10.1016/j.scriptamat.2019.02.022.

[82] Q. Huang, H. Han, R. Liu, G. Lei, L. Yan, J. Zhou, Q. Huang, Saturation of ion irradiation effects in MAX phase Cr2AlC, Acta Mater. 110 (2016) 1–7. https://doi.org/10.1016/j.actamat.2016.03.021.

[83] J. Wang, R. Shu, Y. Dong, T. Shao, Q.H. Deng, X.B. Zhou, F. Huang, S.Y. Du, Z.G. Wang, J.M. Xue, Y.G. Wang, Q. Huang, Microstructure evolution of V2AlC coating on Zr substrate under He irradiation and their mechanical behavior, Scr. Mater. 137 (2017) 13–17. https://doi.org/10.1016/j.scriptamat.2017.05.003.

[84] H.H. Qarra, K.M. Knowles, M.E. Vickers, S. Akhmadaliev, K. Lambrinou, Heavy ion irradiation damage in Zr2AlC MAX phase, J. Nucl. Mater. 523 (2019) 1–9. https://doi.org/10.1016/j.jnucmat.2019.05.034.

[85] B. Tunca, T. Lapauw, C. Callaert, J. Hadermann, R. Delville, E.N. Caspi, M. Dahlqvist, J. Rosén, A. Marshal, K.G. Pradeep, J.M. Schneider, J. Vleugels, K. Lambrinou, Compatibility of Zr2AlC MAX phase-based ceramics with oxygen-poor, static liquid lead–bismuth eutectic, Corros. Sci. 171 (2020) 108704. https://doi.org/10.1016/j.corsci.2020.108704.

[86] R.M. German, Powder Injection Molding, Metal Powder Industries Federation, Princeton (New Jersey), ISBN 9780918404954, 1990.

[87] R.M. German, Injection molding of metals and ceramics, Princeton New Jersey : Metal Powder Industries Federation, Princeton (New Jersey), 1997. https://doi.org/doi.org/10.4271/982417.

[88] V.M. Kryachek, Injection Moulding (Review), 43 (2004) 336–348. https://doi.org/1068-1302/04/0708-0336.

[89] M.F.F.A. Hamidi, W.S.W. Harun, M. Samykano, S.A.C. Ghani, Z. Ghazalli, F. Ahmad, A.B. Sulong, A review of biocompatible metal injection moulding process parameters for biomedical applications, Mater. Sci. Eng. C. 78 (2017) 1263–1276. https://doi.org/10.1016/j.msec.2017.05.016.

[90] H. Ye, X.Y. Liu, H. Hong, Fabrication of metal matrix composites by metal injection molding-A review, J. Mater. Process. Technol. 200 (2008) 12–24. https://doi.org/10.1016/j.jmatprotec.2007.10.066.

[91] R.M. German, Metal powder injection molding (MIM): Key trends and markets, 2nd ed., Elsevier Ltd., 2019. https://doi.org/10.1016/b978-0-08-102152-1.00001-5.

[92] A. Dehghan-Manshadi, M.J. Bermingham, M.S. Dargusch, D.H. StJohn, M. Qian, Metal injection moulding of titanium and titanium alloys: Challenges and recent development, Powder Technol. 319 (2017) 289–301. https://doi.org/10.1016/j.powtec.2017.06.053.

[93] R.K. Enneti, V.P. Onbattuvelli, O. Gulsoy, K.H. Kate, S. V Atre, Powder-binder formulation and compound manufacture in metal injection molding (MIM), in: D.F.B.T.-H. of M.I.M. (Second E. Heaney (Ed.), Woodhead Publ. Ser. Met. Surf. Eng., Woodhead Publishing, 2019: pp. 57–88. https://doi.org/https://doi.org/10.1016/B978-0-08-102152-1.00005-2.

[94] T. Li, Powder Injection Molding of Metallic Parts and Structures, in: F.G.B.T.-E. of M.M. and A. Caballero (Ed.), Elsevier, Oxford, 2022: pp. 401–416. https://doi.org/https://doi.org/10.1016/B978-0-12-819726-4.00015-6.

[95] A. Dehghan-Manshadi, P. Yu, M. Dargusch, D. StJohn, M. Qian, Metal injection moulding of surgical tools, biomaterials and medical devices: A review, Powder Technol. 364 (2020) 189–204. https://doi.org/10.1016/j.powtec.2020.01.073.

[96] J. Gonzalez-Gutierrez, G. Beulke, I. Emri, Powder Injection Molding of Metal and Ceramic Parts, Some Crit. Issues Inject. Molding. (2012). https://doi.org/10.5772/38070.

[97] P. Thomas-Vielma, A. Cervera, B. Levenfeld, A. Várez, Production of alumina parts by powder injection molding with a binder system based on high density polyethylene, J. Eur. Ceram. Soc. 28 (2008) 763–771. https://doi.org/10.1016/j.jeurceramsoc.2007.08.004.

[98] J. Gutiérrez-López, E. Rodriguez-Senín, J.Y. Pastor, M.A. Paris, A. Martín, B. Levenfeld, A. Várez, Microstructure, magnetic and mechanical properties of Ni-Zn ferrites prepared by powder injection moulding, Powder Technol. 210 (2011) 29–35. https://doi.org/10.1016/j.powtec.2011.02.008.

[99] B.S. Zlatkov, N.S. Mitrović, M. V. Nikolić, A.M. Maričić, H. Danninger, O.S. Aleksić, E. Halwax, Properties of MnZn ferrites prepared by powder injection molding technology, Mater. Sci. Eng. B Solid-State Mater. Adv. Technol. 175 (2010) 217–222. https://doi.org/10.1016/j.mseb.2010.07.031.

[100] J.S. Han, C.W. Gal, J.H. Kim, S.J. Park, Fabrication of high-aspect-ratio micro piezoelectric array by powder injection molding, Ceram. Int. 42 (2016) 9475–9481. https://doi.org/10.1016/j.ceramint.2016.03.011.

[101] J. Wang, M.J. Edirisinghe, Ceramic Injection Molding, Ref. Modul. Mater. Sci. Mater. Eng. (2016) 1–22. https://doi.org/10.1016/b978-0-12-803581-8.03574-8.

[102] M. Aslam, F. Ahmad, P.S.M.B.M. Yusoff, K. Altaf, M.A. Omar, R.M. German, Powder injection molding of biocompatible stainless steel biodevices, Powder Technol. 295 (2016) 84–95. https://doi.org/10.1016/j.powtec.2016.03.039.

[103] B.N. Mukund, B. Hausnerova, Variation in particle size fraction to optimize metal injection molding of water atomized 17–4PH stainless steel feedstocks, Powder Technol. 368 (2020) 130–136. https://doi.org/10.1016/j.powtec.2020.04.058.

[104] J. González-gutiérrez, G.B. Stringari, I. Emri, Powder Injection Molding of Metal and Ceramic Parts, Some Critical Issues for Injection Molding, in: Some Crit. Issues Inject. Molding, 2012: pp. 65–88. https://doi.org/10.5772/38070.

[105] G.B. Stringari, B. Zupančič, G. Kubyshkina, B. von Bernstorff, I. Emri, Time-dependent properties of bimodal POM - Application in powder injection molding, Powder Technol. 208 (2011) 590–595. https://doi.org/10.1016/j.powtec.2010.12.025.

[106] J. Hidalgo, C. Abajo, A. Jiménez-Morales, J.M. Torralba, Effect of a binder system on the low-pressure powder injection moulding of water-soluble zircon feedstocks, J. Eur. Ceram. Soc. 33 (2013) 3185–3194. https://doi.org/10.1016/j.jeurceramsoc.2013.06.027.

[107] D. Bleyan, B. Hausnerova, P. Svoboda, The development of powder injection moulding binders: A quantification of individual components' interactions, Powder Technol. 286 (2015) 84–89. https://doi.org/10.1016/j.powtec.2015.07.046.

[108] X. Kong, T. Barriere, J.C. Gelin, Determination of critical and optimal powder loadings for 316L fine stainless steel feedstocks for micro-powder injection molding, J. Mater. Process. Technol. 212 (2012) 2173–2182. https://doi.org/10.1016/j.jmatprotec.2012.05.023.

[109] B. Hausnerova, B.N. Mukund, D. Sanetrnik, Rheological properties of gas and water atomized 17-4PH stainless steel MIM feedstocks: Effect of powder shape and size, Powder Technol. 312 (2017) 152–158. https://doi.org/10.1016/j.powtec.2017.02.023.

[110] D. Lin, D. Sanetrnik, H. Cho, S.T. Chung, Y.S. Kwon, K.H. Kate, B. Hausnerova, S. V. Atre, S.J. Park, Rheological and thermal debinding properties of blended elemental Ti-6Al-4V powder injection molding feedstock, Powder Technol. 311 (2017) 357–363. https://doi.org/10.1016/j.powtec.2016.12.071.

[111] R. Supati, N.H. Loh, K.A. Khor, S.B. Tor, Mixing and characterization of feedstock for powder injection molding, Mater. Lett. 46 (2000) 109–114. https://doi.org/10.1016/S0167-577X(00)00151-8.

[112] J. Hidalgo, A. Jiménez-Morales, J.M. Torralba, Torque rheology of zircon feedstocks for powder injection moulding, J. Eur. Ceram. Soc. 32 (2012) 4063–4072. https://doi.org/10.1016/j.jeurceramsoc.2012.06.023.

[113] T. Barriere, B. Liu, J.C. Gelin, Determination of the optimal process parameters in metal injection molding from experiments and numerical modeling, J. Mater. Process. Technol. 143–144 (2003) 636–644. https://doi.org/10.1016/S0924-0136(03)00473-4.

[114] R. Côté, M. Azzouni, V. Demers, Impact of binder constituents on the moldability of titanium-based feedstocks used in low-pressure powder injection molding, Powder Technol. 381 (2021) 255–268. https://doi.org/10.1016/j.powtec.2020.12.008.

[115] O. Ghanmi, V. Demers, Molding properties of titanium-based feedstock used in low-pressure powder injection molding, Powder Technol. 379 (2021) 515–525. https://doi.org/10.1016/j.powtec.2020.10.068.

[116] M. Sardarian, O. Mirzaee, A. Habibolahzadeh, Mold filling simulation of low pressure injection molding (LPIM) of alumina: Effect of temperature and pressure, Ceram. Int. 43 (2017) 28–34. https://doi.org/10.1016/j.ceramint.2016.07.224.

[117] M.S. Moghadam, A. Fayyaz, M. Ardestani, Fabrication of titanium components by low-pressure powder injection moulding using hydride-dehydride titanium powder, Powder Technol. 377 (2021) 70–79. https://doi.org/10.1016/j.powtec.2020.08.075.

[118] W.J. Tseng, C.K. Hsu, Cracking defect and porosity evolution during thermal debinding in ceramic injection moldings, Ceram. Int. 25 (1999) 461–466. https://doi.org/10.1016/S0272-8842(98)00061-3.

[119] H.K. Lin, K.S. Hwang, In situ dimensional changes of powder injection-molded compacts during solvent debinding, Acta Mater. 46 (1998) 4303–4309.

https://doi.org/10.1016/S1359-6454(98)00093-7.

[120] E.J. Westcot, C. Binet, R.M. German, In situ dimensional change, mass loss and mechanisms for solvent debinding of powder injection moulded components, Powder Metall. 46 (2003) 61–67. https://doi.org/10.1179/003258903225010442.

[121] W.W. Yang, K.Y. Yang, M.C. Wang, M.H. Hon, Solvent debinding mechanism for alumina injection molded compacts with water-soluble binders, Ceram. Int. 29 (2003) 745–756. https://doi.org/10.1016/S0272-8842(02)00226-2.

[122] R.V.B. Oliveira, V. Soldi, M.C. Fredel, A.T.N. Pires, Ceramic injection moulding: Influence of specimen dimensions and temperature on solvent debinding kinetics, J. Mater. Process. Technol. 160 (2005) 213–220. https://doi.org/10.1016/j.jmatprotec.2004.06.008.

[123] S.T. Lin, R.M. German, Interaction between binder and powder in injection moulding of alumina, J. Mater. Sci. 29 (1994) 5207–5212. https://doi.org/10.1007/BF01151118.

[124] S. Md Ani, A. Muchtar, N. Muhamad, J.A. Ghani, Binder removal via a two-stage debinding process for ceramic injection molding parts, Ceram. Int. 40 (2014) 2819–2824. https://doi.org/10.1016/j.ceramint.2013.10.032.

[125] A. Royer, T. Barriere, Y. Bienvenu, Influence of supercritical debinding and processing parameters on final properties of injection-moulded Inconel 718, Powder Technol. 336 (2018) 311–317. https://doi.org/10.1016/j.powtec.2018.05.047.

[126] G. Chen, P. Cao, G. Wen, N. Edmonds, Debinding behaviour of a water soluble PEG/PMMA binder for Ti metal injection moulding, Mater. Chem. Phys. 139 (2013) 557–565. https://doi.org/10.1016/j.matchemphys.2013.01.057.

[127] A. Royer, T. Barrière, J.C. Gelin, L. Hilliou, Development and characterisation of a biosourced feedstock of superalloy in metal injection moulding process, Powder Metall. 60 (2017) 105–111. https://doi.org/10.1080/00325899.2016.1269457.

[128] R. Tandon, Metal Injection Molding, in: K.H.J. Buschow, R.W. Cahn, M.C. Flemings, B. Ilschner, E.J. Kramer, S. Mahajan, P.B.T.-E. of M.S. and T. Veyssière (Eds.), Elsevier, Oxford, 2001: pp. 5439–5442. https://doi.org/https://doi.org/10.1016/B0-08-043152-6/00949-9.

[129] C. Abajo, J. Hidalgo, A. Jiménez-Morales, J.M. Torralba, Optimisation of eco-friendly binary binder system for powder injection moulding, Powder Metall. 57

(2014) 196–203. https://doi.org/10.1179/1743290114Y.0000000089.

[130] R.M. German, Powder metallurgy science, Metal Powder Industries Federation, Princeton (New Jersey), ISBN 1878954423, 1994.

[131] S.-J.L. Kang, Sintering: densification, grain growth and microstructure, Elsevier Butterworth-Heinemann, Oxford (UK), ISBN 0080493076, 2004.

[132] D. Annicchiarico, J.R. Alcock, Review of factors that affect shrinkage of molded part in injection molding, Mater. Manuf. Process. 29 (2014) 662–682. https://doi.org/10.1080/10426914.2014.880467.

[133] R.M. German, PIM breaks the $1 bn barrier, Met. Powder Rep. 63 (2008) 8–10. https://doi.org/10.1016/S0026-0657(08)70036-5.

[134] D.F. Heaney, J.D. Gurosik, C. Binet, Isotropic forming of porous structures via metal injection molding, J. Mater. Sci. 40 (2005) 973–981. https://doi.org/10.1007/s10853-005-6516-1.

[135] S.J. Park, D. Kim, D. Lin, S.J. Park, S. Ahn, Rheological characterization of powder mixture including a space holder and its application to metal injection molding, Metals (Basel). 7 (2017). https://doi.org/10.3390/met7040120.

[136] E. Zhang, B. Wang, On the compressive behaviour of sintered porous coppers with low to medium porosities - Part I: Experimental study, Int. J. Mech. Sci. 47 (2005) 744–756. https://doi.org/10.1016/j.ijmecsci.2004.12.011.

[137] A. Manonukul, N. Muenya, F. Léaux, S. Amaranan, Effects of replacing metal powder with powder space holder on metal foam produced by metal injection moulding, J. Mater. Process. Technol. 210 (2010) 529–535. https://doi.org/10.1016/j.jmatprotec.2009.10.016.

[138] A. Dehghan-Manshadi, Y. Chen, Z. Shi, M. Bermingham, D. StJohn, M. Dargusch, M. Qian, Porous Titanium Scaffolds Fabricated by Metal Injection Moulding for Biomedical Applications, Materials (Basel). 11 (2018) 1573. https://doi.org/10.3390/ma11091573.

[139] G. Matula, J. Krzysteczko, Porous material produced by ceramic injection molding, J. Achievemnts Mater. Manuf. Eng. 71 (2015) 14–21. https://doi.org/1734-8412.

[140] Z.M. Sun, A. Murugaiah, T. Zhen, A. Zhou, M.W. Barsoum, Microstructure and mechanical properties of porous Ti3SiC2, Acta Mater. 53 (2005) 4359–4366.

https://doi.org/10.1016/j.actamat.2005.05.034.

[141] É.P. Pechkovskii, S.A. Firstov, Structure and Mechanical Properties of Porous Titanosilicon Carbide Ti3SiC2, Powder Metall. Met. Ceram. 42 (2003) 424–432. https://doi.org/10.1023/B:PMMC.0000004164.63420.14.

[142] S.A. Firstov, V.F. Gorban, I.I. Ivanova, É.P. Pechkovskii, Mechanical properties of porous Ti3SiC2/TiC, Ti3AlC2/TiC, and Ti4AlN3/TiN nanolaminates at 20 to 1300°C, Powder Metall. Met. Ceram. 49 (2010) 414–423.

[143] S.A. Firstov, E.P. Pechkovsky, I.I. Ivanova, N.P. Brodnikovsky, V.F. Gorban', A.N. Demidik, High-temperature mechanical properties of powder metallurgy: Porous lightweight titanium nanolaminates, High Temp. Mater. Process. 25 (2006) 47–58. https://doi.org/10.1515/HTMP.2006.25.1-2.47.

[144] L. Hu, R. Benitez, S. Basu, I. Karaman, M. Radovic, Processing and characterization of porous Ti2AlC with controlled porosity and pore size, Acta Mater. (2012). https://doi.org/10.1016/j.actamat.2012.07.052.

[145] B. Velasco, E. Gordo, L. Hu, M. Radovic, S.A. Tsipas, Influence of porosity on elastic properties of Ti2AlC and Ti3SiC2 MAX phase foams, J. Alloys Compd. 764 (2018) 24–35. https://doi.org/10.1016/j.jallcom.2018.06.027.

[146] B. Velasco, S. Tsipas, B. Ferrari, E. Gordo, MAX phase foams produced via powder metallurgy process using water soluble space holder, Powder Metall. 58 (2015) 95–99. https://doi.org/10.1179/0032589915Z.000000000226.

[147] C.R. Bowen, T. Thomas, Macro-porous Ti2AlC MAX-phase ceramics by the foam replication method, Ceram. Int. 41 (2015) 12178–12185. https://doi.org/10.1016/j.ceramint.2015.06.038.

[148] S. Ziqi, L. Ying, L. Meishuan, Z. Yanchun, Preparation of Reticulated MAX-Phase Support with Morphology-Controllable Nanostructured Ceria Coating for Gas Exhaust Catalyst Devices, J. Am. Ceram. Soc. 93 (2010) 2591–2597. https://doi.org/10.1111/j.1551-2916.2010.03776.x.

[149] J. Gonzalez-Julian, L. Classen, M. Bram, R. Vaßen, O. Guillon, Near Net Shaping of Monolithic and Composite MAX Phases by Injection Molding, J. Am. Ceram. Soc. 99 (2016) 3210–3213. https://doi.org/10.1111/jace.14466.

[150] M. Stumpf, X. Fan, J. Biggemann, P. Greil, T. Fey, Topological interlocking and damage mechanisms in periodic Ti2AlC-Al building block composites, J. Eur.

Ceram. Soc. 39 (2019) 2003–2009. https://doi.org/10.1016/j.jeurceramsoc.2019.01.047.

[151] J. Savolainen, M. Collan, How Additive Manufacturing Technology Changes Business Models? – Review of Literature, Addit. Manuf. 32 (2020) 101070. https://doi.org/10.1016/j.addma.2020.101070.

[152] Z. Chen, Z. Li, J. Li, C. Liu, C. Lao, Y. Fu, C. Liu, Y. Li, P. Wang, Y. He, 3D printing of ceramics: A review, J. Eur. Ceram. Soc. 39 (2019) 661–687. https://doi.org/10.1016/j.jeurceramsoc.2018.11.013.

[153] B. Gadagi, R. Lekurwale, A review on advances in 3D metal printing, Mater. Today Proc. (2020). https://doi.org/10.1016/j.matpr.2020.10.436.

[154] M. Ansari, E. Jabari, E. Toyserkani, Opportunities and challenges in additive manufacturing of functionally graded metallic materials via powder-fed laser directed energy deposition: A review, J. Mater. Process. Technol. 294 (2021) 117117. https://doi.org/10.1016/j.jmatprotec.2021.117117.

[155] A. Singh, S. Kapil, M. Das, A comprehensive review of the methods and mechanisms for powder feedstock handling in directed energy deposition, Addit. Manuf. 35 (2020) 101388. https://doi.org/10.1016/j.addma.2020.101388.

[156] W.E. Frazier, Metal additive manufacturing: A review, J. Mater. Eng. Perform. 23 (2014) 1917–1928. https://doi.org/10.1007/s11665-014-0958-z.

[157] B. Wysocki, P. Maj, R. Sitek, J. Buhagiar, K.J. Kurzydłowski, W. Świeszkowski, Laser and electron beam additive manufacturing methods of fabricating titanium bone implants, Appl. Sci. 7 (2017) 1–20. https://doi.org/10.3390/app7070657.

[158] T.A. Rodrigues, V. Duarte, R.M. Miranda, T.G. Santos, J.P. Oliveira, Current status and perspectives on wire and arc additive manufacturing (WAAM), Materials (Basel). 12 (2019). https://doi.org/10.3390/ma12071121.

[159] V.T. Le, H. Paris, G. Mandil, Process planning for combined additive and subtractive manufacturing technologies in a remanufacturing context, J. Manuf. Syst. 44 (2017) 243–254. https://doi.org/10.1016/j.jmsy.2017.06.003.

[160] J. Wilkes, Y.C. Hagedorn, W. Meiners, K. Wissenbach, Additive manufacturing of ZrO2-Al2O3 ceramic components by selective laser melting, Rapid Prototyp. J. 19 (2013) 51–57. https://doi.org/10.1108/13552541311292736.

[161] N.T. Aboulkhair, M. Simonelli, L. Parry, I. Ashcroft, C. Tuck, R. Hague, 3D printing

of Aluminium alloys: Additive Manufacturing of Aluminium alloys using selective laser melting, Prog. Mater. Sci. 106 (2019) 100578. https://doi.org/10.1016/j.pmatsci.2019.100578.

[162] P. Avrampos, G.-C. Vosniakos, A review of powder deposition in additive manufacturing by powder bed fusion, J. Manuf. Process. 74 (2022) 332–352. https://doi.org/10.1016/j.jmapro.2021.12.021.

[163] S.D. Dobson, T.L. Starr, Powder characterization and part density for powder bed fusion of 17-4 PH stainless steel, Rapid Prototyp. J. 27 (2021) 53–58. https://doi.org/10.1108/RPJ-01-2020-0023.

[164] S. Yi, F. Liu, J. Zhang, S. Xiong, Study of the key technologies of LOM for functional metal parts, J. Mater. Process. Technol. 150 (2004) 175–181. https://doi.org/10.1016/j.jmatprotec.2004.01.035.

[165] D.A. Klosterman, R.P. Chartoff, N.R. Osborne, G.A. Graves, S. Rodrigues, Development of a curved layer LOM process for monolithic ceramics and ceramic matrix composites, Rapid Prototyp. J. 5 (1999) 61–71.

[166] N. Travitzky, A. Bonet, B. Dermeik, T. Fey, I. Filbert-Demut, L. Schlier, T. Schlordt, P. Greil, Additive manufacturing of ceramic-based materials, Adv. Eng. Mater. 16 (2014) 729–754. https://doi.org/10.1002/adem.201400097.

[167] B. Mueller, D. Kochan, Laminated object manufacturing for rapid tooling and patternmaking in foundry industry, Comput. Ind. 39 (1999) 47–53. https://doi.org/10.1016/S0166-3615(98)00127-4.

[168] Diptanshu, G. Miao, C. Ma, Vat photopolymerization 3D printing of ceramics: Effects of fine powder, Manuf. Lett. 21 (2019) 20–23. https://doi.org/10.1016/j.mfglet.2019.07.001.

[169] R.V. Pazhamannil, P. Govindan, Current state and future scope of additive manufacturing technologies via vat photopolymerization, Mater. Today Proc. 43 (2020) 130–136. https://doi.org/10.1016/j.matpr.2020.11.225.

[170] A. Al Rashid, W. Ahmed, M.Y. Khalid, M. Koç, Vat photopolymerization of polymers and polymer composites: Processes and applications, Addit. Manuf. 47 (2021) 102279. https://doi.org/10.1016/j.addma.2021.102279.

[171] M.L. Gatto, R. Groppo, M. Furlani, A. Giuliani, C. Mangano, F. Mangano, Lithography-based Ceramic Manufacturing (LCM) versus Milled Zirconia Blocks under uniaxial compressive loading: An in vitro comparative study, J. Dent. 116

(2022) 103886. https://doi.org/10.1016/j.jdent.2021.103886.

[172] X. Lv, F. Ye, L. Cheng, S. Fan, Y. Liu, Binder jetting of ceramics: Powders, binders, printing parameters, equipment, and post-treatment, Ceram. Int. 45 (2019) 12609–12624. https://doi.org/10.1016/j.ceramint.2019.04.012.

[173] M. Ziaee, N.B. Crane, Binder jetting: A review of process, materials, and methods, Addit. Manuf. 28 (2019) 781–801. https://doi.org/10.1016/j.addma.2019.05.031.

[174] E. Willems, M. Turon-Vinas, B.C. dos Santos, B. Van Hooreweder, F. Zhang, B. Van Meerbeek, J. Vleugels, Additive manufacturing of zirconia ceramics by material jetting, J. Eur. Ceram. Soc. 41 (2021) 5292–5306. https://doi.org/10.1016/j.jeurceramsoc.2021.04.018.

[175] M. Upadhyay, T. Sivarupan, M. El Mansori, 3D printing for rapid sand casting—A review, J. Manuf. Process. 29 (2017) 211–220. https://doi.org/10.1016/j.jmapro.2017.07.017.

[176] A. Mostafaei, E.L. Stevens, J.J. Ference, D.E. Schmidt, M. Chmielus, Binder jetting of a complex-shaped metal partial denture framework, Addit. Manuf. 21 (2018) 63–68. https://doi.org/10.1016/j.addma.2018.02.014.

[177] J.A. Inzana, D. Olvera, S.M. Fuller, J.P. Kelly, O.A. Graeve, E.M. Schwarz, S.L. Kates, H.A. Awad, 3D printing of composite calcium phosphate and collagen scaffolds for bone regeneration, Biomaterials. 35 (2014) 4026–4034. https://doi.org/10.1016/j.biomaterials.2014.01.064.

[178] J. Gonzalez-Gutierrez, F. Arbeiter, T. Schlauf, C. Kukla, C. Holzer, Tensile properties of sintered 17-4PH stainless steel fabricated by material extrusion additive manufacturing, Mater. Lett. 248 (2019) 165–168. https://doi.org/10.1016/j.matlet.2019.04.024.

[179] B. Liu, Y. Wang, Z. Lin, T. Zhang, Creating metal parts by Fused Deposition Modeling and Sintering, Mater. Lett. 263 (2020) 127252. https://doi.org/10.1016/j.matlet.2019.127252.

[180] P. Singh, V.K. Balla, A. Tofangchi, S. V. Atre, K.H. Kate, Printability studies of Ti-6Al-4V by metal fused filament fabrication (MF3), Int. J. Refract. Met. Hard Mater. 91 (2020) 105249. https://doi.org/10.1016/j.ijrmhm.2020.105249.

[181] A.H. Aleni, I.F. Ituarte, A. Mohite, L. St-Pierre, J. Partanen, Comparing stiffness of solid and scaffold nano-TiO2 structures produced by material extrusion method, Ceram. Int. 44 (2018) 2231–2239. https://doi.org/10.1016/j.ceramint.2017.10.181.

[182] A. Ferrandez-Montero, M. Lieblich, R. Benavente, J.L. González-Carrasco, B. Ferrari, New approach to improve polymer-Mg interface in biodegradable PLA/Mg composites through particle surface modification, Surf. Coatings Technol. 383 (2020) 125285. https://doi.org/10.1016/j.surfcoat.2019.125285.

[183] J. Gonzalez-Gutierrez, S. Cano, S. Schuschnigg, C. Kukla, J. Sapkota, C. Holzer, Additive manufacturing of metallic and ceramic components by the material extrusion of highly-filled polymers: A review and future perspectives, Materials (Basel). 11 (2018). https://doi.org/10.3390/ma11050840.

[184] W. Lengauer, I. Duretek, M. Fürst, V. Schwarz, J. Gonzalez-Gutierrez, S. Schuschnigg, C. Kukla, M. Kitzmantel, E. Neubauer, C. Lieberwirth, V. Morrison, Fabrication and properties of extrusion-based 3D-printed hardmetal and cermet components, Int. J. Refract. Met. Hard Mater. 82 (2019) 141–149. https://doi.org/10.1016/j.ijrmhm.2019.04.011.

[185] A.I. Nurhudan, S. Supriadi, Y. Whulanza, A.S. Saragih, Additive manufacturing of metallic based on extrusion process: A review, J. Manuf. Process. 66 (2021) 228–237. https://doi.org/10.1016/j.jmapro.2021.04.018.

[186] P. Parenti, S. Cataldo, M. Annoni, Shape deposition manufacturing of 316L parts via feedstock extrusion and green-state milling, Manuf. Lett. 18 (2018) 6–11. https://doi.org/10.1016/j.mfglet.2018.09.003.

[187] G. Singh, J.M. Missiaen, D. Bouvard, J.M. Chaix, Additive manufacturing of 17–4 PH steel using metal injection molding feedstock: Analysis of 3D extrusion printing, debinding and sintering, Addit. Manuf. 47 (2021) 102287. https://doi.org/10.1016/j.addma.2021.102287.

[188] A. Samaro, B. Shaqour, N.M. Goudarzi, M. Ghijs, L. Cardon, M.N. Boone, B. Verleije, K. Beyers, V. Vanhoorne, P. Cos, C. Vervaet, Can filaments, pellets and powder be used as feedstock to produce highly drug-loaded ethylene-vinyl acetate 3D printed tablets using extrusion-based additive manufacturing?, Int. J. Pharm. 607 (2021). https://doi.org/10.1016/j.ijpharm.2021.120922.

[189] D.J. Dcosta, W. Sun, F. Lin, T. Ei-Raghy, Freeform fabrication of Ti3SiC2 powder-based structures: Part II - Characterization and microstructure evaluation, J. Mater. Process. Technol. 127 (2002) 352–360. https://doi.org/10.1016/S0924-0136(02)00320-5.

[190] M.M.M. Carrijo, H. Lorenz, I. Filbert-Demut, G.M. De Oliveira Barra, D. Hotza, X.

Yin, P. Greil, N. Travitzky, Fabrication of Ti3SiC2-based composites via three-dimensional printing: Influence of processing on the final properties, Ceram. Int. 42 (2016) 9557–9564. https://doi.org/10.1016/j.ceramint.2016.03.036.

[191] B. Nan, X. Yin, L. Zhang, L. Cheng, Three-dimensional printing of Ti3SiC2-based ceramics, J. Am. Ceram. Soc. 94 (2011) 969–972. https://doi.org/10.1111/j.1551-2916.2010.04257.x.

[192] H. Elsayed, A. Chmielarz, M. Potoczek, T. Fey, P. Colombo, Direct ink writing of three dimensional Ti2AlC porous structures, Addit. Manuf. 28 (2019) 365–372. https://doi.org/10.1016/j.addma.2019.05.018.

[193] M. Belmonte, M. Koller, J.J. Moyano, H. Seiner, P. Miranzo, M.I. Osendi, J. González-Julián, Multifunctional 3D-Printed Cellular MAX-Phase Architectures, Adv. Mater. Technol. 4 (2019) 1–8. https://doi.org/10.1002/admt.201900375.

[194] M. Krinitcyn, Z. Fu, J. Harris, K. Kostikov, G.A. Pribytkov, P. Greil, N. Travitzky, Laminated Object Manufacturing of in-situ synthesized MAX-phase composites, Ceram. Int. 43 (2017) 9241–9245. https://doi.org/10.1016/j.ceramint.2017.04.079.

CHAPTER 2

MOTIVATION AND OBJECTIVES

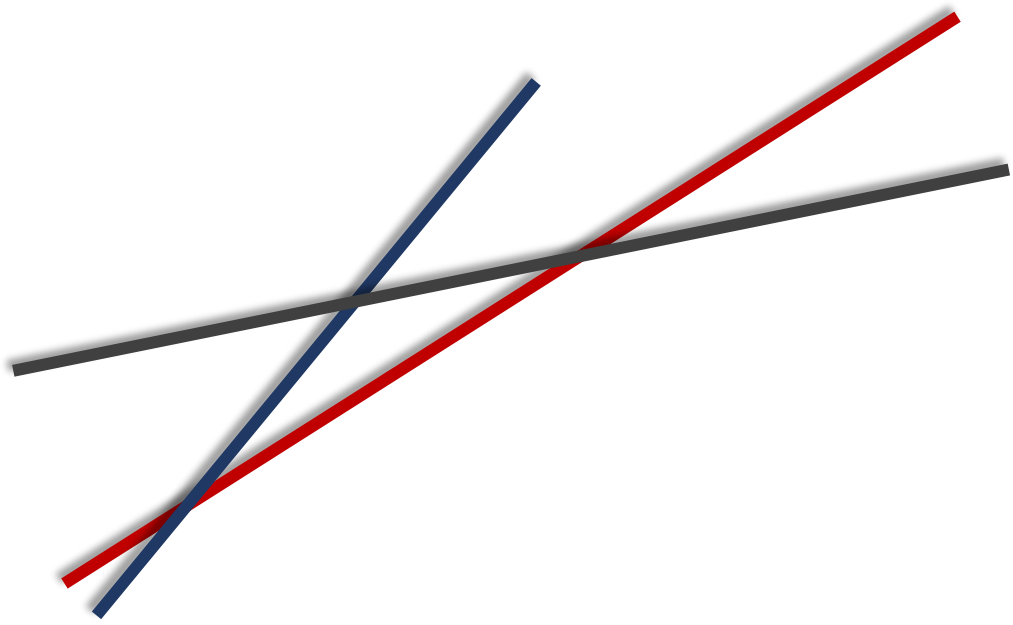

Contents

2.1 Motivation 73

2.2 Objectives 75

References 77

2. Motivation and objectives

2.1 Motivation

The research community is in a constant search of new techniques and innovative materials to accomplish new challenges that the industry demands. Some of those recent cases include discovering new ways of energy production and storage or making existing systems more efficient [1]. As an example, hydrogen energy production is developing as a promising new method that could satisfy the increasing demand of energy supply and reduce the carbon footprint, as established in the agenda 2030. Furthermore, for the production of hydrogen, more efficient heat exchangers are required capable of withstanding more demanding and aggressive environments [2].

For most of these new goals, some key properties that are essential for the development of innovative materials are high melting point, thermal and chemical stability [3], good thermal shock resistance, good oxidation and corrosion behaviour at high temperatures [4] or good wear resistance. Usually, to fulfil these properties a ceramic material is required, and the main issues are the component design and processing routes, for the specific applications of these family of materials.

In the quest to develop materials that can meet the increasing challenges of emerging technologies, this work proposes two different approaches. On one hand, it is essential to develop new materials with excellent properties and, on the other hand, study new processing methods that allow greater freedom in component design, and by doing so, increasing the efficiency and performance of these components.

In this sense, MAX phases have become an excellent candidate for these new requirements, due to their unique combination of ceramic-metallic properties, in terms of high temperature operational resistance, good electrical and thermal conductivity, machinability and high damage tolerance [5].

Regarding the second challenge, freedom of design, Powder Injection Moulding (PIM) and Additive Manufacturing (AM) are two exceptional processing routes to obtain near-net-shape components. Both of these technologies require large quantities of material for the characterisation and optimisation process. Thus, it is important to scale-up the MAX phase powder production process, maintaining high purity in the powders and controlling the powder characteristics, such as particle size for the correct subsequent processing of the material. Conventional consolidation routes need also to be studied for

comparative purposes, in order to understand and analyse the processing properties and behaviour of the raw powders.

Even though AM techniques have many advantages, they also have some significant drawbacks, depending on the material and the specific technique that is going to be used. For example, for powder-bed fusion techniques, it is of great importance to have an optimal powder morphology in order to avoid defects in the processed samples; it is often necessary to use spherical powders, with highly controlled particle size distribution [6,7]. For another widely use AM technique, Fused Deposition Modelling (FDM), a strict control of the filament produced is required in terms of diameter tolerance, feedstock homogeneity and filament flexibility [8].

To overcome these drawbacks with AM techniques, Composite Extrusion Modelling, CEM, is proposed as an alternative method in this work. In CEM the material is printed using feedstocks, in pellet form, as raw starting material and it is extruded through a screw to be deposited layer-by-layer. This processing route not only offers the opportunity of avoiding complex filament production steps using non-specific powder morphologies but, it also allows the use new binder compositions, increasing the range of polymeric systems that can be used in additive manufacturing. Furthermore, this technique poses fewer limitations regarding the powder morphology characteristics required. In addition to this, by increasing the amount of polymers that can be selected for the printing process, it gives the opportunity of selecting sustainable polymeric binders such as polyethylene(glycol) (PEG), as a water solvent polymer, avoiding using organic solvents or cellulose acetate butyrate (CAB) that is a carbon neutral polymer.

2.2 Objectives

The main goal of this thesis is to study and develop new processing routes for MAX phases, starting from the synthesis of MAX phases powders followed by scaling-up of the powder production and the processing of the material. These new processing routes are built on feedstock-based processing such as powder injection moulding (PIM) and additive manufacturing (AM) through composite extrusion modelling (CEM). These objectives are accomplished through the following partial objectives:

- Synthesise, using new synthesis routes, Ti_3SiC_2, Cr_2AlC and Ti_2AlC MAX phases, and characterise and study the different parameters that influence the fabrication of high purity powders.
- Powder production scale-up process, proposing a “simple” route to obtain large amounts of powders, without compromising powder purity. In addition, the powders obtained need to have a controlled particle size distribution, appropriate for the later processing by PIM and CEM.
- Study the processing viability of the synthesised powders by conventional powder metallurgy processes, characterising the mechanical and wear behaviour properties of the consolidated materials.
- Study the rheological behaviour of the feedstocks. Two multicomponent alternative binders are proposed, that use eco-friendly polymers (PEG/CAB and PEG/PP). An in-depth study of the optimal powder solid loadings and rheological behaviour is necessary for the optimization of the feedstocks for the PIM and AM processes.
- Optimisation of the PIM process, starting from the injection parameters and finishing with the sintering step. Control of both solvent and thermal debinding for the optimal removal of the binders.
- Optimisation of the CEM process. Determining the correct parameters for the 3D printing of the MAX phase feedstocks and adjusting the debinding process to ensure the structural integrity of the materials.
- Porosity evaluation of the samples obtained by PIM and CEM and characterisation of the final sintered components.

Through the study and optimisation of each partial objective it is intended to explore and broaden the possible application fields of MAX phases. Furthermore, the powder

production process optimisation and investigation of the suitability of MAX phases for the PIM and AM processing routes is the main objective of this study. With this, new cost-efficient geometries can be built increasing the potential application of this family of materials in the industry, particularly for applications demanding materials resistant to aggressive environments, with complex geometries.

References

[1] C. Luzzatto, A. Morgana, S. Chaudourne, G. Sorbieg, A new concept composite heat exchanger to be applied in high-temperature industrial processes, Appl. Therm. Eng. 17 (1997) 789–797. https://doi.org/https://doi.org/10.1016/S1359-4311(96)00060-9.

[2] J. Schmidt, M. Scheiffele, M. Crippa, P.F. Peterson, E. Urquiza, K. Sridharan, L.C. Olson, M.H. Anderson, T.R. Allen, Y. Chen, Design, fabrication, and testing of ceramic plate-type heat exchangers with integrated flow channel design, Int. J. Appl. Ceram. Technol. 8 (2011) 1073–1086. https://doi.org/10.1111/j.1744-7402.2010.02573.x.

[3] X. Zhang, H. Keramati, M. Arie, F. Singer, R. Tiwari, A. Shooshtari, M. Ohadi, Recent developments in high temperature heat exchangers: A review, Front. Heat Mass Transf. 11 (2018). https://doi.org/10.5098/hmt.11.18.

[4] D. Aquaro, M. Pieve, High temperature heat exchangers for power plants: Performance of advanced metallic recuperators, Appl. Therm. Eng. 27 (2007) 389–400. https://doi.org/10.1016/j.applthermaleng.2006.07.030.

[5] M. Barsoum, MAX phases: Properties of machinable ternary carbides and nitrides, John Wiley & Sons, 2013. https://doi.org/10.1002/9783527654581.

[6] J. Wilkes, Y.C. Hagedorn, W. Meiners, K. Wissenbach, Additive manufacturing of ZrO2-Al2O3 ceramic components by selective laser melting, Rapid Prototyp. J. 19 (2013) 51–57. https://doi.org/10.1108/13552541311292736.

[7] N.T. Aboulkhair, M. Simonelli, L. Parry, I. Ashcroft, C. Tuck, R. Hague, 3D printing of Aluminium alloys: Additive Manufacturing of Aluminium alloys using selective laser melting, Prog. Mater. Sci. 106 (2019) 100578. https://doi.org/10.1016/j.pmatsci.2019.100578.

[8] Z. Chen, Z. Li, J. Li, C. Liu, C. Lao, Y. Fu, C. Liu, Y. Li, P. Wang, Y. He, 3D printing of ceramics: A review, J. Eur. Ceram. Soc. 39 (2019) 661–687. https://doi.org/10.1016/j.jeurceramsoc.2018.11.013.

CHAPTER 3

THEMATIC UNIT, MATERIALS AND METHODS

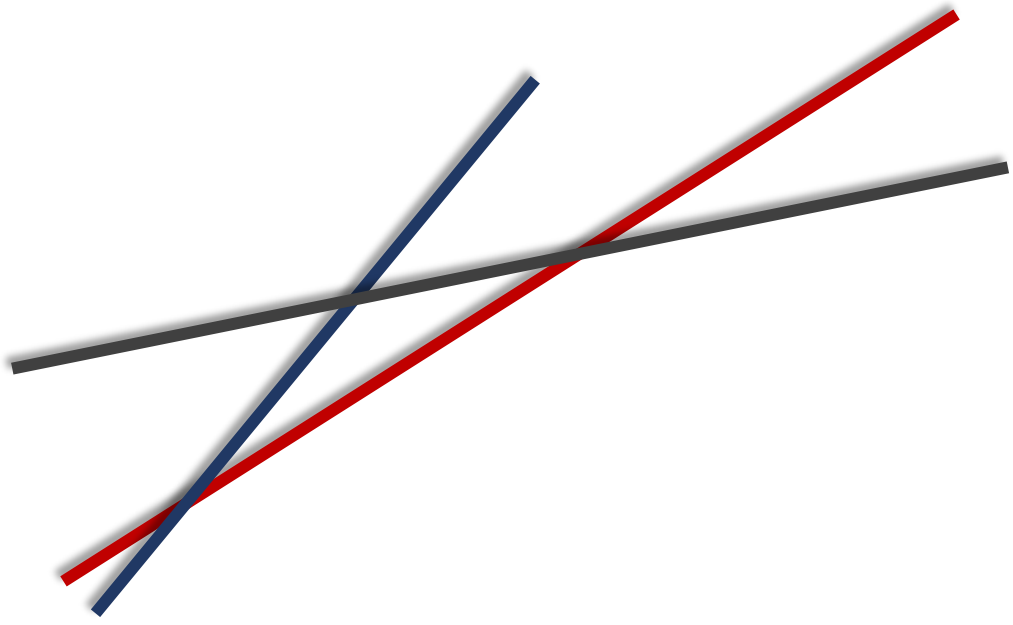

Contents

3.1 Scheme of the experimental work 83

3.2 Initial materials and MAX phase synthesis characterisation 83

3.2.1 Initial powders 84

3.2.2 MAX Phase synthesis 87

3.2.2.1 Cr_2AlC 89

3.2.2.2 Ti_2AlC/Ti_3AlC_2 91

3.2.3 Powder production scale-up 93

3.3 Conventional powder metallurgy consolidation 94

3.3.1 Characterization of consolidated samples 96

3.3.1.1 Density and hardness measurements 96

3.3.1.2 Compressive strength 96

3.3.1.3 Wear properties 96

3.4 Powder injection moulding 98

3.4.1 Initial materials 98

3.4.1.1 PEG/CAB binder 99

3.4.1.2 PEG/PP binder 100

3.4.2 Feedstock solid loading optimisation 101

3.4.2.1 Oil absorption tests 101

3.4.2.2 Multistep torque analysis 102

3.4.2.3 Torque rheology 105

3.4.2.4 Capillary rheology 108

3.4.4 Debinding 111

3.4.5 Sintering and sample characterisation 112

3.5 Composite Extrusion Modelling 113

References 117

3. Thematic unit, materials and methods

3.1 Scheme of the experimental work

In this section, the experimental procedure employed during the implementation of this thesis work is detailed. Figure 1, shows a schematic of the experimental work of all main sections in which this work is divided. Starting from the MAX phase powders synthesis and continuing through the different consolidation processes studied: conventional powder metallurgy, Powder Injection Moulding (PIM) and additive manufacturing through Composite Extrusion Modelling (CEM). In this section, the common thread that encompasses this work as a whole is presented, and the methodology employed for each step of the process will be explained. Readers will be referenced to the published papers shown in the result section (**Chapters 4 to 7**), where most of the relevant results are discussed. In addition, non-published complementary information will be shown in this section along the experimental procedure description.

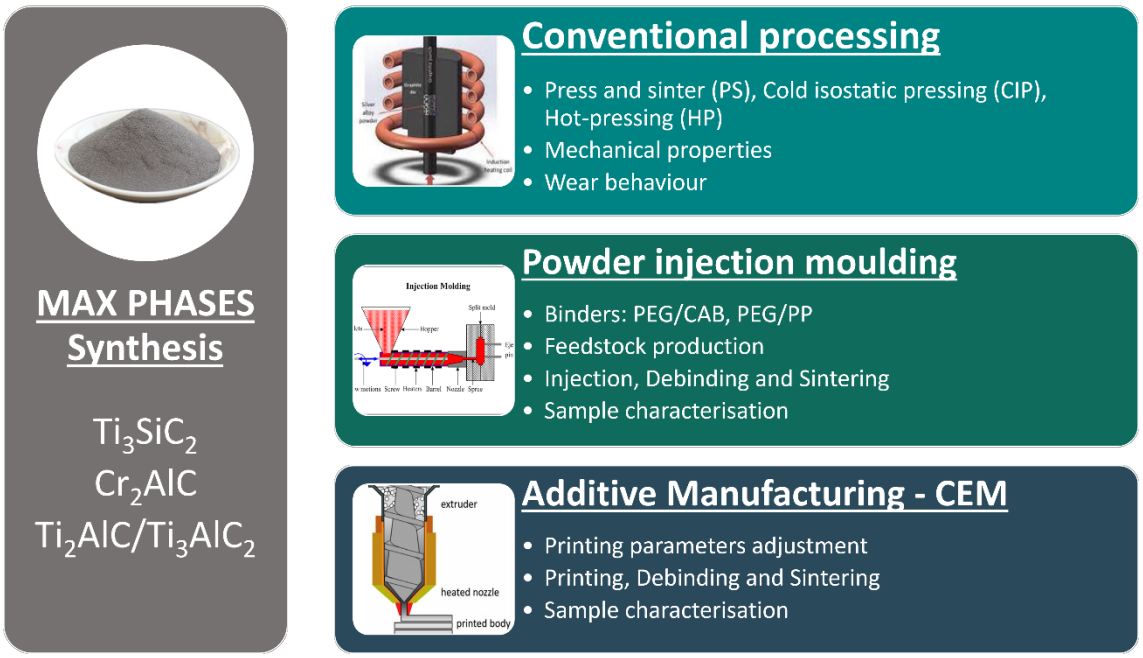

3.2 Initial materials and MAX phase synthesis characterisation

In this work three different MAX phases were synthesised: Ti_3SiC_2, Cr_2AlC and Ti_2AlC/Ti_3AlC_2 starting from different initial powders compositions. Pressureless sintering synthesis was used in order to study the possibility of producing high purity MAX phases through a common and “simple” technique. Furthermore, after optimising the synthesis parameters, a scale-up process was developed to produce high quantity of powders without compromising the purity achieved.

3.2.1 Initial powders

Powders used for the synthesis of MAX phases are listed below. Different carbides (SiC, TiC) and elemental powders (Ti, Si, C, Cr, Al) were used during the optimisation of the MAX phases synthesis. In addition, several particle size distributions of the powders were selected to study the influence of the powder size on the synthesis process. All powders particle size distributions are shown in Figure 2 and characteristics detailed in Table 1. Micrographs of the powders are shown in Figure 3. Powder density was obtained by helium picnometry (AccuPyc 1330, Micrometrics, US). Mean particle size distribution of the powders represented in number, was obtained by Dynamic Light Scattering (MasterSizer 2000, Malvern Instruments, UK). Measurements were performed in an aqueous solution using a dispersant to avoid the agglomeration of the powders during the test. In addition, micrographs of the powders and microstructural analysis performed throughout this work were performed with two scanning electron microscopy (SEM) equipment: a SEM XL-30 Philips (US) coupled with Energy-Dispersive X-ray Spectroscopy (EDS, EDAX, US) and a SEM TENEO-FEI (Netherlands) coupled with EDS, DX-4-EDAX (USA).

Table 1. Detailed list of initial powders used, density and particle distribution characterization.

Powder	Supplier	Density (g/cm^3)	D50 (µm)	D90 (µm)	Purity (%)
Ti	TLS Technik GmbH, Germany	4,5	8	14	99
Si	Alfa Aesar GmbH, Germany	2,3	4	10	99,9
Cr	Goodfellow Ltd., UK	7,2	30	53	99,5
Al	AEE, USA	2,7	38	79	99,5
C_c	Ismaf S.L., Spain	2,8	24	58	99,5
C_f	Alfa Aesar, GmbH, Germany	2,9	13	31	99
SiC_c	Alfa Aesar, GmbH, Germany	3,2	35	53	99
SiC_f	Navarro S.A., Spain	3,2	12	21	99,5
TiC	MaTeck GmbH, Germany	4,9	9	23	99

*Subscripts c and f in the elements' nomenclature throughout the text stands for the coarse (c) or fine (f) particle size used.

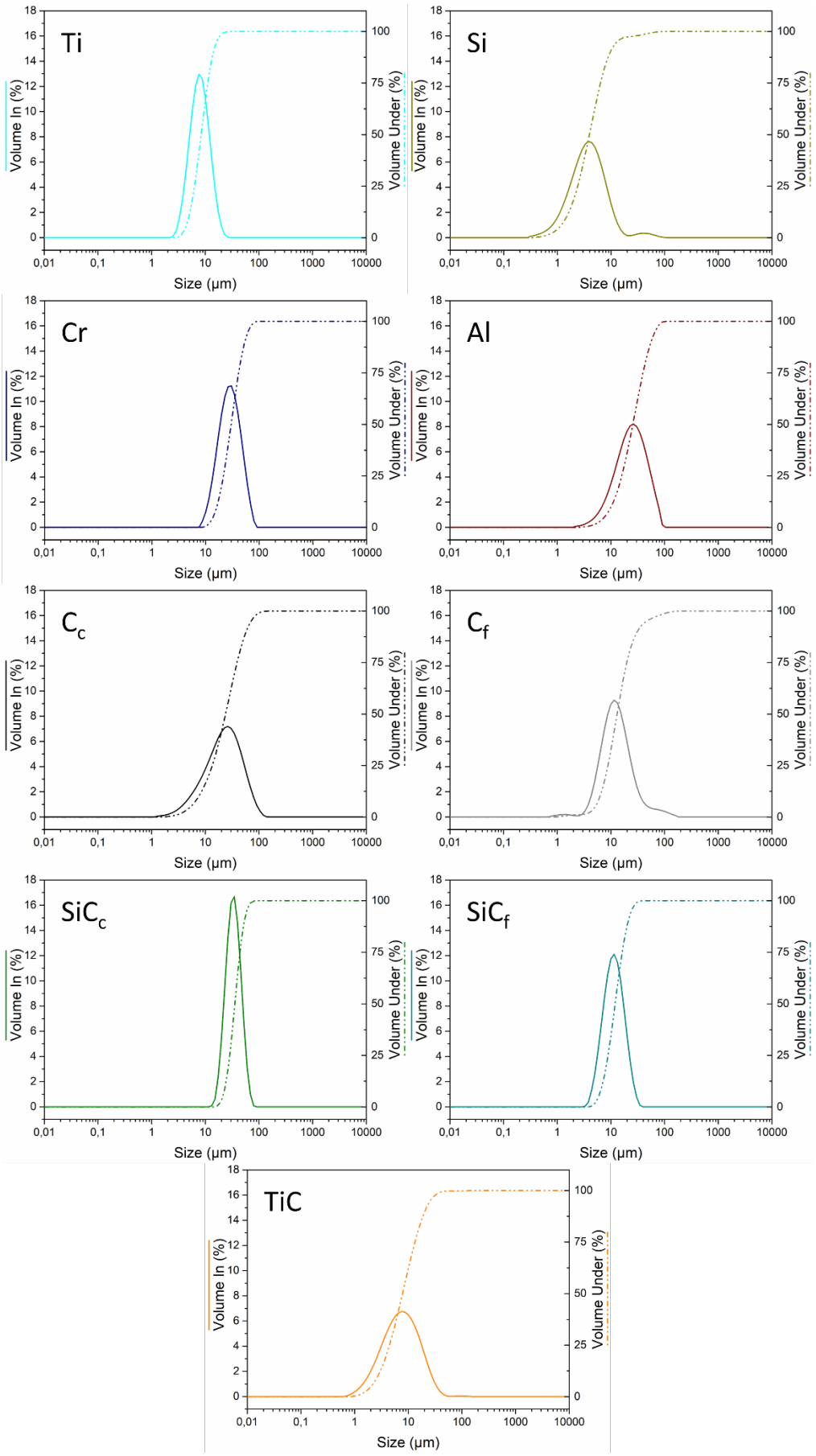

Figure 2. Particle size distribution of all powders used for the synthesis of MAX phases Ti_3SiC_2, Cr_2AlC and Ti_2AlC/Ti_3AlC_2.

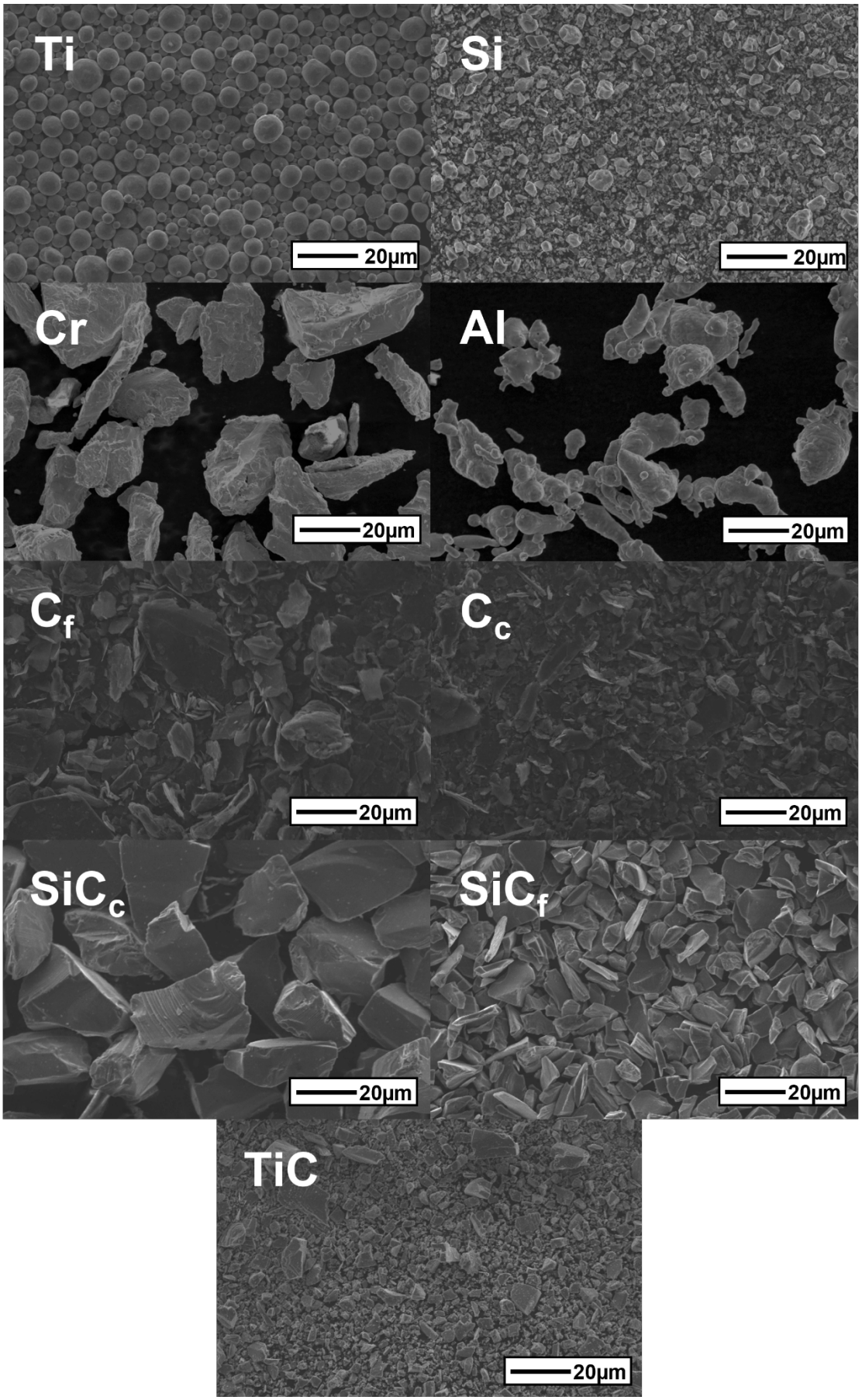

Figure 3. SEM micrographs of the initial powders used for the synthesis of MAX phases Ti_3SiC_2, Cr_2AlC and Ti_2AlC/Ti_3AlC_2.

3.2.2 MAX Phase synthesis

Max phase synthesis was performed by pressureless sintering and the optimisation process started using different initial powders and molar ratios. Due to the novelty of this synthesis route, Ti_3SiC_2 optimisation is reported in **Chapter 4 Section 4.1** where the main results are presented in the scientific journal publication [1]. Results not included in this scientific publication, as well as more detailed experimental descriptions, are presented here. The steps followed for the synthesis were mixing the initial powders mixtures with a specific molar ratio in a Turbula shaker mixer (WAB, Switzerland) for 1 hour. Mixed powders were uniaxially pressed at 200 MPa, obtaining compacted samples of 16 mm diameter and 3 mm thickness. Compacted samples were introduced in an alumina crucible covered with zirconia balls of about 1 mm diameter to avoid the contamination during the heat treatment. Synthesis was performed under different atmospheres, to analyse the influence of this parameter during MAX phase Ti_3SiC_2 formation. A tubular high vacuum furnace (HVT-15/50/450, Carbolite, UK) and a tubular furnace (STF-15/757450, Carbolite, UK), using argon as protective atmosphere, were used, varying the synthesis parameters. An in-depth study of the optimal conditions for high purity synthesis of Ti_3SiC_2 was performed. Synthesised samples were then crushed in an agate mortar, in order to analyse the composition of the final powder for each initial mixture and synthesis parameters, quantifying the purity of the MAX phase. Phase purity analysis was performed by X-Ray diffractometry (XRD, Philips X'pert, Netherlands) using copper Kα radiation at 40 kV and 40 mA. Quantification of the powder composition was calculated by least-square procedure of the integrated area of most intense peaks in the XRD patterns, following Equation 1; where I_x corresponds to the integrated area of the most intense peak of the phase to be quantified and I_t is the summation of the integrated areas of the most intense peaks of all present phases [2]. In order to validate this quantification technique, Rietveld refinement was performed and compared to this method.

Equation 1 $$\% \text{ Phase} = \frac{I_x}{I_t}$$

Differential Thermal Analysis (DTA) and Differential Scanning Calorimetry (DSC) was performed to the powders (SETSYS Evolution, SETARAM Instrumentation, France) with a heating rate of 10 ºC/min up to 1500 ºC in order to study the MAX phase formation temperatures. A complementary evaluation off the possible reaction mechanisms during the synthesis was carried out by thermodynamic calculations of ΔG using Thermo-Calc software (Sweden) with databases SSOL5 and SSUB5 [3].

The same procedure was performed for the synthesis of MAX phases Cr_2AlC and Ti_2AlC. A detailed list of the molar ratios used for the synthesis of these MAX phases is shown in Table 2. Similarly to the procedure followed for Ti_3SiC_2, the molar ratios for Cr_2AlC and Ti_2AlC were selected from successful bibliography high purity synthesis by different techniques and compared to pressureless sintering.

Table 2. List of initial compositions, molar ratios and phases present after heat treatments for successful bibliography Cr_2AlC and Ti_2AlC high purity synthesis.

Author	Initial Powder	Molar ratios	Technique	Phases
Gonzalez-Julian [4]	Cr:Al:C	2:1.1:1	PS/SPS	Cr_2AlC
Xiao [5]	Cr:Al:C	2:1.2:1	PS/HP	Cr_2AlC
Hashimoto [6]	Ti:Al:TiC	1:1:0.75	PS	Ti_2AlC
Ping [7]	Ti:Al:TiC:C	1.5:1:0.5:0.5	HP	Ti_2AlC/Ti_3AlC_2

Selection of the synthesis temperature range for Cr_2AlC and Ti_2AlC was obtained by DSC analysis. Firstly, from the analysis showed in Figure 4, an exothermic peak can be observed for both mixtures at around 640 ºC, which is lower than the melting temperature of Al. This peak corresponds to the formation of a new phase from the initial powder during this first stage: Al_8Cr_5 [8] is formed for mixture Cr:Al:C and TiAl + Ti_3Al [9] for the Ti:TiC:Al mixture. From 1250 ºC to 1400 ºC in Figure 4-a two exothermic peaks can be observed, that correspond to a later reaction of the intermediate Al_8Cr_5 phase with C, to generate MAX phase Cr_2AlC. In Figure 4-b the formation of a secondary phase can be observed at around 1430 ºC, with a small exothermic peak, before the endothermic reaction at 1450 ºC that corresponds to the melting of some of the generated phases. From this analysis a temperature range from 1200 ºC to 1400 ºC was selected for the synthesis study of the selected compacted mixtures.

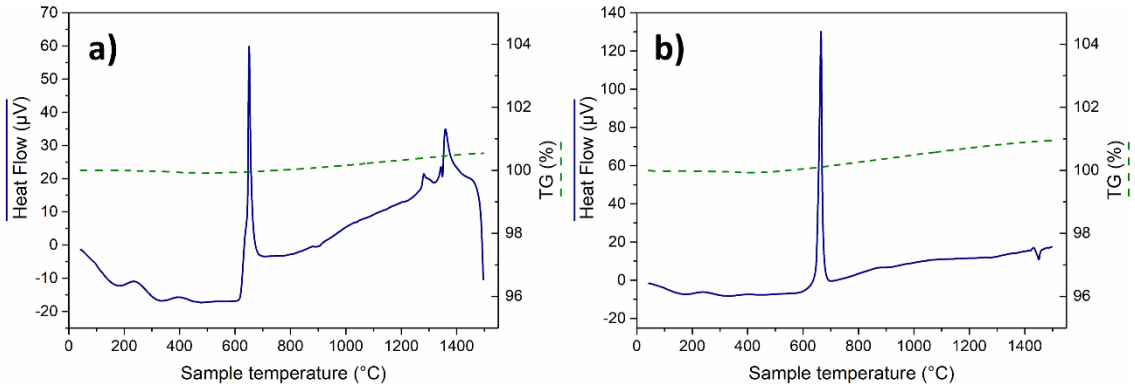

Figure 4. Differential Thermal Analysis (DTA) and Differential Scanning Calorimetry (DSC) curves of a) Cr:Al:C with a molar ratio of 2:1,2:1 and b) Ti:TiC:Al with a molar ratio of 1:1:0,75.

Due to the evaporation of aluminium in vacuum, a protective argon atmosphere was selected for the synthesis of Cr_2AlC and Ti_2AlC MAX phases. Three synthesis

temperatures were selected 1200, 1300 and 1400 ºC with heating and cooling rates of 5 ºC/min and an initial holding time of 4 h.

3.2.2.1 Cr_2AlC

Synthesis using mixtures of Cr:Al:C with molar ratios of 2:1.1:1 and 2:1.2:1 were carried out, and crushed powders obtained after synthesis were analysed by XRD (Figure 5). Table 3 shows the amount of MAX phases and secondary phases obtained after this preliminary synthesis route for both mixtures. Firstly, for the mixture with a molar ratio of 2:1.1:1 at 1200 ºC it is possible to observe the presence of Al_8Cr_5 intermediate phase and unreacted C, suggesting an insufficient synthesis process. By increasing the temperature to 1300 ºC, the presence of unreacted graphite is no longer seen, achieving a purity of 73 %. At 1400 ºC the formation of Cr_2AlC decreases, indicating an excessive temperature for the synthesis of the MAX phase. From the phase evolution analysis represented in Figure 6-a it can be observed how the amount of carbon present at 1300 °C decreases as the temperature increases, due to its reaction with the secondary elements present. Consequently, the amount of Al_8Cr_5 increases with the increase of temperature, as a result of an enhanced reaction. Although there is no presence of any other secondary phase at 1400 ºC, the decrease of the amount of MAX phase could be due to the decomposition of this phase at higher temperature, in the presence of other intermediate phases, as it has been observed for Ti_3SiC_2 [1]. Secondly, the mixture with a molar ratio of 2:1.2:1 shows an increase in the final amount of Cr_2AlC for all temperatures (Figure 6-b). The slight increase of aluminium in the initial molar ratio allows more amount of this material to react with the chromium during the first stage and later with the graphite for the formation of the MAX phase. The A element in the MAX phases is commonly volatile at high temperature, and it is a common strategy to increase the amount of this element compared to the stoichiometric value, to prevent the lack of material and allow for the reactions to occur [2,5,10,11].

With all this, the selected mixture was Cr:Al:C with a molar ratio of 2:1.2:1 and the heat treatment process was set at 1300 ºC, adjusting the holding time to 6 hours to enhance the purity of Cr_2AlC. XRD analysis of the synthesised powders are shown in Figure 7, obtaining a purity of 98 % of MAX phase Cr_2AlC and, in this case, Cr_5C_3 as secondary phase. Due to the longer permanence of the mixture at the synthesis temperature (6 hours at 1300 ºC), the intermediate phases of Al_8Cr_5 seems to have reacted with the remaining graphite in the mixture, generating Cr_2AlC and Cr_5C_3. Furthermore, micrographs of the powder can be observed in Figure 8, where the typical nanolaminated structure of MAX phases can be observed.

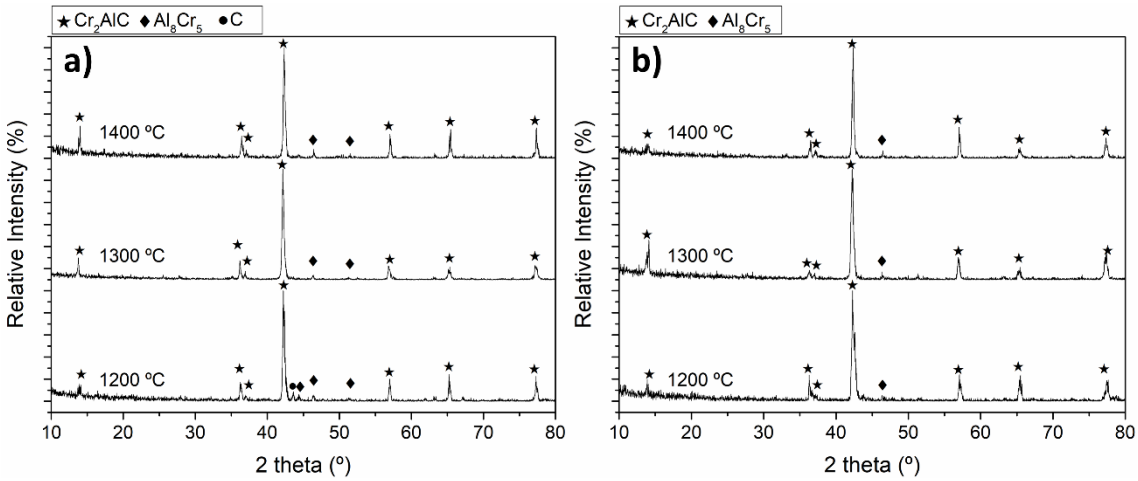

Figure 5. X-ray diffraction patterns of mixture a) Cr:Al:C with a molar ratio of 2:1.1:1 and b) Cr:Al:C with a molar ratio of 2:1.2:1 heat treated under argon atmosphere at different temperatures with a holding time of 4 h.

Table 3. Quantification of detected phases (XRD) present in selected mixtures after heat treatment in argon atmosphere at 1200, 1300 and 1400 ºC temperature for 4 h for Cr_2AlC synthesis.

Initial Mixture Cr:Al:C	**Synthesis temperature (ºC)**	**Detected phases (%)**		
		Cr_2AlC	**Al_8Cr_5**	**C**
2:1.1:1	1200	66	18	16
	1300	73	27	-
	1400	68	32	-
2:1.2:1	1200	92	8	-
	1300	94	6	-
	1400	93	7	-

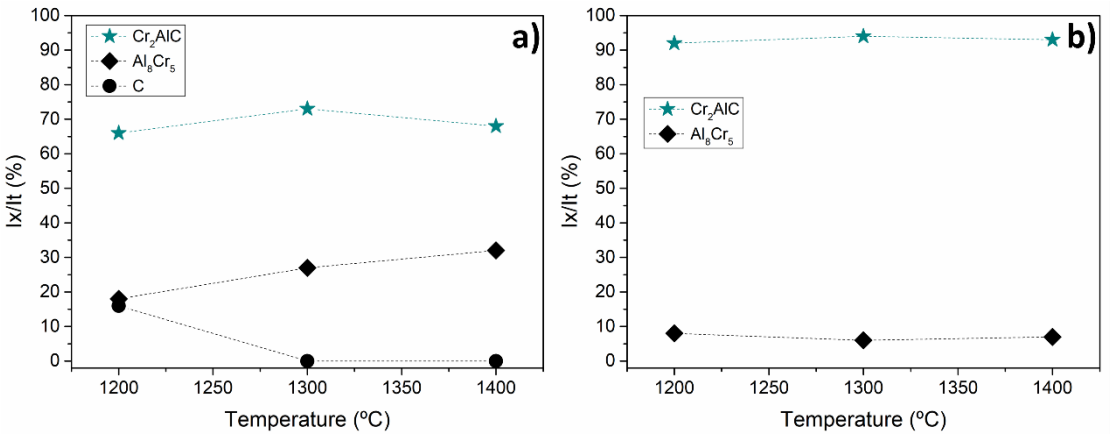

Figure 6. Phase evolution obtained by XRD profiles for a) Cr:Al:C with a molar ratio of 2:1.1:1 and b) Cr:Al:C with a molar ratio of 2:1.2:1 after heat treatment in argon atmosphere at different temperatures for 4 h for Cr_2AlC synthesis.

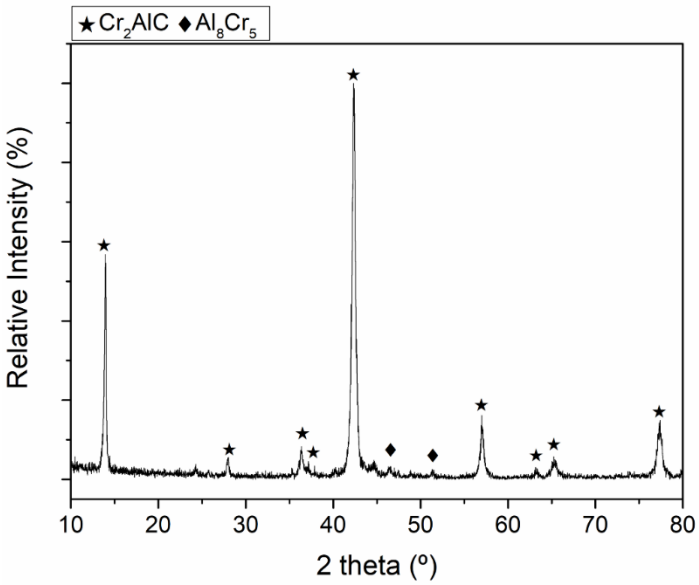

Figure 7. X-ray diffraction patterns of mixture Cr:Al:C with a molar ratio of 2:1.2:1 heat treated under argon atmosphere at 1300 ºC with a holding time of 6 h.

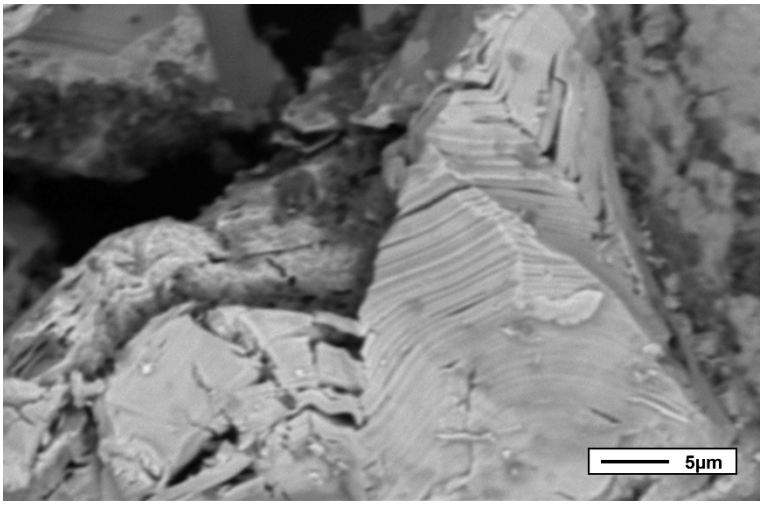

Figure 8. SEM micrographs of synthesised Cr_2AlC after a heat treatment under argon atmosphere at 1300 ºC for 6 h starting from a mixture of Cr:Al:C with a molar ratio of 2:1.2:1.

3.2.2.2 Ti_2AlC/Ti_3AlC_2

Synthesis of MAX phase Ti_2AlC was studied starting from Ti:Al:TiC with a molar ratio of 1:1:0.75 and a mixture of Ti:Al:TiC:C with a molar ratio of 1.5:1:0.5:0.5. XRD synthesis profiles of the powders from 1200 to 1400 ºC are shown in Figure 9. The calculated amount of the different phases obtained during the process are summarised in Table 4. Firstly, for Ti:Al:TiC mixture with a molar ratio of 1:1:0.75, it can be observed that the amount of MAX phase Ti_2AlC, increases with the increase of the heat treatment temperature, reaching its maximum at 1400 °C with a 77% of Ti_2AlC phase. As opposed to other MAX phases, titanium aluminium carbide exhibits two different stable compounds with n being 1 and 2 in the $M_{n+1}AX_n$ formula: Ti_2AlC and Ti_3AlC_2. The presence of this other MAX phase (Ti_3AlC_2) is also observed in the final product in the

same amount for all the temperatures analysed (16-17%). In addition, an incomplete reaction of the product can be observed by the presence of intermediate phases of $TiAl_3$ and TiAl. The increase of temperature enhances the synthesis of the MAX phase, reducing the amount of secondary phases present in the final produced powders. Also, for mixture Ti:Al:TiC:C with a molar ratio of 1.5:1:0.5:0.5, a similar effect on the synthesis process can be observed. The increase of temperature increases the amount of synthesised Ti_2AlC MAX phase, reaching its maximum at 1400 °C with a purity of 75%. Furthermore, Ti_3AlC_2 is still present in the mixture and it remains constant for all the heat treatment temperatures. In this case, the secondary phases found in the final products are $TiAl_3$ and TiC, the former produced by the reaction of Ti+Al and the latter both by the presence of unreacted initial TiC powder and by the reaction of Ti+C. These products are observed at all temperatures and decrease as the MAX phase formation is enhanced, with the increase of the process temperature. The phase evolution during the heat treatment of Ti_2AlC synthesis is shown in Figure 10.

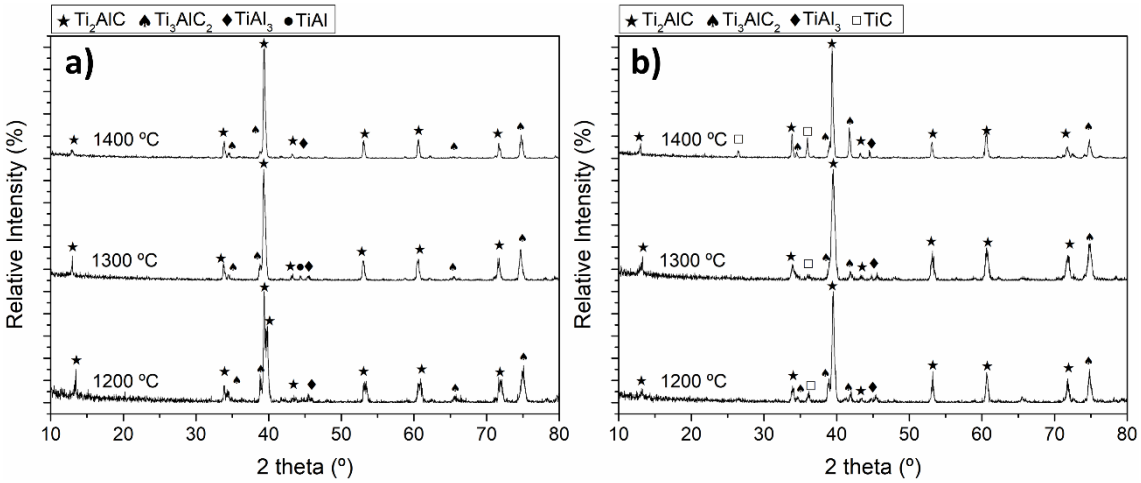

Figure 9. X-ray diffraction patterns of mixture a) Ti:Al:C with a molar ratio of 1:1:0.75 and b) Ti:Al:TiC:C with a molar ratio of 1.5:1:0.5:0.5 heat treated under argon atmosphere at different temperatures with a holding time of 4 h.

Table 4. Quantification of detected phases (XRD) present in selected mixtures after heat treatment in argon atmosphere at 1200 ºC, 1300 ºC and 1400 ºC for 4 h for Ti_2AlC/Ti_3AlC_2 synthesis.

Initial Mixture	Synthesis temperature (ºC)	Detected phases (%)				
		Ti_2AlC	Ti_3AlC_2	$TiAl_3$	TiAl	TiC
Ti:Al:TiC 1:1:0.75	1200	61	17	22	-	-
	1300	62	16	12	10	-
	1400	77	16	7	-	-
Ti:Al:TiC:C 1.5:1:0.5:0.5	1200	66	15	11	-	8
	1300	73	15	5	-	7
	1400	75	17	4	-	4

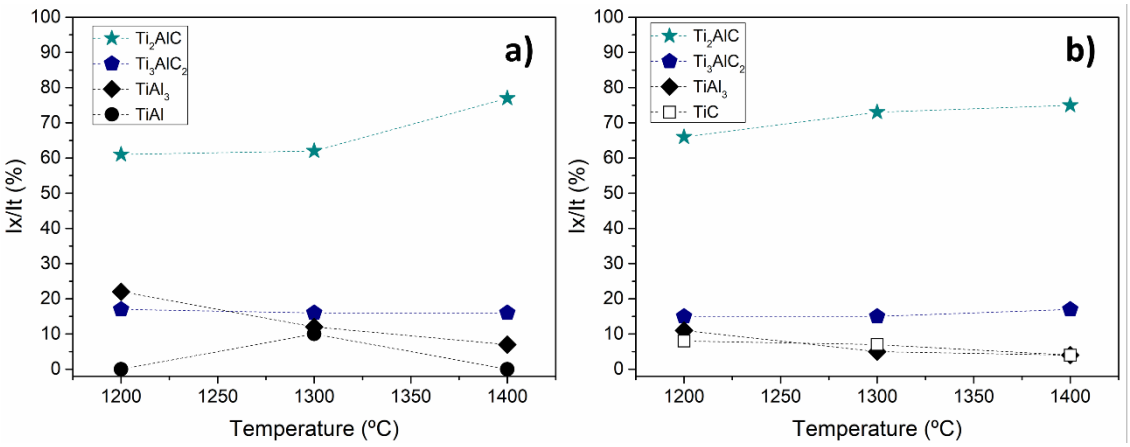

Figure 10. Phase evolution obtained by XRD profiles for Ti:Al:C with a molar ratio of 1:1:0.75 and b) Ti:Al:TiC:C with a molar ratio of 1.5:1:0.5:0.5 after heat treatment in argon atmosphere at different temperatures for 4 h for Ti_2AlC/Ti_3AlC_2 synthesis.

For this MAX phase the best purity results obtained were for initial powder mixture of Ti:Al:TiC with a molar ratio of 1:1:0.75 at 1400 ºC with a holding time of 4 h. For Ti_2AlC it is also possible to observe the nanolaminated structure of the synthesised powders characteristic of MAX phases (Figure 11).

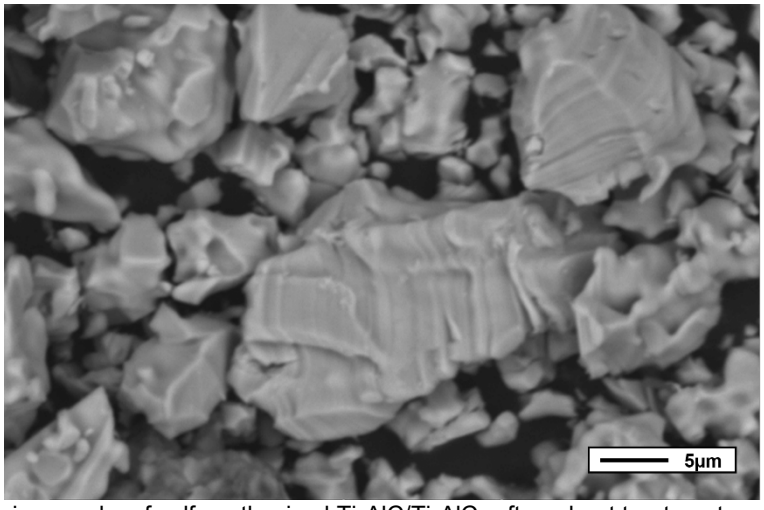

Figure 11. SEM micrographs of self-synthesised Ti_2AlC/Ti_3AlC_2 after a heat treatment under argon at 1400 ºC for 4 h starting from a mixture of Ti:Al:C with a molar ratio of 1:1:0.75.

3.2.3 Powder production scale-up

After analysing and optimising the different synthesis routes for high purity MAX phases, the next step in the powder production is to study its scalability. For this, two of the three synthesised MAX phases were selected: Ti_3SiC_2 and Cr_2AlC. Powder production scalability of MAX phases is an important matter since the scale-up process could compromise the purity of the powders. Ti_3SiC_2 is one of the most widely studied MAX phase and a great candidate for newer processing techniques, as is intended in this work. Furthermore, since this MAX phase is commercially available, the production technique used for high quantity of powder production used in this work can be compared

in terms of purity, to commercially available powders. In addition, Cr_2AlC was also selected as a promising MAX phase for alternative processing techniques and due to the high purity achieved during the synthesis optimisation (98%), it stands as a great candidate for further analysis. In the case of Ti_2AlC, although the final purity obtained was relatively high (77%) and even higher considering the secondary Ti_3SiC_2 found in the mixture (93%), the production of high quantity of powders for this MAX phase was disregarded, due to this dual presence of Ti_2AlC/Ti_3AlC_2.

For this purpose, silicon moulds were prepared to fit higher quantities of powders that were to be consolidated by cold isostatic pressing (CIP). The press used was an EPSI Systems CIP (Belgium), and vacuum-sealed moulds were pressed at 400 MPa. Compacted samples were then synthesised with the optimised cycles presented in Section 3.2.2 (Ti_3SiC_2: vacuum, 1300 ºC for 6 hours and Cr_2AlC: argon, 1300 ºC for 6 hours). Heat treated samples were then milled in a planetary ball mill (Pulverisette 5/2, Fritsch, Germany) using a ball to powder ratio of 10:1 and argon atmosphere and isopropanol as protective agents against oxidation of the powders during the milling.

Final purity obtained for both MAX phases was of 92 % for Ti_3SiC_2 and 96 % for Cr_2AlC, resulting in an optimum scale-up process for the production of high quantities of MAX phase powder obtaining up to 50 times more amount of material. Furthermore, the particle size distribution of the powders was controlled during the process, obtaining optimal distribution for the different processing routes established for this thesis work. Further information on the powders characteristics after this process can be seen in **Chapter 5 Section 5.1** where the most important results are presented in a scientific publication.

3.3 Conventional powder metallurgy consolidation

In order to establish the suitability of synthesised powders for different processing routes, common MAX phases consolidation techniques were applied to study and compare the properties of the synthesised materials processed by conventional press and sintering, analysing the differences between uniaxial, cold isostatic pressing, and hot pressing.

Firstly, sinterability of the powders was studied by uniaxial press and sintering, varying the pressure from 100 to 500 MPa. Green samples were sintered under vacuum for MAX phase Ti_3SiC_2 and argon for Cr_2AlC. The sintering thermal cycle program was set to 1300 ºC during 6 h for both MAX phases. In addition to uniaxial pressing, cold isostatic pressing was used for consolidating MAX phase powders at 4000 bar. Furthermore, as an alternative consolidation technique for MAX phase consolidation, inductive hot

pressing was used to obtain Ti_3SiC_2 and Cr_2AlC samples. Inductive hot pressing is a field-assisted sintering process (FAST), where an electrical current is applied to a coil to generate high heating rates for the consolidation of the powders. This is performed while a uniaxial pressure is applied to the powders and is used commonly to obtain high density consolidated samples. The schematics of the set-up used for Ti_3SiC_2 and Cr_2AlC consolidation are shown in Figure 12. A 20 mm graphite die was used, protected with a graphite foil sprayed with a boron nitride (BN) coating, to avoid reactions between the powders and the die. Boron nitride-Graphite foils were also placed between the powders and the graphite spacers. The top and bottom punches inserted in the die are the responsible for the pressure transfer to the sample during the cycle. This cycle consisted of a heating rate of 50 ºC/min, lowering this rate to 25 ºC/min when reaching a temperature of 100 ºC lower than the selected final consolidation temperature, in order to have a better control on the maximum cycle temperatures. Different dwell times were analysed, from 15 to 60 minutes. After this, the cooling rate was set to 50 ºC/min to room temperature. Hot pressing tests were mainly performed under vacuum (10^{-3} bar), although argon atmosphere was also used to study the possible influence of the sintering atmosphere on the MAX phase consolidation. In addition, the pressure applied was also varied from 30 to 50 MPa, to analyse the influence on the final density of the samples. Hot-pressing of the samples was performed at RHP Technology GmbH, located in Seibersdorf (Austria) during a research stay.

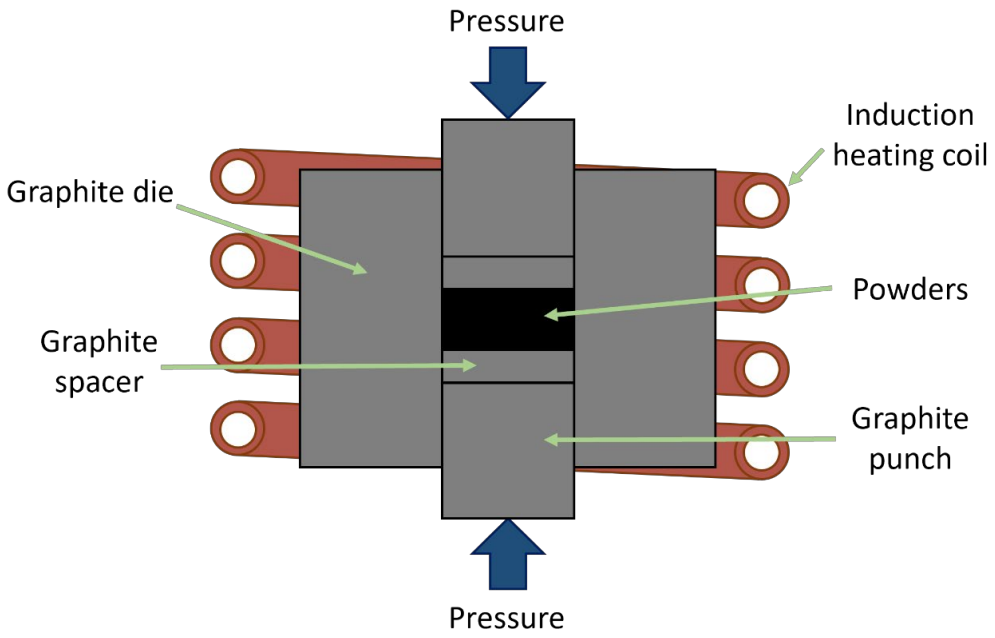

Figure 12. Schematic representation of the inductive hot-pressing process.

3.3.1 Characterization of consolidated samples

3.3.1.1 Density and hardness measurements

Ti_3SiC_2 and Cr_2AlC consolidated samples by these different techniques were characterised in terms of porosity, compressive strength and wear behaviour. In order to study the effect of pressure on green and sintered samples, Archimedes density was calculated using distilled water for the immersed body weight measurements following Equation 2 and Equation 3:

Equation 2 $$\rho = W_d \cdot \rho_{destilled\ water} / W_w - W_d$$

Equation 3 $$Porosity_{total}(\%) = (1 - \rho/\rho_t) \cdot 100$$

where, *W* is the weight of the samples at different stages of the test (w=wet and *d*=dry), *ρ* is the calculated density and ρ_t the theoretical density.

Additionally, hardness of the samples was evaluated by Vickers hardness using a Zwick Roell Z 2.5 (Germany) hardness tester applying a load of 10 N for 10 s. Values reported correspond to the average value of 10 different indentations randomly done in the surface of the samples.

3.3.1.2 Compressive strength

From the consolidated samples produced using cold isostatic pressing and sintering and hot-pressing, 6 mm height by 3 mm diameter cylindrical samples were obtained by wire cutting for cyclic micro-compressive test (Microtest, EM2/5/FR, Spain). Test parameters were set as follows: a preload of 20 N at a speed rate of 0,1 mm/min to guarantee the contact between the pressure clamps and the samples. Subsequently, cyclic test were performed at 1 N/s up to 500 N for 5 cycles at room temperature. An analysis of the deformation behaviour of the samples tested in these conditions was performed.

3.3.1.3 Wear properties

Wear characterisation was performed by reciprocating linear sliding; for this purpose, a UMT tribometer (Bruker, Germany) was used for the tests. Two different loads were set for the wear analysis, at 5 and 10 N, in order to study the behaviour of the consolidated samples and the influence of pressure in the wear behaviour of the MAX phases. As counter materials, 5 mm alumina balls were used under unlubricated conditions in air. Three different wear tracks were performed for each consolidation technique and load applied, while monitoring the coefficient of friction (COF) of the samples in order to study the wear mechanism. In addition, the length of stroke used during the test was fixed at 5

mm and the test frequency speed was 1 Hz. All wear tests were performed for 30 minutes and the wear tracks were characterised in an optical profilometer (DSX500, Opto-Digital Microscope, Japan). 3D models of the tracks were obtained, and several track measurements of each test were acquired to calculate the wear rate of the processed MAX phases. The schematic representation of the wear track model is represented in Figure 13.

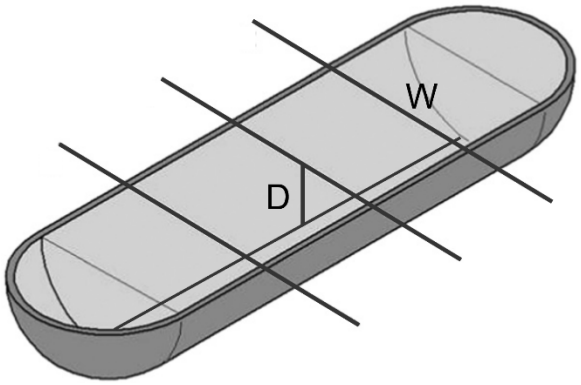

Figure 13. Wear track model used for the calculation of specific wear rates [12].

Specific wear rates (W_v) were calculated using Equation 4-Equation 6 reported by Doni et al. [13]. From the wear tracks, average depth ($\bar{D}$) was calculated from the average wear loss area ($\bar{A}_w$) and the average width of the track ($\bar{W}$).

Equation 4 $$\bar{D} = \bar{A}_w / \bar{W}$$

Volume lost during the test (V), was calculated using the radius (R) of the counter material ball used, the average depth of the wear track previously calculated ($\bar{D}$), the average wear loss area ($\bar{A}_w$) obtained from the 2D profiles of the track, and the stroke length (l).

Equation 5 $$\Delta V = [(1/3) \cdot \pi \cdot \bar{D}^2 (3R - \bar{D})] + \bar{A}_w \cdot l$$

Finally, specific wear rates (W_v) were calculated from the volume loss (ΔV) divided by the load applied (N) and total sliding distance (S):

Equation 6 $$W_V = \Delta V / N \cdot S$$

Results related to the materials obtained with all the conventional consolidation processes as well as the mechanical and wear characterisation of Ti_3SiC_2 and Cr_2AlC MAX phases can be found in **Chapter 5 Section 5.1** where a scientific journal article is presented.

3.4 Powder injection moulding

After assessing the viability of the self-synthesised MAX phases and the scale-up process of the powder production, non-conventional processing routes such as powder injection moulding were explored. With this approach, near-net-shape samples can be obtained, increasing the possible application range of MAX phases.

3.4.1 Initial materials

Firstly, in order to understand the particle behaviour of the synthesised MAX phases, tap and apparent densities were calculated. This procedure was performed following standards ASTM B212-17 and ASTM B527-15, respectively. These values are indicative of the packaging behaviour of the powders depending on their characteristics, such as particle size distribution, morphology or tendency to agglomerate. In the case of tap density, a value higher than 50% of theoretical density would correlate to an optimal powder to obtain dense samples through the injection process [14]. A beneficial aspect of the scaling process of the powder production is the possibility to tailor the particle size distribution during the ball milling of the powders. From particle size distribution measurements of the powders, it is possible to predict their theoretical suitability for powder injection moulding. This is performed calculating the slope (S_w) parameter of the powder following Equation 7 [14]:

Equation 7 $$S_w = 2{,}56\frac{D_{90}}{D_{10}}$$

S_w, values between 2-4 mean that the particle size distribution is broad, and the powders will exhibit a low viscosity (easy-to-mould). Values corresponding to a narrow particle size distribution (S_w = 4-7) are characteristic of powders that exhibit a high viscosity. All these values can be found alongside a deeper analysis in **Chapter 6 Section 6.2** and **Chapter 7 Section 7.1** where the most relevant results are presented in scientific publications [15,16].

Furthermore, MAX phases Ti_3SiC_2 and Cr_2AlC feedstocks were developed using non-conventional binders. In-line with the green objectives of this work, to not only increase the added value of MAX phases, but to reduce the carbon footprint, several sustainable polymeric binders were used for the feedstock production. Two different multicomponent binders were selected for this purpose: PEG/CAB and PEG/PP. Multicomponent binders allow us to achieve a correct viscosity, crucial for the injection process, and the possibility of performing a two-step debinding process that will ease the optimal removal of the

polymeric system, preserving the structural integrity of the samples, while reducing the amount of defects introduced during the process prior to the sintering step.

All details on the commercially available polymers and additives used for the production of PEG/CAB binders are listed in Table 5, as well as the molecular weight used and their density calculated by helium pycnometry.

Table 5. Detailed list of initial binders used and their density characterisation.

Material	Supplier	Molecular Weight (g/mol)	Density (g/cm^3)
Polyethylene glycol	Sigma-Aldrich, Spain	4.000	1,23
Polyethylene glycol	Sigma-Aldrich, Spain	20.000	1,23
Cellulose Acetate Butyrate	Eastman, USA	30.000	1,24
Polypropylene	Sabic, SA	20.000	0,90
Stearic Acid	Panreac Química, Spain	-	0,94
Phenothiazine	Sigma-Aldrich, Spain	-	1,34

3.4.1.1 PEG/CAB binder

For this binder, two different polyethylene glycol (PEG) polymers, with different molecular weights, were used (4.000 and 20.000 g/mol). PEG is a polyether derived from petroleum, but what makes this polymer a “green” solution is its solubility in water, which allows the degradation of PEG using water, instead of utilising organic solvents for the degradation of this polymer. As backbone, cellulose acetate butyrate (CAB) was used with a molecular weight of 30.000 g/mol. CAB is a thermoplastic, which derives from the cellulose acetate, which exhibits excellent mechanical properties. CAB properties depend on the composition of functional groups butyrate and acetate [17]. It is not soluble in water and its degradation doesn’t produce toxic emissions [18]; this preserves the sustainable trademark of this multicomponent binder. Furthermore, as additives in the system, Phenothiazine (PTZ) is used as an antioxidant and stearic acid (SA) as a surfactant. Further information on the optimisation process of the binder systems can be found elsewhere [19].

Furthermore, the polymers that constitute the binder were characterised by Simultaneous Thermal Analysis (STA 6000, PerkinElmer, US). The Thermogravimetry (TGA) and Differential Scanning Calorimetry (DSC) results can be seen in Figure 14. From the results obtained, it can be seen that onset degradation temperatures for both polyethylene glycol (PEG) polymers used, which have different molecular weights, are similar and above 360 ºC. Degradation temperature for this polymer is not critical for

establishing the debinding process, due to the fact that its elimination will be done through solvent, rather than by thermal debinding. Acetate butyrate cellulose (CAB) onset degradation temperature is near 325 ºC and offset 406 ºC, which is going to be an important parameter for selecting thermal debinding conditions. Considering the thermal behaviour of the polymers in the binder, the feedstock mixing temperature was chosen below the onset of degradation of any of the polymeric binders, at 180 ºC, in order to prevent premature binder degradation.

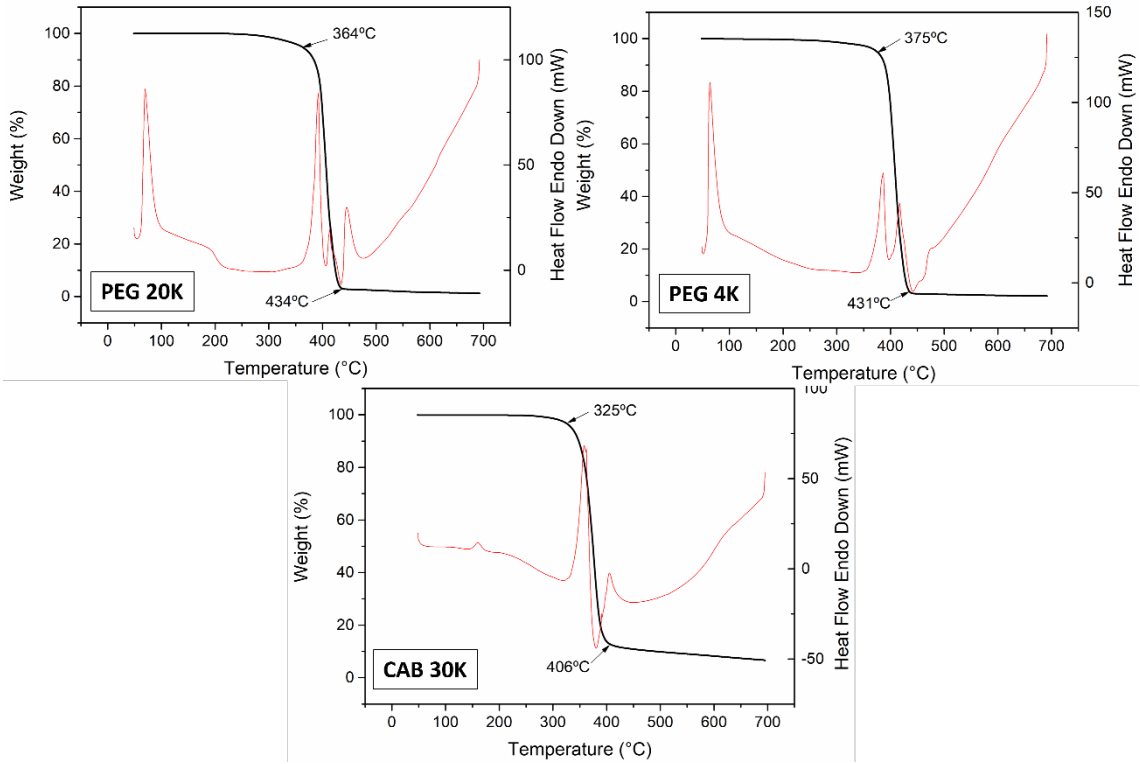

Figure 14. DSC and TG analysis for the polymers used for the PEG/CAB binder system.

3.4.1.2 PEG/PP binder

The second polymeric system used in this work was composed of Polyethylene glycol, to maintain the two-step debinding process strategy, and polypropylene (PP) acting as a backbone. The molecular weight of the PEG used for the development of this binder is 20K. PP used in this work is a commercially available polymer (PP 670Kh) especially suited for injection moulding processes, with medium melt flow and high demoulding temperature. From the STA analysis (Figure 15) it is possible to observe a degradation temperature onset at 379 ºC and a complete degradation of the polymer (offset) at 484 ºC. The degradation temperature of this polymers will determine the thermal debinding temperatures of the injected samples.

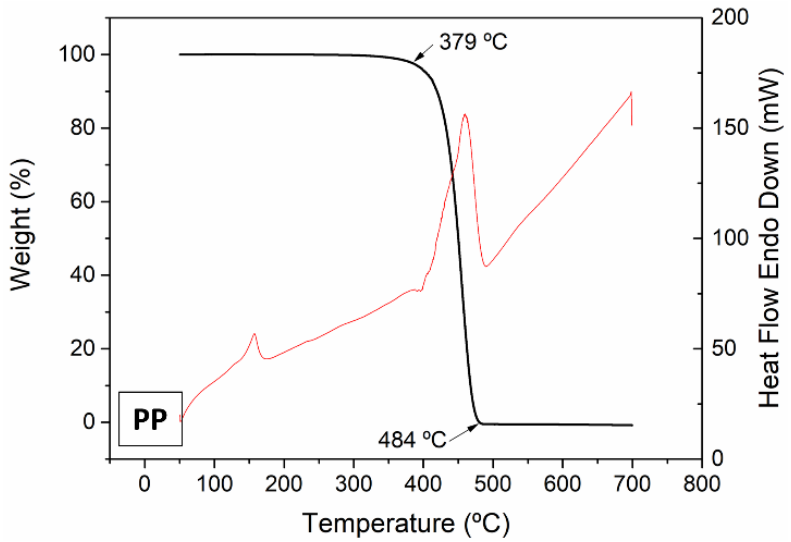

Figure 15. DSC and TG analysis for PP used in the PEG/PP binder system.

3.4.2 Feedstock solid loading optimisation

Feedstock optimisation was carried out using a rotatory mixing machine (Haake Polylab QC, Thermofisher, US). This equipment consists of a heated chamber with two rotors, which rotate in opposite directions to ease the mixing of the feedstocks. The temperature inside the chamber can be monitored in different parts and can reach up to 450 ºC. In addition, rotation speed can also be modified, depending on the material to be mixed, to as high as 100 rpm. The chamber volume is 69 cm^3 and to ensure a correct mixing of the material a 70% of the total volume is filled. Torque is represented as a function of time during mixing of the material. Torque is the force generated by the rotors during mixing and is directly related to the viscosity of the mixtures, giving information about the fluid behaviour during mixing (Newtonian, pseudoplastic or dilatant). The optimisation and selection of the solid loading of the feedstocks has been performed in a progressive order to determine the best rheological behaviour of the feedstocks to be injected. The schematic order of this process is represented in Figure 16 and details on each of the steps are detailed in the following subsections.

3.4.2.1 Oil absorption tests

Since the rheological behaviour of MAX phases has not been yet analysed in depth, and its rheological behaviour with non-conventional binders is unknown, a first approximation study was carried out for Ti_3SiC_2 MAX phase to determine the minimum volume of binder necessary to ensure a complete homogenisation with the powder. This test is called Oil absorption method, and it is performed by introducing a known amount of powders into the heated chamber and adding oil while recording the torque generated against time, up to the stabilisation of the torque, for every fraction of oil added. All torque rheology analyses were performed at a fixed rotation speed and temperature, since these two

parameters directly affect the viscosity behaviour of the mixture, and if different rotation speeds were used it would not allow for comparison between materials to be made. In this case, a 50 rpm rotation speed at a temperature of 180 ºC was selected. In addition, 1 mL of oil was introduced every 5 min, to ensure the correct stabilisation of the torque value. From the maximum torque obtained during the test and following Equation 8, the approximate critical solid loading of the mixture can be determined:

Equation 8 $$CPVC = \frac{V_p}{V_p + V_o}$$

Where, CPVC corresponds to the critical powder volume concentration of the mixture, V_p is the powder volume introduced in the chamber and V_o is the volume of oil at the maximum torque. Oil absorption tests results can be found in **Chapter 6 Section 6.2** [15] where the most relevant findings are shown in a scientific publication**.**

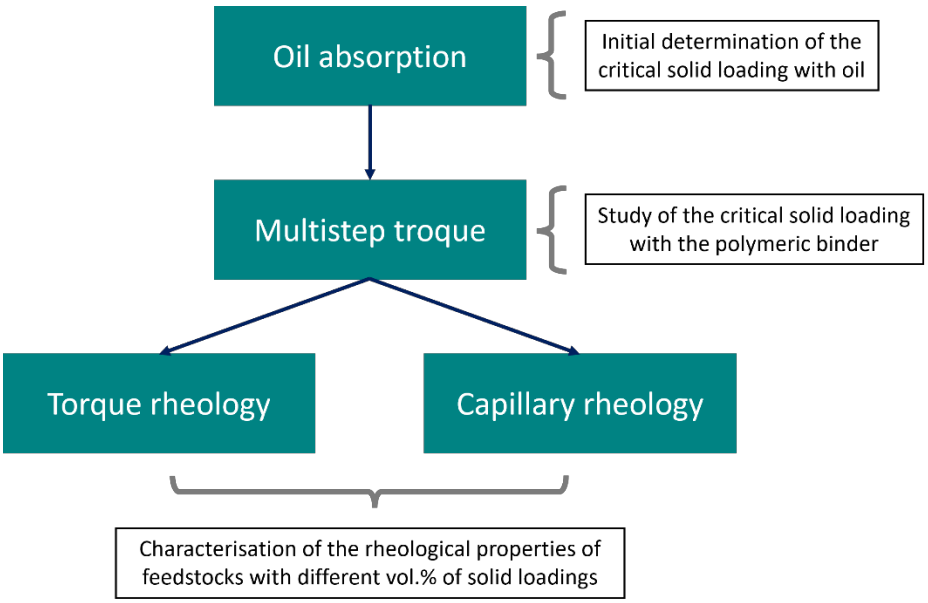

Figure 16. Schematic representation of the procedure followed for the optimisation of MAX phase feedstocks.

3.4.2.2 Multistep torque analysis

Using the estimated values obtained from the oil absorption tests as a starting point, multistep torque analysis was performed to all the binder systems, in order to determine the optimal solid loading of the mixtures. In this test, a selected range of solid loadings is analysed, and the initial and final solid loading values have to be calculated and known before starting the test [20]. This is due to the fact that when the maximum solid loading value is analysed the volume of the feedstock should not exceed the 70 % of total chamber volume filled. In our study, a range of different solid loadings were analysed considering the values obtained for the oil absorption test. As the critical solid loading

obtained from the oil absorption test was 55 vol.%, a range between 45 and 65 vol.% solid loading was analysed, with the real binder system (PEG/CAB or PEG/PP). The procedure for this test is to introduce the binder proportions and heat it up until it melts. Once the biner is melted the corresponding amount of powder for the lowest solid loading (45 vol.%) is added into the chamber. Subsequently, after the stabilisation of the previous mixture, 1 vol.% of the powders is introduced into the chamber, increasing gradually the solid loading of the feedstock, all this, while measuring the torque response during the mixing, until the maximum selected solid loading (65 vol.% in this case) is reached.

Multistep torque analysis of the Ti_3SiC_2 PEG/CAB feedstocks can be found in **Chapter 6 Section 6.1** [15] and those corresponding to the feedstock of Cr_2AlC PEG/CAB in **Chapter 7 Section 7.1** [16]**.**

For the PEG/PP binder systems the multistep torque analysis for MAX phases Ti_3SiC_2 and Cr_2AlC are detailed in this section. Firstly, the multistep analyses of the Ti_3SiC_2 PEG/PP feedstock are shown in Figure 17. Figure 17-a shows the torque response to the increase of powder to the mixture, where vertical grey lines indicate the addition of the corresponding amount of powder to increase by 1 vol.% the solid loading of the mixture; and Figure 17-b shows the torque as a function of the solid loading in the chamber after stabilisation. For initial solid loading increments, from 45 to 49 vol.% (light green in Figure 17), it is possible to observe an increase on the torque values while increasing the amount of powder in the mixture. This steady increase in the stabilised torque value is also detected for the next range of solid loading (50 to 55 vol.%, light brown in Figure 17). For these solid loadings it is possible to see a change in the torque stabilisation process. First, mixtures show an increase of the initial torque when the powder is poured into the chamber which gradually reduces while the mixture is homogenised. At 53 vol.% this behaviour changes, and an increase of the torque value is observed once the powder is added to the mixture while the mixture homogenises. From the studies performed on the PEG/CAB feedstocks, this change in the behaviour indicates that the feedstock is close to reaching the critical solid loading [15,16]. For the next range of solid loadings (56 to 62 vol.%, blue in Figure 17) analysed it is possible to observe a steady final value of the torque and a big decrease of this torque values while increasing the solid loading. At this point, the critical solid loading of the feedstock has been surpassed and the binder is not able to accept more powder and still remain homogeneous. This would normally result in a drastic increase in the torque values of the feedstocks; however, this effect is not observed for the MAX phases feedstock. The decrease on the torque values is directly related to the graphitic-like properties of MAX phases, acting as a lubricant to the mixtures and, henceforth, resulting in a decrease of

the torque values. Nevertheless, even though the feedstocks exhibit this low torque values, they have an excess of powder, creating a heterogeneous mixture that is not suited for the injection process. For a better analysis of these values and to determine the optimal solid loading range of the feedstocks, stabilised torque values are represented as a function of the solid loading (Figure 17-b). From these values it is possible to observe a change in the slope of the torque behaviour of the material, which allows to determine an initial optimal solid loading of the feedstock at 49 vol.%. and a critical solid loading value of 55 vol.% for the Ti_3SiC_2 PEG/PP feedstock.

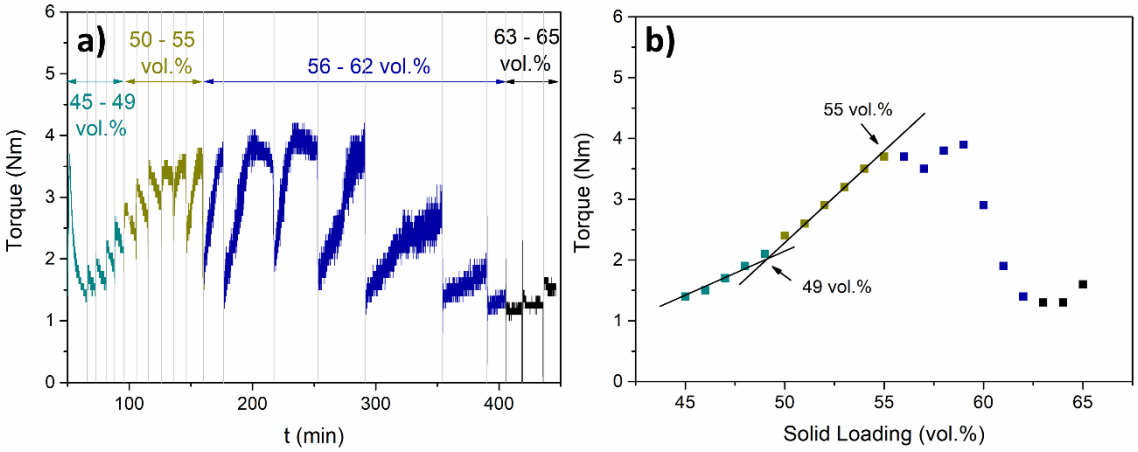

Figure 17. Analysis of the Ti_3SiC_2 PEG/PP feedstocks by a) multistep torque analysis and b) final torque values obtained after stabilisation of mixture with solid loading from 45 to 65 vol.%.

This same study was performed for the production of Cr_2AlC feedstocks using PEG/PP as a binder. Figure 18-a shows the evolution of the torque while the solid loading increases. For this material the range of solid loadings analysed was from 45 vol.% to 56 vol.%. Since all three previous feedstocks produced exhibited a reduction of the torque once the critical solid loading was exceeded, in this case, once a change on the tendency was observed no further powder was added. This change of the tendency occurs for solid loadings highlighted in blue in Figure 17 and Figure 18, where the torque gradually increases with holding time. In addition, it is possible to observe for this material that the initial 45 vol.% solid loading takes a longer time to stabilise, compared to the previous materials analysed. PEG/CAB feedstocks did not show this behaviour and could probably be due to the different rheological properties of the two binder systems. This can be clearly observed by comparing the initial torque values of all feedstocks with 45 vol.% solid loading which are as follows: 1 Nm for Ti_3SiC_2 with a binder system of PEG/CAB [15], as compared to 3,7 Nm for Ti_3SiC_2 with a binder system of PEG/PP and 0,6 Nm for Cr_2AlC with a binder system of PEG/CAB [16], as compared to 5 Nm for Cr_2AlC for a binder system of PEG/PP. It is clear that the PEG/PP binder exhibits higher torque values for the initial solid loading for both materials. On the other hand, the difference between stabilisation times between Ti_3SiC_2 and Cr_2AlC 45 vol.% could be

related to their difference in particle size distribution (**Chapter 5 Section 5.1)** of the synthesised powders: Cr_2AlC has a bigger particle size (D90 = 23 µm) compared to Ti_3SiC_2 (D90 = 20 µm), which could contribute to different rheological behaviour and hence higher stabilization times.

From the differences in slope of the stabilised torque values observed in Figure 18-b the optimal initial solid loading was selected to be 51 vol.% for the Cr_2AlC with PEG/PP as a binder system.

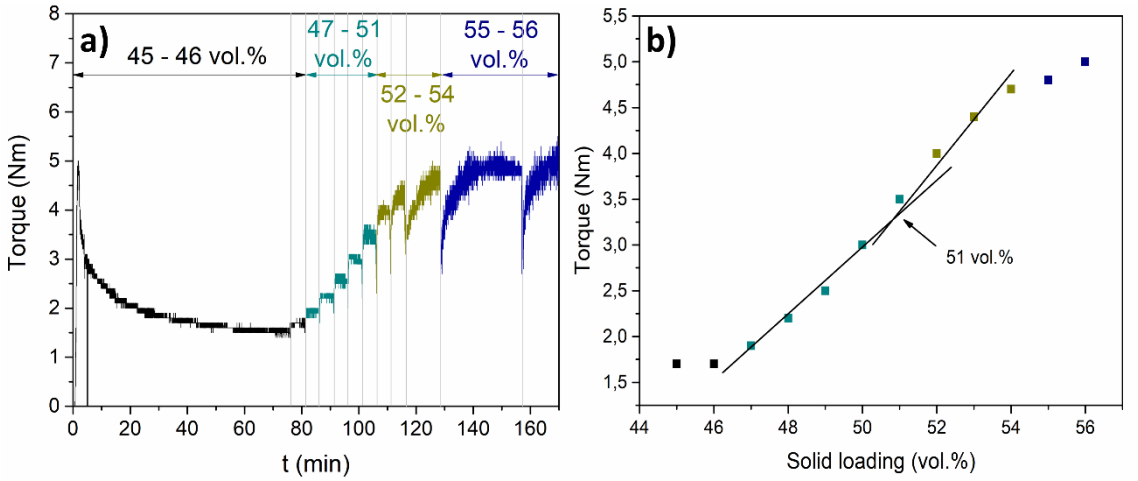

Figure 18. Analysis of the Cr_2AlC PEG/PP feedstocks by a) multistep torque analysis and b) final torque values obtained after stabilisation of mixture with solid loading from 45 to 56 vol.%.

3.4.2.3 Torque rheology

Torque rheology was performed for several solid loadings percentages, below and above the critical solid loading determined from the torque multistep analysis discussed above, in order to study in depth their properties and select an optimal loading for each feedstock system. In this case, after melting the binder at 180 ºC in the chamber, the complete amount of powders for each solid loading were introduced into the chamber, at a fixed roller rotation speed of 50 rpm, and the torque behaviour after 1 hour was analysed. During this time, the powder-binder system has enough time to stabilise, assuming that the solid content has not exceeded the critical solid loading of the mixtures.

In addition, from the results of the torque rheology it is possible to calculate the totalised torque (TTQ). This value is the energy that the system is receiving at a given time. This value is calculated by the area under the curve of the torque behaviour with time and it can be calculated following Equation 9 [21]:

Equation 9 $$TTQ = \frac{E_t}{2 \cdot \pi \cdot N}$$

where E_t is the energy being put into the system by the rotor, and N is the angular speed of the rotor.

Torque rheology of the Ti_3SiC_2 PEG/CAB feedstocks can be found in **Chapter 6 Section 6.1** [15] and those corresponding to the feedstock of Cr_2AlC PEG/CAB in **Chapter 7 Section 7.1** [16]. In the case of PEG/PP binder system, torque rheology is detailed below for Ti_3SiC_2 an Cr_2AlC.

Firstly, Ti_3SiC_2 was analysed by examining the behaviour of the optimal solid loading and critical solid loading obtained during the multistep tests shown in Figure 17. For this purpose, and to have a better understanding of how the amount of solid loading affects the rheological properties of the feedstocks, 49 vol.% was selected as the optimal solid loading for this material and 55 vol.% as the critical solid loading. Torque rheology of these two solid loadings can be observed in Figure 19. It is possible to see how the selected optimal solid loading (49 vol.%) has a similar behaviour as the ones studied for the PEG/CAB system [15,16]. That is, once the powder is poured into the chamber, torque value rapidly increases as a response of the powder generating a resistance on the blades. When the mixture starts to homogenise at around 10 minutes, the torque starts to decrease reaching low final torque values. The initial resistance of the powders to be mixed can also be seen on the chamber temperature values. For this mixture there is an initial increase of the temperature with a steady decrease when the feedstock homogenises.

On the other hand, Ti_3SiC_2 PEG/PP feedstock with a solid loading of 55 vol.% exhibits a low torque value initially, with an increase of that torque value while the feedstock attempts to homogenise, reaching its maximum value at 30 minutes, followed by with a small decrease of torque with time. It is important to note that the expected behaviour for this feedstock with 55 vol.% solid loading would be: an initial increase of the torque value to higher values, compared to the 49 vol.% feedstocks, with a gradual decrease until reaching the final torque value. One of the reasons for this different behaviour could be the lubricant effect of the MAX phase powders while mixing, when the optimal solid loading value has been exceeded. As the powder is poured into the chamber, the 49 vol.% feedstock starts to create agglomerates with the binder in the chamber, resulting in an increase of the initial torque values. In contrast, the 55 vol.% feedstock, due to the higher amount of solid content that it is just at the critical solid loading, the mixture cannot create those agglomerates in the initial state, and the torque observed is a result of the lubricant effect of the powders that the binder cannot accommodate. Nevertheless, the amount of powder in the mixture has not surpassed the critical solid loading, thus, the feedstock is eventually able to create those agglomerates, increasing the torque values of the mixtures, and with time stabilise as a highly filled feedstock, decreasing the torque of the mixture.

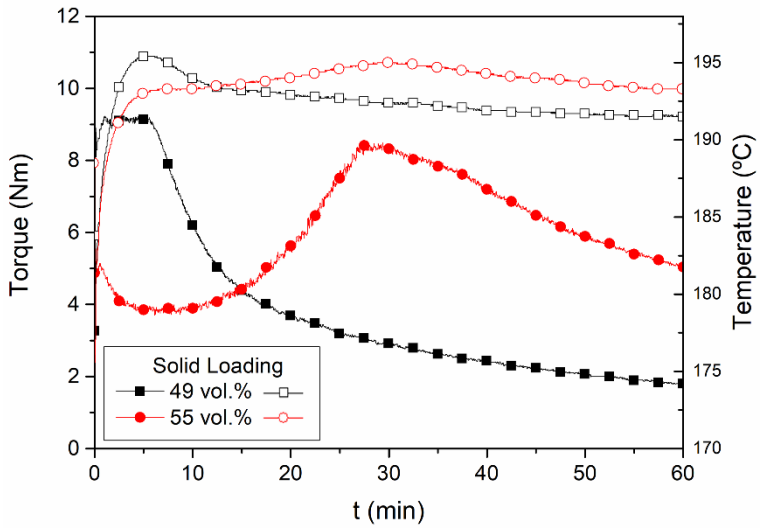

Figure 19. Torque rheology analysis of the Ti_3SiC_2 PEG/PP feedstock with solid loadings of 49 vol.% and 55 vol.%. Filled symbols correspond to the torque values and empty symbols to the temperature of the chamber for each feedstock.

Cr_2AlC PEG/PP feedstocks were studied following the same methodology. In this case, a wider range of solid loadings were analysed from 46 to 52 vol.%. From the results shown in Figure 20, a similar behaviour for all solid loading can be seen with an increase of torque values when the powders are poured into the chamber and, when the system starts to homogenise, a gradual decrease of the torque values that stabilises with time. In the case of the feedstock with a 52 vol.% an increase of the torque at 10 minutes can be observed, followed by a considerable drop after 13 minutes of mixing. Although this behaviour is not entirely understood, this could be generated by the same effect seen for the Ti_3SiC_2 PEG/PP system previously. Thus, a formation of big agglomerates (powder/binder) due to the excess of powder in the mixture and due to the fact that the amount of powder has not yet surpassed the critical solid loading (54 vol.% shown in Figure 18) the system is able to recover its initial homogeneous properties rapidly.

Nevertheless, it can be observed how the final torque values progressively increases with the increase of the solid loading in the mixture, except for the feedstock with 51 vol.% solid loading. In this case, the final torque value obtained is similar to the one obtained for the mixture with a 48 vol.% of solid loading. This effect was also seen during the optimisation of the Ti_3SiC_2 PEG/CAB and Cr_2AlC PEG/CAB feedstocks, detailed in **Chapter 6 Section 6.1** and **Chapter 7 Section 7.1**, respectively. For these feedstocks, the decrease of the final torque values, compared to those with a lower solid loading, defined the optimal solid loading for each system. Thus, for the Cr_2AlC PEG/PP feedstock a solid loading of 51 vol.% can be considered to be the optimal solid loading of this MAX phase-binder combination.

For these feedstocks, there are no big differences in terms of the chamber temperature. It is possible to see the same behaviour for all mixtures, with an increase of the temperature at the initial stage, when the powders have been poured into the chamber and the rotors start to blend the mixtures. After this, and while the mixture is homogenising this temperature remains relatively constant.

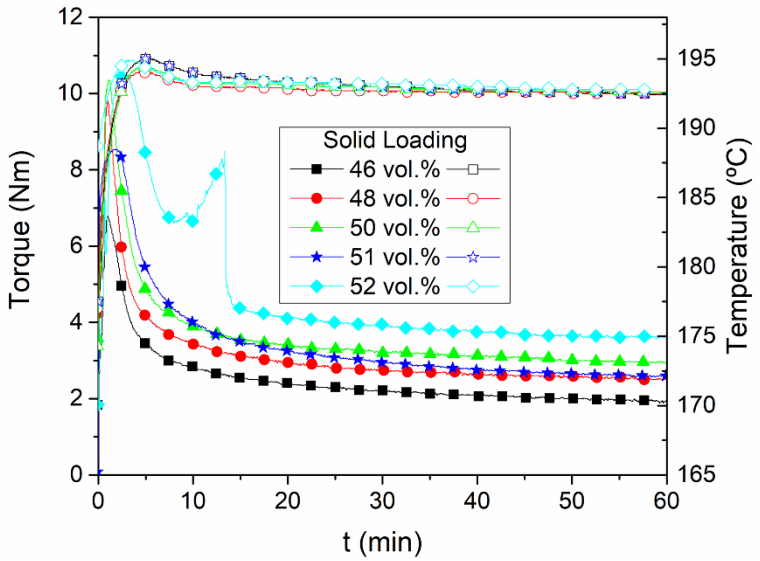

Figure 20. Torque rheology analysis of the Cr_2AlC PEG/PP feedstock with solid loadings from 46 to 52 vol.%. Filled symbols correspond to the torque values and empty symbols to the temperature of the chamber for each feedstock.

3.4.2.4 Capillary rheology

Viscosity off the feedstocks was analysed by capillary rheology. The viscosity of a material depends mainly on the temperature, shear rate and pressure applied. This test consists in filling a barrel with the feedstock and forcing the material to flow through a small diameter. The viscosity of the fluid feedstock is measured while varying the shear rate. Capillary rheology is considered the best way to predict the flow behaviour of feedstocks.

Viscosity measurements were performed in a Haake Rheocap S20 (Thermofisher, US) with a length/diameter ratio of 30:1. Tests were performed at 180 ºC, varying the shear rates from 100 to 10000 s^{-1}. In addition, fluid index (n) of the feedstocks was measured following Equation 10 [22]:

Equation 10 $$\tau = k \cdot \gamma^n$$

Where, τ is the shear effort, k is the consistency index of the fluid and γ is the shear rate. Calculating the shear effort as a function of the viscosity (η) and the shear rate (γ) as showed in Equation 11:

Equation 11 $$\tau = \eta \cdot \gamma$$

From this analysis it is also possible to stablish the fluid nature of the feedstocks being pseudoplastic (n<1), newtonian (n=1) or dilatant (n>1) as discussed in Chapter 1, Section 1.2.1.2. Mainly, a pseudoplastic behaviour of a feedstock is requested to ensure the optimal injection of the materials [23,24].

Capillary rheology of the Ti_3SiC_2 PEG/CAB feedstocks can be found in **Chapter 6 Section 6.1** [15] and those corresponding to the feedstock of Cr_2AlC PEG/CAB in **Chapter 7 Section 7.1** [16]. The capillary rheology properties of the PEG/PP feedstocks are detailed below.

The viscosity measurements for the Ti_3SiC_2 PEG/PP feedstocks with the two different solid loadings selected are shown in Figure 21. Both feedstocks exhibit a pseudoplastic behaviour, meeting the requirements for PIM. Furthermore, viscosity values are below 1000 Pa·s which is the recommended value for powder injection moulding processes [14,23]. The viscosity of the feedstock with 49 vol.% of solid loading steadily decreases with the increase of the shear rate. In the case of the feedstock with 55 vol.% of solid loading the decrease of the viscosity values with the increase of shear rate is more pronounced, reaching lower viscosity values compared to the ones obtained for the 49 vol.% feedstock. Although this is not expected when considering that this feedstock contains a higher amount of powders in the mixture, this excess of powder is what causes the decrease of the viscosity values. As stated earlier in the multistep torque analysis and torque rheology (**Section 3.4.2.3 and 3.4.2.4**, respectively), the excess of powder in the feedstock once the critical solid loading is reached, generates heterogeneities in the mixture. This means that the powder is not entirely mixed with the rest of the polymeric system. While this would result in a drastic increase of the viscosity for other materials [25], the lubricant effect of the MAX phases produces the decrease of this value. From all the rheological characterisation performed, a 49 vol.% of solid loading was selected as the optimal solid loading for the production of Ti_3SiC_2 PEG/PP feedstock.

Cr_2AlC PEG/PP feedstocks viscosity measurements obtained by capillary rheology are shown in Figure 22. As for previous feedstocks, it is possible to see a pseudoplastic behaviour, with viscosity values below the recommended for injection moulding process. For this material, an increase of the viscosity values can be observed as the solid loading increases in the mixture, except for 51 vol.%. Again, as it was observed in the torque rheology measurements shown in Figure 20, there is a decrease of the viscosity values of the feedstock with 51 vol.% solid loading which shows values comparable to those

with a lower amount of solid loading (i.e., 50 vol.%). In this case, 51 vol.% was selected as the optimal solid loading for the production of Cr_2AlC PEG/PP feedstocks.

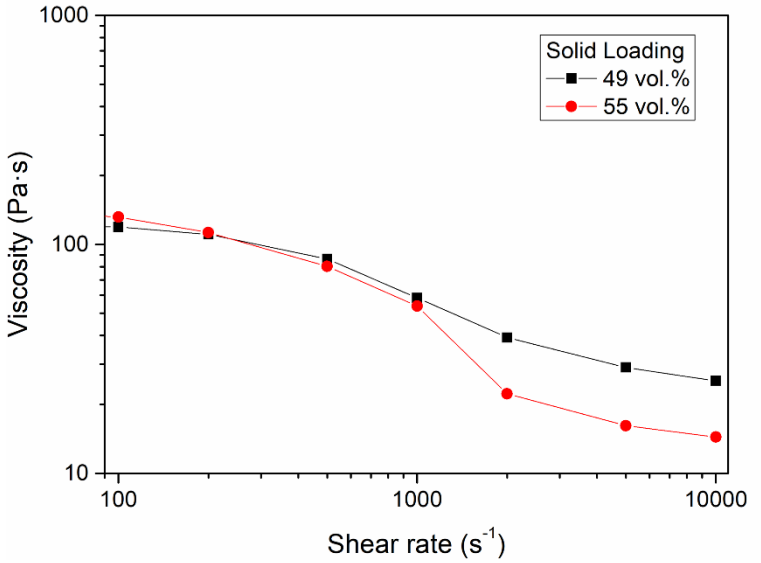

Figure 21. Viscosity behaviour of the Ti_3SiC_2 PEG/PP feedstocks at shear rates between 100 and 10000 s^{-1}.

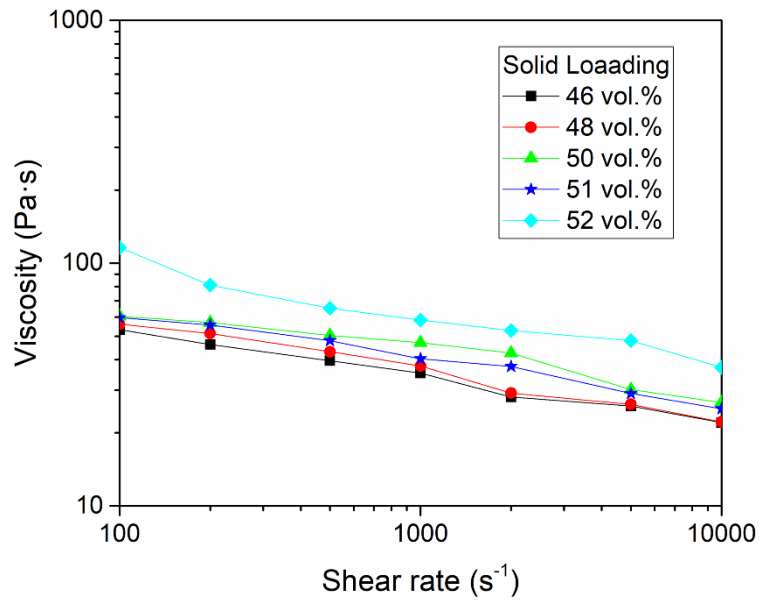

Figure 22. Viscosity behaviour of the Cr_2AlC PEG/PP feedstocks at shear rates between 100 and 10000 s^{-1}.

With all this, PEG/PP feedstocks of Ti_3SiC_2 and Cr_2AlC MAX phases were developed and characterised in terms of their rheological properties. The optimal solid loadings were selected at 49 vol.% and 51 vol.% for Ti_3SiC_2 and Cr_2AlC feedstocks, respectively. Although some injection trials were carried out for these feedstocks, no further results are shown for these materials. PEG/PP feedstocks were used for the additive manufacturing process as it can be seen in **Section 3.6**.

After verifying the ability of the feedstocks to be injected a semi-automatic low-pressure injector was used (AB-400, A.B. Machinery, US). This equipment allows using smaller

amounts of feedstocks for a laboratory scale production. Pneumatic pressure is applied by a cylinder to the barrel filled with material with an approximate volume of 100 cm^3. The parameters that can be controlled in the equipment are temperature, injection pressure, clamp pressure and injection and waiting times. The mould used was rectangular shaped with 60x8x4 mm dimensions. Mould temperature can also be adjusted, although for all injected samples the mould was at room temperature since the variation of this parameter didn't affect noticeably the quality of the injected parts. Ti_3SiC_2 PEG/CAB feedstocks were injected at 200 ºC with an injection time of 5 seconds and a pressure of 600 kPa. On the other hand, Cr_2AlC PEG/CAB feedstocks were injected at 220 ºC with an injection time of 5 seconds applying 600 kPa for the injection pressure.

Results of powder injection moulding of Ti_3SiC_2 PEG/CAB feedstocks can be found in **Chapter 6 Section 6.2** [15] where the most relevant findings of the PIM process are shown in a scientific publication.

3.4.4 Debinding

As commented earlier, a two-step debinding process was selected for the correct elimination of the polymeric binder. Firstly, PEG was removed from the green samples by solvent debinding. For this purpose, distilled water was employed at 60 ºC. Samples were placed in a metal grate used to raise the samples, favouring a greater contact of the samples with water. In addition, a magnetic stirrer was used to promote binder degradation. The process was carried out for 5 h and samples were dried in air at 90 ºC for 2 h, to eliminate all the water content in the samples.

To eliminate the backbone from the green samples, a thermal debinding process was carried out, placing the sample in an alumina crucible covered with 1 mm diameter zirconia balls. Samples were introduced in a debinding furnace (GD-DC-50, Goceram, Sweden) and the conditions used for the correct degradation of the polymers were for PEG/CAB feedstocks: heating rate of 2 ºC/min, holding time of 1 h at 360 ºC and a cooling rate of 5 ºC/min. All the process was performed under argon protective atmosphere. In the case of PEG/PP feedstocks, the same heating and cooling rates were used, but this time the maximum temperature was raised to 450 ºC.

Samples were weighted before and after each debinding step to calculate the amount of polymer loss during the processes. This calculation was done following Equation 12 and Equation 13:

Equation 12 $$\%PEG\ Removed = \frac{w_i - w_{sd}}{w_{PEG}} \cdot 100$$

Equation 13 $$\%Backbone\ Removed = \frac{w_{sd} - w_{td}}{w_{Backbone}}$$

Where, w_i corresponds to the initial weight of the samples, w_{sd} to the weight after solvent debinding, w_{PEG} is the theoretical amount of PEG in the feedstock, w_{td} is the weight after thermal debinding and $w_{Backbone}$ the theoretical amount of Backbone (CAB or PP) in the mixtures.

Debinding tests of Ti_3SiC_2 PEG/CAB feedstocks can be found in **Chapter 6 Section 6.2** [15] where the most relevant findings of the PIM process are shown in a scientific publication..

3.4.5 Sintering and sample characterisation

Brown samples were sintered under vacuum ($2{,}5x10^{-5}$) atmosphere in a tubular furnace (HVT-15/50/450, Carbolite, UK) with heating and cooling rates of 5 ºC/min and a holding time of 6 hours at 1300 ºC.

Density of the samples was measured by Archimedes method explained in **Section 3.3.1**, although, for a better calculation of the porosity of the samples, density was measured by vacuum infiltration, following Archimedes principles but, in this case, introducing the samples in ethanol and applying vacuum for 30 minutes, to ensure a correct infiltration of the ethanol through the open porosity in the samples. Weight measurements of the samples directly correlates to the amount of porosity, and it is possible to calculate open and closed porosity using Equation 14 to Equation 17:

Equation 14 $$\rho = W_d \cdot \rho_{ethanol} / W_i - W_a$$

Equation 15 $$Porosity_{total}(\%) = (1 - \rho/\rho_t) \cdot 100$$

Equation 16 $$Porosity_{open}(\%) = (W_i - W_d / W_i - W_a) \cdot 100$$

Equation 17 $$Porosity_{closed}(\%) = Porosity_{total} - Porosity_{open}$$

where, *W* is the weight of the samples at different stages of the test (*d*=dry, *i*=infiltrated and *a*=after infiltration). ρ is the calculated density and ρ_t the theoretical density. In addition, and similarly to the weight measurements, dimensions of the samples were measured to calculate the shrinkage (dimensional change) of the samples during the process following Equation 18:

Equation 18 $$Shrinkage(\%) = \frac{d_{sintered} - d_{green}}{d_{green}} \cdot 100$$

Where d corresponds to the dimension to be measured (volume, length, height or width) for the sintered and green samples.

Furthermore, mechanical properties of the sintered samples were measured. Vickers hardness measurements were performed in a Zwick Roell Z 2.5 tester with a force of 10 N. Additionally, Young's modulus and elastic and plastic work was measured using a load application speed of 1 mm/min and a speed of 2 mm/min for load removal during the indentation.

Sintering and characterisation of Ti_3SiC_2 PEG/CAB feedstocks can be found in **Chapter 6 Section 6.2** [15] where the most relevant findings of the PIM process are shown in a scientific publication.

As an example, Cr_2AlC PEG/CAB samples at different stages of the injection process are shown in Figure 23. It is possible to observe the shrinkage of the samples while performing the debinding processes and, more noticeably, after the sintering. Total volumetric shrinkage of the Cr_2AlC samples is 22,5%. Sintered samples obtained from the Cr_2AlC feedstocks with 51 vol.% of solid loading exhibited a total porosity of 30%.

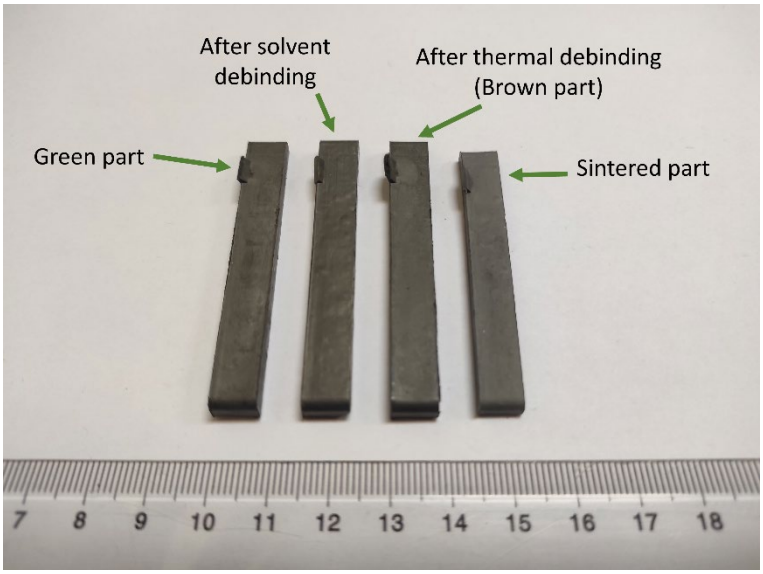

Figure 23. Samples of Cr_2AlC PEG/CAB at different stages of the injection process.

3.5 Composite Extrusion Modelling

Within all the techniques that encompasses additive manufacturing, Composite Extrusion Modelling (CEM) is the best suited for the 3D printing of powder with irregular morphology, due to the lack of the flexibility requirements of filament production. This technique is based on the material extrusion of feedstocks in pellet form. By heating the material inside the barrel, a screw is responsible for the extrusion of the fused feedstock through a nozzle and deposited layer-by-layer in the bed.

3.6.1 Sample design and 3D printing

In 3D printing the geometry to be printed needs to be modelled firstly in a Computer-Aided Design (CAD) program. In this work, Solid Edge 2021 (Siemens, Germany) was used for the design of the geometries. After design, files need to be configured in a layer-based object, defining the strokes that the printer needs to do in order to build the printed samples. This process is called slicing and there is a big number of programs that offer this tool. In this research different programs were used indistinctly to create the ".stl" (sliced files) for the printing: Ultimaker Cura and Simplify 3D. Printing parameters most commonly are defined by the geometry to be printed and the feedstock being used. Although the exact parameters are discussed in depth in **Chapter 7 Section 7.1** [16] and **Section 7.2**, a summary of the most common printing parameters for MAX phases Ti_3SiC_2 and Cr_2AlC PEG/CAB feedstocks used in this work are shown in Table 6.

Table 6. Printing parameters of Ti_3SiC_2 and Cr_2AlC MAX phase PEG/CAB feedstocks.

Material	Ti_3SiC_2	Cr_2AlC
Nozzle Diameter (mm)	0,6	0,6
Extrusion speed (steps per unit)	550	650
Extruder Temperature (ºC)	210	230
Bed Temperature (ºC)	50	50
Printing speed (mm/s)	5	5

Two different printers were used during this work. First of all, ExAM 255 3D printer (AIM3D, Germany) (Figure 24-a) was used as an initial trial for the printing of MAX phases. This equipment is a large-scale printer with the possibility of printing continuously, thanks to the automatic material feeder that can contain up to 1 litre of material. The second one was a pellet extrusion head (V4 Pellet Extruder, IAMTech, Spain) (Figure 24-b) that can be mounted in most of the commercially available polymer filament printers. In this case, the extruder head was mounted in a TL-D3 Pro (Tenlog, China). It is worth noting that all published results in **Chapter 7** are results from the V4 pellet extruder.

Firstly, different nozzle diameters were used (0,2 - 0,8 mm), and although with 0,4 mm good quality samples were obtained, some obstruction problems appeared with this nozzle size. Finally, a 0,6 mm nozzle was selected for all the printing adjustments. Printing parameter optimisation was performed by obtaining good quality samples and analysing the cross-section of the printed parts in an optical microscope (VHX 500 3D microscope, Keyence, Japan). Delamination on the cross section of the samples implies defects at later stages (debinding and sintering) so, printing parameters were varied until no defects in the internal zones of the samples were found. Furthermore, once a sample

was obtained without mayor internal defects and good surface quality, temperature and extrusion speed were varied to analyse the improvement of the printing parts, performing a subsequent printing parameter optimisation if necessary. In addition, Archimedes density of the samples was measured to be compared to the theoretical density in order to select the optimal printing parameters. Some of the geometries printed during this optimisation process are shown in Figure 25. Samples showed in this figure were printed at RHP Technology GmbH, located in Seibersdorf (Austria) during a research stay.

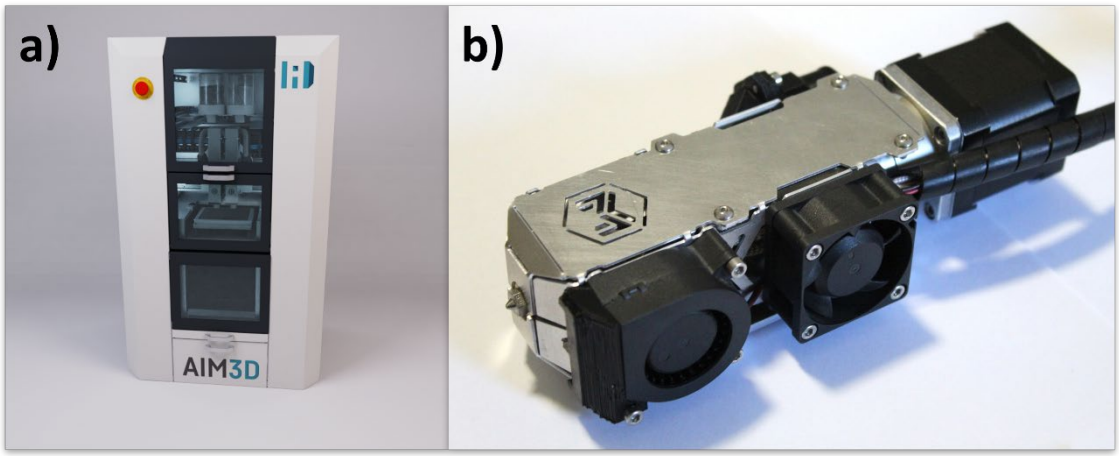

Figure 24. Composite extrusion modelling (CEM) equipments used in this work, a) ExAM 255 and b) V4 pellet extruder.

Figure 25. Image of some of the geometries printed for the optimisation process during this work.

In addition, printing conditions of Ti_3SiC_2 and Cr_2AlC PEG/PP feedstocks were also adjusted. In this case, printing reproducibility wasn't achieved for the PEG/PP feedstocks. Even with a low solid content of the Ti_3SiC_2 feedstock of 49 vol%, the screw extrusion of the feedstock through the small nozzles used for 3D printing caused the cough of the nozzle creating inconsistencies in the deposition of the material. Some of the printed trials were successful, but due to the lack of printing reproducibility with the same printing parameters, results on these feedstocks are not shown in this work.

3.6.2. Debinding, sintering and sample characterisation

A two-step debinding process was selected for the printed samples, similarly to the PIM samples. Firstly, a solvent debinding was performed, using stirred distilled water at 60 ºC for 5 h for the PEG removal. Subsequently, and after drying the samples, a thermal debinding was performed, in a debinding furnace, for 1 h at 500 ºC, with heating and cooling rates of 0,5 ºC/min and 1 ºC/min, respectively for both MAX phases. Compared to the PIM process, lower heating and cooling rates are selected in this case to avoid the delamination of the samples during the process. In addition, a higher temperature is selected this time to ensure a complete elimination of the binders, thus, reducing the apparition of mayor defects during the sintering process, due to the brittle nature of the printed samples.

Sintering was performed under vacuum atmosphere (2,5 x 10^{-5}) in a tubular furnace, at 1300 ºC for 6 h, with heating and cooling rates of 5 ºC/min for both MAX phases. As for PIM, samples were weighted and measured after every step of the process, in order to control the amount of binder removed, densities and shrinkage of the samples. Further information on the debinding and sintering properties of Ti_3SiC_2 and Cr_2AlC PEG/CAB feedstocks can be found in **Chapter 7 Section 7.1** [16] and **Section 7.2** where the most relevant findings of the CEM process are shown in a scientific publication.

In addition, mechanical properties of the sintered samples were measured. Vickers hardness measurements were performed in a Zwick Roell Z 2.5 tester with a force of 10N. Additionally, Young's modulus and elastic and plastic work was measured using a load application speed of 1 mm/min and a speed of 2 mm/min for load removal during the indentation.

References

[1] E. Tabares, A. Jiménez-Morales, S.A. Tsipas, Study of the synthesis of MAX phase Ti3SiC2 powders by pressureless sintering, Bol. La Soc. Esp. Ceram. y Vidr. (2020). https://doi.org/10.1016/j.bsecv.2020.01.004.

[2] J.M. Córdoba, M.J. Sayagués, M.D. Alcalá, F.J. Gotor, Synthesis of Ti3SiC2 powders: Reaction mechanism, J. Am. Ceram. Soc. 90 (2007) 825–830. https://doi.org/10.1111/j.1551-2916.2007.01501.x.

[3] J.O. Andersson, T. Helander, L. Höglund, P.F. Shi, B. Sundman, Thermo-Calc and DICTRA, Computational tools for materials science., Calphad. 26 (2002) 273–312. https://doi.org/S0364-5916(02)00037-8.

[4] J. Gonzalez-Julian, S. Onrubia, M. Bram, O. Guillon, Effect of sintering method on the microstructure of pure Cr2AlC MAX phase ceramics, J. Ceram. Soc. Japan. 124 (2016) 415–420. https://doi.org/10.2109/jcersj2.15263.

[5] L.O. Xiao, S.B. Li, G. Song, W.G. Sloof, Synthesis and thermal stability of Cr2AlC, J. Eur. Ceram. Soc. 31 (2011) 1497–1502. https://doi.org/10.1016/j.jeurceramsoc.2011.01.009.

[6] S. Hashimoto, M. Takeuchi, K. Inoue, S. Honda, H. Awaji, K. Fukuda, S. Zhang, Pressureless sintering and mechanical properties of titanium aluminum carbide, Mater. Lett. 62 (2008) 1480–1483. https://doi.org/10.1016/j.matlet.2007.09.005.

[7] W. Ping, M. Bing-chu, H. Xiao-lin, Z. Wei-bing, Synthesis of Ti2AlC by hot pressing and its mechanical and electrical properties, Trans. Nonferrous Met. Soc. China. 17 (2007) 3–6. https://doi.org/https://doi.org/10.1016/S1003-6326(07)60215-5.

[8] S. Cui, I.H. Jung, J. Kim, J. Xin, A coupled experimental and thermodynamic study of the Al-Cr and Al-Cr-Mg systems, J. Alloys Compd. 698 (2017) 1038–1057. https://doi.org/10.1016/j.jallcom.2016.12.298.

[9] K. Das, P. Choudhury, S. Das, The Al-O-Ti (Aluminum-oxygen-titanium) system, J. Phase Equilibria. 23 (2002) 525–536. https://doi.org/10.1361/105497102770331271.

[10] M.A. El Saeed, F.A. Deorsola, R.M. Rashad, Optimization of the Ti3SiC2 MAX phase synthesis, Int. J. Refract. Met. Hard Mater. (2012). https://doi.org/10.1016/j.ijrmhm.2012.05.001.

[11] S.B. Li, H.X. Zhai, Y. Zhou, Z.L. Zhang, Synthesis of Ti3SiC2 powders by

mechanically activated sintering of elemental powders of Ti, Si and C, Mater. Sci. Eng. A. 407 (2005) 315–321. https://doi.org/10.1016/j.msea.2005.07.043.

[12] J. Ureña, E. Tabares, S. Tsipas, A. Jiménez-Morales, E. Gordo, Dry sliding wear behaviour of β-type Ti-Nb and Ti-Mo surfaces designed by diffusion treatments for biomedical applications, J. Mech. Behav. Biomed. Mater. 91 (2019). https://doi.org/10.1016/j.jmbbm.2018.12.029.

[13] Z. Doni, A.C. Alves, F. Toptan, J.R. Gomes, A. Ramalho, M. Buciumeanu, L. Palaghian, F.S. Silva, Dry sliding and tribocorrosion behaviour of hot pressed CoCrMo biomedical alloy as compared with the cast CoCrMo and Ti6Al4V alloys, Mater. Des. 52 (2013) 47–57. https://doi.org/10.1016/j.matdes.2013.05.032.

[14] R.M. German, Injection molding of metals and ceramics, Princeton New Jersey : Metal Powder Industries Federation, Princeton (New Jersey), 1997. https://doi.org/doi.org/10.4271/982417.

[15] E. Tabares, S.C. Cifuentes, A. Jiménez-Morales, S.A. Tsipas, Injection moulding of porous MAX phase Ti3SiC2 without using space-holder, Powder Technol. 380 (2021) 96–105. https://doi.org/10.1016/j.powtec.2020.11.022.

[16] E. Tabares, M. Kitzmantel, E. Neubauer, A. Jimenez-Morales, S.A. Tsipas, Extrusion-based Additive Manufacturing of Ti3SiC2 and Cr2AlC MAX phases as candidates for High Temperature Heat Exchangers, J. Eur. Ceram. Soc. (2021). https://doi.org/10.1016/j.jeurceramsoc.2021.10.042.

[17] K. Kamide, Molecular properties of cellulose and cellulose derivatives, in: Cellul. Cellul. Deriv., 2005: pp. 189–444. https://doi.org/https://doi.org/10.1016/B978-0-444-82254-3.X5000-0.

[18] P.E. Gongwer, H. Arisawa, T.B. Brill, Kinetics and products from flash pyrolysis of cellulose acetate butyrate (CAB) at 460-600°C, Combust. Flame. 109 (1997) 370–381. https://doi.org/10.1016/S0010-2180(96)00188-5.

[19] C. Abajo, J. Hidalgo, A. Jiménez-Morales, J.M. Torralba, Optimisation of eco-friendly binary binder system for powder injection moulding, Powder Metall. 57 (2014) 196–203. https://doi.org/10.1179/1743290114Y.0000000089.

[20] D. Lin, D. Sanetrnik, H. Cho, S.T. Chung, Y.S. Kwon, K.H. Kate, B. Hausnerova, S. V. Atre, S.J. Park, Rheological and thermal debinding properties of blended elemental Ti-6Al-4V powder injection molding feedstock, Powder Technol. 311 (2017) 357–363. https://doi.org/10.1016/j.powtec.2016.12.071.

[21] N.P. Cheremisinoff, Product design and testing of polymeric materials, Marcel Dekker, New York, USA, 1990. https://doi.org/10.1002/pola.1991.080290918.

[22] A. de Waele, Viscosimetry and plastometry, J. Oil Colour Chem. Assoc. 6 (1923) 33–80.

[23] R.M. German, Powder Injection Molding, Metal Powder Industries Federation, Princeton (New Jersey), ISBN 9780918404954, 1990.

[24] D. Bleyan, B. Hausnerova, P. Svoboda, The development of powder injection moulding binders: A quantification of individual components' interactions, Powder Technol. 286 (2015) 84–89. https://doi.org/10.1016/j.powtec.2015.07.046.

[25] B. Hausnerova, B.N. Mukund, D. Sanetrnik, Rheological properties of gas and water atomized 17-4PH stainless steel MIM feedstocks: Effect of powder shape and size, Powder Technol. 312 (2017) 152–158. https://doi.org/10.1016/j.powtec.2017.02.023.

CHAPTER 4

SYNTHESIS OF MAX PHASES

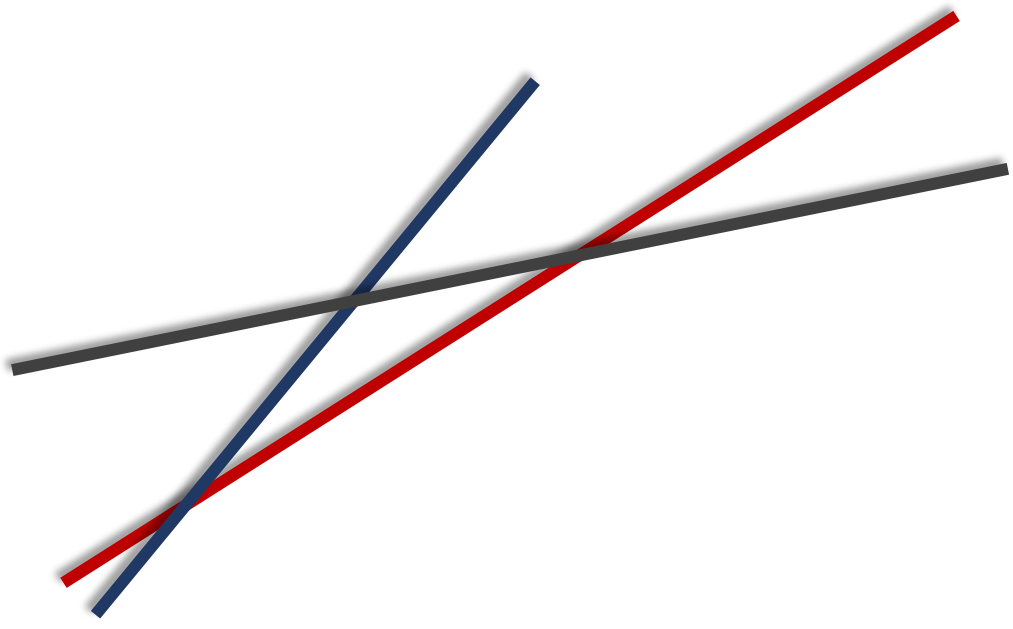

Contents

4.1 Study of the synthesis of MAX phase Ti_3SiC_2 powders by pressureless sintering 125

4.1 Study of the synthesis of MAX phase Ti_3SiC_2 powders by pressureless sintering

Authors: Eduardo Tabares, Antonia Jiménez-Morales, Sophia A. Tsipas

Departamento de Ciencia e Ingeniería de Materiales e Ingeniería Química, IAAB, Universidad Carlos III de Madrid, Avda. de la Universidad, 30, 28911 Leganés, Madrid, Spain

Journal: Boletín de la Sociedad Española de cerámica y vidrio
Publisher: ELSEVIER; ISSN: 0366-3175; Category: Materials Science, Ceramics
Position: 7 of 29 (Q1) IMPACT FACTOR: 2.383 (JCR 2020)

Scope of this paper:

The first objective of this PhD thesis is the synthesis of high purity MAX phases for the later processing by PIM and AM. For this purpose, this scientific publication exhibits the study of the Ti_3SiC_2 MAX phase synthesis. Several molar ratios and initial powders were studied varying the heat treatment temperatures and the phases present after the pressureless sintering process were analysed. All samples were characterised by XRD and SEM to control the phase evolution of the Ti_3SiC_2 synthesis. In addition, the synthesis mechanism was studied through thermodynamic calculations and a reaction mechanism for the selected powder mixtures is proposed. Finally, a specific mixture is further analysed with the variation of the heat treatment time and particle size of the initial powders to study their effect on the Ti_3SiC_2 synthesis, obtaining high purity powders. From this work, powders of Ti_3SiC_2 with a purity of 94 vol.% were synthesised using Ti/SiC/C as initial powders with a molar ratio of 3:1.5:0.5, adjusting the heat treatment at 1300 ºC for 6 h under vacuum conditions.

Graphical Abstract:

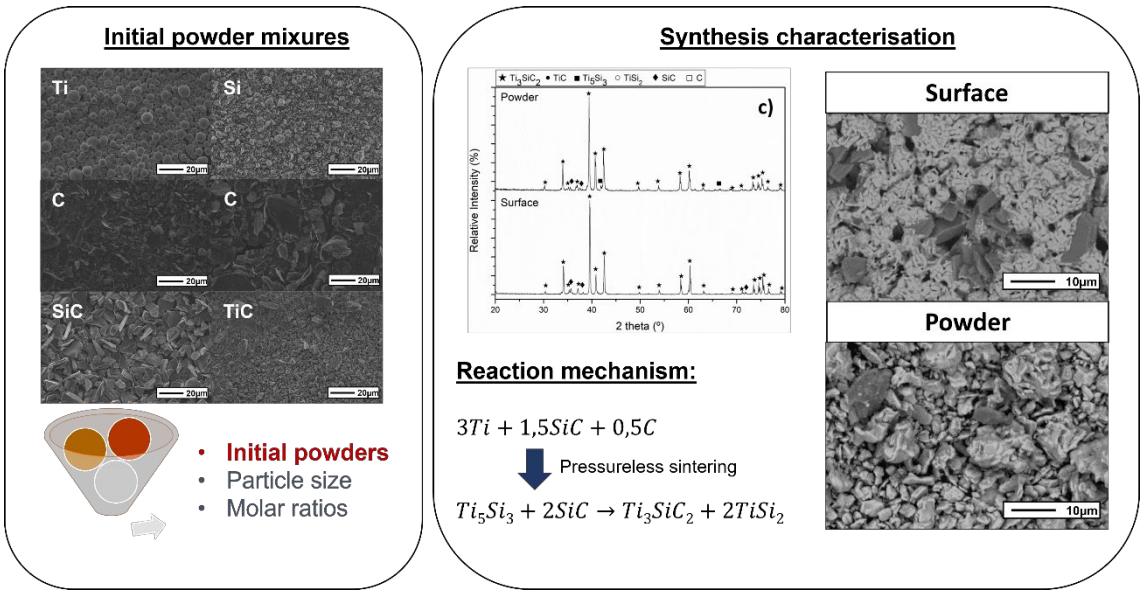

BOLETIN DE LA SOCIEDAD ESPAÑOLA DE
Cerámica y Vidrio
www.elsevier.es/bsecv

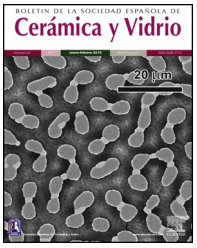

Original

Study of the synthesis of MAX phase Ti_3SiC_2 powders by pressureless sintering

*Eduardo Tabares, Antonia Jiménez-Morales, Sophia Alexandra Tsipas**

Departamento de Ciencia e Ingeniería de Materiales e Ingeniería Química, IAAB, Universidad Carlos III de Madrid, Avda. de la Universidad, 30, 28911 Leganés, Madrid, Spain

ARTICLE INFO

Article history:
Received 29 July 2019
Accepted 10 January 2020
Available online 5 February 2020

Keywords:
MAX phase synthesis
Ti_3SiC_2
Powder metallurgy

ABSTRACT

MAX phases exhibit excellent combination of ceramic and metallic-like properties. In this work, MAX phase Ti_3SiC_2 powder was synthesized starting-off with different combinations of elemental powders and carbides. The powders used were Ti, Si, C, SiC and TiC in different combinations, molar ratios and powder size. Powders were heat treated on a vacuum furnace for different times and temperatures for in situ production of the Ti_3SiC_2 MAX phase. High purity synthesized samples were analyzed by X-ray diffraction (XRD) and scanning electron microscopy (SEM) in order to identify and quantify the different phase constituents present. The main phase constituents in the powders produced were Ti_3SiC_2 and $TiSi_2$. Up to 94% of Ti_3SiC_2 MAX phase was obtained using Ti:SiC:C as starting powders in a molar ratio of 3:1.5:0.5. Different phase constitution was observed on the surface and the centre of the samples. An optimal starting powder composition, molar ratio, heat treatment temperature and time is proposed for the formation of high purity Ti_3SiC_2 MAX phase. Selected mixture was studied thermodynamically and a reaction mechanism of formation of the MAX phase is proposed.

Estudio de la síntesis de polvos de la fase MAX Ti_3SiC_2 por sinterización sin presión

Palabras clave:
Síntesis de fases MAX
Ti_3SiC_2
Pulvimetalurgia

RESUMEN

Las fases MAX presentan una excelente combinación de propiedades cerámicas y metálicas. En este trabajo se sintetizaron polvos de fase MAX Ti_3SiC_2 a partir de diferentes combinaciones de polvos elementales y carburos. Los polvos utilizados fueron Ti, Si, C, SiC y TiC en diferentes combinaciones, proporciones molares y tamaño de partícula. Los polvos se sinterizaron en un horno de vacío a diferentes tiempos y temperaturas para la producción

* *Corresponding author.*
E-mail address: stsipas@ing.uc3m.es (S.A. Tsipas).
https://doi.org/10.1016/j.bsecv.2020.01.004

in situ de la fase MAX Ti_3SiC_2. Las muestras sintetizadas de alta pureza se analizaron mediante difracción de rayos X (XRD) y microscopía electrónica de barrido (SEM) para identificar y cuantificar las diferentes fases constituyentes presentes. Las principales fases constituyentes en los polvos producidos fueron de Ti_3SiC_2 y $TiSi_2$. Se obtuvo hasta un 94% de fase MAX Ti_3SiC_2 utilizando como polvos de partida Ti:SiC:C en una proporción molar de 3:1,5:0,5. Se observó diferente formación de fase en la superficie y en el centro de las muestras. Finalmente, se propone una composición óptima de polvo de partida, relación molar, temperatura de sinterización y tiempo para la formación de la fase MAX de Ti_3SiC_2 de alta pureza. La mezcla seleccionada se estudió termodinámicamente y se propone un mecanismo de reacción para la formación de la fase MAX.

Introduction

MAX phases are known for their excellent combination of both metallic (high electrical and thermal conductivity, machinability, high tolerance to damage) and ceramic (stiffness, good mechanical properties at high temperature, corrosion and oxidation resistance) properties [1]; hence, amongst other, these materials are promising candidates as high temperature components for both structural and functional applications [2]. These family of materials are defined like ternary compounds with a general formula of $M_{n+1}AX_n$ where M is an early transition metal, A is an element from groups IIIA and IVA of the periodic table, X either carbon or nitrogen and n a number between 1 and 3 [1,3]. They show a hexagonal crystalline structure (space group $P6_3/mmc$) where layers of the elements M and X are intercalated with a layer of the element A. Furthermore, due to their nanolaminated structure, MAX phases show good shock absorption resistance by the formation of kink bands. In particular, Ti_3SiC_2 presents low density ($\rho = 4.52\ g/cm^3$), high Young's modulus ($E = 339–343\ GPa$) and higher fracture toughness than ceramics ($K_{IC} = 5–20\ MPa\ m^{1/2}$). Additionally, Ti_3SiC_2 has a good thermal and electrical conductivity ($\lambda = 34\ W/m\ K$, $\sigma_e = 4.5 \times 10^6\ S/m$) [3–6].

Titanium silicon carbide (Ti_3SiC_2) has been one of the most widely studied compounds of MAX phases. The difficulty in synthesizing high purity or single phase in either powder or bulk form has lead researchers to study different processing approaches and optimize its synthesis since Ti_3SiC_2 was firstly synthesized in the 1960s [7]. For bulk Ti_3SiC_2 samples some of the synthesis routes reported are summarized below. Goto and Hirai [8] reported on the synthesis of the MAX phase by chemical vapour deposition (CVD) using $TiCl_4$, $SiCl_4$ and CCl_4 and applying an electronic current to a graphite substrate at deposition temperatures of 1300–1600 °C. Barsoum and El-Raghy reported the synthesis of Ti_3SiC_2 by hot pressing (HP) [6] applying pressures of 40 MPa at 1600 °C starting from Ti, Si and C powders in a stoichiometric proportion of 3:1:2. Later, they published a work based on the synthesis of the MAX phase by hot isostatic pressing (HIP) [3] with temperatures ranging from 1450 to 1700 °C applying 40 MPa of pressure starting with a mixture containing SiC instead of elemental Si. They study the reaction path of the mixture proposing as intermediate phases during the synthesis TiC_x and Ti_3SiC_x. Ti:Si:TiC mixtures in a molar ratio of 1:1:2 have been used by Gao et al. to obtain Ti_3SiC_2 through spark plasma sintering (SPS) [9], with pressures from 20 to 60 MPa and temperatures between 1125 and 1400 °C obtaining dense samples with a 2 wt.% of TiC impurities. Through pulse discharge sintering (PDS) nearly full density Ti_3SiC_2 (99 wt.%) has been obtained with TiC as a secondary phase and at a temperature range between 1200 and 1450 °C [10].

Furthermore, the production of Ti_3SiC_2 powders has also been extensively investigated through different techniques. Sun et al. [11] obtained an 81 wt.% of Ti_3SiC_2 through solid–liquid reaction (S–L) using NaF in the mixture of Ti, Si and graphite at 1300 °C. Self-propagating high temperature synthesis (SHS) has also been studied as a cost efficient technique; El Saeed et al. obtained purity as high as 88% starting from a mixture of Ti:SiC:C with a molar ratio of 3:1.2:0.8 [12] obtaining TiC as secondary phase. Pressureless sintering (PS) has also been studied by Córdoba et al. [13] for the synthesis of MAX phase Ti_3SiC_2. In this work they studied different molar ratios and starting powders under Ar atmosphere obtaining up to a 98% purity at 1400 °C. Most common starting point of these methods is the use of elemental powders of the MAX phase (Ti, Si, C) and carbides (SiC, TiC) in different molar ratios. Other works propose the formation of Ti_3SiC_2 by using titanium hydride (TiH_2) as starting powder [14]. In these works, authors report a secondary or intermediate phase present during the synthesis, generally, titanium or silicon carbides and titanium silicides. An excess of silicon in the initial stoichiometric composition is a common strategy used for a higher purity of Ti_3SiC_2 in order to compensate the evaporation of Si during heat treatments [12,13,15] and therefore the formation of secondary phase TiC. Nevertheless, this excess Si has to be controlled since it can produce high amounts of titanium silicides ($TiSi_2$, Ti_5Si_3). In addition, the presence of titanium carbide can be an indicator of a decomposition process of Ti_3SiC_2 [16]. Also, other studies propose the addition of aluminium in the starting mixtures in low quantities to activate the reaction mechanism of the synthesis [17–20]. An overall important problematic of these techniques is the high temperatures needed, the sophisticated and expensive equipment required for high purity synthesis of Ti_3SiC_2 MAX phase and the low yield of MAX phase.

This work pretends to propose and study thoroughly a cost-efficient route (pressureless sintering) of MAX phase powder

Table 1 – Summary of initial mixtures reported for successful synthesis of Ti_3SiC_2 used in this work.

Authors	Initial powders	Molar ratios	Technique	Phases
Sun [10]	Ti:Si:C	5:2:3	PDS	Ti_3SiC_2, TiC, $TiSi_2$
Sun [10]	Ti:SiC:C	5:2:1	PDS	Ti_3SiC_2, TiC, $TiSi_2$
El Saeed [12]	Ti:SiC:C	3:1.2:0.8	SHS	Ti_3SiC_2, TiC
Córdoba [13]	TiC:Si	3:1	PS	Ti_3SiC_2, TiC, Ti_5Si_3
Córdoba [13]	Ti:SiC	3:2	PS	Ti_3SiC_2, TiC, $TiSi_2$, Ti_5Si_3
Córdoba [13]	Ti:SiC:C	3:1.5:0.5	PS	Ti_3SiC_2, TiC
Li [15]	Ti:SiC:C	3:1.1:2	SHS	Ti_3SiC_2, TiC, Ti_5Si_3
Ngai [21]	Ti:Si:C	3:1.2:1.8	MA-PS	Ti_3SiC_2, SiC, $TiSi_2$
Yang [22]	Ti:Si:TiC	1:1:2	PS	Ti_3SiC_2, TiC
Yang [22]	Ti:Si:TiC	2:2:3	PS	Ti_3SiC_2, TiC

Table 2 – Detailed list of initial powders used and their characterization.

Powder	Supplier	D_{50} (μm)	D_{90} (μm)	Purity (%)
Ti	TLS Technik GmbH, Germany	8.36	14.23	99
Si	Alfa Aesar GmbH, Germany	3.95	9.68	99.9
C_c	Ismaf, Spain	23.78	57.60	99.5
C_f	Alfa Aesar GmbH, Germany	13.03	30.81	99
SiC	Navarro SiC S.A., Spain	11.98	20.89	99.5
TiC	MaTeck GmbH, Germany	7.81	20.36	99

preparation with high purity content of Ti_3SiC_2 using a simple synthesis technique. For this purpose, different initial conditions in terms of starting powder and molar ratios have been analyzed and varied to achieve this objective, starting from initial mixtures based on the literature described in the previous paragraphs, summarized in Table 1, as well as novel ratios. In addition, the technique proposed allows for easy scaling-up process in order to be able to produce high amount of MAX phase in powder form. Finally, in order to understand the formation of the Ti_3SiC_2 phase, the ΔG of different possible reactions is calculated and a formation mechanism is proposed and discussed.

Materials and methods

Synthesis of the MAX phase Ti_3SiC_2 was studied starting from commercially available elemental powders and carbides, summarized in Table 2. Particle size distribution was obtained by laser diffraction obtaining mean particle size of the powders represented in number (MasterSizer2000, Malvern Instruments, UK). In addition, initial powders micrographs are shown in Fig. 1. All powders have an irregular morphology except for titanium powders that have spherical shape. Moreover, two types of graphite have been used, nomenclature stands for their particle size distribution: C_c for a coarser powder and C_f for fine particles.

Different mixtures were prepared, varying initial powders, powder particle size and molar ratios. Each powder combination was mixed in a Turbula shaker mixer (WAB, Switzerland) for 1 h and compacted uniaxially at 200 MPa to obtain discs of 16 mm diameter and 3 mm thickness. Green samples were heat treated in an alumina crucible with heating and cooling rates of 5 °C/min up to the selected heat treatment temperature for 2 h; vacuum atmosphere (2.5×10^{-5} bar) was employed (HVT-15/50/450, Carbolite, UK). Heat treated samples were analyzed by X-ray diffractometry (XRD, Philips X'pert, Netherlands) with Cu K_α radiation at 40 kV and 40 mA as well as scanning electron microscopy (SEM, XL-30 Philips, US) coupled with energy-dispersive X-ray spectroscopy (EDS, EDAX, US) in order to study and quantify the phases present after the thermal cycle. XRD spectra can

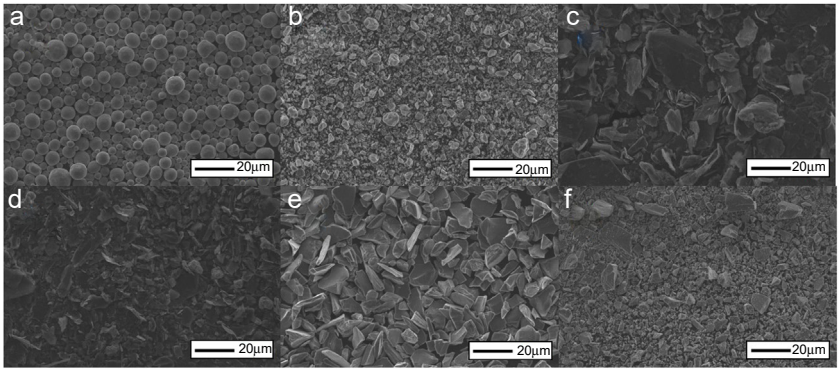

Fig. 1 – Micrographs of commercial powders used in this work: (a) Ti, (b) Si, (c) coarse graphite (C_c), (d) fine graphite (C_f), (e) SiC and (f) TiC.

be found as supplementary information. Due to the layered structure of Ti_3SiC_2, prior to quantification it was verified that the relative intensities of XRD peaks were consistent with random orientation. Quantification of phases was calculated as reported elsewhere [13], using Eq. (1), where I_x is the integrated area of most intense peak of the phase to be analyzed (Ti_3SiC_2 (104), Ti_8C_5 (024), TiC (200), Ti_5Si_3 (211), $TiSi_2$ (131), SiC (111) and C (002)) and I_t the total sum of the integrated area of most intense peak for all representative present phases. Integrated areas were calculated by least-square procedure. These calculated percentages were compared to Rietveld refinement to study the validity of this quantification method.

$$\% \ \text{Phase} = \frac{I_x}{I_t} \quad (1)$$

After heat treatment, selected samples were crushed in an agate mortar and studied thoroughly comparing the XRD patterns and SEM micrographs of powders obtained with those of the bulk sample surface. Differential thermal analysis (DTA, SETSYS Evolution, SETARAM Instrumentation, France) was performed at a heating rate of 10 °C/min to 1500 °C to study the reaction. Furthermore, reaction mechanism and intermediate phase reactions have been studied by thermodynamic calculations of ΔG using Thermo-Calc software (Sweden) with database SSOL5 and SSUB5 [23].

Results and discussions

Effect of initial powder molar ratio and surface diffusion on phase constitution

In order to be able to narrow down and determine optimal powder ratios, different mixtures of powders and molar ratios were produced. As commented in the introduction, these mixtures were selected attending to previous reported work using different synthesis techniques [10,12,13,15,21,22] as well as self-established ratios. Table 3 shows the detected phases for mixtures prepared with different molar ratios, initial powders and graphite size. In order to reduce the number of variables, the heat treatment temperature was set to 1300 °C for 2 h, with the objective of studying in depth the compositions with higher formation or MAX phase at these conditions. Although this temperature might not be the optimum for some of the mixtures prepared, it is selected as a relatively low temperature compared to reported synthesis conditions presented previously.

Table 3 – List of initial compositions, molar ratios and phases present (XRD) after heat treatment at 1300 °C for 2 h in vacuum atmosphere. Graphite nomenclature stands for c (coarse) and f (fine), according to their powder size distribution. In brackets, calculated amount of phase for mixtures with Ti_3SiC_2 formation.

Initial powders	Molar ratios	Phases
Ti:Si:C_c	3:1.2:1.8	Ti_5Si_3/C/Ti_8C_5
Ti:Si:C_f	3:1.2:1.8	Ti_5Si_3/TiC/C
Ti:SiC:C_c	3:1.2:0.6	Ti_8C_5/C/Ti_5Si_3
Ti:SiC:C_f	3:1.2:0.6	Ti_8C_5/C/Ti_5Si_3
Ti:Si:C_c	3:1.2:0.9	TiC/Ti_5Si_3/C
Ti:Si:TiC	1:1:2	Ti_3SiC_2(47)/TiC(53)
Ti:Si:TiC	2:2:3	Ti_3SiC_2(34)/TiC(66)
TiC:Si	3:1	Ti_3SiC_2(85)/TiC(15)
Ti:SiC:C_c	3:1.5:0.5	Ti_3SiC_2(94)/SiC(6)
Ti:SiC:C_f	3:1.5:0.5	Ti_3SiC_2(93)/SiC(5)/C(2)
Ti:Si:C_f	3:1.1:2	Ti_3SiC_2(71)/C(9)/TiC(20)
Ti:SiC:C_c	5:2:1	Ti_3SiC_2(71)/Ti_8C_5(28)/C(2)
Ti:SiC:C_f	5:2:1	Ti_3SiC_2(65)/Ti_8C_5(34)/C(1)
Ti:Si:C_c	3:1.1:3.1	Ti_3SiC_2(63)/Ti_8C_5(18)/C(5)/SiC(5)/TiC(9)
Ti:Si:C_f	3:1.1:3.1	Ti_3SiC_2(82)/TiC(13)/C(5)
Ti:Si:C_c	3:1.1:2	Ti_3SiC_2(67)/C(7)/TiC(26)
Ti:SiC	3:2	Ti_3SiC_2(90)/SiC(6)/$TiSi_2$(4)
Ti:Si:C_c	5:2:3	Ti_3SiC_2(59)/C(11)/TiC(30)
Ti:Si:C_f	5:2:3	Ti_3SiC_2(71)/Ti_8C_5(29)

To validate the method used for the quantification of phases, which uses the integrated area of the most representative peaks, a Rietveld refinement was performed on selected diffractograms to determine and compare the adjustment of this technique. Results for both methods as well as goodness of fit (GOF) value of the Rietveld analysis are shown in Table 4; GOF is a quality value and it is established that for values between 1.09 and 1.28 there is a good refinement [24]. Rietveld refinement shows a similar phase constitution as the calculated with the integrated areas, with a maximum difference of 6% in phase constitution. Although 6% can be a high difference, all results for Rietveld refinement show higher purity than the studied with integrated area. Taking into account that Rietveld analysis might yield a higher purity, integrated area analysis is considered as a valid method and used for further quantification.

Regarding initial molar ratios, it is noticeable how selecting optimal molar ratios is essential to ensure MAX phase formation. From the phase quantifications performed and shown in Table 3, it can be seen that near stoichiometry ratios tend to have a higher Ti_3SiC_2 content during the synthesis.

Table 4 – Comparison of phase quantification with Rietveld refinement and integrated areas calculations.

Mixture analyzed		Ti_3SiC_2 phase amount with Rietveld analysis (%)	Ti_3SiC_2 phase amount with Integrated areas analysis (%)	GOF
Ti:Si:C 3:1.1:3.1	[a]	67	63	1.16
Ti:SiC:C 3:1.1:2	[b]	98	92	1.29

[a] Sample heat treated at 1300 °C for 2 h.
[b] Sample heat treated at 1400 °C for 2 h.

Table 5 – Quatification of detected phases (XRD) present in selected mixtures (surface and powders) after heat treatment in vacuum atmosphere at 1300 °C temperature for 2 h.

Initial mixture	Sample	Detected phases (%)					
		Ti_3SiC_2	TiC	$TiSi_2$	Ti_5Si_3	C	SiC
Ti:Si:C_f	Surface	82	13	–	–	5	–
3:1.1:3.1	Powder	83	10	–	–	7	–
Ti:SiC	Surface	91	–	3	–	–	6
3:2	Powder	83	–	11	–	–	6
Ti:SiC:C_c	Surface	94	–	–	–	–	6
3:1.5:0.5	Powder	90	–	–	5	–	5

Furthermore, as commented previously, increasing the amount of atomic percentage of silicon also increases MAX phase formation due to the sublimation during heat treatment at high temperatures [12,13,15]. The influence of graphite particle size is not clear since, depending on the mixture, it appears to either increase or reduce the amount of MAX phase formation. From these results three different mixtures were selected for further analysis (Ti:Si:C_f = 3:1.1:3.1, Ti:SiC = 3:2 and Ti:SiC:C_c = 3:1.5:0.5) attending to the final content of Ti_3SiC_2 and intermediate phases produced during the synthesis.

In addition to initial molar ratios, diffusion also plays an important role on the samples' final phase constitution. Detected phases on the surface of the samples often differ from those present on the interior of the sample [25]. Selected mixtures, according to the amount of Ti_3SiC_2 phase formed, were crushed into powders to study and identify the phases present in the internal zone of the sample (Table 5 and Fig. 2). As expected, diffusion on the surface of samples is different than at the centre. Generally, there is a loss of purity in the synthesis and in some cases, new phases

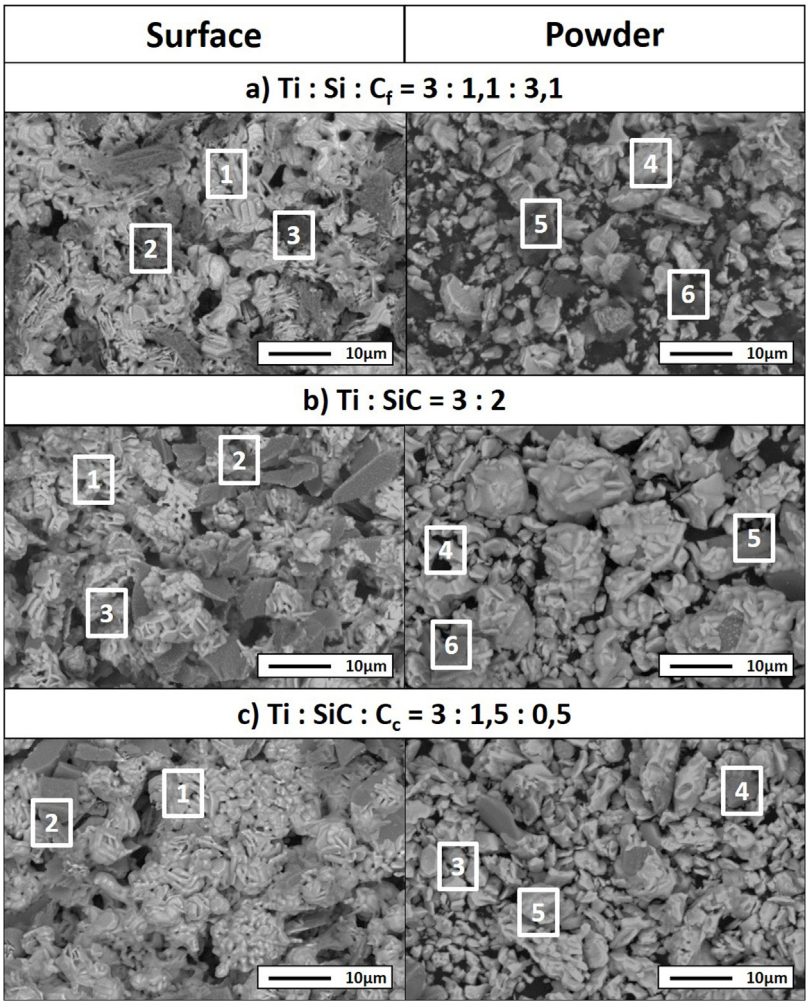

Fig. 2 – SEM micrographs of (a) Ti:Si:C_f = 3:1.1:3.1, (b) Ti:SiC = 3:2 and (c) Ti:SiC:C_c = 3:1.5:0.5 of surface (left) and powders (right).

Table 6 – EDS point analysis of mixtures Ti:Si:C_f = 3:1.1:3.1, Ti:SiC = 3:2 and Ti:SiC:C_c = 3:1.5:0.5 for points shown in Fig. 2.

Sample	Sample	Analysis point	Element (at %)			Phase
			Ti	Si	C	
Ti:Si:C_f	Surface	1	58	20	22	Ti_3SiC_2
3:1.1:3.1		2	67	2	31	TiC
		3	1	4	95	C
	Powder	4	52	16	32	Ti_3SiC_2
		5	7	49	53	SiC
		6	2	2	96	C
Ti:SiC	Surface	1	49	23	28	Ti_3SiC_2
3:2		2	7	44	49	SiC
		3	31	69	–	$TiSi_2$
	Powder	4	56	23	21	Ti_3SiC_2
		5	5	54	41	SiC
		6	27	70	3	$TiSi_2$
Ti:SiC:C_c	Surface	1	57	23	20	Ti_3SiC_2
3:1.5:0.5		2	3	71	26	SiC
	Powder	3	47	24	29	Ti_3SiC_2
		4	1	53	46	SiC
		5	65	34	1	Ti_5Si_3

appear that are not present on the surface (Ti_5Si_3). These new phases are intermediate products produced during the synthesis process, corroborating the diffusion difference between zones in the sample. Decrease in purity is observed once powders are obtained (Table 5) for samples Ti:SiC = 3:2 and Ti:SiC:C_c = 3:1.5:0.5. However, for mixture Ti:Si:C_f with a molar ratio of 3:1.1:3.1 there is a small increase on the final amount of Ti_3SiC_2 in the powder. This can be due to the higher reactivity of elemental silicon, having in this case a better diffusion compared to the SiC, which is present in the other mixtures studied.

From micrographs in Fig. 2 it is clear how there is a different reaction mechanism occurring depending on the starting mixture. Point analysis results are shown in Table 6. For mixture (a) (Ti:Si:C_f = 3:1.1:3.1) the formation of the MAX phase is combined with second phases of TiC and C that has not reacted, according to XRD. In the microstructure (Fig. 2a) a lighter majoritarian phase is observed, corresponding to Ti_3SiC_2, and also secondary darker phases can be seen (Points 2, 3, 5 and 6 in Fig. 2a) which probably correspond to TiC, C and SiC, respectively, attending to EDS analysis. The presence of TiC during the synthesis of Ti_3SiC_2 from elemental powders can be either an intermediate product prior to the formation of the Ti_3SiC_2 phase, or a result of its decomposition [16]. Examination of the milled powder shows the presence of SiC (Point 5 in Fig. 2a); however, this phase was not detected by XRD. Unreacted graphite was detected both in the surface and in the milled powder, suggesting that the initial powder ratios where not optimal. Therefore, this starting composition is disregarded as an optimal mixture.

For Ti:SiC = 3:2 (mixture (b) in Fig. 2), XRD shows the presence of SiC and $TiSi_2$ in addition to Ti_3SiC_2, and this is in accordance with the microstructure observed by SEM. However, in the SEM micrographs, a great difference can be observed between the phases detected at the surface, where a large amount of secondary darker phase can be distinguished, and the milled powder, where less amount of this secondary phase is observed. The presence of intermediate phases such as $TiSi_2$ suggests that the synthesis of Ti_3SiC_2 could be optimized with this initial powder ratio, by adjusting the thermal cycle. However, due to the large differences between the microstructures observed and the amount of MAX phase present in the milled powders and in the surface, this mixture was not considered for further optimization.

A good candidate is mixture Ti:SiC:C_c = 3:1.5:0.5 (mixture (c) in Fig. 2) since there is a high amount of Ti_3SiC_2 phase both at the surface and in the milled powders (Points 1 and 2 in Fig. 2c). At the surface it can be observed how the only secondary phase present is SiC (Point 2 in Fig. 2c, darker zones in the micrographs), that exists in lower amount compared to Ti:SiC = 3:2. Analyzing the microstructure of the milled powders it can be seen how the lighter phase predominates, corresponding to MAX phase Ti_3SiC_2. Darker zones correspond to SiC that still is present from the initial powder mixture (Point 4 in Fig. 2c), but in a low amount. Another intermediate phase is present in the powders due to the different diffusion mechanism depending on the zone of the sample. From EDS analysis it can be deduced that this phase corresponds to Ti_5Si_3 (Point 5 in Fig. 2c). The absence of remnant graphite from the initial mixture and the intermediate phases present suggest that the formation of MAX phase is incomplete but still possible, an adjustment of the thermal cycle could further enhance the formation of Ti_3SiC_2 for this molar ratio. Therefore, this molar ratio was selected for further optimization and study of the synthesis mechanism.

Reaction mechanism of the Ti_3SiC_2 synthesis

There are different intermediate reactions that can be occurring during the synthesis process, some of them are shown in Table 7, together with their calculated ΔG. These proposed reactions have been calculated in concordance with the secondary/intermediate phases obtained during the synthesis. According to the thermodynamic calculations performed using Thermo-Calc, over 1000 °C all of the reactions are spontaneous, with the exception of reaction $Ti + 2SiC \rightarrow TiSi_2 + 2C$,

Table 7 – Gibbs free energy calculation of different possible reactions during the synthesis process at temperature range from 1000 °C to 1400 °C.

Reaction	ΔG [J]				
	1000 °C	1100 °C	1200 °C	1300 °C	1400 °C
$3Ti + SiC + C \rightarrow Ti_3SiC_2$ (I)	-3.45×10^5	-3.43×10^5	-3.40×10^5	-3.37×10^5	-3.34×10^5
$Ti + C \rightarrow TiC$ (II)	-1.69×10^5	-1.67×10^5	-1.66×10^5	-1.64×10^5	-1.63×10^5
$5Ti + 3SiC \rightarrow Ti_5Si_3 + 3C$ (III)	-3.96×10^5	-3.98×10^5	-4.00×10^5	-4.02×10^5	-4.04×10^5
$Ti + 2SiC \rightarrow TiSi_2 + 2C$ (IV)	1.18×10^3	5.38×10^2	-1.56×10^2	-9.05×10^2	-1.71×10^3
$6Ti + 5SiC \rightarrow Ti_5Si_3 + TiSi_2 + 5C$ (V)	-3.95×10^5	-3.98×10^5	-4.00×10^5	-4.03×10^5	-4.05×10^5
$Ti_5Si_3 + 2SiC \rightarrow Ti_3SiC_2 + 2TiSi_2$ (VI)	-7.83×10^4	-8.19×10^4	-8.56×10^4	-8.96×10^4	-9.37×10^4
$TiC + Ti_5Si_3 + 3SiC \rightarrow 2Ti_3SiC_2 + 4Si_{(g)}$ (VII)	4.73×10^5	4.37×10^5	4.01×10^5	3.64×10^5	3.28×10^5
$TiC + 2TiSi_2 + SiC \rightarrow Ti_3SiC_2 + 4Si_{(g)}$ (VIII)	5.60×10^5	5.27×10^5	4.94×10^5	4.61×10^5	4.27×10^5

that is spontaneous over 1200 °C, and reactions (VII) and (VIII) that are not favourable for all temperatures. The first reaction presented corresponds to the formation of the MAX phase from the initial powder mixture that has been selected for optimization. This powder mixture starts from Ti, SiC and C to produce Ti_3SiC_2; this reaction is spontaneous for all temperatures analyzed, so it could be a possible formation mechanism. The reactions and ΔG for the formation of intermediate compounds Ti_5Si_3 and $TiSi_2$ are also presented. The ΔG for the formation of these compounds is in the same order of magnitude and slightly more negative than the formation of Ti_3SiC_2, with the exception of the formation of $TiSi_2$ from Ti and SiC. Therefore, it is energetically favourable that these compounds will form as secondary phases, as observed previously. The reaction products of the formation of these secondary phases, include C, that could promote the formation of Ti_3SiC_2 at other stages of the synthesis.

Differential thermal analysis (DTA) was carried out to the mixture Ti/SiC/C_c with a molar ratio of 3:1.5:0.5 to understand further the reaction mechanism (Fig. 3a). It can be seen that there is a big range of temperatures where a phase transformation is happening and for further analysis, compacted samples were heat treated at these different temperatures to identify the phases present after each thermal treatment performed under vacuum atmosphere for 6 h. Evolution of calculated phases obtained from XRD analysis is shown in Fig. 3b.

It is observed that at 1000 °C elemental titanium, from the starting mixture, has fully reacted to form TiC and intermetallic Ti_5Si_3; and MAX phase Ti_3SiC_2 begins to form. Indeed, ΔG calculation presented in Table 7 corroborated that the formation of Ti_5Si_3 is energetically favourable at this temperature. With the increase of temperature there is a higher amount of formation of MAX phase Ti_3SiC_2 and a decrease in the amount of the intermediate phases. In addition, graphite has completely reacted at 1300 °C and no more graphite appears to be present at higher temperatures. TiC that forms during the initial stages of the synthesis process is not detected at 1300 °C and, subsequently, at 1400 °C is again detected. This is in concordance with work reported by other authors [16] where the presence of TiC as final element when this phase is not present in the initial mixture is an indication of a possible decomposition of the Ti_3SiC_2 phase. The amount of Ti_3SiC_2 synthesized in the mixture increases with temperature and reaches the highest at 1300 °C. Graphite, SiC and Ti_5Si_3 slowly decrease with the increase of temperature as a sign of a reaction with the rest of elements. TiC and Ti_5Si_3 are the two intermediate phases formed at 1000 °C in this representation of the synthesis process. These intermediate phases react with the rest of phases (C and SiC) present to form the MAX phase. At 1300 °C $TiSi_2$ starts to be present as an intermediate product of the synthesis and this is also in concordance with the ΔG calculations performed

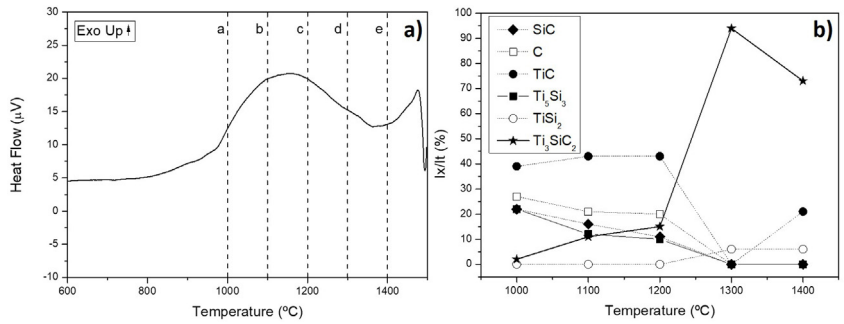

Fig. 3 – (a) DTA analysis of mixture Ti:SiC:C_c with a molar ratio of 3:1.5:0.5 and (b) phase evolution obtained by XRD profiles after a heat treatment under vacuum atmosphere for 6 h at different temperatures (a – 1000 °C, b – 1100 °C, c – 1200 °C, d – 1300 °C, e – 1400 °C).

Table 8 – Summary of phase percentage of mixture Ti:SiC:C_c = 3:1.5:0.5 heat treated at 1300 °C increasing the isothermal time from 2 to 6 h.

Time	Sample	Detected phases (%)			
		Ti_3SiC_2	Ti_5Si_3	$TiSi_2$	SiC
2 h	Surface	94	–	–	6
	Powder	90	5	–	5
4 h	Surface	95	2	–	3
	Powder	92	–	–	8
6 h	Surface	98	2	–	–
	Powder	94	–	6	–

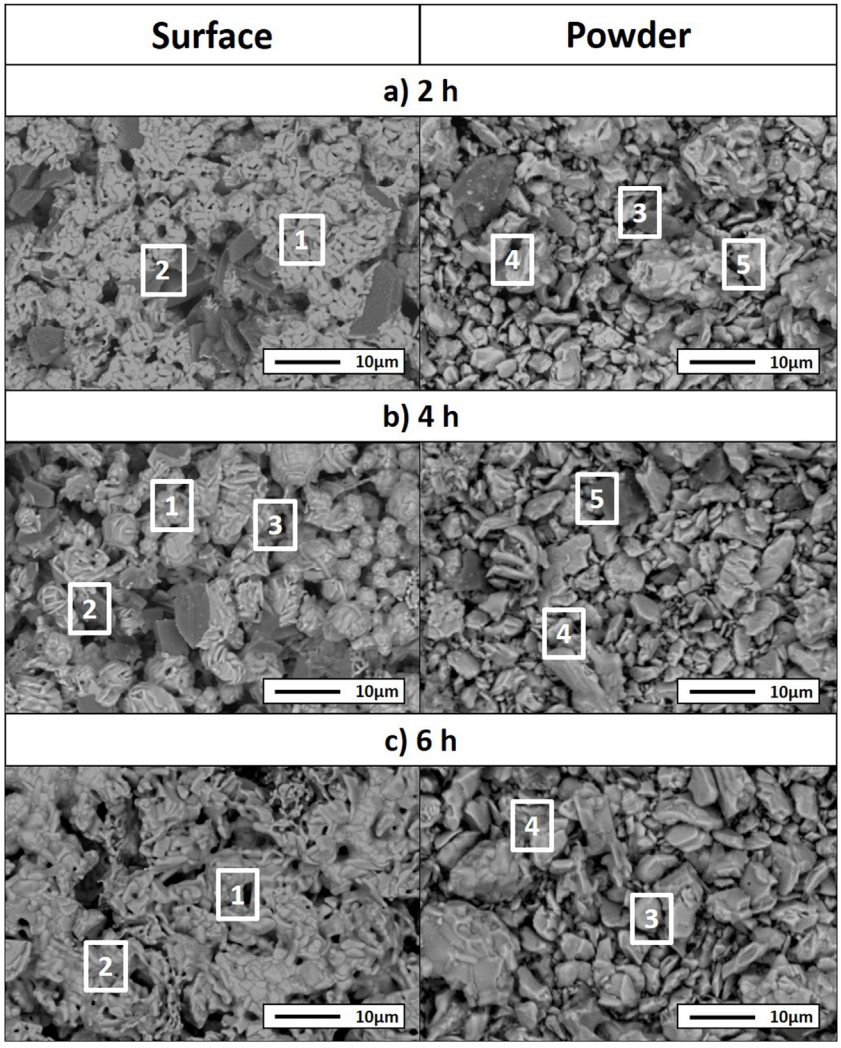

Fig. 4 – SEM micrographs of the surface (left) and powders (right) of the samples Ti:SiC:C_c with a molar ratio of 3:1.5:0.5 heat treated at 1300 °C for different holding times: (a) 2 h, (b) 4 h and (c) 6 h.

where this subproduct reaction begins to be spontaneous at 1200 °C.

Considering that the highest amount of Ti_3SiC_2 was obtained from the selected mixture at a temperature of 1300 °C, this was established as the optimum synthesis temperature. Subsequently, isothermal holding times were varied, to further study the reaction mechanism. In this case, time was increased from 2 h to 4 and 6 h and, as before, bulk sample surface and powders were analyzed to study diffusion differences. Table 8 shows the influence that the isothermal holding time has on the synthesis of Ti_3SiC_2 through XRD analysis of the samples. Formation of the MAX phase is higher with the increment of time. Up to a 94% of Ti_3SiC_2 is obtained for a heat treatment temperature of 1300 °C and an isothermal time of 6 h. Micrographs in Fig. 4 show how from SiC powders a phase transformation occurs, where in a first stage the intermediate phase Ti_5Si_3 is formed. The reaction of SiC with Ti to form Ti_5Si_3 (reaction (III) in Table 7)

Table 9 – EDS point analysis of mixture Ti:SiC:C_c = 3:1.5:0.5 heat treated at 1300 °C for points shown in Fig. 4.

Heat treatment time	Sample	Analysis point	Element (at %)			Possible phase
			Ti	Si	C	
2 h	Surface	1	51	19	30	Ti_3SiC_2
		2	1	55	44	SiC
	Powder	3	45	19	36	Ti_3SiC_2
		4	5	51	44	SiC
		5	60	37	3	Ti_5Si_3
4 h	Surface	1	50	21	29	Ti_3SiC_2
		2	1	57	42	SiC
		3	59	36	5	Ti_5Si_3
	Powder	4	58	20	22	Ti_3SiC_2
		5	1	53	46	SiC
6 h	Surface	1	53	22	25	Ti_3SiC_2
		2	62	35	3	Ti_5Si_3
	Powder	3	55	22	23	Ti_3SiC_2
		4	32	64	4	$TiSi_2$

is thermodynamically favourable for all the temperature range studied. Subsequently transforms Ti_5Si_3 into Ti_3SiC_2 by reaction with SiC and TiC (reaction (VI) in Table 7) which are also thermodynamically favourable. At higher times, there is a complete transformation of SiC into the intermediate phase $TiSi_2$ and MAX phase with no presence of TiC, a phase generally present when the decomposition of Ti_3SiC_2 occurs [16]. The formation of $TiSi_2$ at 1300 °C is in concordance with the thermodynamic calculations preformed that corroborate that it is energetically favourable for temperatures above 1200 °C (reaction (IV) in Table 7). Reactions of the intermediate phases to yield Ti_3SiC_2 and $Si_{(g)}$ (reactions (VII) and (VIII) in Table 7) do not seem to be energetically favourable, and therefore are not proposed as a synthesis mechanism.

Microstructures of the surface and the powders for the different holding times at 1300 °C were studied (as shown in Fig. 4) and composition of the phases present was analyzed by EDS (Point analysis in Table 9). Synthesis for 2 h at 1300 °C, as discussed in the section "Reaction mechanism of the Ti_3SiC_2 synthesis", shows a majority of a lighter phase corresponding to Ti_3SiC_2 (Points 1 and 3 in Fig. 4a) with different second phases. In the surface analysis, there is only presence of a darker phase that corresponds to SiC (Point 2 in Fig. 4). Analyzing milled powders, there are two different darker phases corresponding to SiC and Ti_5Si_3 (Points 4 and 5 in Fig. 4a, respectively). By increasing the holding time to 4 h it can be seen how the amount of SiC (Points 2 and 5 in Fig. 4b) is lower because of its transformation into Ti_3SiC_2 (Points 1 and 4 in Fig. 4b), corresponding to the lighter phase. Again, an intermediate phase appears as a sign of an incomplete transformation into Ti_3SiC_2 (Point 5 in Fig. 4b) that corresponds to Ti_5Si_3. In Fig. 4c the holding time was increased to 6 h, and it can be seen how there is an almost complete transformation to Ti_3SiC_2 (lighter phase Points 1 and 3). There is a difference in the intermediate phases detected considering surface and powders (Points 2 and 4 in Fig. 4c) analyzed corresponding to Ti_5Si_3 and $TiSi_2$ for the surface and powder, respectively, nevertheless the formation of both phases is energetically favourable. It is possible that the addition of C into the starting mixture could enhance the formation of MAX phase with these processing conditions. Nevertheless, the purity reached for this synthesis (94%), with the condition proposed is considered optimal. Although this value is lower than the obtained by Córdoba et al. also by pressureless sintering (98%), in their work they study the synthesis of different mixtures using 100 mg of the initial powders and a more complex synthesis route. In our case, we have developed an easy to scale process also through a simple technique.

From these results, analyzing the variation of isothermal times during the heat treatment, it is possible to establish a reaction mechanism that explains the transformation process with time. Powder analysis after 2 h of heat treatment shows that, in addition to Ti_3SiC_2, the intermediate phases found are SiC, which is present in the initial mixture, and Ti_5Si_3 which is formed according to reaction (III) from Table 7. Increasing heat treatment time to 6 h the phases present are Ti_3SiC_2 and $TiSi_2$. Therefore, SiC has reacted with Ti_5Si_3 to form Ti_3SiC_2, according to Eq. (VI) in Table 7, with impurities of $TiSi_2$. Along with the Ti_3SiC_2 that has already been formed at 2 h (probably according to reaction (I) in Table 7 which is also thermodynamically favourable). The intermediate phases present at this holding

Table 10 – Summary of phase percentage of mixture Ti:SiC:C_f = 3:1.5:0.5 heat treated at 1300 °C increasing the isothermal time from 2 to 6 h.

Time	Sample	Detected phases (%)			
		Ti_3SiC_2	Ti_5Si_3	$TiSi_2$	SiC
2 h	Powder	86	4	5	5
4 h	Powder	90	–	5	5
6 h	Powder	91	–	6	3

time react to produce more Ti_3SiC_2 and $TiSi_2$ (reaction (VI) in Table 7) that is not formed at lower times and temperatures.

Effect of graphite particle size in the synthesis of Ti_3SiC_2

In order to analyze the influence of graphite particle size in the initial mixture during the synthesis process, initial mixture of Ti:SiC:C with a molar ratio of 3:1.5:0.5 starting with smaller graphite particle size (D_{50} = 13.03 μm) was prepared. In this case, the heat treatment temperature was set to 1300 °C and the synthesis process was analyzed with the increase of holding times, as done in the section "Reaction mechanism of the Ti_3SiC_2 synthesis". It is possible to observe from the phase calculations shown in Table 10 how the amount of MAX phase synthesized increases with the increase of isothermal time. Although, in this case, at 6 h there is still presence of SiC in the final powders.

From micrographs, shown in Fig. 5, it is possible to see the same tendency as analyzed before for the mixture with coarser graphite. At 2 h darker areas can be seen that are intermediate phases corresponding to SiC, $TiSi_2$ and Ti_5Si_3 (Points 2, 3 and 4, respectively, in Fig. 5a). At 4 h, intermediate phase Ti_5Si_3 is no longer seen as confirmed by XRD results and EDS analysis, as reported before in the proposed mechanism, this phase reacts with SiC to form Ti_3SiC_2 and $TiSi_2$. These two phases (SiC and $TiSi_2$) are present in the final powders, Points 2 and 3 in Fig. 5b. Increasing the time up to 6 h for this mixture with a finer graphite does not enhance the Ti_3SiC_2 synthesis as studied before. It can be seen how there is still presence of SiC in the final powders as well as intermediate phase $TiSi_2$ (Points 2 and 3 in Fig. 5c). Although phase transformation has not been complete as in the case of Ti:SiC:C_c, there is still a majority of a lighter phase corresponding to Ti_3SiC_2 (Point 1 in Fig. 5) in the final powders (all EDS point analysis are summarized in Table 11). Fig. 6 shows the evolution of detected phases of XRD phase analysis, shown in Tables 8 and 9, for different holding times during the heat treatment process of the two graphite particle sizes analyzed. Comparing these results, it can be seen that the amount of Ti_3SiC_2 formed during the synthesis is of great purity even for the finer graphite (91% at 6 h), but there is a clear difference between both mixtures in terms of secondary phases and final purity. Particle size in the initial mixture does affect to the synthesis process of MAX phase Ti_3SiC_2. In this case, a coarser graphite enhances the synthesis of the MAX phase. In terms of difference between the powders, both of the graphite powders used have a flake-like morphology. Regarding purity, the coarser powders have a higher purity (as showed in Table 1), however, this does not seem to be a determining factor in the synthesis process. Analyzing these results and comparing them to Table 3, it appears that when elemental Si is used as starting powder, the particle size of C has a larger influence on the amount of MAX phase produced. In this case, is more beneficial to use a finer particle size distribution of graphite. On the other hand, when silicon carbide is used in the initial mixture (as for the final mixture selected) there is a smaller influence on the particle size of graphite, but in all cases the use of coarser C seems to favour MAX phase formation. These effects might be due to the reactivity of finer powders that are more critical when using elemental powders in the starting mixture (i.e. Si). When a more

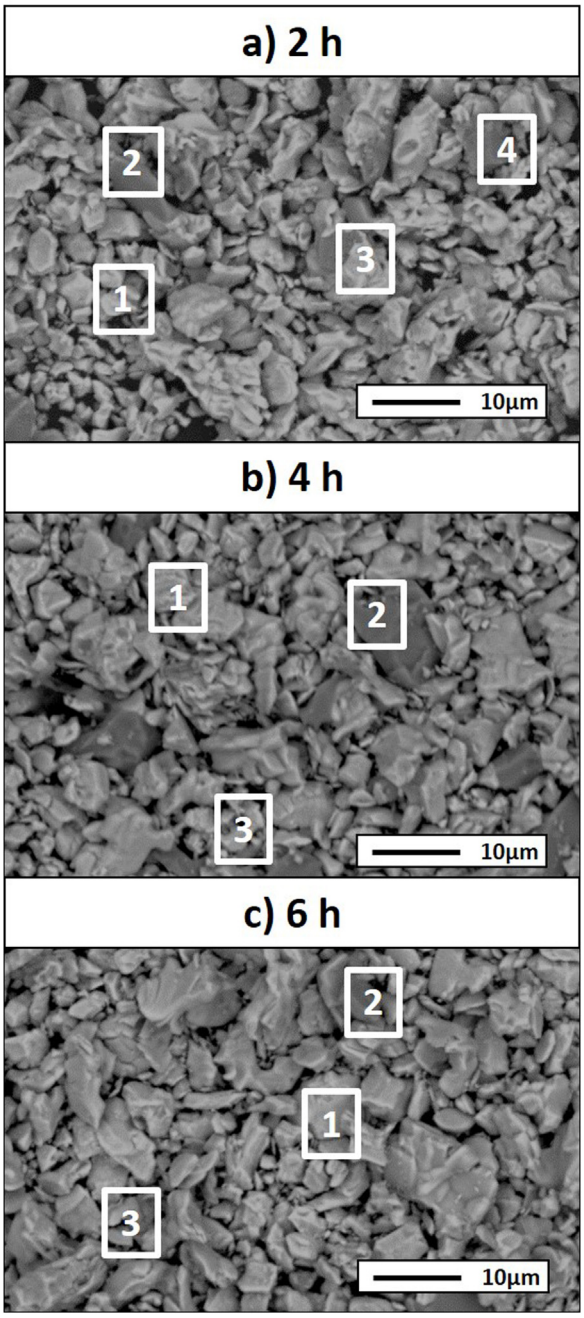

Fig. 5 – SEM micrographs of powders of the samples Ti:SiC:C_f with a molar ratio of 3:1.5:0.5 heat treated at 1300 °C for different holding times: (a) 2 h, (b) 4 h and (c) 6 h.

chemically stable compound is selected, as SiC, the particle size of C is not as determinant. Nevertheless, for SiC in the starting mixture it appears that the use of coarser graphite yields a slightly higher amount of MAX phase. According to XRD results (Fig. 3b), when SiC is used in the starting mixture, even after 2 h at 1000 °C all the Ti present has reacted to form TiC, Ti_5Si_3, and Ti_3SiC_2, since these are the only Ti containing phases and no elemental Ti is present. Reactions (I), (II), (III) and (V) in Table 7 for the reaction of Ti are all thermodynamically favourable at this temperature. It is possible that, when SiC is present, instead of Si, the size

Table 11 – EDS point analysis of mixture Ti:SiC:C_f = 3:1.5:0.5 heat treated at 1300 °C for points shown in Fig. 5.

Heat treatment time	Sample	Analysis point	Element (at %)			Possible phase
			Ti	Si	C	
2 h	Powder	1	50	28	21	Ti_3SiC_2
		2	1	61	38	SiC
		3	32	63	5	$TiSi_2$
		4	61	36	3	Ti_5Si_3
4 h	Powder	1	53	20	27	Ti_3SiC_2
		2	2	55	43	SiC
		3	32	67	1	$TiSi_2$
6 h	Powder	1	63	15	22	Ti_3SiC_2
		2	1	59	40	SiC
		3	38	60	2	$TiSi_2$

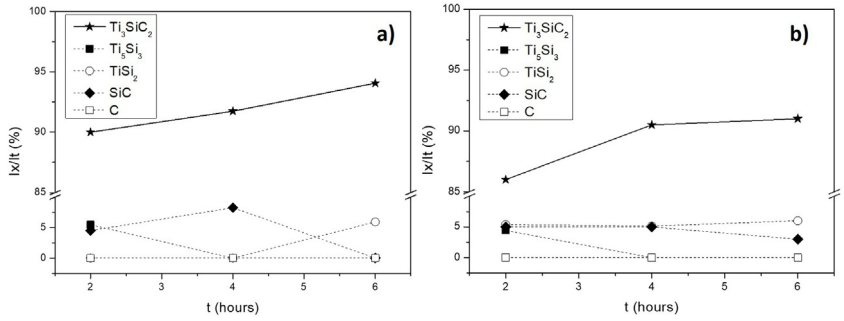

Fig. 6 – Evolution of phases obtained by XRD profiles of mixture (a) Ti:SiC:C_c and (b) Ti:SiC:C_f powders with a molar ratio of 3:1.5:0.5 heat treated at 1300 °C for 2, 4 and 6 h.

of C does not affect significantly due to the high stability of the compound TiC, and C is mostly consumed by reaction with Ti to form TiC. When elemental Si is used, there are more competing reactions and hence a finer more reactive C particle size favours a higher reaction to form Ti_3SiC_2.

Conclusions

Ti_3SiC_2 has been successfully synthesized through pressureless sintering for powder production of this MAX phase. Different conditions of the synthesis have been studied such as, initial compositions (molar ratios, initial powder, particle size) and heat treatment conditions (atmosphere, temperature, time). An optimal synthesis route is proposed with starting powder of Ti:SiC:C_c with a molar ratio of 3:1.5:0.5. The effect on graphite particle size has been studied for this mixture. For the mixture selected, graphite size does not have a significant effect, however, using a coarser graphite enhances slightly the formation of the MAX phase. It has been determined that for mixtures starting from elemental silicon, using a finer particle size of C will be beneficial for the Ti_3SiC_2 synthesis, probably due to the higher reactivity of elemental Si as compared to SiC. A heat treatment cycle at 1300 °C for 6 h under vacuum has been the optimal process for the selected mixture, reaching up to a 94% of Ti_3SiC_2 in an easy to scale-up process. Thermodynamic calculations have been performed and intermediate reactions for the synthesis of MAX phase are proposed considering the intermediate phases observed during the synthesis. A thermodynamically favourable mechanism for the formation of Ti_3SiC_2 is proposed, were intermediate phases of Ti_5Si_3 and SiC react to form Ti_3SiC_2 and $TiSi_2$, in concordance with the evolution of phases observed during the heat treatment process.

Acknowledgements

The authors would like to thank the funding provided for this research by the Regional Government of Madrid (Dir. Gral. Universidades e Investigación) through the project P2018/NMT4411 (ADITIMAT-CM), the Spanish Government through the Ramón y Cajal contract RYC-2014-15014 and the project MAT2012-38650-C02-01.

Appendix A. Supplementary data

Supplementary data associated with this article can be found, in the online version, at doi:10.1016/j.bsecv.2020.01.004.

REFERENCES

[1] M. Barsoum, T. El-Raghy, The MAX Phases: Unique New Carbide and Nitride Materials, 2001, http://dx.doi.org/10.1511/2001.28.736.
[2] G. Song, Y. Wang, Y. Zhou, MAX Phases and Ultra-High Temperature Ceramics for Extreme Environments, IGI Global, USA, 2013, http://dx.doi.org/10.4018/978-1-4666-4066-5.
[3] T. El-Raghy, M.W. Barsoum, Processing and mechanical properties of Ti_3SiC_2: I. Reaction path and microstructure evolution, J. Am. Ceram. Soc. 82 (1999) 2849–2854, http://dx.doi.org/10.1111/j.1151-2916.1999.tb02167.x.

[4] T. El-raghy, M.W. Barsoum, A. Zavaliangos, S.R. Kalidindi, Processing and mechanical properties of Ti_3SiC_2: II. Effect of grain size and deformation temperature, J. Am. Ceram. Soc. 82 (1999) 2855–2860.
[5] M.W. Barsoum, M. Radovic, Elastic and mechanical properties of the MAX phases, Annu. Rev. Mater. Res. 41 (2011) 195–227, http://dx.doi.org/10.1146/annurev-matsci-062910-100448.
[6] M. Barsoum, T. El-Raghy, ChemInform Abstract: Synthesis and Characterization of a Remarkable Ceramic: Ti_3SiC_2, 1996, http://dx.doi.org/10.1111/j.1151-2916.1996.tb08018.x.
[7] W. Jeitschko, H. Nowotny, Die Kristallstruktur von Ti_3SiC_2: ein neuer Komplexcarbid-Typ Monatshefte Für Chemie, Chem. Mon. 98 (1967) 329–337, http://dx.doi.org/10.1007/BF00899949.
[8] T. Goto, T. Hirai, Chemically vapor deposited Ti_3SiC_2, Mater. Res. Bull. 22 (1987) 1195–1201, http://dx.doi.org/10.1016/0025-5408(87)90128-0.
[9] N.F. Gao, J.T. Li, D. Zhang, Y. Miyamoto, Rapid synthesis of dense Ti3SiC2 by spark plasma sintering, J. Eur. Ceram. Soc. 22 (2002) 2365–2370. doi:10.1016/S0955-2219(02)00021-3.
[10] Z.M. Sun, H. Hashimoto, Z.F. Zhang, S.L. Yang, S. Tada, Synthesis and characterization of a metallic ceramic material–Ti_3SiC_2, Mater. Trans. 47 (2006) 170–174, http://dx.doi.org/10.2320/matertrans.47.170.
[11] Z. Sun, Z. Yi, Y. Zhou, Synthesis of Ti_3SiC_2 powders by a solid–liquid reaction process, Scr. Mater. 41 (1999) 61–66, http://dx.doi.org/10.1016/S1359-6462(99)00054-8.
[12] M.A. El Saeed, F.A. Deorsola, R.M. Rashad, Optimization of the Ti_3SiC_2 MAX phase synthesis, Int. J. Refract. Met. Hard Mater. (2012), http://dx.doi.org/10.1016/j.ijrmhm.2012.05.001.
[13] J.M. Córdoba, M.J. Sayagués, M.D. Alcalá, F.J. Gotor, Synthesis of Ti_3SiC_2 powders: reaction mechanism, J. Am. Ceram. Soc. 90 (2007) 825–830, http://dx.doi.org/10.1111/j.1551-2916.2007.01501.x.
[14] J. Yang, X. Zhang, Z. Wang, P. He, L. Gao, S. Dong, Fabrication of Ti_3SiC_2 powders using TiH_2 as the source of Ti 38 (2012) 3509–3512, http://dx.doi.org/10.1016/j.ceramint.2011.12.037.
[15] S.B. Li, H.X. Zhai, Y. Zhou, Z.L. Zhang, Synthesis of Ti_3SiC_2 powders by mechanically activated sintering of elemental powders of Ti, Si and C, Mater. Sci. Eng. A 407 (2005) 315–321, http://dx.doi.org/10.1016/j.msea.2005.07.043.
[16] C. Racault, F. Langlais, R. Naslain, Solid-state synthesis and characterization of the ternary phase Ti_3SiC_2, J. Mater. Sci. 29 (1994) 3384–3392, http://dx.doi.org/10.1007/BF00352037.
[17] H.B. Zhang, Y.C. Zhou, Y.W. Bao, M.S. Li, J.Y. Wang, Intermediate phases in synthesis of Ti_3SiC_2 and $Ti_3Si(Al)C_2$ solid solutions from elemental powders, J. Eur. Ceram. Soc. 26 (2006) 2373–2380, http://dx.doi.org/10.1016/j.jeurceramsoc.2005.04.010.
[18] B. Xu, Q. Chen, X. Li, C. Meng, H. Zhang, M. Xu, J. Li, Z. Wang, C. Deng, Synthesis of single-phase Ti_3SiC_2 from coarse elemental powders and the effects of excess Al, Ceram. Int. 45 (2019) 948–953, http://dx.doi.org/10.1016/j.ceramint.2018.09.270.
[19] Y. Zou, Z. Sun, S. Tada, H. Hashimoto, Effect of Al addition on low-temperature synthesis of Ti_3SiC_2 powder, J. Alloys Compd. 461 (2008) 579–584, http://dx.doi.org/10.1016/j.jallcom.2007.07.090.
[20] Z. Sun, S. Yang, H. Hashimoto, Effect of Al on the synthesis of Ti_3SiC_2 by reactively sintering Ti–SiC–C powder mixtures, J. Alloys Compd. 439 (2007) 321–325, http://dx.doi.org/10.1016/j.jallcom.2006.08.079.
[21] T.L. Ngai, Y. Kuang, Y. Li, Impurity control in pressureless reactive synthesis of pure Ti_3SiC_2 bulk from elemental powders, Ceram. Int. 38 (2012) 463–469, http://dx.doi.org/10.1016/j.ceramint.2011.07.028.
[22] S. Yang, Z.M. Sun, H. Hashimoto, T. Abe, Ti_3SiC_2 Powder Synthesis from Ti/Si/TiC Powder Mixtures, 2003, http://dx.doi.org/10.1016/S0925-8388(03)00039-2.
[23] J.O. Andersson, T. Helander, L. Höglund, P.F. Shi, B. Sundman, Thermo-Calc and DICTRA, computational tools for materials science, Calphad 26 (2002) 273–312, http://dx.doi.org/10.1016/S0364-5916(02)00037-8.
[24] S. Bid, S.K. Pradhan, Preparation of zinc ferrite by high-energy ball-milling and microstructure characterization by Rietveld's analysis, Mater. Chem. Phys. 82 (2003) 27–37, http://dx.doi.org/10.1016/S0254-0584(03)00169-X.
[25] M. Peng, X. Shi, Z. Zhu, M. Wang, Q. Zhang, Facile synthesis of Ti_3SiC_2 powder by high energy ball-milling and vacuum pressureless heat-treating process from Ti–TiC–SiC–Al powder mixtures, Ceram. Int. 38 (2012) 2027–2033, http://dx.doi.org/10.1016/j.ceramint.2011.10.038.

CHAPTER 5

CONVENTIONAL PROCESSING OF MAX PHASES

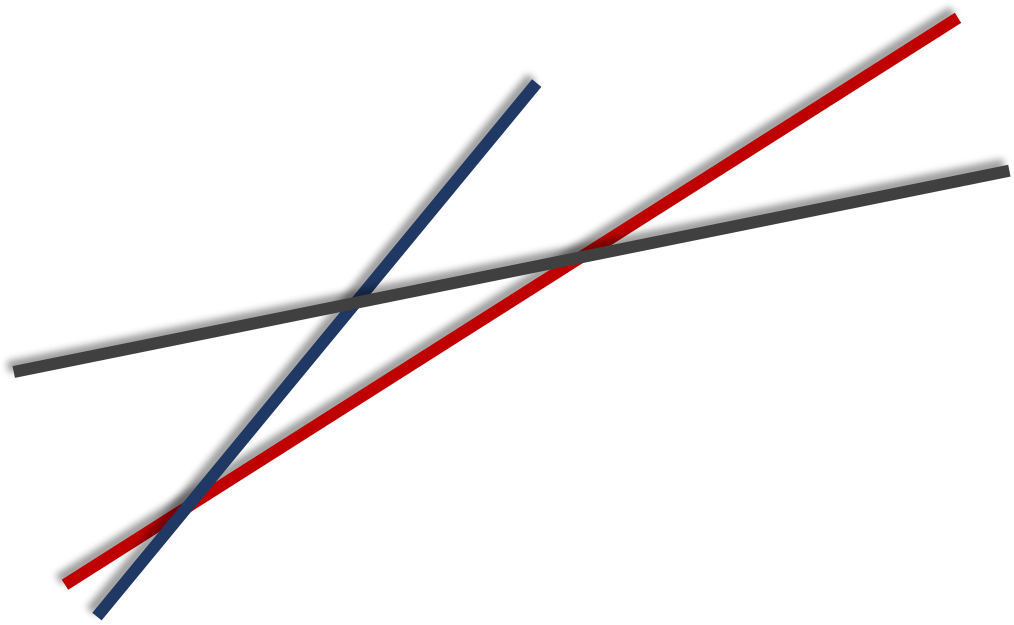

Contents

5.1 Sinterability, mechanical properties and wear behaviour of Ti_3SiC_2 and Cr_2AlC MAX phases 143

5.1 Sinterability, mechanical properties and wear behaviour of Ti_3SiC_2 and Cr_2AlC MAX phases

Authors: Eduardo Tabares[a], Michael Kitzmantel[b], Erich Neubauer[b], Antonia Jiménez-Morales[a], Sophia A. Tsipas[a]

[a] Departamento de Ciencia e Ingeniería de Materiales e Ingeniería Química, IAAB, Universidad Carlos lll de Madrid, Avda. De la Universidad 30, 38911 Leganés, Spain

[b] RHP-Technology GmbH, Forschungs- und Technologiezentrum, A-2444 Seibersdorf, Austria

Journal: Ceramics
Publisher: MDPI; ISSN: 2571-6131; Category: Materials Science, Multidisciplinary | Materials Science

Scope of this paper:

After the study of the synthesis and powder production of MAX phases Ti_3SiC_2 (**Chapter 4**) and Cr_2AlC (**Chapter 3, Section 3.2**) and in order to validate the properties of the synthesised powders, this work intends to analyse different processing techniques. First of all, MAX phase powders were consolidated by uniaxial pressing and sintering, cold isostatic pressing and sintering and hot-pressing. After the optimisation of the sample production, densification of the powders was analysed while maintaining high purity levels of MAX phase. Mechanical characterisation of the samples was carried out by cyclic compressive test. Furthermore, the wear behaviour of the samples was studied by reciprocating sliding, analysing the wear tracks and wear rate of the samples, in order to establish a wear mechanism. From this work, and after analysing the effect of the different processing routes, the stability of the synthesised powders was proven obtaining samples with good mechanical properties and wear behaviour, despite the porosity obtained.

Graphical Abstract:

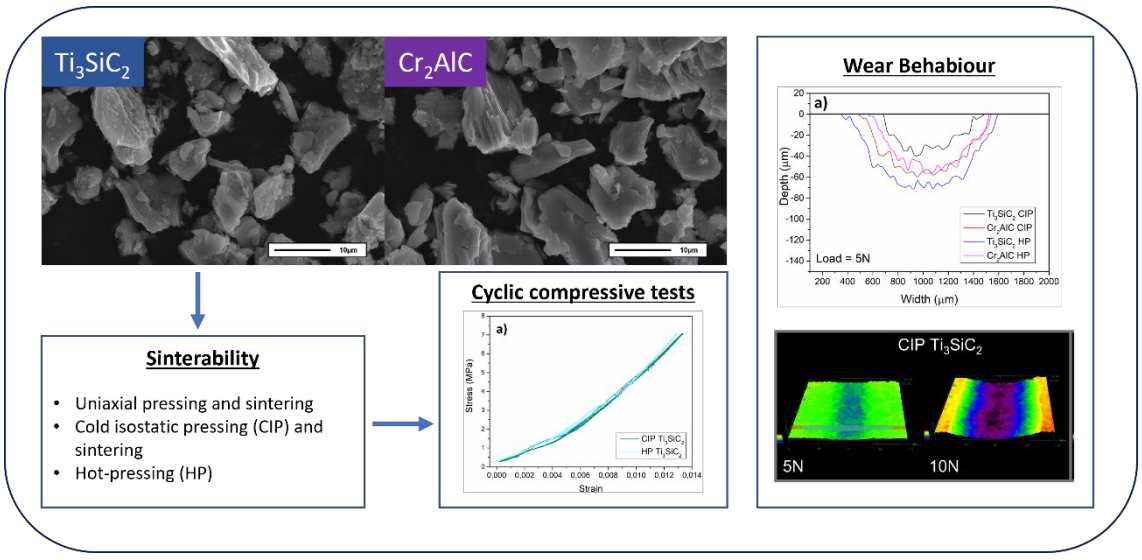

ceramics

MDPI

Article

Sinterability, Mechanical Properties and Wear Behavior of Ti_3SiC_2 and Cr_2AlC MAX Phases

Eduardo Tabares [1], Michael Kitzmantel [2], Erich Neubauer [2], Antonia Jimenez-Morales [1] and Sophia A. Tsipas [1,*]

[1] Departamento de Ciencia e Ingeniería de Materiales e Ingeniería Química, IAAB, Universidad Carlos lll de Madrid, Avda. De la Universidad 30, 38911 Leganés, Spain; etabares@ing.uc3m.es (E.T.); toni@ing.uc3m.es (A.J.-M.)

[2] RHP-Technology GmbH, Forschungs- und Technologiezentrum, 2444 Seibersdorf, Austria; m.ki@rhp.at (M.K.); e.ne@rhp.at (E.N.)

* Correspondence: stsipas@ing.uc3m.es

Abstract: MAX phases are a promising family of materials for several demanding, high-temperature applications and severe conditions. Their combination of metallic and ceramic properties makes MAX phases great candidates to be applied in energy production processes, such as high temperature heat exchangers for catalytic devices. For their successful application, however, the effect of the processing method on properties such as wear and mechanical behavior needs to be further established. In this work, the mechanical and wear properties of self-synthesized Ti_3SiC_2 and Cr_2AlC MAX phase powders consolidated by different powder metallurgy routes are evaluated. Uniaxial pressing and sintering, cold isostatic pressing and sintering and hot pressing were explored as processing routes, and samples were characterized by analyzing microstructure, phase constitution and porosity. Wear behavior was studied by reciprocating-sliding tests, evaluating the wear rate by the loss of material and the wear mechanism.

Keywords: Ti_3SiC_2; Cr_2AlC; MAX phases; reciprocating-sliding; wear behavior; mechanical properties; hot isostatic pressing; powder processing

Citation: Tabares, E.; Kitzmantel, M.; Neubauer, E.; Jimenez-Morales, A.; Tsipas, S.A. Sinterability, Mechanical Properties and Wear Behavior of Ti_3SiC_2 and Cr_2AlC MAX Phases. *Ceramics* **2022**, *5*, 55–74. https://doi.org/10.3390/ceramics5010006

Academic Editors: Margarita A. Torresani and Elisa Torresani

Received: 14 December 2021
Accepted: 29 January 2022
Published: 31 January 2022

1. Introduction

Nanolaminated ternary carbides and nitrides, MAX Phases, are a new family of materials with great potential for different highly demanding and aggressive environments [1,2]. Due to their structure, MAX phases show good mechanical properties at high temperatures [3] with good oxidation and corrosion behaviors, and at the same time, exhibit good electrical and thermal conductivity and are easily machinable [4,5]. MAX phases' name comes from the elements that configure the ternary compound: M is an early transition metal, A is an element of the groups IIIA and IVA of the periodic table and X is either carbon or nitrogen. They exhibit a fixed stoichiometry and a general formula of $M_{n+1}AX_n$, where n is a number between 1 and 3 [4,6]. This excellent combination of ceramic and metallic-like properties occurs as a result of the layered disposition of the elements in the structure, alternating layers of elements MX and layers of element A, making this family of materials a good candidate for several applications [3]. In recent years, there has been a search for different applications for the use of this family of materials. Their use as heat exchangers [7] or catalytic devices using porous Ti_3SiC_2 and Ti_2AlC [8], thermal barriers using Cr_2AlC [9] or as fuel cladding material in nuclear reactors using Zr_2AlC [10] are some of the possible applications of these materials.

As for the wear behavior of MAX phases, several works have characterized the resistance of this family of materials under abrasive conditions. El-Raghy et al. [11] studied the effect of the grain size on the wear behavior of hot-isostatically-pressed (HIP) Ti_3SiC_2 samples by pin-on-disk tests and found a large difference in the coefficient of friction (COF)

at initial stages and a similar final COF once the debris started acting as a third body. Magnus et al. [12] explored the wear mechanism of a dual Ti_3AlC_2-Ti_2AlC MAX phase and the evolution of the microstructure by the pin-on-disk test, proposing a three-body abrasive wear with a wear rate of 10^{-4} mm^3/Nm. Shamsipoor et al. [13] analyzed the effect of the spark plasma sintering (SPS) parameters on the wear behavior of Cr_2AlC. Although the SPS parameters mainly affected the final MAX phase composition, which was synthesized in situ from elemental powders, wear behavior improved with the presence of the Cr_2AlC phase, with mainly adhesion and delamination wear mechanisms. In addition to this, MAX phases have been studied as a reinforcement for other materials in order to improve wear behavior. Yu et al. [14] produced an AZ91 magnesium composite reinforced with the Ti_2AlC MAX phase, improving the wear resistance in pin-on-disk wear tests with the addition of a MAX phase when compared to the raw magnesium alloy. From these works, it can be observed that the wear behavior of MAX phases is commonly studied in samples that are synthesized during the consolidation process and not starting from raw MAX phases powders, as it is in the scope of this work.

One of the main issues of pin-on-disk tests is the control of the constant load when starting the test; generally, the surface is smooth, but as time passes, wear products build up, causing the bolt that contains the counter material to vibrate. Although reciprocating-sliding tests do not maintain a constant velocity during the test, they offer a study of the reciprocal slip generated in the samples that is interesting for real industry behaviors, mainly in the biomedical industry [15]. Reciprocating-sliding tests are based on the application of a constant normal load over the sample through a bolt enclosing the counter material. This bolt performs a reciprocal movement with a previously defined stroke at the desired frequency. This method has the advantage of producing many repetitions of the sliding cycles, which causes the friction and wear processes to reach a stable value faster than other techniques [16].

As commented before, MAX phases are most frequently synthesized during their consolidation step and characterized after the optimization of the process [17–19]. Nevertheless, this work aims to study the consolidation process of already self-synthesized high purity Ti_3SiC_2 and Cr_2AlC MAX phase powders in order to validate the powder production process and analyze the sinterability of the powder through different consolidation methods: uniaxial pressing and sintering, cold isostatic pressing and sintering and hot pressing. Sintered samples were analyzed in order to determine the relative density of the processed samples, and the mechanical properties and wear behavior of selected samples were studied.

2. Materials and Methods

2.1. Powder Characterization

Self-synthesized and high purity Ti_3SiC_2 and Cr_2AlC MAX phases were produced from the commercially available powders detailed in Table 1, and the powder synthesis was scaled-up for large-quantity powder production. Ti_3SiC_2 was obtained starting from Ti:SiC:C with a molar ratio of 3:1,5:0,5 [20] and Cr_2AlC MAX phase was obtained by the synthesis of the elemental powders of Cr:Al:C with a molar ratio of 2:1,2;1.

Table 1. A list and the characteristics of commercially available powders for the synthesis of Ti_3SiC_2 and Cr_2AlC MAX phases.

Powder	Supplier	D50 (μm)	D90 (μm)	Purity (%)
Ti	TLS Technik GmbH, Bitterfeld-Wolfen, Germany	8	14	99
SiC	Navarro S.A., León, Spain	12	21	99.5
C	Ismaf S.L., Zamudio, Spain	24	58	99.5
Cr	Goodfellow Ltd., Huntingdon, UK	30	53	99.5
Al	AEE, Upper Saddle River, NJ USA	38	79	99.5

After mixing the initial powders in a Turbula shaker mixer (WAB Group, Muttenz, Switzerland) for 1 h, the powders were isostatically cold pressed at 4000 bar (EPSI Systems, Temse, Belgium). The synthesis of the pressed pellets was achieved by pressureless sintering. For the Ti_3SiC_2 MAX phase, a tubular high vacuum furnace was used (2.5×10^{-5}, HVT-15/50/450, Carbolite, Hope, UK) at 1300 °C for 6 h, with heating and cooling rates of 5 °C/min; for the Cr_2AlC MAX phase, a tubular furnace (STF-15/757450, Carbolite, Hope, UK) with an argon atmosphere was used at 1300 °C for 4 h, with heating and cooling rates of 5 °C/min. Synthesized consolidated samples were then crushed in a planetary ball mill (Pulverisette 5/2, Fritsch, Weimar, Germany) using a powder to ball ratio of 10:1, with isopropanol as a mixing medium and an argon protective atmosphere. After drying the synthesized powder in air at 100 °C, a comprehensive characterization was performed to study the purity and properties of the powders. Detected phases were analyzed by X-ray diffraction (XRD, Philips X'pert, Almelo, Netherlands) with Cu Kα radiation at 40 kV and 40 mV. The purity of the powders was determined by a least-squared procedure of the most intense peaks of the diffraction spectrum, as reported elsewhere [17]. This method has been previously compared to a Rietveld analysis [20], obtaining similar results for phase quantification. The calculation was done following Equation (1), where I_x corresponds to the integrated area of the most intense peak of the phase to be quantified and I_t to the sum of the integrated area of the most intense peaks detected in the XRD analysis:

$$\% \, Phase = I_x / I_t, \tag{1}$$

In addition, the morphology of the powders was studied with Scanning Electron Microscopy (SEM, TENEO-FEI, Eindhoven, Netherlands) coupled with energy-dispersive X-ray spectroscopy (EDS, DX-4-EDAX, Mahwah, NJ, USA). Furthermore, the mean particle size distribution of the initial powders was measured by Dynamic Light Scattering (MasterSizer 2000, Malvern Instruments, Malvern, UK).

2.2. Consolidation Techniques and Mechanical Properties Characterization

The sinterability of the powders by conventional powder metallurgy, press and sintering, was analyzed in order to understand the consolidation process of the synthesized MAX phase powders. For this purpose, the powders were uniaxially pressed from 100 to 500 MPa and sintered at 1300 °C for 6 h. The Archimedes density was measured for both green and sintered samples to study the effect of the pressure on the densification of the samples.

Alternative powder processing routes were explored. First, instead of uniaxial pressing, powders were cold isostatically pressed (CIP) at 4000 bar and then sintered under the same conditions. Second, inductive hot pressing was optimized to consolidate the MAX phase powders. The influences of pressure, time and temperature on the density of the MAX phase samples were analyzed. For the inductive hot-pressed samples, a 20 mm graphite die was used. The die was covered with a graphite foil with a sprayed coating of boron nitride to reduce the possible reaction of the powders with the die and to facilitate the sample release after the process. The process was performed using two heating rates. First, the heat was increased at a rate of 50 °C/min up to 100 °C below the selected consolidation temperature, then the rate was lowered to 25 °C/min in order to maintain better control of the process temperature. After the programmed dwell time, a cooling rate of 50 °C/min was applied. All processed samples were characterized by SEM and XRD in order to control MAX phase purity after consolidation. In order to understand the reaction mechanism of the hot-pressed samples, thermodynamic calculations of ΔG were performed using Thermo-Calc software (Stockholm, Sweden) with databases SSOL5 and SSUB5 [21].

Vickers hardness measurements were performed in a Zwick Roell Z 2.5 tester with a force of 10 N. Additionally, Young's modulus and elastic and plastic work were measured using a speed for the load applied of 1 mm/min and a speed of 2 mm/min for load removal during the indentation. In addition, cyclic micro-compressive tests (Microtest, EM2/5/FR, Madrid, Spain) were performed to wire-cut cylindrical samples with a height of 6 mm and a diameter of 3 mm. A preload speed of 0.1 mm/min was selected up to 20 N to ensure the

correct contact between the sample and the clamp. Tests were performed at 1 N/s up to 500 N for 5 cycles at room temperature.

2.3. Wear Tests

For the wear characterization of the selected samples, a reciprocating lineal sliding tribometer was used (UMT, Bruker, Mannheim, Germany). A 5 mm alumina ball was used as the counter material for the test, in air, under unlubricated conditions. All of the tests were performed using a 5 mm stroke distance with a frequency of 1 Hz for 30 min. Applied loads were varied from 5 to 10 N, to study the influence of this parameter on the wear rate. Three wear tests were performed for each condition, and the coefficient of friction (COF) was measured during each test. Specific wear rates (W_v) were calculated using the following Equations (2)–(4) reported by Doni et al. [16] to calculate the volume loss (V) divided by the load applied (N) and the total sliding distance (S):

$$W_V = \Delta V / N \cdot S, \tag{2}$$

The volume loss (V) is calculated using the radius (R) of the ball used as counter material, the average depth of the wear track ($\overline{D}$), the average wear loss area ($\overline{A}_w$) from the 2D profiles of the track and the stroke length (l).

$$\Delta V = \left[(1/3) \cdot \pi \cdot \overline{D}^2 \left(3R - \overline{D}\right)\right] + \overline{A}_w \cdot l, \tag{3}$$

Calculating the average depth ($\overline{D}$), through the average wear loss area ($\overline{A}_w$) and the average width of the track ($\overline{W}$).

$$\overline{D} = \overline{A}_w / \overline{W}, \tag{4}$$

Track measurements for the wear rate calculations were performed in an optical profilometer (DSX500, Opto-Digital Microscope, Tokio, Japan) to evaluate three different profiles in the center, top and bottom parts of the track, averaging the width, depth and area of the profiles.

3. Results and Discussion

3.1. Powders Characterization and Sinterability of Ti_3SiC_2 and Cr_2AlC MAX Phases

MAX phase Ti_3SiC_2 and Cr_2AlC synthesized powders are shown in Figure 1. From the micrographs, the irregular morphology of the powders can be observed. In addition, it is possible to see the characteristic nanolaminated structure of the MAX phases [4]. Complementary to the X-ray diffraction patterns of the powders shown in Figure 2, it is possible to observe the presence of some secondary phases, corresponding to $TiSi_2$ in the case of the production of Ti_3SiC_2, and Cr_5C_3 for Cr_2AlC. From the least-square analysis performed on the XRD diffractograms, a total purity of 92 vol.% and 96 vol.% has been calculated for Ti_3SiC_2 and Cr_2AlC, respectively. No other intermediate phase, unreacted powders or contamination from the milling was found from the XRD and EDS analyses of the synthesized powders. Furthermore, the particle size distribution of the powders produced exhibited a high control of the powders' production, with unimodal distribution for both MAX phases and a relatively low mean particle size, obtaining a D_{90} of 20 μm for Ti_3SiC_2 and 23 μm for Cr_2AlC.

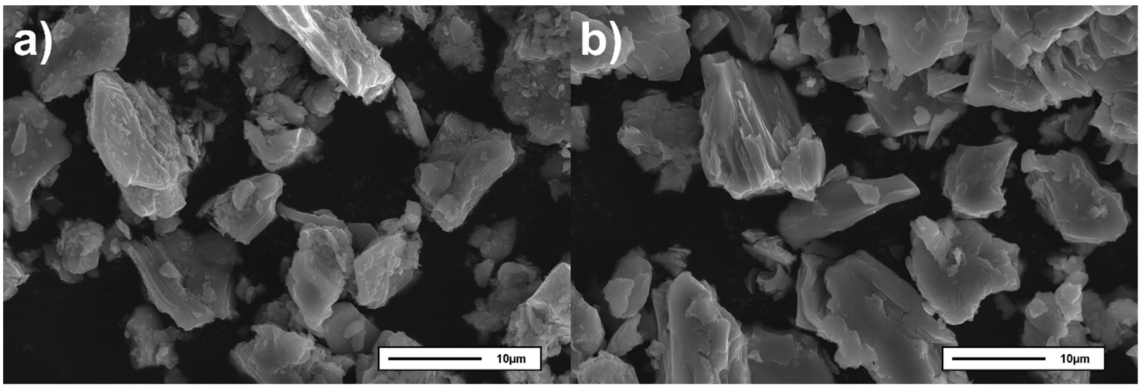

Figure 1. SEM micrographs of self-synthesized powders of (**a**) Ti3SiC2 and (**b**) Cr2AlC MAX phases.

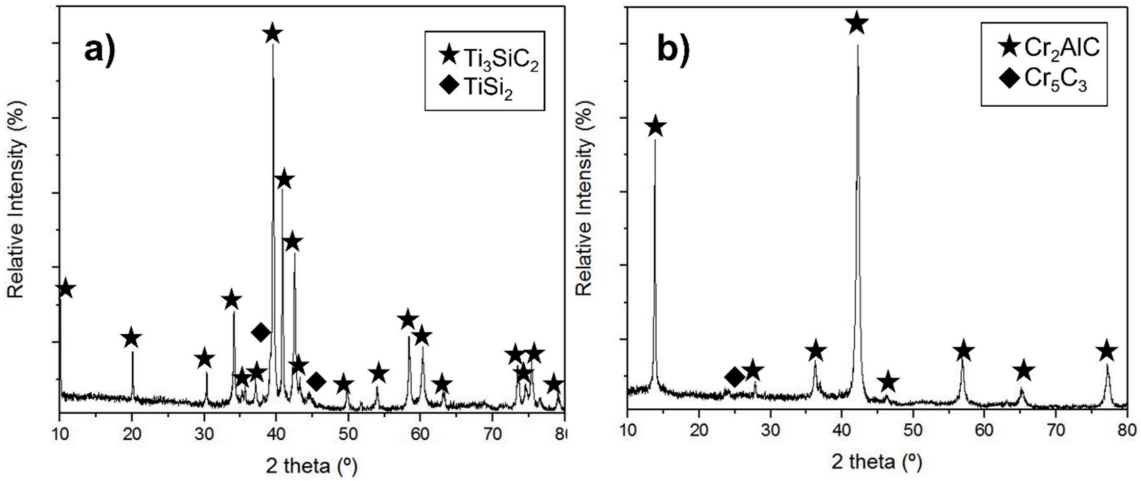

Figure 2. The X-Ray diffraction patterns of self-synthesized powders of (**a**) Ti_3SiC_2 and (**b**) Cr_2AlC MAX phases.

The sinterability properties of both self-synthesized MAX phase powders through conventional powder metallurgy processes were analyzed in order to study the densification of the powders for comparison with other production methods. It is important to note that compressibility tests of the powders through press and sintering establish a starting point to improve the densification or tailor the porosity of the samples, depending on the application. In Figure 3a, the evolution of the relative green density of the samples related to the pressure applied during the consolidation can be observed. A typical behavior is observed, wherein the green density increases with the increase of pressure for both MAX phases. A similar green relative density is exhibited for these samples with up to 63% for Ti_3SiC_2 and 61% for Cr_2AlC at 500 MPa. Both MAX phases show a similar slope while increasing the pressure. In addition, the evolution of the volumetric relative density after sintering was calculated (Figure 3b). It is possible to observe an increase in the relative density of the samples with the increase of the pressure up to 400 MPa and a stabilization of the value after this value, obtaining a relative density of 75% and 88% for Ti_3SiC_2 and Cr_2AlC, respectively, after sintering. Although the green density slopes showed a similar behavior in the green state, it is possible to observe a difference in the final relative density of the sintered samples. Generally, the hardness values of the materials have a direct correlation with the compressibility properties of the powders. From the theoretical values of Ti_3SiC_2 (4 GPa) [22] and Cr_2AlC (5.5 GPa) [23], it can be seen how this effect is not correlated. The lower compressibility of the powders appears to be an effect of the different particle size distribution of the powders, obtaining a lower compressibility for Ti3SiC2 (D_{90} = 20 µm) than for Cr_2AlC (D_{90} = 23 µm). These relative density values, albeit

low, might prove beneficial for applications such as catalytic substrates [24] electrodes [25], volumetric solar receivers [26] or hot gas filters [27].

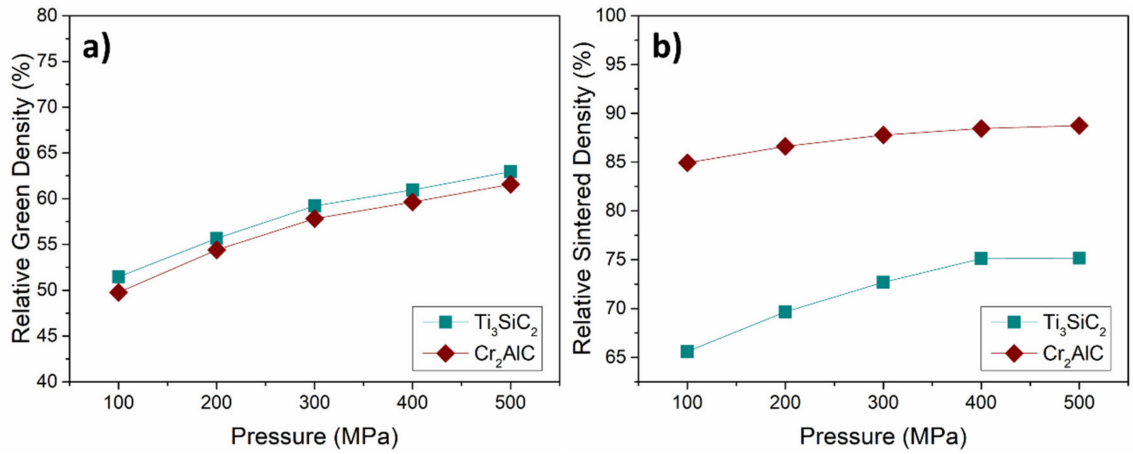

Figure 3. The press and sintering density measurements of Ti_3SiC_2 and Cr_2AlC: (**a**) relative green density and (**b**) relative sintered density.

The optimization of the hot-pressing process was done by analyzing the possible decomposition of the MAX phases after the process. First, the Ti_3SiC_2 MAX phase was hot pressed at a range of temperatures using a fixed pressure (30 MPa) and holding time of 15 min. XRD analysis of the samples after the process showed the limiting temperatures to avoid decomposition of the Ti_3SiC_2 phase. As can be observed in Figure 4, at a low temperature of 1050 °C, the phases present in the final samples correspond to Ti_3SiC_2 and the intermediate phase $TiSi_2$, which is also present in the initial composition of the powders. As the temperature begins to increase, the formation of TiC begins, reaching a maximum in its formation at 1250 °C, along with the decomposition of the MAX phase. This effect can be better seen in Figure 4b, where the amount of TiC at 1150 °C is 8%, increasing to 85% at 1250 °C. The phase formation of TiC could be due to the reactions produced by different effects, as discussed below. First, inductive heating, combined with pressure, accelerates the reactions that occur inside the graphite mold, altering the reactions studied in the pressureless sintering processes [20]. In addition to this, although a B/N sprayed coating is applied, it is possible that the powders react with the graphite foil; this could enhance the formation of TiC by reacting with the impurities of $TiSi_2$. These effects are correlated with the Gibbs free energy calculations of the possible reactions occurring during the hot pressing process, as shown in Table 2. Reaction 1 corroborates the stability of the MAX phase Ti_3SiC_2, which should not decompose at these temperatures, although from experimental synthesis of this MAX phase, it was observed that decomposition is possible at temperatures above 1300 °C [20]. TiC presence at temperatures of 1050 °C is in accordance with reaction 2, where the existence of the intermediate phase $TiSi_2$ and C produces TiC and $Si_{(gas)}$. Comparing the Gibbs free energy values from 1050 °C to 1350 °C to those presented elsewhere [20], it is possible to observe that the formation of TiC is more thermodynamically stable than the formation of Ti_3SiC_2, enhancing the appearance of TiC while the decomposition of Ti_3SiC_2 is occurring. Argon was used during the hot-pressing of the Ti_3SiC_2 to study the possible influence of using a protective atmosphere during the process; nevertheless, this effect could not be controlled, obtaining the same decomposition products in the final samples. With all this in mind, a temperature of 1150 °C was selected as optimal for the consolidation of Ti_3SiC_2 by inductive hot pressing. In addition to the temperature analysis, pressure and holding time at maximum temperature were varied to study the final density of the consolidated sample. By increasing the pressure on the sample to 50 MPa, it was possible to improve the density by 5%, reaching a total of 74% relative density, and by increasing the holding time to 1 h, up to an 80% densification was reached. On the other hand, for Cr_2AlC,

from the XRD analysis in Figure 5, there is no decomposition or increase in the secondary phase formation during the consolidation of the powders for all tested temperatures, and a temperature of 1200 °C was selected for this process.

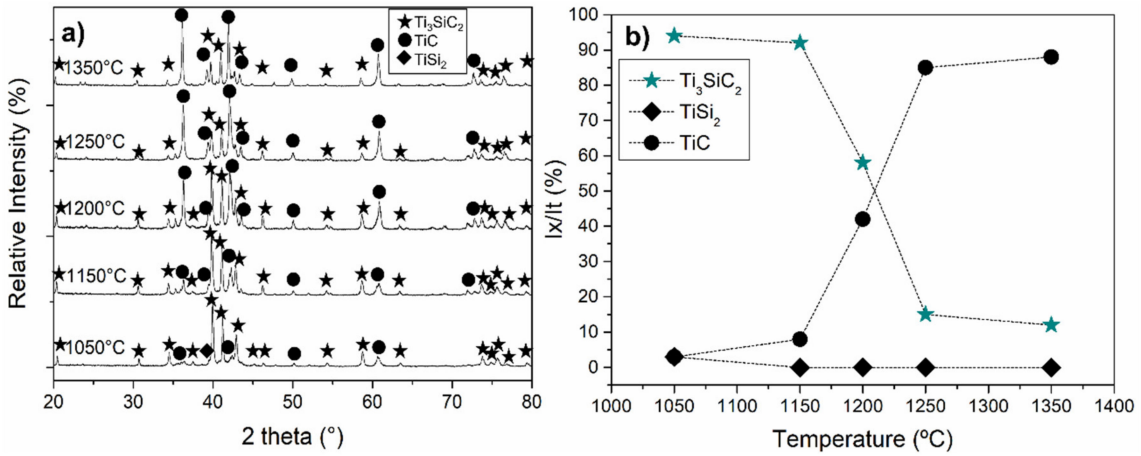

Figure 4. (**a**) The X-ray diffraction patterns of hot-pressed Ti_3SiC_2 powders from 1050 °C to 1350 °C and (**b**) the phase evolution from the XRD profiles.

Table 2. The Gibbs free energy calculations of different possible reactions during the hot pressing process at temperatures ranging from 1050 °C to 1350 °C.

Reaction	ΔG [J] 1050 °C	1150 °C	1200 °C	1250 °C	1350 °C
$Ti_3SiC_2 + C \rightarrow 3TiC + Si(g)$	4.47×10^3	2.83×10^4	4.06×10^4	5.31×10^4	7.87×10^4
$TiSi_2 + C \rightarrow TiC + 2Si(g)$	-4.80×10^5	-4.47×10^5	-4.31×10^5	-4.13×10^5	-3.79×10^5

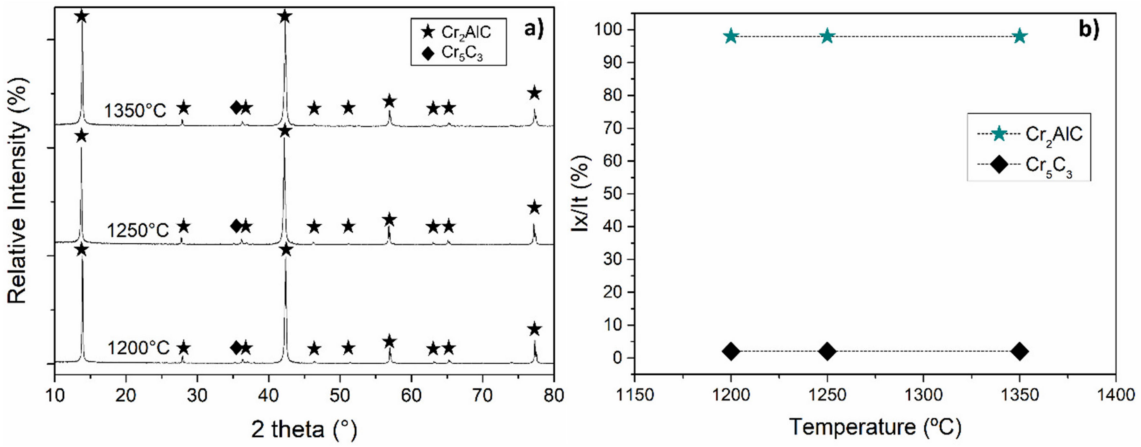

Figure 5. (**a**) The X-ray diffraction patterns of hot-pressed Cr_2AlC powders from 1200 °C to 1350 °C and (**b**) the phase evolution from the XRD profiles.

A summary of the microstructures obtained for the three different processes is shown in Figure 6, and the relative densities of each process are shown in Table 3. Isostatic pressing improves the densification of the samples when compared to press and sintering, and hot pressing enhances the densification of the Cr_2AlC MAX phase even further. For Ti_3SiC_2, density doesn't improve with the hot pressing process; the lower particle size distribution of this powder, combined with the reaction of the powder with the die and decomposition during the process, may have a negative effect on the consolidation of this MAX phase. From the XRD analysis of the consolidated samples shown in Figure 7, the high purity of

the processed samples is corroborated. For pressed and sintered samples (uniaxially and cold isostatically), it is possible to see remnants of secondary $TiSi_2$ from the initial powder synthesis for Ti_3SiC_2 (Figure 7a) and the minor presence of Cr_5C_3 in the Cr_2AlC (Figure 7b) consolidated samples. For hot-pressed samples, no decomposition of Ti_3SiC_2 was found after the consolidation process, with only TiC as a secondary phase (Figure 7a). In the case of Cr_2AlC, the XRD analysis (Figure 7b) shows a minor presence of Cr_5C_3 as secondary phase. In addition, the relative densities of the processed samples are shown in Table 3 to study the influence of the processes on the MAX phase samples. Densification of the powders was enhanced by this process obtaining up to 80% of relative density for Ti_3SiC_2 and 95% for Cr_2AlC.

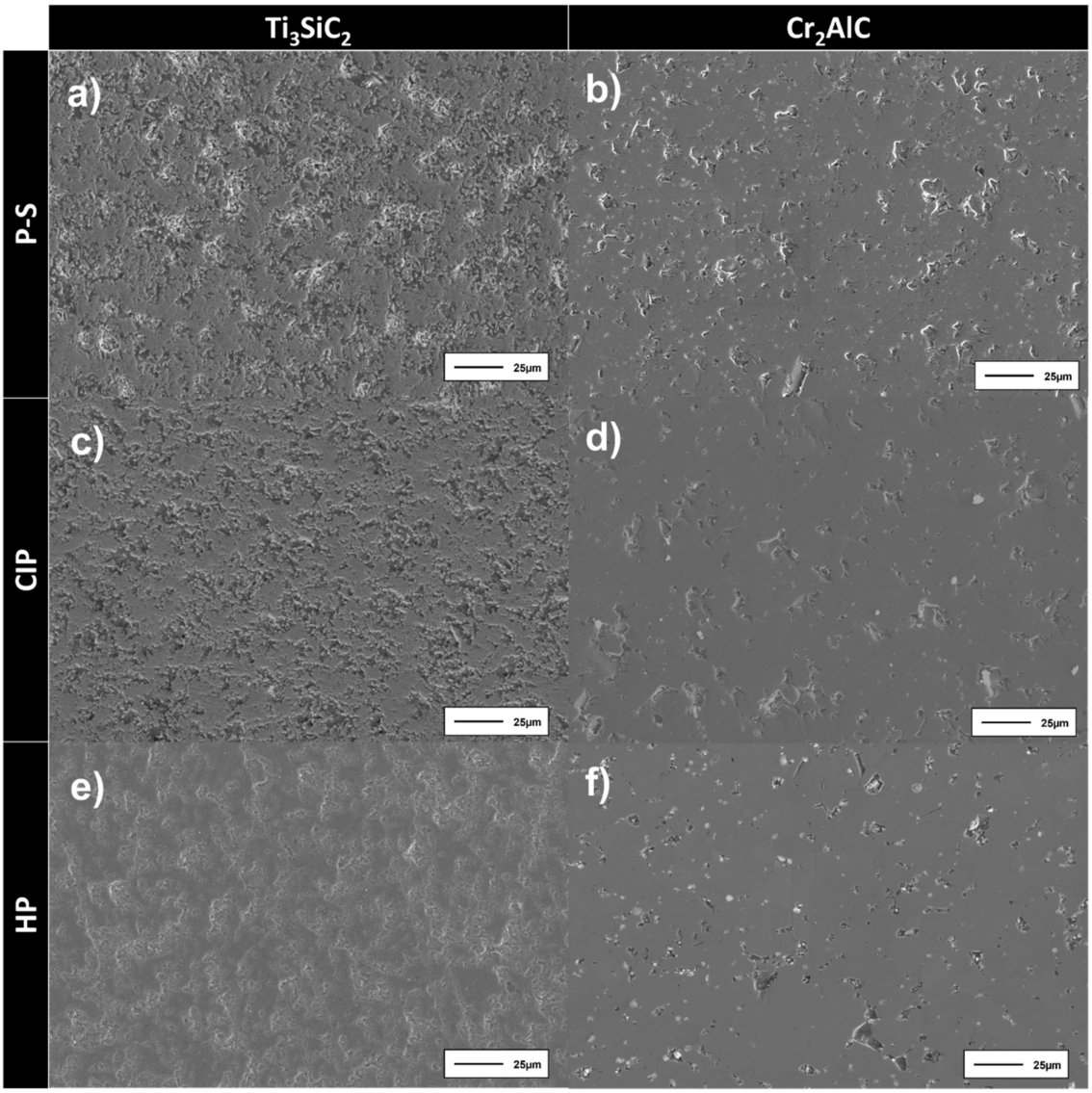

Figure 6. SEM micrographs of consolidated samples by different routes: (**a**) uniaxially pressed and sintered (P-S) Ti_3SiC_2; (**b**) uniaxially pressed and sintered (P-S) Cr_2AlC; (**c**) cold isostatic pressed and sintered (CIP) Ti_3SiC_2; (**d**) cold isostatic pressed and sintered (CIP) Cr_2AlC; (**e**) hot-pressed (HP) Ti_3SiC_2 and (**f**) hot-pressed (HP) Cr_2AlC.

Table 3. The relative densities of the consolidated Ti_3SiC_2 and Cr_2AlC MAX phases by press and sintering (P-S), cold isostatic pressing and sintering (CIP) and hot-pressing (HP).

Material	Process	Relative Density (%)
Ti_3SiC_2	P-S	75
	CIP	83
	HP	80
Cr_2AlC	P-S	88
	CIP	95
	HP	96

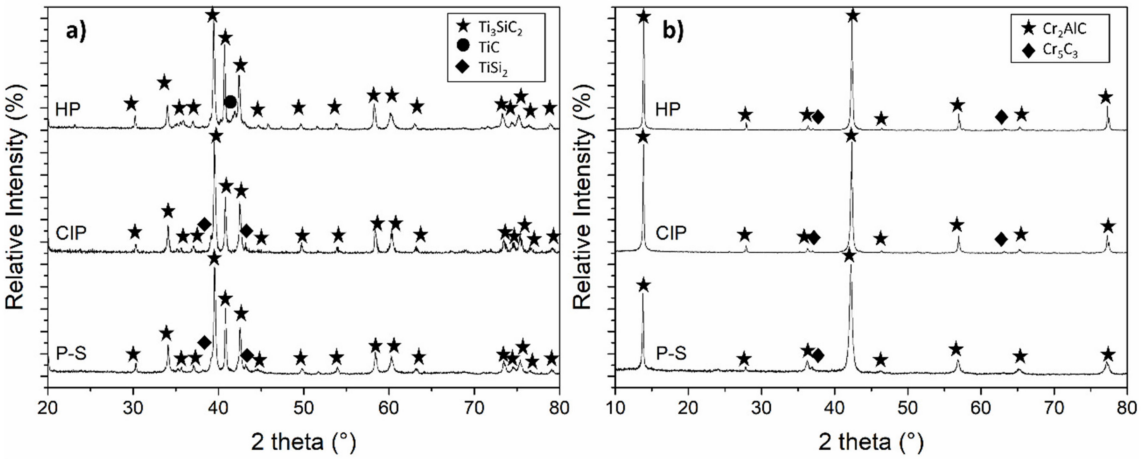

Figure 7. The X-ray diffraction patterns of uniaxially pressed and sintered (P-S), cold isostatic pressed and sintered (CIP) and hot-pressed (HP) consolidated samples after optimization of the process for (**a**) Ti_3SiC_2 at 1150 °C for 1 h and (**b**) Cr_2AlC at 1200 °C for 15 min.

3.2. Effect of the Consolidation Technique on the Mechanical Properties

The hardness, Youngs modulus, elastic and plastic work and recovery indexes calculated for the three processing routes used to consolidate Ti_3SiC_2 and Cr_2AlC are shown in Table 4. From the hardness values, it is possible to see an increase of the value for Ti_3SiC_2 as the consolidation technique is improved, from 136 HV for the P-S sample to 322 HV for the hot-pressed material. Although this value it is not directly correlated to the porosities obtained for each process, the amount of porosity in the samples increases the standard deviation of the measurements. Hardness is mainly dependent on the grain size generated in each process, with hot-pressed samples having a smaller grain size due to their fast consolidation. The same occurs for Cr_2AlC, where hot-pressed samples have a higher hardness value (535 HV) than the P-S (427 HV) and CIP (398 HV), due to the smaller grain size. Hardness values reported for Ti_3SiC_2 obtained through in situ synthesis reach values around 600 HV [5], which are higher than those obtained in this work (322 HV). In the case of Cr_2AlC, hardness values obtained for the hot-pressed samples (535 HV) are similar to those previously reported (530 HV) [5]. From the elastic and plastic work of the samples, it is important to note a higher value for the plastic work, a behavior that is characteristic of ceramic materials. This plastic work value is higher for the Ti_3SiC_2 MAX phase, and this should have an effect on the wear mechanism of this material, favoring a lower wear resistance and lowering the coefficient of friction as compared to Cr_2AlC for the same porosity values. In terms of the recovery index of the samples, similar values for P-S and CIP samples can be observed, although there is a clear difference in porosity between these samples and the hot-pressed samples; the appearance of localized porosity could have a big effect in this matter, reducing the elastic recovery of the surface after the test. In addition, the smaller grain size of the hot-pressed Ti_3SiC_2 appears to have an influence on the recovery properties of this material. Cr_2AlC recovery indexes are similar

for all the consolidation processes. All consolidated Cr_2AlC samples showed a high relative density and hence the effect of porosity in this recovery value is not significant. In terms of elastic modulus, this value has a great dependence on both the porosity in the sample and the grain size of the material. It can be observed in Figure 8 that lower E modulus values are obtained compared to those previously reported (343 kN/mm^2 for Ti_3SiC_2 and 245 kN/mm^2 for Cr_2AlC) [5]. As the porosity changes depending on the consolidation method in Ti_3SiC_2, and it is lower for cold isostatic pressing and higher for consolidation by hot pressing, the elastic modulus varies in this same manner. In the case of Cr_2AlC, the influence of the grain size directly relates to the higher E modulus obtained for the hot-pressed samples. A decrease in the elastic modulus for the CIP samples can also be observed; this in in accordance with the hardness values obtained and could be due to localized porosity in the sample.

Table 4. A summary of the measured mechanical properties of uniaxially (P-S), cold isostatic pressed and sintering (CIP) and hot-pressed (HP) Ti_3SiC_2 and Cr_2AlC MAX phases. W_{elast} and W_{plast} stand for the elastic and plastic work during the indentation and μ_{IT} for the recovery index after releasing the indentation.

Material	Zone	Hardness (HV10)	W_{elast} (Nmm)	W_{plast} (Nmm)	μ_{IT} (%)
Ti_3SiC_2	P-S	136	0.008 ± 0.001	0.055 ± 0.001	12.5 ± 0.6
	CIP	139	0.008 ± 0.001	0.054 ± 0.002	12.2 ± 0.8
	HP	322	0.021 ± 0.004	0.040 ± 0.004	34.2 ± 4.5
Cr_2AlC	P-S	427	0.008 ± 0.001	0.027 ± 0.002	22.3 ± 1.5
	CIP	398	0.008 ± 0.002	0.029 ± 0.002	22.3 ± 4.0
	HP	535	0.017 ± 0.001	0.024 ± 0.001	24.7 ± 2.5

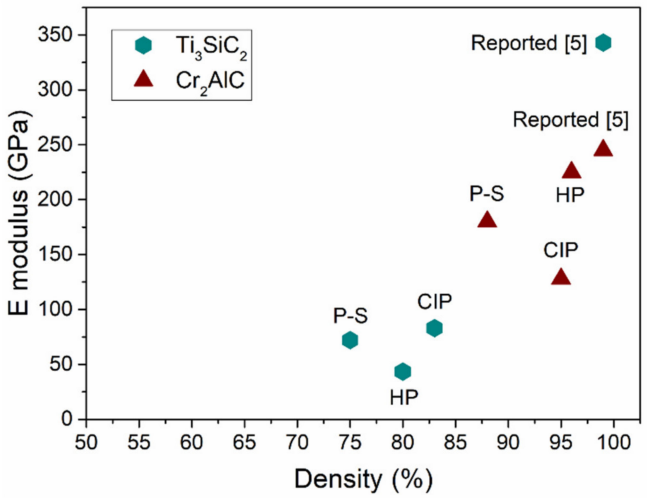

Figure 8. The E modulus of uniaxially (P-S), cold isostatic pressed and sintering (CIP) and hot- pressed (HP) Ti_3SiC_2 and Cr_2AlC MAX phases compared with the reported values from Barsoum, M. 2013.

The cyclic micro-compressive behaviors of cold isostatic pressed and sintered and hot-pressed samples are shown in Figure 9. It is possible to observe for both materials a kinking non-linear elastic behavior characteristic of MAX phases. The twisting that is generated by the energy dissipation during the compression is produced by the formation of incipient kinking bands (IKB) dislocations [4]. It is also possible to observe the lack of hysteresis during the different cycles, since it is not possible to differentiate the load and unload for any of the material. At loads under a specific threshold, IKB dislocations contract, producing a reversible process, thus generating the same values for every cycle and an elastic behavior due to the absence of plastic deformation at this load (500 N). This

effect produces a fully reversible loop for the uniaxial compression of MAX phases, as previous works have shown, for dense and porous MAX phases [28,29].

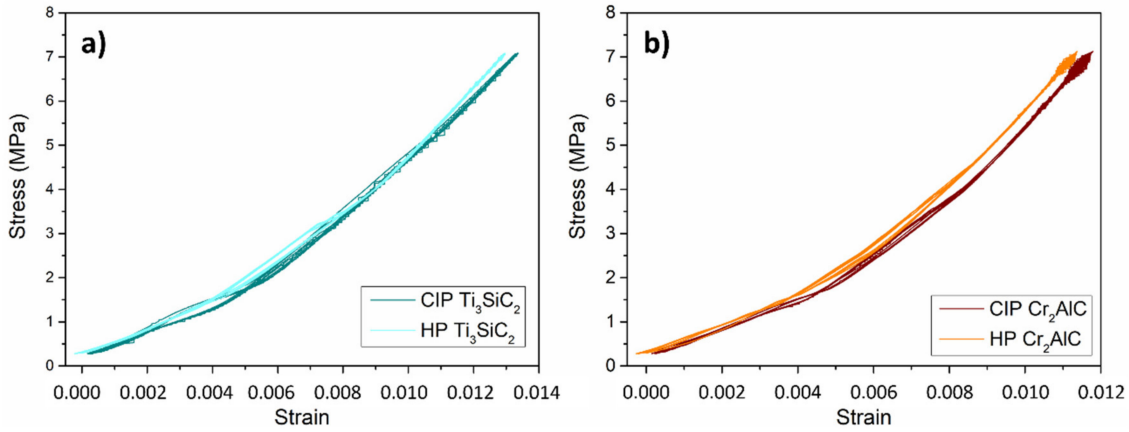

Figure 9. The cyclic micro-compressive stress-strain behavior of CIP and sintered and HP samples of (**a**) Ti_3SiC_2 and (**b**) Cr_2AlC at a load of 500 N with a pressure rate of 1 N/s.

In Figure 9a,b, it is also possible to observe a slight difference between the cold isostatic pressed and sintered and the hot-pressed samples. Although there is a porosity difference between the different sample production routes, this disparity should not be the main factor in the differences of compressive behavior. The main reason for the slight change in rigidity values during the micro-compressive test is the grain size generated during the sample production. This has a strong dependence on the cyclic compressive behavior of MAX phases [3], resulting in a lower strain on the material.

3.3. Effect of the Consolidation Technique on the Wear Behavior of Ti_3SiC_2 and Cr_2AlC MAX Phases and Influence of the Test Load on the Wear Properties

Initially, in order to assess the influence of the grain size on the wear behavior of the samples according to the processing route, a qualitative evaluation of the grain sizes was performed by micrographic analysis, as shown in Figure 10. It is possible to observe the presence of porosity at the grain boundaries of the MAX phases in all of the micrographs. The Ti_3SiC_2 samples exhibit smaller grains, shown in Figure 10a,c (~8 μm for CIP and ~4.5 μm for HP), compared to the Cr_2AlC samples (~32 μm for CIP and ~18 μm for HP) shown in Figure 10b,d. When comparing the different processing routes, it is possible to observe a common trend: Hot-pressed samples exhibit a smaller grain size when compared to the samples processed by cold isostatic pressing and sintering. This could be an effect of the cooling rate of the processes, with lower grain sizes for higher cooling rates.

The evolution of the friction coefficients (COF) during the wear tests is shown in Figure 11 for the Ti_3SiC_2 samples and Figure 12 for the Cr_2AlC samples. It is possible to observe different behaviors for different Ti_3SiC_2 samples (Figure 11). The CIP Ti_3SiC_2 sample tested with a load of 5 N shows a steady increase in the friction coefficient that stabilizes at around 300 s at a COF of 0.65. By increasing the load on the CIP Ti_3SiC_2 sample, it is possible to observe a higher initial coefficient, probably due to the initial debris generated in the track, and after less than a minute, the delamination of this generated debris reduces the abrasive effect, acting as a lubricant and lowering the coefficient value, stabilizing at values close to those of the sample tested at 5 N. This self-lubricant effect has been previously reported for both MAX phases and is intrinsic to the layered hexagonal crystalline structure of MAX phases [12], causing a reduction in the friction coefficient. Furthermore, this lubricating effect is also a result of the oxidation of the loose wear material, reducing the abrasion during the tests [30].

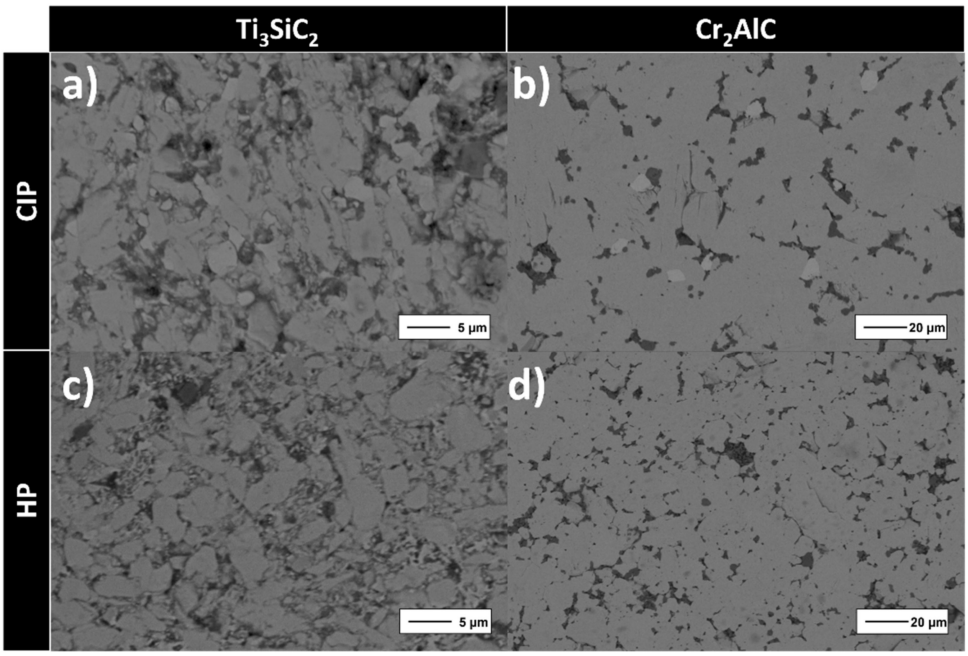

Figure 10. SEM micrographs of (**a**) cold isostatic pressed and sintered (CIP) Ti_3SiC_2; (**b**) cold isostatic pressed and sintered (CIP) Cr_2AlC; (**c**) hot-pressed (HP) Ti_3SiC_2 and (**d**) hot-pressed (HP) Cr_2AlC.

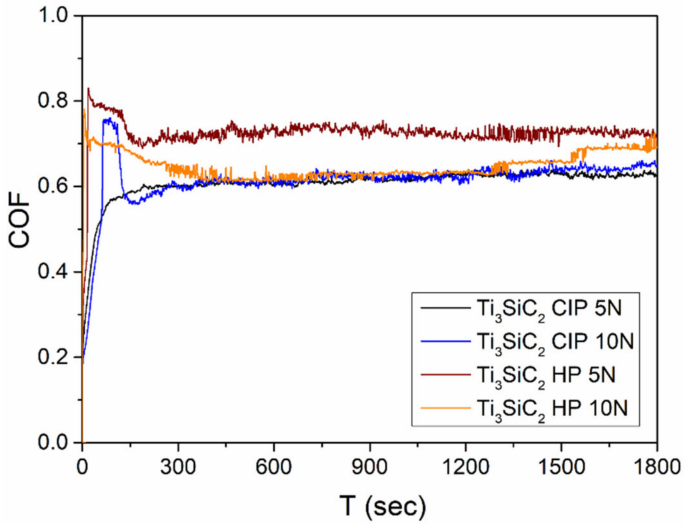

Figure 11. The coefficients of friction of the cold isostatic pressing and sintering (CIP) and hot-pressed (HP) samples during the reciprocating-sliding test with a load of 5 and 10 N of the Ti_3SiC_2 MAX phase.

On the other hand, hot-pressed Ti_3SiC_2 samples tested at 5 N and 10 N have higher final coefficients of friction, with a stabilization value at around 0.72 for both loads. In this case, a slightly higher coefficient during the test for the lowest load (5N) can be observed. Although this behavior is not expected, it could be due to the effect of the load in the delamination of the debris: in more aggressive conditions, it is easier to delaminate the material and generate a "lubricating" third body [12]. In Figure 12, it is possible to observe a higher final coefficient of friction for Cr_2AlC compared to those seen for Ti_3SiC_2. A possible explanation of this effect is the difficulty to produce wear in materials with a higher hardness (Ti_3SiC_2 = 4 GPa [22] and Cr_2AlC = 5.5 GPa [23]). The higher hardness of the Cr_2AlC MAX phase makes the wear debris more difficult to delaminate, thus reducing the self-lubricating effect and increasing the coefficient of friction. This double effect generated by the materials' hardness can also explain the difference between the CIP and

HP samples. HP samples have lower coefficients of friction and behave better than the CIP samples. It is important to note that hot pressing is a fast consolidation technique and the grain growth in this process is lower than for the CIP sample. This lower grain growth enhances the wear resistance of the HP samples [11]. In addition, as for the Ti_3SiC_2 hot-pressed samples, it is possible to see a lower COF for the Cr_2AlC HP 10 N than for the 5 N; this could be the effect of quicker delamination and faster oxidation of the debris [30], improving the wear resistance on the sample. When having more aggressive conditions set in the test, the higher load applied proves beneficial for the delamination of the debris, improving the self-lubricating effect of the MAX phases during wear.

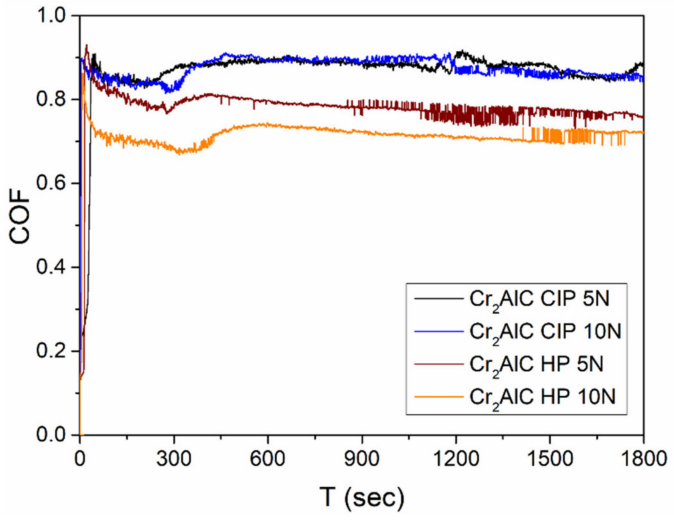

Figure 12. The coefficients of friction of the cold isostatic pressing and sintering (CIP) and hot-pressed (HP) samples during the reciprocating-sliding test with a load of 5 and 10 N of the Cr_2AlC MAX phase.

To better analyze the influence of the processing routes applied to obtain consolidated MAX phase samples, the wear rate was calculated. Figure 13 shows a representation of the 2D profiles of the wear tracks for different samples and loading conditions. In Figure 13a, the tracks of the cold isostatic and hot-pressed samples applying a load of 5N can be observed. From the track profiles, it can be noted that there is a better wear behavior for the Ti_3SiC_2 CIP sample that exhibits the smallest depth and width of the track. This effect is directly related to the porosity of the samples; with higher porosity, a higher amount of material is lost during the wear test. Thus, the cold isostatic pressed samples, which have lower porosity, have a smaller wear track profile compared to the hot-pressed samples that have higher porosity. This effect is also noticeable with the Cr_2AlC: both CIP and HP samples have similar porosity and similar wear track profiles. When comparing isostatic pressed samples, it is possible to observe a better wear behavior for MAX phase Ti_3SiC_2 compared to Cr_2AlC. This could be due to the differences between the self-lubricating effects of these MAX phase powders. As has been previously established, Ti_3SiC_2 has an intrinsic self-lubricating behavior [31] and Cr_2AlC has a strong dependence on the oxidation of the debris to generate this lubricating effect [30]. Furthermore, in terms of the debris formation, the difficulty of delaminating the torn material to produce this lubricating effect is also affected by the presence of secondary phases, which help to pin the MAX phase grains, delaying debris generation [31]. As can be seen in Figure 13a, this pinning effect is more noticeable for denser samples. As the porosity increases (hot-pressed Ti_3SiC_2), this pinning effect is no longer predominant and the debris generated could contain more secondary phases, creating more torn debris material with higher hardness and resulting in worse wear behavior. At higher loads (Figure 13b), as expected, the wear tracks are wider and deeper than those observed at 5 N. With these more aggressive conditions, we are able to observe a similar behavior for both MAX phases, no matter the processing route. The similarity of the CIP and HP 2D profiles for both MAX phases was not expected, since the

grain growth enhanced by the CIP sintering process should have had a negative effect on the wear behavior of the samples [11]. This effect is better understood with the wear rate calculation of the worn surfaces.

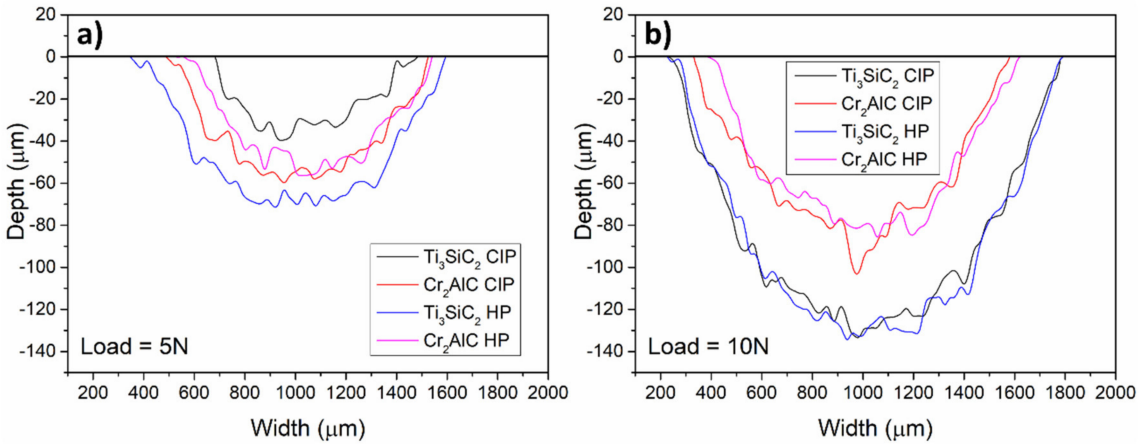

Figure 13. The 2D profiles at the center of the wear track of cold isostatic pressed and sintered (CIP) and hot-pressed (HP) Ti_3SiC_2 and Cr_2AlC applying (**a**) 5 N and (**b**) 10 N.

Although 2D profiles give a first approximation of the wear resistance of the materials, it is only a qualitative approach, and wear behavior should be studied by the wear rate, taking the complete track into consideration. The mean values of the profiles along the track and are shown in Table 5. In addition, the wear rates calculated following Equations (2)–(4) are shown in Figure 14.

Table 5. The wear track mean values extracted from the 2D profiles and the wear rate calculations for the Ti_3SiC_2 and Cr_2AlC MAX phases processed by CIP and HP.

MAX Phase	Process	Load (N)	Width (μm)	Depth (μm)	Area (mm^2)
Ti_3SiC_2	CIP	5	859.23	34.59	1.60×10^{-2}
		10	1610.72	133.59	1.46×10^{-1}
	HP	5	1006.23	55.76	3.86×10^{-2}
		10	1197.43	93.39	6.21×10^{-2}
Cr_2AlC	CIP	5	1212.16	77.10	5.54×10^{-2}
		10	1504.15	113.32	1.18×10^{-1}
	HP	5	977.78	48.10	2.87×10^{-2}
		10	1235.12	79.68	6.09×10^{-2}

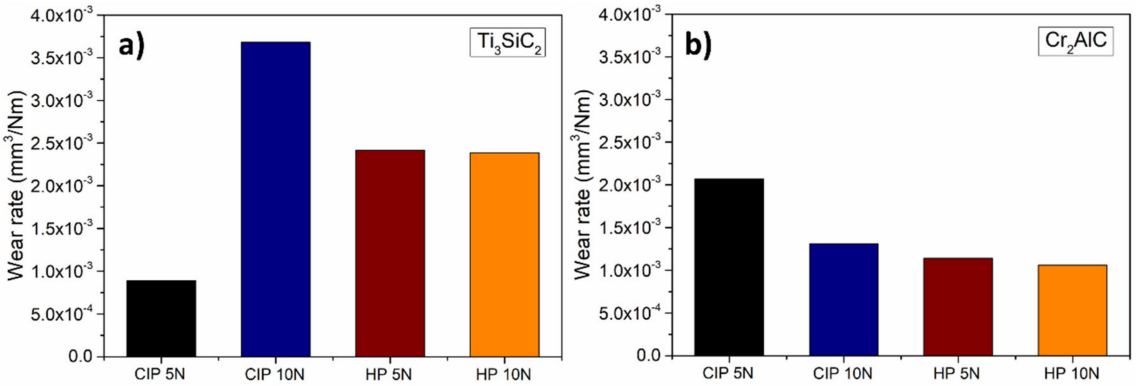

Figure 14. The wear rate calculations of samples processed by cold isostatic pressing and sintering (CIP) and hot pressing (HP) for (**a**) Ti_3SiC_2 and (**b**) Cr_2AlC.

It is possible to observe a high difference between the wear rates of CIP samples of Ti_3SiC_2 at different test loads. The CIP samples have the lowest porosity for this MAX phase, and under 5 N, exhibit the lowest wear rate of all the tested samples (8.91×10^{-4} mm^3/Nm). At higher loads, this wear rate increases greatly, reaching the highest value of all tested samples (3.68×10^{-3} mm^3/Nm). It appears that the larger grain size produced during the cold isostatic pressing and sintering has a detrimental effect on the wear behavior of these samples, as already seen in the hardness measurement shown in Table 4. At high loads, the CIP Ti_3SiC_2 sample dramatically decreases its wear properties. In this case, the amount of material removed during the test is not acting as lubricant debris, and as suspected from the COF measurements, the larger the grain size produced, the higher the difficulty in delaminating the debris. On the other hand, the hot-pressed Ti_3SiC_2 samples exhibit similar specific wear rates for 5 N and 10 N loads: 2.42×10^{-3} and 2.38×10^{-3} mm^3/Nm, respectively. This effect is directly related to the good wear behavior of the material and to an optimal consolidation of the samples, since a similar specific wear rate indicates a similar wear behavior under different conditions for the same sample.

The Cr_2AlC CIP sample exhibits an increase in the wear properties with an increase in the load, having specific wear rates of 2.07×10^{-3} mm^3/Nm at a load of 5 N and 1.31×10^{-3} mm^3/Nm at a load of 10 N. This could be due to the self-lubricating effect being enhanced in more severe loading conditions, which increases the delamination of the debris and improves the wear properties. In addition, the hot-pressed Cr_2AlC shows better wear properties and, similarly to HP Ti_3SiC_2, due to the lower grain size produced during the consolidation, indicates a good consolidation of the MAX phase samples and a good wear behavior of Cr_2AlC.

Complementary 3D profiles of the wear tracks are represented in Figure 15, where the color map representing the depth of each track depending on the load applied is shown.

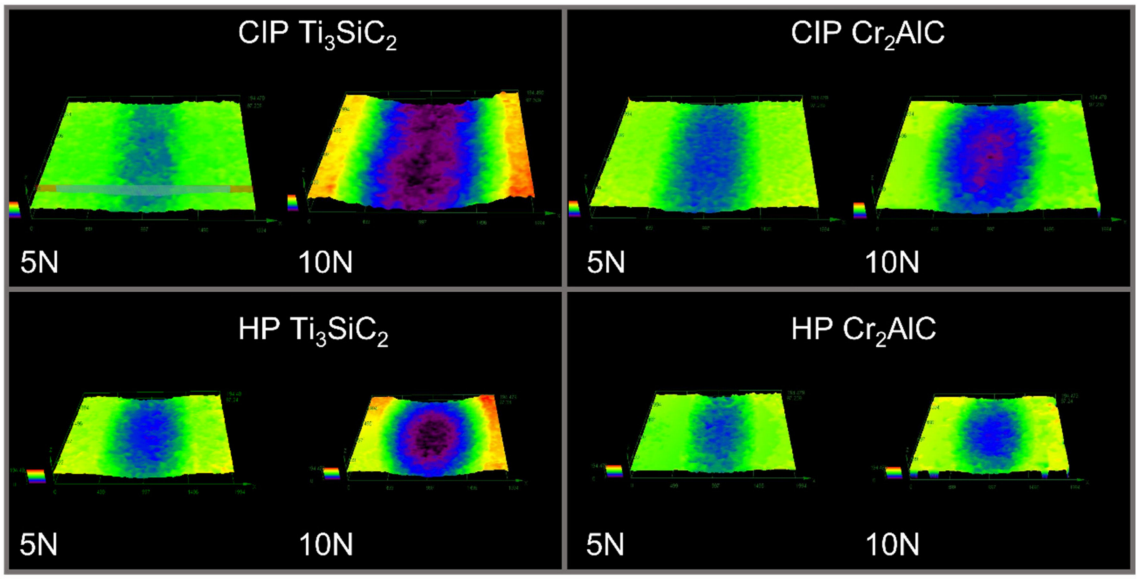

Figure 15. 3D profile images of the wear tracks for the Ti_3SiC_2 and Cr_2AlC MAX phases produced by cold isostatic pressing (CIP) and hot pressing (HP) at different wear test loads.

In order to study the wear mechanism produced during the tests, both secondary electron and back scattered detectors were analyzed to examine the nature of the wear. Wear test tracks for the 5 N load are shown in Figure 16 with an area analysis to study. If any amounts of oxygen and aluminum are found, that would suggest an adhesion of the aluminum ball used as counter material. An EDS analysis of the areas studied in Figure 16 is detailed in Table 6.

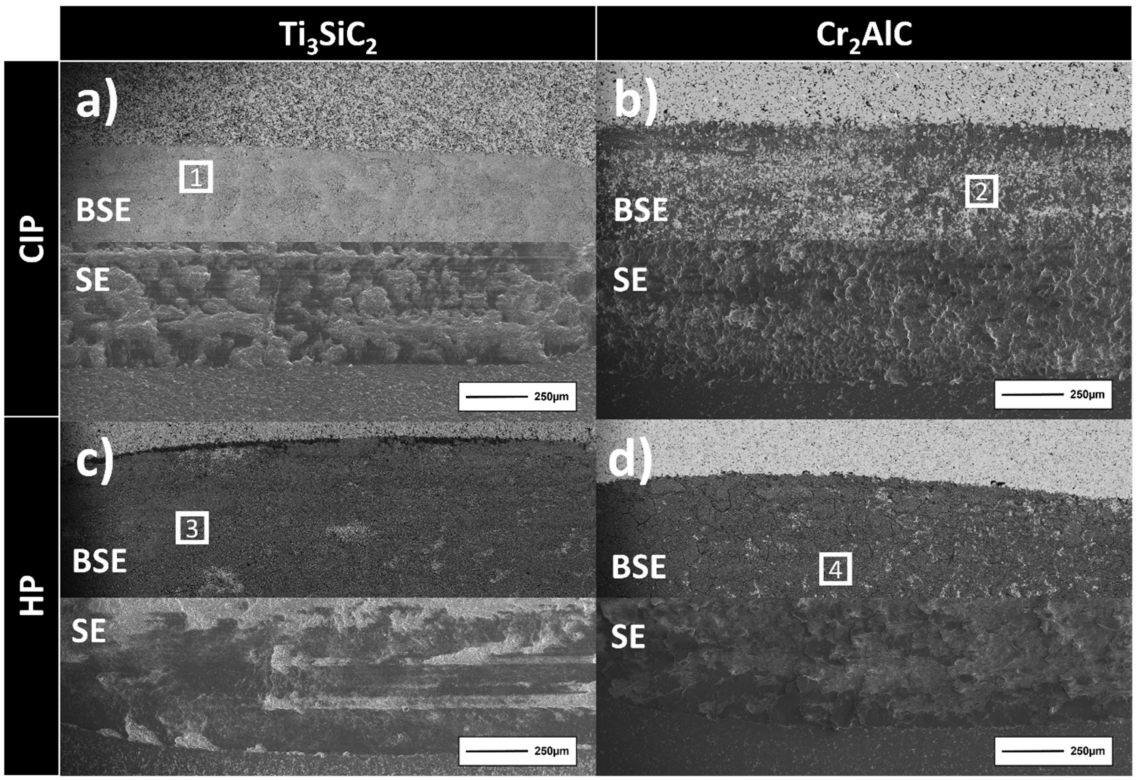

Figure 16. SEM secondary electron and back-scattered detectors micrographs of the reciprocating-sliding wear test with an applied load of 5 N for (**a**) cold isostatic pressed and sintered (CIP) Ti_3SiC_2; (**b**) cold isostatic pressed and sintered (CIP) Cr_2AlC; (**c**) hot-pressed (HP) Ti_3SiC_2 and (**d**) hot-pressed (HP) Cr_2AlC.

Table 6. An EDS area analysis of the wear tracks produced with a load of 5 N shown in the micrographs in Figure 16 for the cold isostatic pressing (CIP) and hot-pressed (HP) samples of the Ti_3SiC_2 and Cr_2AlC MAX phases.

Material/Process	Area	Ti (wt.%)	Cr (wt.%)	Si (wt.%)	Al (wt.%)	C (wt.%)	O (wt.%)
Ti_3SiC_2-CIP	1	36	-	12	10	26	16
Cr_2AlC-CIP	2	-	25	-	14	34	27
Ti_3SiC_2-HP	3	26	-	10	15	16	33
Cr_2AlC-HP	4	-	22	-	13	19	46

From the SEM micrographs, it is possible to observe a clear difference between MAX phases Ti_3SiC_2 and Cr_2AlC. The secondary electron detector shows horizontal lines corresponding to an abrasive mechanism in the Ti_3SiC_2 samples (Figure 16a,c) and some material accumulation in the form of stains corresponding to an adhesion of the counter material. Cr_2AlC (Figure 16b,d), on the other hand, exhibits a predominant adhesive mechanism, with no clear horizontal lines indicating abrasion. As reported elsewhere [32], it is possible to differentiate the wear behavior between both MAX phases. Ti_3SiC_2 behaves with a quasi-plastic deformation, with the formation of kink bands on the edges of the wear tracks (darker lines between the wear track and the substrate in Figure 16c). This is corroborated with the properties shown in Table 4, where the plastic work is higher for Ti_3SiC_2.

On the other hand, on Cr_2AlC, there is a formation of adhesive cracks within the wear track. Although in our work the adhesive behavior in worn Cr_2AlC is predominant, it is possible to observe those cracks in Figure 16b. This adhesive behavior, where the delamination of the MAX phase has been also previously reported [13] showing the adhesive nature of Cr_2AlC wear mechanism, reduces the coefficient of friction for samples with a higher

purity of Cr_2AlC. An EDS analysis in Table 6 confirms the adhesive mechanism through the detection of aluminum and oxygen in all the tracks and the predominant adhesive nature of the wear behavior for Cr_2AlC, exhibiting a higher oxygen content compared to that in the Ti_3SiC_2 produced by the same processing route. It is important to note that the presence of Al and O in Cr_2AlC could also be due to the formation and oxidation of debris, rather than from the Al_2O_3 counter material. Additionally, it is possible to observe a higher aluminum content for the Cr_2AlC samples tested at 5 N produced by hot pressing. These samples have a lower porosity, which should reduce the amount of debris created during the test and increase the adhesive wear mechanism in the samples.

The reciprocating-sliding wear tracks applying a load of 10 N are shown in Figure 17. It is possible to see the increase in the width of the wear tracks compared to those at a load of 5 N, as also seen in the 2D profiles. In this case, the horizontal lines indicating an abrasive wear observed previously are not seen at this higher load. This can be clearly seen in the Ti_3SiC_2 samples (Figure 17a,c), where big stains of adhered materials can be found in the BSE micrographs. The presence of more adherence zones at these higher loads is in accordance with the coefficient of friction and wear rates calculated, demonstrating a higher delamination of the MAX phases with the increase of the load to 10 N and improving the wear behavior of the material by increasing the self-lubricating effect during the test. Cr_2AlC (Figure 17b,d) exhibits this same behavior at 10 N. Under more aggressive conditions, it is possible to clearly observe in Figure 17d the cracking of the adhered debris formed during the test. As seen in the 5 N tests, the HP samples show a higher amount of adhered materials on the wear tracks when compared to the CIP samples; this can be attributed to the smaller grain size of the processed samples, which improves the delamination of the MAX phases. From the EDS analysis in Table 7, it is possible to demonstrate the predominant adhesive nature of the wear mechanism, mostly for the MAX phase Cr_2AlC with an increase in the oxygen found in the areas analyzed.

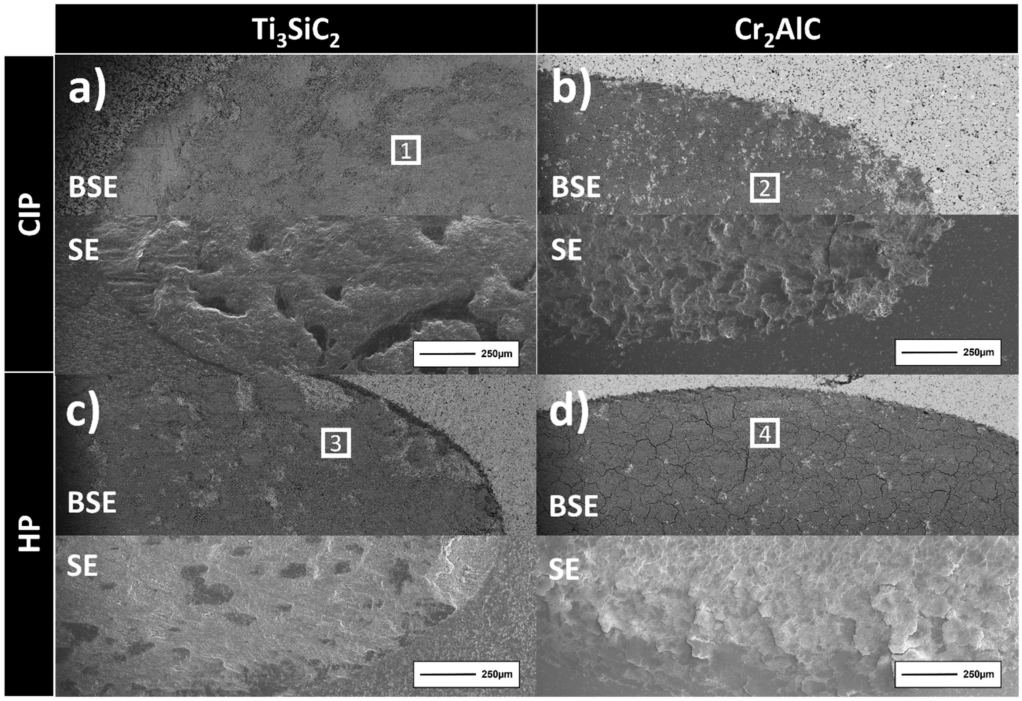

Figure 17. SEM secondary electron and back-scattered detectors micrographs of the reciprocating-sliding wear test with an applied load of 10 N for (**a**) cold isostatic pressed and sintered (CIP) Ti_3SiC_2; (**b**) cold isostatic pressed and sintered (CIP) Cr_2AlC; (**c**) hot-pressed (HP) Ti_3SiC_2 and (**d**) hot-pressed (HP) Cr_2AlC.

Table 7. An EDS area analysis of the wear tracks produced with a load of 10 N shown in the micrographs in Figure 17 for cold isostatic pressing (CIP) and hot-pressed (HP) samples of the Ti_3SiC_2 and Cr_2AlC MAX phases.

Material/Process	Area	Ti (wt.%)	Cr (wt.%)	Si (wt.%)	Al (wt.%)	C (wt.%)	O (wt.%)
Ti_3SiC_2-CIP	1	36	-	13	8	23	20
Cr_2AlC-CIP	2	-	17	-	11	20	52
Ti_3SiC_2-HP	3	30	-	12	15	19	24
Cr_2AlC-HP	4	-	18	-	11	21	50

4. Conclusions

The consolidation of self-synthesized Ti_3SiC_2 and Cr_2AlC was studied by three different processing techniques: uniaxial pressing and sintering, cold isostatic pressing and sintering and hot pressing. Each processing route has an effect on the final density of the samples and on the mechanical properties and wear behavior of the MAX phases. In terms of sinterability, hot pressing was the best processing technique for Cr_2AlC and cold isostatic pressing was the best processing technique for Ti_3SiC_2 due to the decomposition of the MAX phase during the inductive hot pressing of the powders, which lost most of their purity in the case of Ti_3SiC_2. An elastic modulus showed a close dependence on the porosity and the grain size of the sample. The CIP and sintered Ti_3SiC_2 samples exhibited the best properties, due to the reduction of porosity through the consolidation process. In the case of Cr_2AlC, an elastic modulus showed similar values for the HP samples compared to those previously reported. The compressive strength properties of the Ti_3SiC_2 and Cr_2AlC processed by CIP and HP were unaffected by the porosity and grain size and showed no hysteresis during the cyclic tests, with a similar behavior for the different processing routes.

The wear behavior of the MAX phases processed by CIP and HP was determined by comparing the different consolidation processes (CIP and HP) and varying the loads applied during the tests (5 and 10 N). For both MAX phases, wear behavior seems to have a dependence on the porosity of the samples. The CIP Ti_3SiC_2 exhibits the best wear properties at 5 N, which drastically decrease when increasing the load. However, in the case of hot-pressed samples, the wear behavior is similar for both applied loads. This effect is a combination of the grain size produced during the consolidation route and the self-lubricating effect of the MAX phases' debris generated during the tests. Cr_2AlC exhibits the same behavior for both consolidation routes, with a reduction on the wear rate when increasing the load; this reduction is higher for the CIP samples. This reduction is related to the ease of delaminating the debris by applying higher loads, which creates a self-lubricant effect during the wear test. Although both MAX phases revealed a self-lubricant effect, demonstrating the good wear properties of these materials, the wear mechanism of both MAX phases can be differentiated by a quasi-plastic deformation with a combination of abrasive and adhesive wear and a predominant adhesive wear mechanism for Cr_2AlC.

Author Contributions: E.T.: Writing—original draft, Conceptualization, Methodology, Investigation and Formal analysis. E.N.: Review and editing, Conceptualization, Methodology, Investigation and Formal analysis. M.K.: Review and editing, Conceptualization, Methodology, Investigation and Formal analysis. A.J.-M.: Review and editing, Conceptualization, Methodology, Investigation, Formal analysis and Resources. S.A.T.: Review and editing, Conceptualization, Methodology, Investigation, Formal analysis and Resources. All authors have read and agreed to the published version of the manuscript.

Funding: The authors would like to thank the funding provided for this research by the Regional Government of Madrid (Dra. Gral. Universidades e Investigación) through the project P2018/NMT4411 (ADITIMAT-CM), and the Spanish Government through the projects PID2019-106631GB-C43 and RTC2019-007049-4.

Institutional Review Board Statement: Not applicable.

Conflicts of Interest: The authors declare that they have no known competing financial interests or personal relationships that could have appeared to influence the work reported in this paper.

References

1. Hoffman, E.N.; Vinson, D.W.; Sindelar, R.L.; Tallman, D.J.; Kohse, G.; Barsoum, M.W. MAX phase carbides and nitrides: Properties for future nuclear power plant in-core applications and neutron transmutation analysis. *Nucl. Eng. Des.* **2012**, *244*, 17–24. [CrossRef]
2. Song, G.; Wang, Y.; Zhou, Y. *MAX Phases and Ultra-High Temperature Ceramics for Extreme Environments*; IGI Global: Hershey, PA, USA, 2013; ISBN 9781466640665.
3. Barsoum, M.W.; Radovic, M. Elastic and Mechanical Properties of the MAX Phases. *Annu. Rev. Mater. Res.* **2011**, *41*, 195–227. [CrossRef]
4. Barsoum, M.W. The Mn+1AXn Phases: A New Class of Solids. *Prog. Solid State Chem.* **2000**, *28*, 201–281. [CrossRef]
5. Barsoum, M. *MAX Phases: Properties of Machinable Ternary Carbides and Nitrides*; John Wiley & Sons: Hoboken, NJ, USA, 2013.
6. Jeitschko, W.; Nowotny, H. Die Kristallstruktur von Ti3SiC2: Ein neuer Komplexcarbid-Typ. *Mon. Für Chem.–Chem. Mon.* **1967**, *98*, 329–337. [CrossRef]
7. Tsipas, S.A.; Tabares, E.; Weissgaerber, T.; Hutsch, T.; Sket, F.; Velasco, B. Thermophysical properties of porous Ti2AlC and Ti3SiC2 produced by powder metallurgy. *J. Alloy. Compd.* **2021**, *857*, 158145. [CrossRef]
8. Velasco, B.; Gordo, E.; Hu, L.; Radovic, M.; Tsipas, S.A. Influence of porosity on elastic properties of Ti2AlC and Ti3SiC2 MAX phase foams. *J. Alloy. Compd.* **2018**, *764*, 24–35. [CrossRef]
9. Gonzalez-Julian, J.; Go, T.; Mack, D.E.; Vaßen, R. Thermal cycling testing of TBCs on Cr2AlC MAX phase substrates. *Surf. Coat. Technol.* **2018**, *340*, 17–24. [CrossRef]
10. Qarra, H.H.; Knowles, K.M.; Vickers, M.E.; Akhmadaliev, S.; Lambrinou, K. Heavy ion irradiation damage in Zr2AlC MAX phase. *J. Nucl. Mater.* **2019**, *523*, 1–9. [CrossRef]
11. El-Raghy, T.; Blau, P.; Barsoum, M.W. Effect of grain size on friction and wear behavior of Ti3SiC2. *Wear* **2000**, *238*, 125–130. [CrossRef]
12. Magnus, C.; Cooper, D.; Sharp, J.; Rainforth, W.M. Microstructural evolution and wear mechanism of Ti3AlC2—Ti2AlC dual MAX phase composite consolidated by spark plasma sintering (SPS). *Wear* **2019**, *438–439*, 203013. [CrossRef]
13. Shamsipoor, A.; Farvizi, M.; Razavi, M.; Keyvani, A. Influences of processing parameters on the microstructure and wear performance of Cr2AlC MAX phase prepared by spark plasma sintering method. *J. Alloy. Compd.* **2020**, *815*, 152345. [CrossRef]
14. Yu, W.; Chen, D.; Tian, L.; Zhao, H.; Wang, X. Self-lubricate and anisotropic wear behavior of AZ91D magnesium alloy reinforced with ternary Ti2AlC MAX phases. *J. Mater. Sci. Technol.* **2019**, *35*, 275–284. [CrossRef]
15. Ureña, J.; Tabares, E.; Tsipas, S.; Jiménez-Morales, A.; Gordo, E. Dry sliding wear behaviour of β-type Ti-Nb and Ti-Mo surfaces designed by diffusion treatments for biomedical applications. *J. Mech. Behav. Biomed. Mater.* **2019**, *91*, 335–344. [CrossRef] [PubMed]
16. Doni, Z.; Alves, A.C.; Toptan, F.; Gomes, J.R.; Ramalho, A.; Buciumeanu, M.; Palaghian, L.; Silva, F.S. Dry sliding and tribocorrosion behaviour of hot pressed CoCrMo biomedical alloy as compared with the cast CoCrMo and Ti6Al4V alloys. *Mater. Des.* **2013**, *52*, 47–57. [CrossRef]
17. Córdoba, J.M.; Sayagués, M.J.; Alcalá, M.D.; Gotor, F.J. Synthesis of Ti3SiC2 powders: Reaction mechanism. *J. Am. Ceram. Soc.* **2007**, *90*, 825–830. [CrossRef]
18. Gonzalez-Julian, J.; Onrubia, S.; Bram, M.; Guillon, O. Effect of sintering method on the microstructure of pure Cr2AlC MAX phase ceramics. *J. Ceram. Soc. Jpn.* **2016**, *124*, 415–420. [CrossRef]
19. Liu, X.L.; Jiang, Y.; Zhang, H.B.; He, Y.H. Corrosion behavior of porous Ti3SiC2 in nitric acid and aqua regia. *Trans. Nonferrous Met. Soc. China* **2017**, *27*, 584–590. [CrossRef]
20. Tabares, E.; Jiménez-Morales, A.; Tsipas, S.A. Study of the synthesis of MAX phase Ti3SiC2 powders by pressureless sintering. *Bol. La Soc. Esp. Ceram. Y Vidr.* **2020**, *60*, 41–52. [CrossRef]
21. Andersson, J.O.; Helander, T.; Höglund, L.; Shi, P.F.; Sundman, B. Thermo-Calc and DICTRA, Computational tools for materials science. *Calphad* **2002**, *26*, 273–312. [CrossRef]
22. El Saeed, M.A.; Deorsola, F.A.; Rashad, R.M. Optimization of the Ti3SiC2 MAX phase synthesis. *Int. J. Refract. Met. Hard Mater.* **2012**, *35*, 127–131. [CrossRef]
23. Lin, Z.; Zhou, Y.; Li, M.; Wang, J. In-situ hot pressing/solid-liquid reaction synthesis of bulk Cr2AlC. *Z. Fuer Met. Res. Adv. Tech.* **2005**, *96*, 291–296. [CrossRef]
24. Chen, Y.; Wang, N.; Ola, O.; Xia, Y.; Zhu, Y. Porous ceramics: Light in weight but heavy in energy and environment technologies. *Mater. Sci. Eng. R Rep.* **2021**, *143*, 100589. [CrossRef]
25. Hedayat, N.; Du, Y.; Ilkhani, H. Review on fabrication techniques for porous electrodes of solid oxide fuel cells by sacrificial template methods. *Renew. Sustain. Energy Rev.* **2017**, *77*, 1221–1239. [CrossRef]
26. Chen, X.; Xia, X.L.; Yan, X.W.; Sun, C. Heat transfer analysis of a volumetric solar receiver with composite porous structure. *Energy Convers. Manag.* **2017**, *136*, 262–269. [CrossRef]
27. Hammel, E.C.; Ighodaro, O.L.R.; Okoli, O.I. Processing and properties of advanced porous ceramics: An application based review. *Ceram. Int.* **2014**, *40*, 15351–15370. [CrossRef]

28. Fraczkiewicz, M.; Zhou, A.G.; Barsoum, M.W. Mechanical damping in porous Ti3SiC2. *Acta Mater.* **2006**, *54*, 5261–5270. [CrossRef]
29. Sun, Z.M.; Murugaiah, A.; Zhen, T.; Zhou, A.; Barsoum, M.W. Microstructure and mechanical properties of porous Ti3SiC2. *Acta Mater.* **2005**, *53*, 4359–4366. [CrossRef]
30. Gupta, S.; Filimonov, D.; Palanisamy, T.; Barsoum, M.W. Tribological behavior of select MAX phases against Al2O3 at elevated temperatures. *Wear* **2008**, *265*, 560–565. [CrossRef]
31. Magnus, C.; Cooper, D.; Ma, L.; Rainforth, W.M. Microstructures and intrinsic lubricity of in situ Ti3SiC2–TiSi2–TiC MAX phase composite fabricated by reactive spark plasma sintering (SPS). *Wear* **2020**, *448*, 203169. [CrossRef]
32. Qu, L.; Bei, G.; Nijemeisland, M.; Cao, D.; van der Zwaag, S.; Sloof, W.G. Point contact abrasive wear behavior of MAX phase materials. *Ceram. Int.* **2020**, *46*, 1722–1729. [CrossRef]

CHAPTER 6

POWDER INJECTION MOULDING OF MAX PHASES

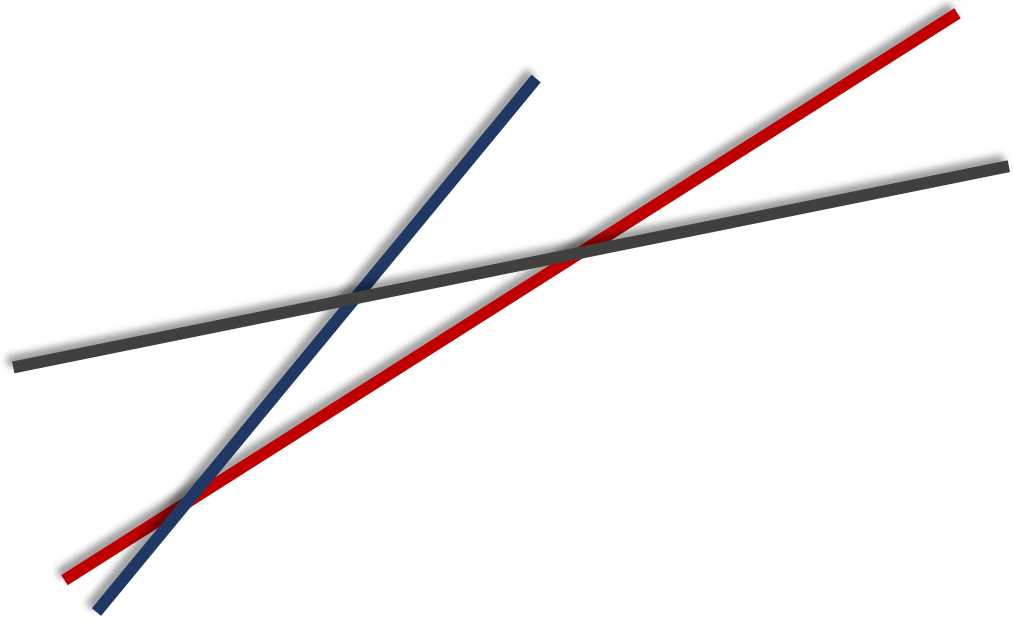

Contents

6.1 Powder injection moulding of MAX phase Ti_3SiC_2 169
6.2 Injection moulding of porous MAX phase Ti_3SiC_2 without using space-holder 177

6.1 Powder injection moulding of MAX phase Ti_3SiC_2

Authors: Eduardo Tabares, Sandra C. Cifuentes, Antonia Jiménez-Morales, Sophia A. Tsipas

Departamento de Ciencia e Ingeniería de Materiales e Ingeniería Química, IAAB, Universidad Carlos lll de Madrid, Avda. De la Universidad 30, 38911 Leganés, Spain

Journal: Proceedings of the Euro PM 2019 Congress and Exhibition (Conference Paper), Euro PM 2019, Maastricht, 13-16October 2019 Code 167182, ISBN: 978-189907251-4

Scope of this paper:

After validating the stability of the synthesised powders, alternative processing routes are explored for MAX phases. In this peer-reviewed conference paper, a first approximation study of powder injection moulding (PIM) is analysed, studying the suitability of MAX phase Ti_3SiC_2 for the production of injected samples. Powder characteristics and a first look at the rheological properties of Ti_3SiC_2 are presented, using PEG/CAB as a polymeric binder. Several solid loadings feedstocks ranging from 49 to 54 vol.% were injected and the microstructure analysed to study the homogeneity of the mixtures. Furthermore, a two-step debinding process was analysed, controlling the amount of polymeric binder removed. From this work, the first steps for the processing of MAX phases by PIM were explored obtaining good torque properties for binders between 49 and 54 vol.% with an almost complete degradation of the polymeric system, while maintaining the structural integrity of the samples.

Graphical Abstract:

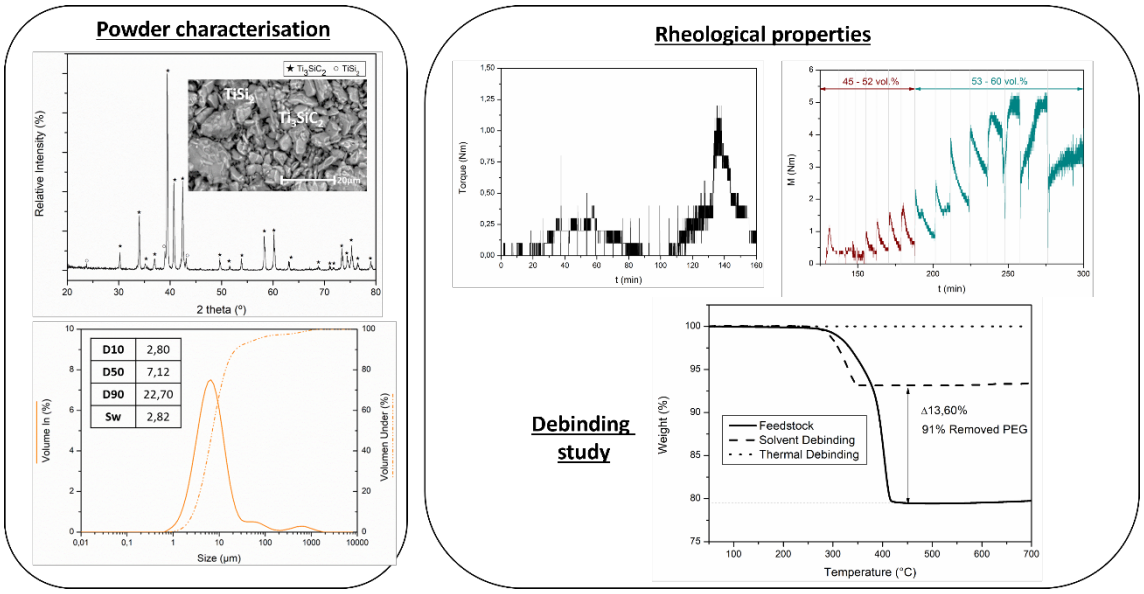

Manuscript refereed by Prof Thierry Barrière (University of Franche-Comte, France)

Powder Injection Moulding of MAX Phase Ti_3SiC_2

E. Tabares etabares@ing.uc3m.es; S. C. Cifuentes scifuent@ing.uc3m.es; A. Jimenez-Morales toni@ing.uc3m.es; S.A. Tsipas stsipas@ing.uc3m.es

Departamento de Ciencia e Ingeniería de Materiales e Ingeniería Química, IAAB, Universidad Carlos III de Madrid, Avda. de la Universidad, 30, 28911 Leganés, Madrid, Spain.

Abstract

The excellent combination of metallic and ceramic like properties of MAX phases have caught the attention of researchers in the recent years. New applications for these materials are being studied due to their unique characteristics. In this work, a new processing route is studied for MAX phase Ti_3SiC_2, Powder injection Moulding (PIM). Self-synthesized powders were mixed with a multicomponent binder for the production of sustainable feedstocks, using a combination of water soluble and low CO_2 emission polymers. A critical solid loading has been determined and rheological properties, debinding conditions and sintering parameters have been adjusted to achieve good quality samples. Furthermore, in depth characterization of all PIM stages has been done to control porosity in the final parts. The main goal of this work is to give added value to MAX Phases components and broaden their application fields through PIM technology.

Keywords: Ti_3SiC_2, powder injection moulding, sustainable feedstock.

Introduction

MAX phases are a group of ternary compounds whose general formula is $M_{n+1}AX_n$ (where M is a transition element, A an element generally from groups IIIA o IVA from the periodic table and X may be C or N, and n=1-3) [1]. They have a nanolaminated structure that gives them unusual properties. MAX phases combine typical metal and ceramic properties, such as high rigidity, good mechanical properties at high temperatures, high resistance to corrosion and oxidation and good thermal and electrical conductivity. Furthermore, they show the mechanical damping characteristics (shock-absorption) of laminated materials: they deform forming kink bands, which allow them to absorb large amounts of energy [2].

To date, most of the research focus has been on the synthesis and characterization of different MAX phases to explore possible applications of this material. Thus, samples obtained have the shape characteristic of the synthesis route or they are crushed to produce powder. Near net shaping, such as, powder injection moulding (PIM) stands as an interesting processing route to obtain final samples with the geometry desired. With PIM it is possible to produce complex shaped samples with high reproducibility at a low cost [3]. During the synthesis of MAX phase powders it is possible to adapt powder production in order to make them suitable for the injection process since it is known that initial powders characteristics (particle size, morphology) affect the processing route [4]. Furthermore, the binder system used has a great influence since it gives the material the necessary viscosity properties for a correct filling of the mould. In addition, this polymer system has to be removed from the samples before densification retaining the structural properties and avoiding defects in the sample. In this work, synthesized powders have been characterized and tailored for the PIM processing. Several feedstocks were produced combining MAX phase Ti_3SiC_2 powders, and a sustainable binder composed of Polyethylene glycol (PEG) and cellulose acetate butyrate (CAB). All steps of the processing route where characterized and controlled.

Experimental procedure

MAX phase Ti_3SiC_2 powders were synthesized starting from powders of Ti (TLS Technik GmbH, 99% purity, D_{50} = 8,36 µm), SiC (Navarro SiC S.A., 99,5% purity, D_{50} = 11,98 µm) and C (Ismaf, 99,5% purity, D_{50} = 23,78 µm) with a molar ratios of 3:1,5:0,5. Initial powders mixture was mixed in a turbula shaker mixer for 1 hour. Powders were then cold isostatic pressed (CIP) at 400 MPa for 10 minutes and green compacts were sintered under vacuum atmosphere (2,5 x 10^{-5} bar) at 1300 ºC for 6 hours. These heat treatment parameters have been adjusted to ensure a high purity of the MAX phase powders. Microstructural and phase composition was analysed combining x-ray diffractometry (XRD,

Philips X'pert) and scanning electron microscopy (SEM, Philips XL-30) coupled with Energy-Dispersive X-ray Spectroscopy (EDS, EDAX)

Different density measurements can also help to predict the suitability of a powder for the injection process. For that purpose, Helium pycnometry (AccuPYC 1330, Micrometrics) was done to measure the real density of the powders produced. In addition, standard test method ASTM B527 – 15 was carried out to determine the tap density of the powders. Moreover, to calculate the apparent density of the powders standard test method ASTM B417 – 18 was followed. These two densities are directly related with the morphology, packaging capacity and particle size distribution of the powders.

Determination of critical solid loadings was done following different routes. In first place, oil adsorption test was carried out in order to determine the minimum volume of oil that is necessary to cover the particles. In this test, the chamber of a rotor mixing machine (Haake Polylab QC, Thermofisher) with a fixed powder volume is filled by adding oil. With this procedure is it possible to observe torque variations and determine the critical solid loading for a specific powder with Equation 1:

$$CPVC = \frac{V_p}{V_p + V_o}$$

Equation 1

where CPVC is the critical powder volume concentration, V_p is the powder volume in the chamber and V_o is the oil volume poured at a specific time in the chamber.

In addition, a multistep torque analysis was done at CPVC values close the obtained from the oil adsorption test. In this test, a fixed volume of binder is poured into the mixing chamber and melted. Torque variations are analysed with respect to the incremental addition of solid loading into the chamber, thus, increasing the CPVC of the mixture, simulating torque response of feedstocks with different solid loadings.

For the production of feedstock, powders were mixed in a Haake Polylab QC torque rheometer with a multicomponent binder composed of polyethylene glycol (PEG) and cellulose acetate butyrate (CAB) with different solid loadings.

For the binder removal, a two-step process was done to ensure the structural integrity of the samples. PEG removal was carried out though solvent debinding: samples were immersed in distilled water for 5 hours at 60 ºC. Dried samples were then introduced in a debinding furnace (GD-DC-50, Goceram) at 360 ºC for 1 hour under argon atmosphere, heating and cooling rates were set at 2 ºC/min to ensure the correct elimination of the polymeric binder. With every step of the debinding process, thermogravimetric analysis was performed (STA 6000, PerkinElmer) to study the elimination process of the binder analysing mass loss of the samples.

Results and discussion

Ti_3SiC_2 synthesized powders have a purity of 90% and $TiSi_2$ as secondary phase, as shown in Figure 1-Left, in addition, micrographic analysis of the powders confirm the presence of $TiSi_2$ as an secondary phase. Table 1 shows EDS analysis done to the synthesized powders, there is a lighter zone corresponding to MAX phase Ti_3SiC_2 (Point 1 in Figure 1-Right) and a darker zone that corresponds to the secondary phase $TiSi_2$ (Point 2 in Figure 1-Right). Furthermore, powders exhibit a broad particle size distribution (Figure 2 and Table 2), ranging from 2,80 µm (D_{10}) to 22,70 µm (D_{90}).The slope parameter, Sw, indicates a low viscosity, easy to mould powders, an important parameter as it can predict powders behaviour and suitability during the injection process.

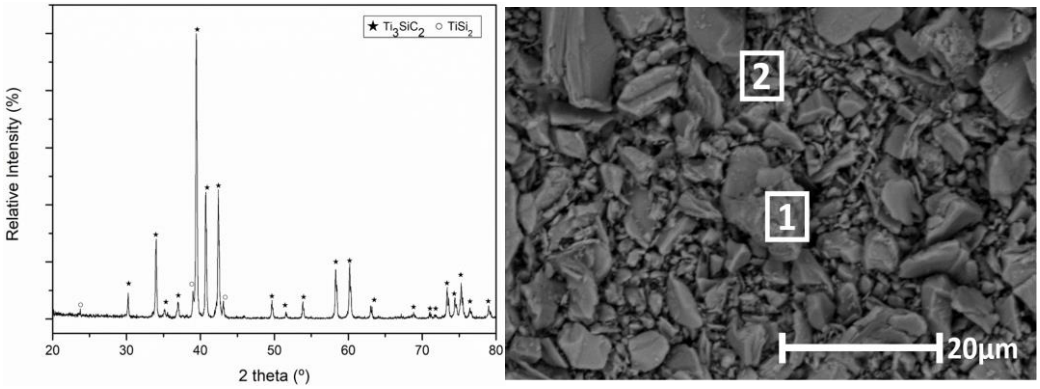

Figure 1. Characterization of synthesized powders. (Left) DRX analysis and (Right) SEM micrograph of the powders produced

Table 1. EDS point analysis of powders represented in Figure 1

Point	Ti	Si	C	Possible Phase
1	56	20	24	Ti_3SiC_2
2	25	74	1	$TiSi_2$

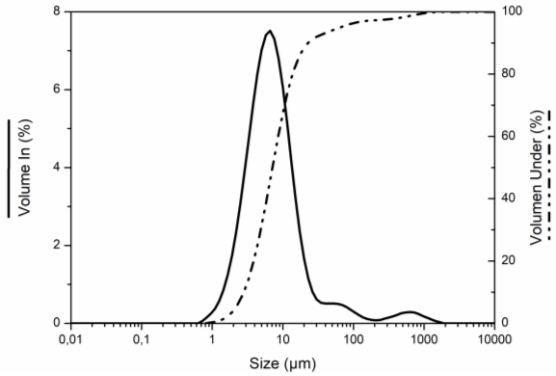

Figure 2. Particle size distribution of synthesized powders of MAX phase Ti_3SiC_2

Table 2. Mean particle size of MAX phase Ti_3SiC_2 powders produced, obtained from Particle size distribution analysis

D_{10} (µm)	D_{50} (µm)	D_{90} (µm)	Sw (µm)
2,80	7,12	22,70	2,82

Density measurement (summarised in Table 3) shows a lower density than the theoretical for MAX phase Ti_3SiC_2 (4,52 gr/cm^3). This lower value could be due to the presence of the secondary phase $TiSi_2$ with a theoretical density of 4,02 gr/cm^3 and as a result of microporosity in the synthesized powder. As it can be seen both apparent density and tap density of the powders are below 50% of the real density; this value should be above that 50% as an ideal property for powder injection moulding. Even though apparent and tap density are not theoretically optimal, previous work has determined that, although it is an important factor, is not critical to disregard the suitability of the powders [6].

Table 3. Real, apparent and tap densities of the synthesized MAX phase powders Ti_3SiC_2

ρ_{real} (gr/cm^3)	ρ_{tap} (%real)	ρ_{app} (%real)
4,44 ± 0,03	38	21

Solid loading determination and rheological properties of feedstocks

Critical solid loading, as a first approximation, was determined analysing torque behaviour with the oil absorption test. Vertical lines in Figure 3 represent the opening of the chamber to introduce oil after each stabilization of torque. With time, viscosity of the mixture decreases and consequently torque. At these first stages, there is an excess of powder in the mixture. Once a homogenous mixture is achieved, torque increases indicating a critical solid loading. After reaching this point, excess of oil decreases constantly torque values. In this test, it is observed how there is a maximum torque value

achieved at 140 min corresponding to a 53 vol. %. This value represents the critical solid loading of the mixture for the oil adsorption test, indicating a starting point for further analysis with the polymeric binder used for the feedstock production.

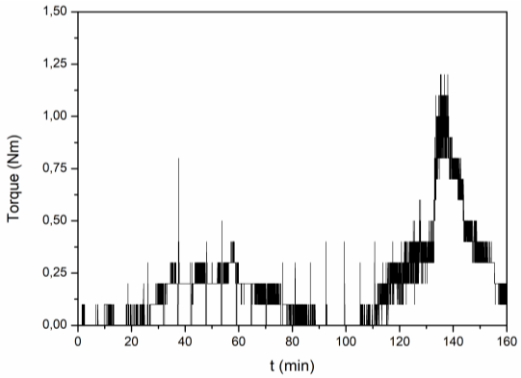

Figure 3. Oil absorption test of Ti_3SiC_2 powders

After this preliminary test, torque analysis of the compositions using the polymeric binder was studied from 45 to 65 vol. % through multistep torque analysis. In this case, vertical lines are added in Figure 4 to clarify powder addition into the chamber. In the first stage (45-52 vol. %), there is a low torque response. Once higher volumetric fraction of powder is added, there is an increase in torque when the mixing chamber is being closed and with time this value decreases stabilizing when the mixture is homogenous. Feedstock behaviour changes when the mixture approaches the critical solid loading (53-59 vol. %). In this case, it is clear how torque values are higher, also how the stabilization of the feedstock varies with solid loading addition. Initially, stabilization of the mixtures follows the same trend: torque increases with the addition of powders and decreases while homogenising, but at higher torque values than the previous stage. This changes with the increase in solid loading: once the chamber is closed torque values increase with time. This indicates that for the polymeric binder is hard to accommodate more powders into the mixture, creating non-homogenous feedstock with non-mixed powder.

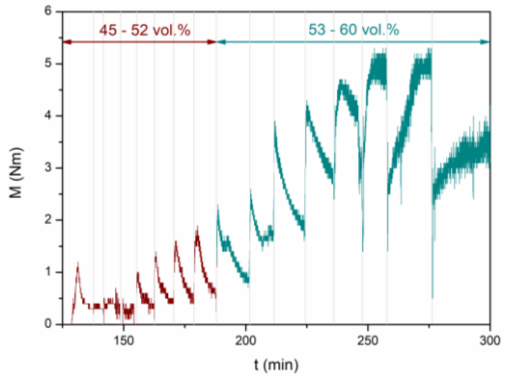

Figure 4. Variation of torque with time during multistep torque analysis of feedstocks with solid loadings from 45 to 59 vol. %

Characterization of green and brown samples

Green samples were obtained by compaction moulding of the feedstocks and micrographs of the cross sections are shown in Figure 5. Lighter zones represent MAX phases Ti_3SiC_2 powders and darker ones to the binder. Feedstock with a 49 vol. % of solid loading is not homogenous due to the lack of solid content in the mixture. It is clear how homogeneity of the feedstocks increases with the increase of solid loading. During solvent debinding, mass of the samples was controlled to measure the elimination of PEG, and after drying, mass variation calculations showed an elimination of the polymer above 90 wt. %. The same procedure was done after thermal debinding, where mass variation exhibited a loss of 95 wt. % and above for all feedstocks. After the debinding processes, no defects were found superficially and the structural integrity of samples maintained, validating the two-step debinding process and conditions as it can be seen in Figure 6.

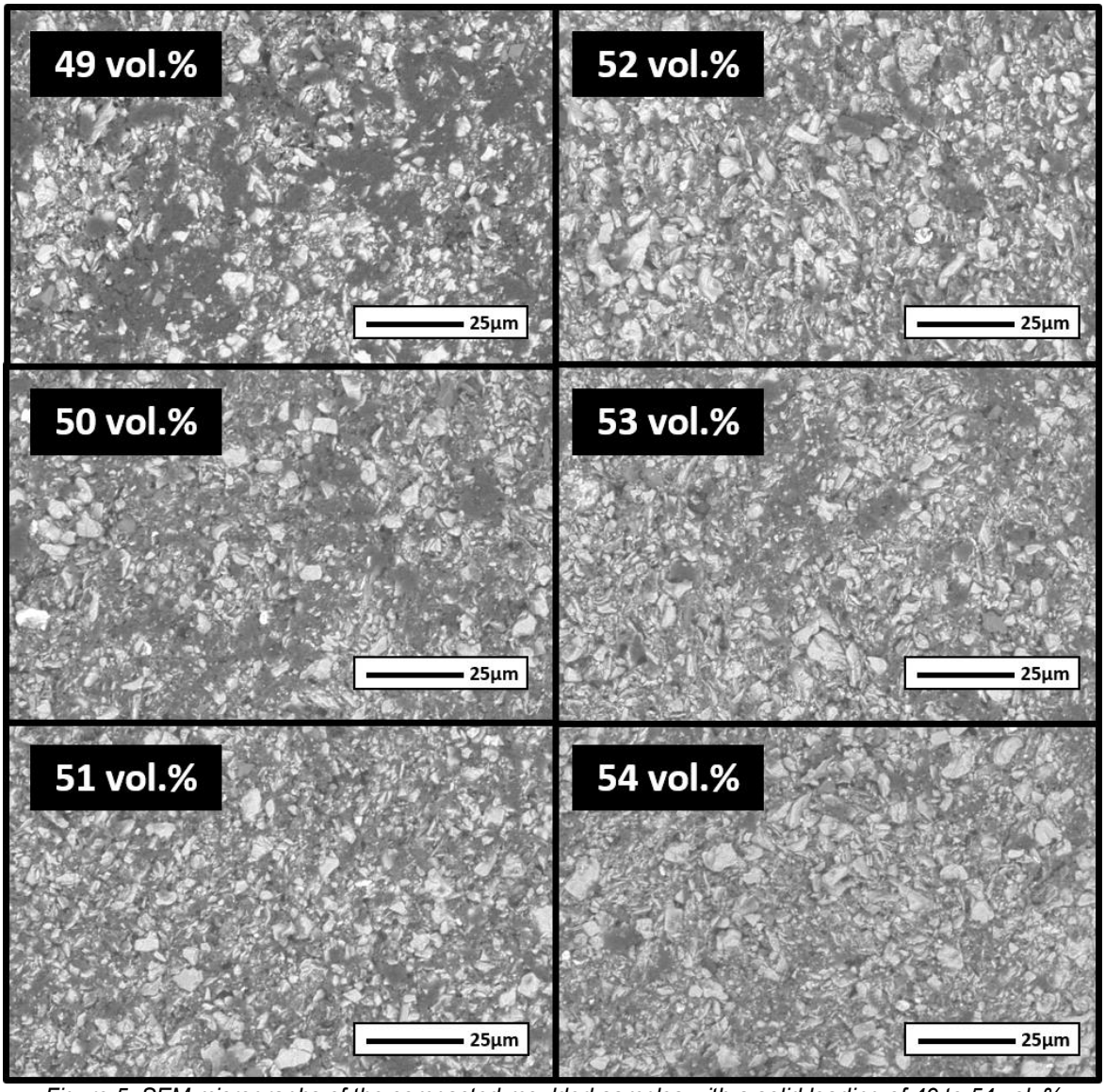

Figure 5. SEM micrographs of the compacted moulded samples with a solid loading of 49 to 54 vol. %

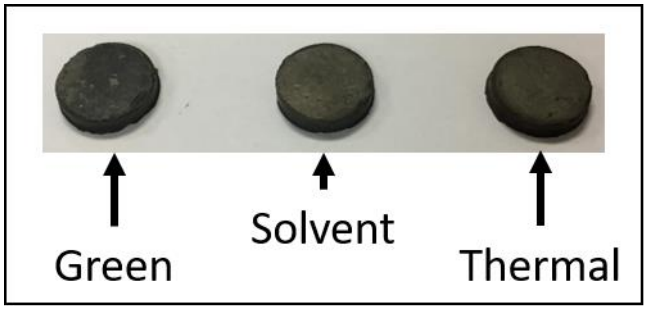

Figure 6. Samples during different injection steps. (Left) Green sample, (Centre) after solvent debinding and (Right) after thermal debinding

Furthermore, these calculations were contrasted with thermogravimetric analysis, Figure 7 shows as a representative example of the results obtained for feedstock with a 49 vol. % of solid loading. Feedstock curve represents the green sample where that 79,5 wt. % corresponds to the 51 vol. % of binder in the mixture. After solvent debinding, the amount of mass difference compared to the green sample matches that of the PEG removed during the process, in this case the amount to polymer removed reaches a 91 wt. % of the total amount of polymer added. After thermal debinding, thermogravimetric analysis shows no mass loss, indicating almost complete elimination of the binder, confirming the mass loss calculations results.

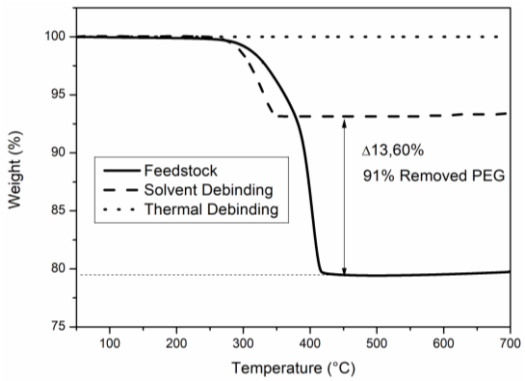

Figure 7. Thermogravimetric analysis of different stages of the debinding process for feedstock with a 49 vol. % of solid loading

Conclusions

MAX phase Ti_3SiC_2 powders with high purity were successfully produced starting from an initial mixture of Ti:SiC:C with a molar ratio of 3:1,5:0,5. Characterization of the powder produced showed an optimal particle size distribution and easy to mould powders. Critical solid loading of the mixtures was determined and feedstocks with different solid loadings were successfully produced. Green samples were obtained showing good homogeneity for feedstocks with a 50 vol. % of solid loading and above. The debinding process was adjusted achieving almost total removal of the binder in a two-step debinding, combining solvent and thermal debinding. In addition, structural integrity of the samples was maintained after the removal of the binder.

Acknowledgements

The authors would like to thank the funding provided for this research by the Regional Government of Madrid (Dir. Gral. Universidades e Investigación) through the project P2018/NMT4411 (ADITIMAT-CM), the Spanish Government through the Ramón y Cajal contract RYC-2014-15014 and the project MAT2012-38650-C02-01.

References

[1] M.W. Barsoum, The Mn+1AXn Phases: A New Class of Solids, Prog. Solid State Chem. 28 (2000) 201–281. doi:10.1016/S0079-6786(00)00006-6.

[2] M. Barsoum, T. El-Raghy, The MAX phases: unique new carbide and nitride materials ternary ceramics turn out to be surprisingly soft and machinable, yet also heat-tolerant, strong and lightweight, 2001.

[3] R.M. German, Injection molding of metals and ceramics, Princeton New Jersey : Metal Powder Industries Federation, Princeton (New Jersey), 1997.

[4] R.M. German, Powder metallurgy science, Met. Powder Ind. Fed. 105 Coll. Rd. E, Princeton, N. J. 08540, U. S. A, 1984. 279. (1984).

[5] A. de Waele, Viscosimetry and plastometry, J. Oil Colour Chem. Assoc. 6 (1923) 33–80.

[6] J. Hidalgo, C. Abajo, A. Jiménez-morales, J.M. Torralba, Effect of a binder system on the low-pressure powder injection moulding of water-soluble zircon feedstocks, J. Eur. Ceram. Soc. 33 (2013) 3185–3194. doi:10.1016/j.jeurceramsoc.2013.06.027.

[7] D. Lin, D. Sanetrnik, H. Cho, S.T. Chung, Y.S. Kwon, K.H. Kate, B. Hausnerova, S. V. Atre, S.J. Park, Rheological and thermal debinding properties of blended elemental Ti-6Al-4V powder injection molding feedstock, Powder Technol. 311 (2017) 357–363. doi:10.1016/j.powtec.2016.12.071.

6.2 Injection moulding of porous MAX phase Ti_3SiC_2 without using space-holder

Authors: Eduardo Tabares[a], Sandra C. Cifuentes[b], Antonia Jiménez-Morales[a], Sophia A. Tsipas[a]

[a] Departamento de Ciencia e Ingeniería de Materiales e Ingeniería Química, IAAB, Universidad Carlos lll de Madrid, Avda. De la Universidad 30, 38911 Leganés, Spain

[b] Área de Ciencia e Ingeniería de Materiales, ESCET, Universidad Rey Juan Carlos, C/ Tulipán s/n, 28933 Móstoles, Madrid, Spain

Journal: Powder Technology
Publisher: ELSEVIER; ISSN: 032-5810; Category: Engineering, Chemical: 30 of 143 (Q1); IMPACT FACTOR: 5.134 (JCR 2020)

Scope of this paper:

After the first approximation of the injection process shown in **Section 6.1**, this scientific publication shows an in-depth study of the rheological properties and characteristics of the Ti_3SiC_2-PEG/CAB feedstocks. This work intends to validate the use of powder injection moulding as a processing route for complex shaped samples, increasing the application range of MAX phases, as well as taking advantage of the polymeric binder as porosity former, instead of using sacrificial elements to obtain tailored porous materials. Feedstocks with different solid loading were characterised and optimised to produce porous samples, obtaining a controlled porosity that depended on the solid loading of each feedstock. The binders produced exhibited good rheological behaviour with viscosity values at a recommended range for the injection process, allowing the final porosity of the samples to be tailored depending on the solid loading of the feedstocks. In this way, PIM is used for producing porous MAX phase samples, without the use of space-holders.

Graphical Abstract:

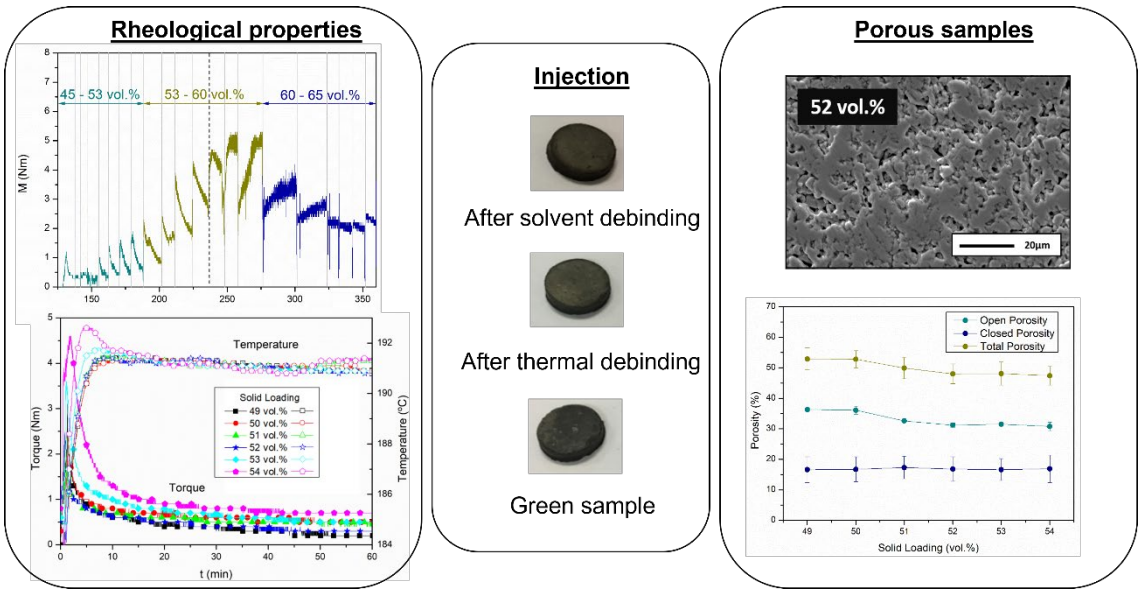

Powder Technology 380 (2021) 96–105

Contents lists available at ScienceDirect

Powder Technology

journal homepage: www.elsevier.com/locate/powtec

Injection moulding of porous MAX phase Ti_3SiC_2 without using space-holder

Eduardo Tabares [a], Sandra C. Cifuentes [a,b], Antonia Jiménez-Morales [a], Sophia A. Tsipas [a,*]

[a] Departamento de Ciencia e Ingeniería de Materiales e Ingeniería Química, IAAB, Universidad Carlos III de Madrid, Avda. de la Universidad, 30, 28911 Leganés, Madrid, Spain
[b] Área de Ciencia e Ingeniería de Materiales, ESCET, Universidad Rey Juan Carlos, C/Tulipán s/n, 28933 Móstoles, Madrid, Spain

ARTICLE INFO

Article history:
Received 14 July 2020
Received in revised form 26 October 2020
Accepted 12 November 2020
Available online 18 November 2020

Keywords:
Ti_3SiC_2
MAX phase
Powder injection moulding
Porous material
Rheology

ABSTRACT

Ti_3SiC_2 is one of the most studied MAX phase due to its unique combination of metallic and ceramic like properties. In this work, Powder Injection Moulding (PIM) is proposed as a new processing route to manufacture porous MAX phase Ti_3SiC_2, without the need of a space holder. The main goal of this work is to broaden MAX phase application fields through powder injection moulding technology. In depth characterization of all process stages has been done to control porosity in the final parts. Self-synthesized powders were mixed with a multicomponent binder for the production of sustainable feedstocks. The binder selection was carried out considering the design of a process with the reduction of the carbon footprint. In this sense, the binder consists of a combination of water soluble and low CO_2 emission polymers. Feedstocks produced exhibit good properties for injection moulding. Critical solid loading (52 vol%) and a set of debinding debinding conditions has been determined for a two-step process without producing any defects in the samples. In addition, sintering parameters have been adjusted to successfully achieve porous MAX phase samples.

1. Introduction

MAX phase family stands as a promising material for transport, communication and even biomedical industries due to their unique combination of properties. These materials have some of the best attributes of ceramic materials, such as, high corrosion and oxidation resistance and good mechanical properties at high temperature; and metallic properties, such as, high electrical and thermal conductivity and machinability, among others [1–3]. These materials have a fixed stoichiometry with a general formula of $M_{n+1}AX_n$, being M a transition element, A an element from groups IIIA or IVA and X either C or N, with $n = 1–3$ [3].

Within the different MAX phases, Ti_3SiC_2 is one of the most studied due to its unique mechanical and electrical behaviour [4]. The synthesis process of MAX phase Ti_3SiC_2 can be done using different starting powder combinations and techniques, and the aim is usually to obtain dense samples. MAX phase materials are often proposed as an alternative for high temperature applications and aggressive conditions where most materials lose their mechanical properties, or as heat exchangers. Thus, bulk dense samples are frequently obtained through synthesis [5,6] or they are crushed to produce powder for further processing [7].

For the production of porous MAX phases or foams, different techniques have been followed. Gonzalez-Julian et al. [8] used the space holder technique to produce materials with macroporosity using NH_4HCO_3, being able to control the porosity by selecting the amount of space holder in the prepared Cr_2AlC MAX phase materials. In addition, Velasco et al. [9] proposed the use of saccharose as a space holder to facilitate space holder removal before the sintering step using water to avoid possible corrosion effects in the samples and controlling the macroporosity in Ti_2AlC foams. The main reason for using these techniques is to control the amount of porosity and pore size achieved through these methods. Regarding Ti_3SiC_2, the predominant method used is a one-step process to synthesize the MAX phase and create porosity in the sample through reactive synthesis. Liu et al. [10] present a corrosion study for filtration/separation applications of the porous Ti_3SiC_2 showing high corrosion resistance of the porous samples prepared after immersion in different acid solutions. In addition, Ziqi et al. [11] proposed this MAX phase for catalytic devices, producing Ti_3SiC_2 supports with 80 vol% open porosity due to the excellent electrical conductivity of this material. In addition, for MAX phase Ti_3SiC_2, Wang et al. [12] reported the production of porous samples and the synthesis of the MAX phase with the addition of Al to control Ti_3SiC_2 purity; porosity in the samples was controlled with the variation of the titanium particle size in the initial mixture and through reactive sintering. In general terms, all of this MAX phase porous production lack of a controlled final shape of the samples compared to near-net shape techniques.

The injection process has been demonstrated as a reliable method to produce near net shaped components with high surface quality, of monolithic and composite MAX phase materials including Ti_3SiC_2,with theoretical density of 80,8% [13]. The production of porous samples by

* Corresponding author.
E-mail address: stsipas@ing.uc3m.es (S.A. Tsipas).

https://doi.org/10.1016/j.powtec.2020.11.022
0032-5910/

powder injection moulding (PIM), have been usually performed decreasing the amount of solid loading in the feedstocks or by adding a secondary polymeric binder in the mixture to act as a space holder reducing the solid loading during the PIM process [14,15].

This work proposes the production of porous MAX phase by powder injection moulding without the need of a space holder nor the addition of secondary-sacrificial binders. In this sense, PIM stands as an interesting processing route to obtain final components with the desired geometry and offers the possibility to produce complex shaped porous samples with high reproducibility at a low cost. For this purpose, MAX phase powders produced have to be suitable for the injection process, namely, the initial powders characteristics (particle size, morphology, packaging behaviour) must be analysed [16,17]. A processing route is presented to obtain porous MAX phases by PIM without the need of a space holder. In-depth characterization of the complete process (from feedstock optimization to sintered porous materials) is presented. Several feedstocks were produced combining MAX phase Ti_3SiC_2 powders, and a sustainable binder composed of Polyethylene glycol (PEG) and cellulose acetate butyrate (CAB). Feedstocks rheology was studied as well as moulding, debinding and sintering stages. All steps of the processing route were controlled to achieve porous materials. Thus, from this comprehensive study, it can be concluded that this work validates the PIM process as an effective production technique for porous MAX phase materials.

2. Experimental procedure

2.1. Powder synthesis and characterization

Titanium silicon carbide powders were prepared starting from Ti:SiC:C with a molar ratio of 3:1,5:0,5. The powder synthesis was previously optimized for the production of high purity MAX phase [18]. Summarising, initial powders were mixed in a Turbula shaker mixer for 1 h and compacted at 400 MPa by cold isostatic pressing (EPSI systems, Belgium). For the synthesis of MAX phase Ti_3SiC_2, compacted samples were sintered at 1300 °C for 6 h in a vacuum furnace. Sintered pellets were then milled in a planetary ball mill (Pulverisette 5/2, Fritsch, Germany) to obtain the powders. XRD profile of the synthesized powders indicates an average phase purity of 92 vol% and the presence of a secondary intermediate phase of $TiSi_2$ (Fig. 1a), which is confirmed in the micrographic analysis of the powders, that shows a wide majority of the MAX phase (Fig. 1b). Other intermediate phases or evidence of contamination during the milling process was not detected using XRD and micrographic analysis.

The suitability of the powders for the injection process was predicted calculating the slope parameter of this distribution called S_w [19]. Values of S_w, between 2 and 4 mean that the particle size distribution is broad, and the powders will exhibit a low viscosity (easy-to-mould) [19]. Values corresponding to a narrow particle size distribution (S_w= 4–7) are characteristic of powders that exhibit a high viscosity. Particle size distribution was determined by MasterSizer 2000 analyser (Malvern Instruments, UK). With the milling of sintered pellets, it is possible to tailor the resulting powders to produce broad particle size distributions, which are optimal for injection. Fig. 2 shows the average particle size distribution of the synthesized powders. MAX phase powders exhibit a wide range of particle sizes. The slope parameter of the powders produced has a value of 2,82 (between 2 and 4), predicting an easy-to-mould powder with a low viscosity. Therefore, the synthesis method employed is capable of producing powders with appropriate characteristics for PIM.

Powders density was measured with a helium pycnometer (AccuPyc 1330, Micrometrics, US). Apparent density and tap density were measured following standards ASTM B212-17 and ASTM B527-15, respectively. These values are indicative of the packaging behaviour of the powders depending on their characteristics, such as particle size distribution, morphology or tendency to agglomerate. In the case of tap density, a value higher than 50% of theoretical density would correlate to an optimal powder to obtain dense samples through the injection process [19].

The composition of the multicomponent binder selected for the production of the feedstocks is detailed in Table 1. This binder has been successfully used for processing zircon feedstocks [20] showing good torque and viscosity behaviour of the feedstocks for injection moulding. Two different PEGs were used with molecular weight of 4.000 and 20.000 g/mol, respectively, this polymeric binder was selected due to its sustainable characteristics. Polyethylene glycol (PEG) is a water-soluble polymer, preventing the use of organic solvents for its removal. In addition, cellulose acetate butyrate (CAB) with a molecular weight of 30.000 g/mol was used. This polymer exhibits good mechanical properties, acting as a backbone during the debinding process: Furthermore, CAB produces non-toxic emissions during degradation process. The PEG/CAB system is an excellent binder for controlled debinding. Different additives are used as surfactant (stearic acid, SA) and antioxidant (Phenothiazine, PTZ).

2.2. Feedstock production

Feedstock optimal composition was determined employing various methods. A first approximation of the critical solid loading was done

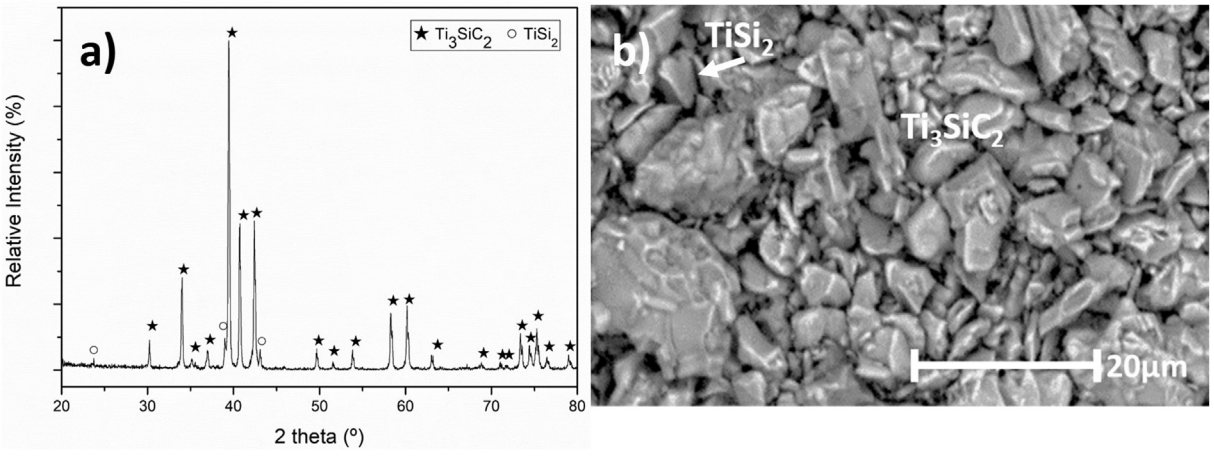

Fig. 1. a) XRD profile of Ti_3SiC_2 synthesized powders from an initial mixture of Ti:SiC:C with a molar ratio of 3:1,5:0,5 and b) SEM micrographs of synthesized powder of MAX phase Ti_3SiC_2.

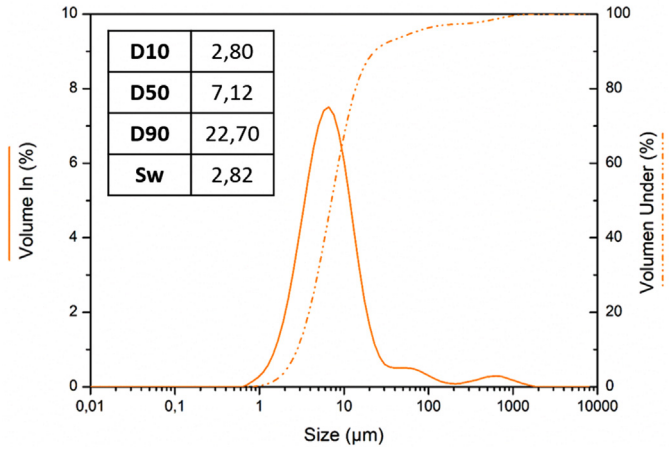

Fig. 2. Particle size distribution of synthesized powder of MAX phase Ti_3SiC_2.

Table 1
Composition of multicomponent binder and molecular mass of the polymers used.

	PEG	CAB
vol%	70	30
Molecular weight (gr/mol)	4.000–20.000	30.000
Supplier	Sigma-Aldrich	Eastman

by oil absorption (Haake Polylab QC, Thermofisher, US). Subsequently, torque rheology was studied by multistep torque analysis [21]. In this test, binder was melted in the torque rheometer at 180 °C and then powders were added increasing the solid loading of the feedstocks. In addition, after selecting several solid loadings, torque rheology was studied maintaining a fixed volume for all the feedstocks. Rollers were set at 50 rpm and torque stabilization was analysed for 1 h. Furthermore, viscosity of the feedstocks was studied through capillary rheology (Haake Rheocap S20, Thermofisher, US) with a relation between the length and diameter of the die of 30:1. Tests were performed varying shear rates from 100 to 10,000 s^{-1} at 180 °C.

2.3. Powder injection moulding process

A first analysis was carried out to obtain green samples through an injection-like process, compaction moulding (OPAL 460, ATM-Advance Materialography, Germany). Green samples were obtained by melting the feedstock at 180 °C and filling the mould applying a pressure of 130 bar. Heating and cooling rates were adjusted to achieve optimal densification (16 and 8 °C/min, respectively).

For the debinding process, the removal of the polymeric binder was achieved using a multistep process: solvent and thermal debinding was combined to control the structural integrity of samples. Solvent debinding was carried out to remove PEG from green samples. In this step, samples were immersed in distilled water at 60 °C for 5 h under stirring. Samples were weighted and measured every hour to control the progressive elimination of the polymer. After the process, samples were dried in a furnace for 3 h at 70 °C. For the removal of CAB, thermal debinding process was carried out at a heating rate of 2 °C/min and a holding time of 1 h at 360 °C under argon atmosphere in a debinding furnace (GD-DC-50, Goceram, Sweden), obtaining samples without any polymeric binder after solvent and thermal debinding, referred as brown samples. Thermogravimetric analysis (STA 6000, PerkinElmer, US) was done for all samples to verify binder loss during after both stages of the debinding processes under argon atmosphere with a heating rate of 20 °C/min and a final temperature of 700 °C.

In addition, thermal analysis was performed for the selection of the sintering parameters through Differential Thermal analysis (SETSYS Evolution DTA/DSC, Setaram Instrumentation, France) under argon atmosphere with a heating rate of 10 °C/min and a final temperature of 1500 °C. After determining optimal sintering temperatures, brown samples were sintered in high vacuum (2×10^{-5} bar) at 1300 °C for 4 h and with heating and cooling rates of 5 °C/min.

2.4. Sample characterization

During different stages of the PIM process samples were characterized. Microstructural analysis was performed in a Scanning Electron Microscopy (SEM, Philips XL-30, US) coupled with Energy-Dispersive X-ray Spectroscopy (EDS, EDAX, US). Phase identification was obtained by X-Ray diffractometry (XRD, Philips X'pert, Netherlands) with Cu Kα radiation at 40 kV and 40 mA. In addition, porosity of sintered samples was measured by vacuum infiltration, following Archimedes' principle. For this, samples were introduced in ethanol and vacuum was applied for 30 min to guarantee the infiltration of ethanol in the samples. Weight variation of the samples correlates with the amount of porosity and it is possible to determine open and closed porosity using the following equations:

$$\rho = W_d \cdot \rho_{ethanol} / W_i - W_a \quad (1)$$

$$Porosity_{total}(\%) = (1 - \rho/\rho_t) \cdot 100 \quad (2)$$

$$Porosity_{open}(\%) = (W_i - W_d / W_i - W_a) \cdot 100 \quad (3)$$

$$Porosity_{closed}(\%) = Porosity_{total} - Porosity_{open} \quad (4)$$

where, W is the weight of the samples in different stages of the test (d = dry, i = infiltrated and a = after infiltration). ρ is the calculated density and ρ_t the theoretical density.

3. Results and discussions

3.1. Initial materials characterization

Density measurements of the powders produced show an experimental density of 4,44 g/cm^3; in addition, tap and apparent densities are a 39% and 21% of the powders value, respectively. As it can be seen from density measurements, powders have a relatively low packing value which, as a first approximation, would indicate the production of porous samples. However, determining final sample porosity is not trivial, and it is necessary to study the packaging behaviour of powders to predict density/porosity of sintered samples [17]. The packaging behaviour of powders depends on the particle size distribution, powder morphology and its tendency to create agglomerates. A tap density value lower than 50% of the theoretical value would be a first indication that porous samples will be obtained, although, it has been shown that even with a low tap density almost fully dense samples can be obtained [22], having this value lower than 50% of the theoretical value would be a first indication that porous samples will be obtained. In this sense, the synthesized powder would be suitable for the production of porous samples by injection moulding.

3.2. Critical solid loading determination and rheological characterization

As a first approximation, critical solid loading, was determined analysing torque behaviour with the oil absorption test (Fig. 3). This test is performed in order to determine a solid loading where increase of solid loading affects the torque. Determining this value prior to the multistep test is important, since analysing a high solid content powder feedstock with a low chamber fill could show a low torque value and lead to misrepresentation of the values. Since there is no information

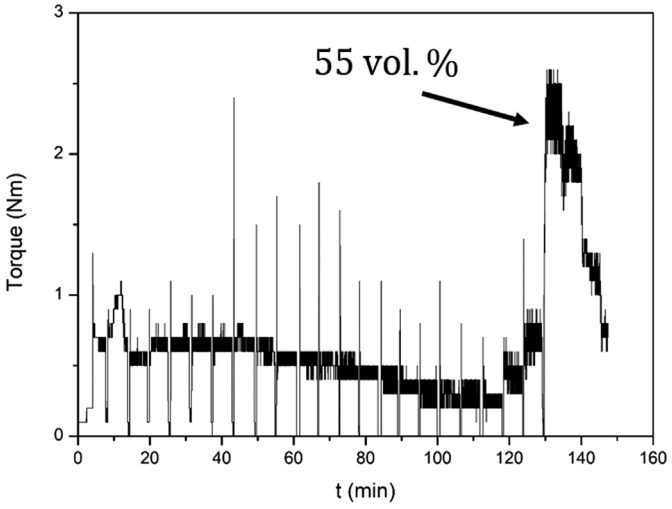

Fig. 3. Oil absorption test of Ti_3SiC_2 powders.

on the optimal solid content of the feedstock developed, oil absorption test gives a first idea on the solid loading to be analysed. Vertical lines in Fig. 3 represent opening of the chamber to introduce oil after each stabilization of torque. With time, viscosity of the mixture decreases and, consequently, torque decreases due to blending of the powder with the oil. During the initial stages, there is an excess of powder in the mixture. Once a homogenous mixture is achieved, torque increases noticeably (at around 55 vol%), indicating that a critical point in the amount of solid loading has been reached. After reaching this point, the oil added in excess causes a progressive decrement in torque values. From this test, mixture of powders and oil indicates a critical solid loading of 55 vol% as a starting point for further analysis.

Considering the results of this preliminary test, compositions below and above the critical solid loading (55 vol%) were selected for rheological studies. Feedstocks with 45 to 65 vol% of MAX phases were studied through multistep torque analysis. Fig. 4 shows the results of this study. Vertical lines indicate the addition of powder into the chamber. The graph can be divided in three distinct regions, where different tendencies can be observed. In the first stage (45–52 vol%), the mixtures have, in general, a low torque response. The powder is added progressively in higher volumetric fractions and there is an increase in torque when closing the mixing chamber which decreases progressively and stabilizes with time at a relatively low torque value when the mixture is homogeneous. Feedstock behaviour changes when the mixture approaches the critical solid loading (53–59 vol%). In this second stage, for solid loadings of 53–59 vol%, it is clear how final torque values are higher and how the stabilization of the feedstock varies with solid loading addition. Initially, stabilization of the mixtures follows the same trend as in the first stage: torque increases with the addition of powders and decreases after homogenizing, but at higher final torque values than those observed during the first stage. This behaviour changes when solid loading reaches 57 vol% (marked as a dash line in Fig. 4): for this solid loading, once the chamber is closed, torque values appear to increase with time. What occurs is that the polymeric binder cannot accommodate more powder into the mixture, creating non-homogenous feedstock with un-mixed powder. Lastly, in the third stage, when the amount of solid loading into the mixture is excessive (60–65 vol%) torque behaviour changes, decreasing its value. This can be explained due to the lubricating, behaviour of MAX phases, as a result of its layered, nanolaminated structure. With the increase of powder in the mixture and with a binder that is not able to accommodate more solid loading, unmixed powders with a lubricating behaviour decrease torque values.

Representing final torque values, after stabilization, against solid loading (Fig. 5), it is possible to determine a critical solid loading of powder with the selected polymeric binder that is going to be used for the injection process. The critical solid loading corresponds to the composition where there is a change of slopes in the torque behaviour. From the values obtained, critical solid loading is determined as 53 vol%. After reaching the maximum torque value at 59 vol% of solid loading, torque starts to decrease with the addition of solid loading as commented above. Mixtures within this range are composed of some mixed feedstock material and loose powders that cause the observed decrease in torque. They are not homogenous and, therefore, are not adequate for injection. These solid loadings were not considered optimum.

Solid loadings from 49 to 54 vol% were selected to study their rheological behaviour. Firstly, torque rheology of the feedstocks was analysed as shown in Fig. 6. For all mixtures, there is an increase in torque values as the powders are being introduced in the chamber and, as expected, torque values increase with higher solid loading. After 20 min of mixing, torque values of all feedstocks completely stabilize. Final torque values (M) are summarized in Table 2. Analysing M values, it can be seen that for feedstock with 52 vol% of solid loading there is a change in the increasing behaviour of the final torque value (M). In this case, final torque is lower than feedstocks with lower solid

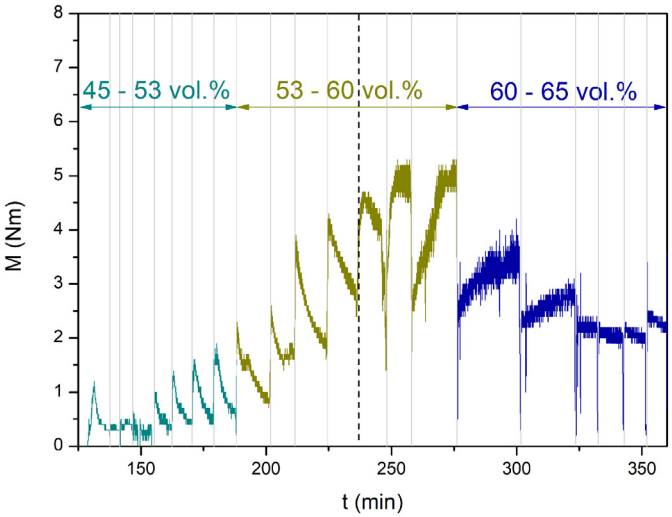

Fig. 4. Multistep torque analysis. Feedstocks with solid loadings from 45 to 65 vol%.

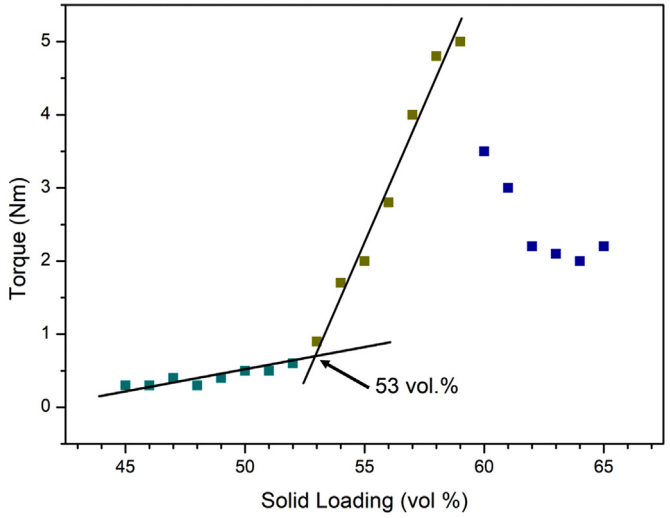

Fig. 5. Final torque of mixtures with solid loadings from 45 to 65 vol%.

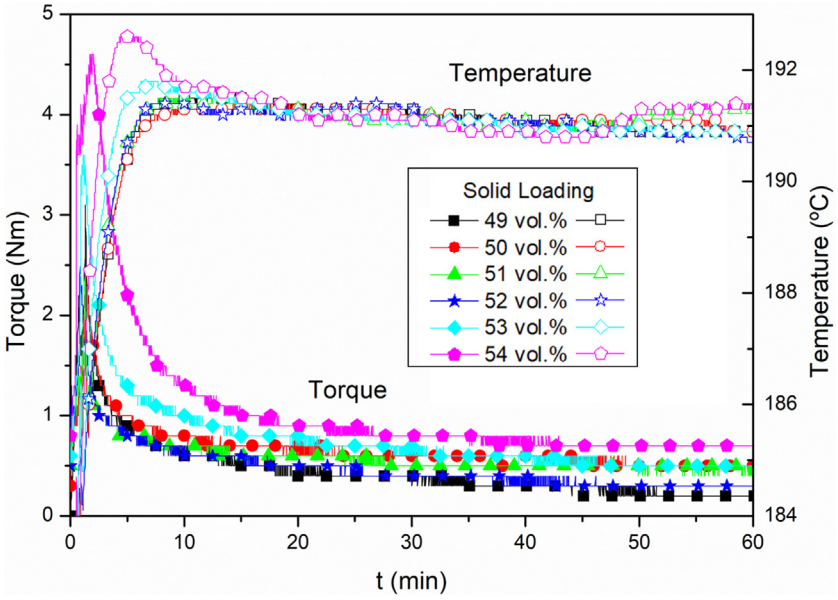

Fig. 6. Torque analysis of the feedstocks with solid loadings from 49 to 54 vol%.

Table 2
Torque mixing parameters for stabilized mixtures at 60 min for feedstocks produced.

Feedstock (vol%)	M* (Nm)	ΔM* (Nm)	T* (°C)	E_t* (kJ)	TTQ* (Nm min)
49	0,2	0,33	190,9	7,13	28,35
50	0,5	0,25	190,9	10,48	41,68
51	0,5	0,17	191,3	9,34	37,15
52	0,3	0,26	190,7	7,61	30,29
53	0,5	0,43	190,9	11,78	46,89
54	0,7	0,74	191,4	16,62	66,12

* *M* (final torque), *ΔM* (average deviation of torque), *T* (temperature), E_t (energy being put into the system) and *TTQ* (totalized torque).

content. This indicates that there is a better rheological behaviour of this particular feedstock, which presents the optimal mix for the injection process. This behaviour could be explained by a better powder-binder homogeneity of the mixture. A stable proportion between the amount of solid loading and binder can affect the dispersion of the powder within the polymer resulting in a lower friction with the blades causing a decrease in torque. In addition to torque values, internal temperature was monitored. Although the temperature was set at 180 °C for the test, mean value of the temperature reached values around 191 °C for all feedstocks, due to the internal friction during the mixing process, but not as high to produce the degradation of the binder. At lower mixing times, this effect is more noticeable; with higher solid loading, friction is higher and temperature in the chamber increases. With these results, it is possible to determine the totalized torque (*TTQ*). This value is the energy that the system is receiving at a given time. This value is considered as the area under the curve of the torque behaviour with time and it can be calculated by$TTQ = E_t/2 \cdot \pi \cdot N$ Eq. 5 [23]:

$$TTQ = E_t/2{\cdot}\pi{\cdot}N \tag{5}$$

where E_t is the energy being put into the system by the blades, and N is the angular speed of the blades. Fig. 7 shows the evolution of *TTQ* with time. As observed in the torque analysis, there is an increase in the energy being put into the system with the increment of solid loading, with the exception of feedstock with a 52 vol% of solid loading. This feedstock exhibits an energy for mixing that is lower than feedstocks with solid loadings of 51%, 50% and a similar energy of mixing to feedstock with

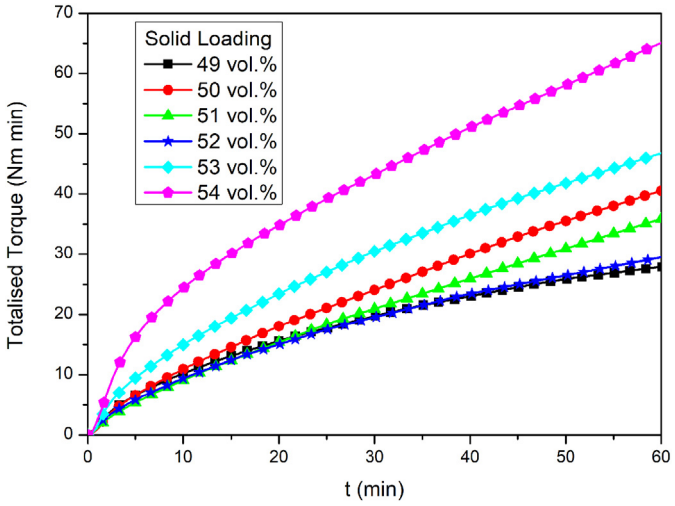

Fig. 7. Totalized torque values with time of the feedstocks with a solid loading from 49 to 54 vol%.

solid loading of 49%. Table 2 shows the final values of torque and TTQ, obtained after 60 min of mixing. It is evident that with a solid loading of 52 vol%, besides the decrement of the torque (M), the energy required during mixing (TTQ) also decreases.

Viscosity of the feedstocks was studied through capillary rheology. Fig. 8a represents viscosity values of the studied feedstocks at different shear rates. All mixtures show a pseudoplastic behaviour, where viscosity decreases with higher shear rates. There is a small increase in viscosity with the increase of solid loadings. However, similarly to as observed for torque rheology analysis, feedstock with solid loading of 52 vol% shows a behaviour comparable to feedstocks with lower solid loading (51 vol%), as mentioned earlier, homogeneity of the feedstock could have a major role in this: when the binder-powder composition is balanced for this particular material the mixing of the feedstock creates more homogenous regions decreasing the viscosity of the mixture. Furthermore, fluid index of the feedstocks (Table 3) demonstrates the pseudoplastic behaviour of all mixtures ($n < 1$) [24], in addition

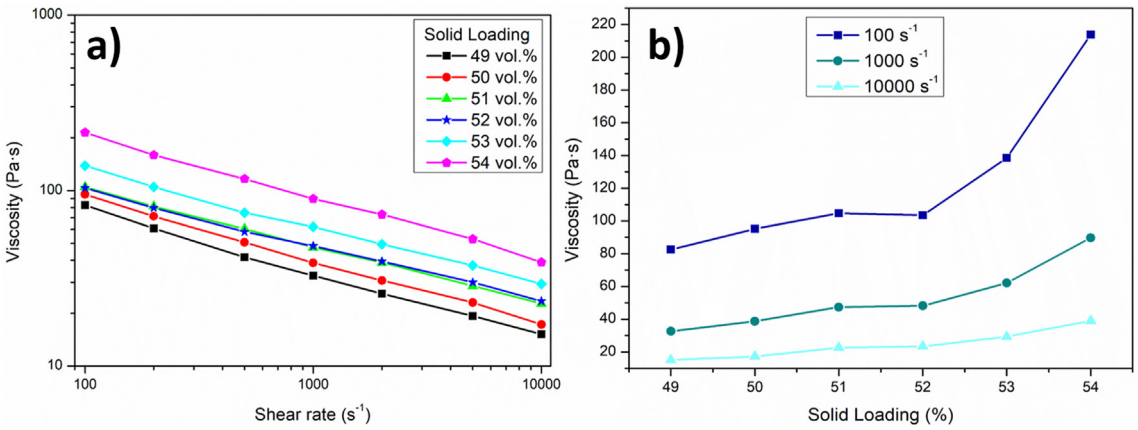

Fig. 8. a) Viscosity at different shear rates of the feedstocks and b) Viscosity behaviour of the feedstocks at different shear rates.

Table 3
Fluid index of the feedstocks and chi-square adjustments.

Feed stock	49 vol%	50 vol%	51 vol%	52 vol%	53 vol%	54 vol%
n	0,41	0,40	0,42	0,43	0,41	0,38
R	0,99	0,99	0,99	0,99	0,99	0,99

although all values are similar, it can be observed how the feedstock with solid loading of 52 vol% shows a higher fluid index, and thus, the best behaviour compared to the rest of the prepared feedstocks.

Moreover, viscosity was studied at different shear rates (Fig. 8b). Here, it is clearer how viscosity increases with the increase of the solid loading, except for solid loading of 52 vol% where viscosity exhibits the same value as the feedstock with 51 vol%. Also, for lower shear rates, the increase of viscosity is more noticeable at higher solid loadings (53–54 vol%) but always lower than recommended viscosities for powder injection moulding (1000 Pa·s) [19]. As mentioned earlier, CAB acts as the backbone in this polymeric binder and PEG gives the flowability to the mixtures. The selected molecular weights of PEG reduce the viscosity permitting highly load feedstocks [25].

These values are lower compared to reported viscosities for Ti_3SiC_2 and Ti_2AlC [13] using a mixture of paraffin and a PE resin as binder. This difference is due to a combination of the flowability of the binders used, but most importantly, due to the friction generated by the solid content in the feedstocks (62 vol% compared to 48–54 vol% used in this work). Overall, it is clear from the various techniques applied that, although the rheological behaviour is adequate for PIM process for all the solid loadings studied, a different behaviour is clearly observed at 52 vol%.

3.3. Effect of solid loading on microstructure and properties of samples during the injection steps

The injection process was studied for the different feedstocks in order to determine an optimal solid loading. Fig. 9 shows BSE micrographs of the cross section of samples obtained where lighter zones correspond to the MAX phase Ti_3SiC_2 powders and darker zones to the polymeric binder (PEG-CAB). From micrographs, it can be observed how the homogeneity of powder distribution varies depending on the solid loading. With less loading of solid particles in the mixture there is a worst dispersion of the powders (lighter zones in Fig. 9) in the polymeric binder (darker zones in Fig. 9). For the feedstock with a solid loading of 49 vol%, there are big gaps of polymer creating heterogeneous areas; in this case, there is not enough amount of powder to be surrounded by the binder even after 1 h of mixing. With the increase of solid loading these big gaps of polymer start to disappear reaching a point where the dispersion of powder-binder is homogenous. Analysing densities of the green samples it is possible to predict optimal solid loadings of feedstocks. Commonly, experimental density approaches theoretical values when the feedstocks is at an optimal solid loading and once it surpasses this value experimental density diverges from theoretical values. Fig. 10 shows calculated densities by helium pycnometry and theoretical density values of the mixtures. Analysing density values, it is clear how at 52 vol% of solid loading the experimental value is near the theoretical one and after this point density values tend to diverge from the theoretical value.

The amount of polymer removed after both processes is represented in Table 4. After solvent debinding the amount of PEG removed for all samples is between 90 and 93 wt% of the total PEG in the sample and after thermal debinding the amount of CAB and residual PEG degraded for all samples is between 96 and 98 wt% of the total CAB. With these results it can be concluded that the debinding process for this binder is optimal.

In addition to the mass loss calculations, thermogravimetric analysis was carried out to confirm the elimination of the polymeric binder. Fig. 11 shows different thermogravimetric analysis for the material with a solid loading of 49 vol%. The first analysis (grey line) corresponds to the green sample (feedstocks), there is a mass loss starting at 270 °C and finishing at 410 °C, this mass lost reaches to 79,9 wt% corresponding to the degradation of 51 vol% of the binder. The second analysis (green dashed line) belongs to the sample after solvent debinding, where PEG is removed from the system. In can be observed that the sample looses a 13,60% less of mass corresponding to a 91 vol% of PEG removed after the debinding process, this value agrees with the one calculated by weight difference of the samples shown in Table 4. Finally, the third analysis (red dotted line) shows that after the thermal cycle all the polymeric binder in the mixture has been removed, including both, the residuary PEG and all the CAB in the brown sample. There is no mass loss during the third analysis.

After the debinding process, all materials maintained their structural integrity with no defects detected macroscopically by visual inspection. Samples were sintered to obtain final parts. Fig. 12 shows the SE micrographs of the cross-section of sintered materials in order to analyse porosity and internal defects. In first place, it can be observed that it is possible to achieve well distributed irregular porosity without using space holder in the samples. For samples with 49 and 50 vol% some porous zones can be observed at the left of the micrographs and, the porosity on these samples is not well distributed. Samples from 51 to 53 vol% have a better distribution of the porosity through the micrograph exhibiting well disperse pores. Finally, 54 vol% sample again exhibits a lack of homogeneity through the micrograph with a big accumulated porous zone, probably due to the lack of a homogenous dispersion of the powder in the polymeric system at the green stage. Results of

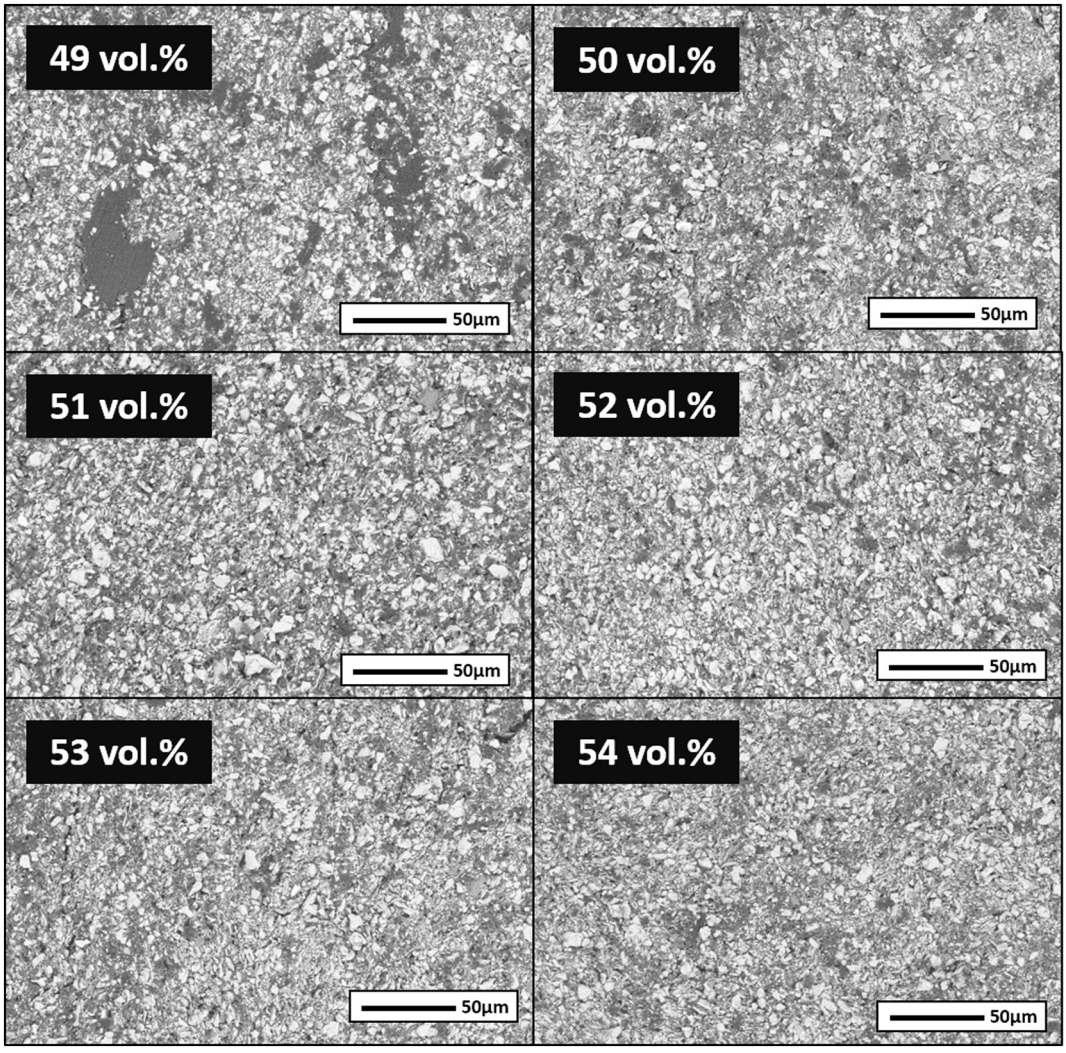

Fig. 9. Cross-section SEM micrographs of compaction moulded samples with solid loading from 49 to 54 vol%.

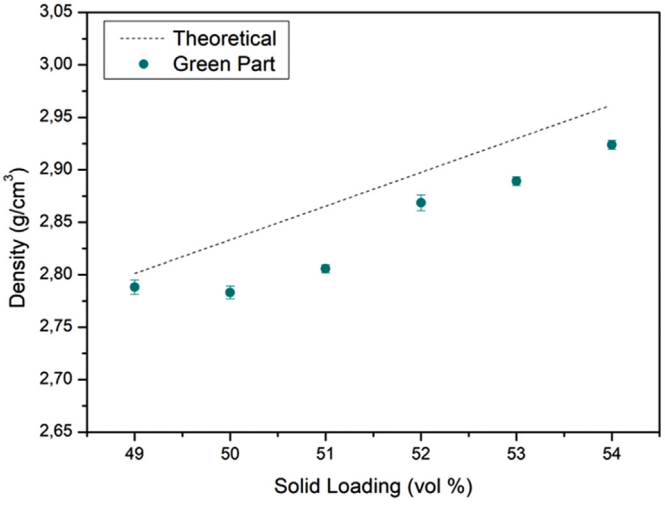

Fig. 10. Density theoretical and measured of green samples of feedstocks with solid loading from 49 to 54 vol%.

open and closed porosity obtained by the vacuum infiltration test can be observed in Fig. 13. Regarding closed porosity, values are constant for all the samples (≈ 16%). This can be related to the microporosity inherent in MAX phase production using pressureless sintering techniques [26]. On the other hand, open porosity has a direct connection with the amount of solid loading in the feedstocks produced. It can be seen how there is a general tendency of decrease in the porosity as solid loading increases. As the material densifies during the sintering process the amount of binder previously on the sample correlates to the total porosity obtained after the process. This value differs from the theoretical as much as a 3% for the mixture with a 50 vol% of solid loading, so it is possible to establish from the beginning of the process the amount of porosity that is desired in the material. Although further characterization of the porosity is not intended in this work, in comparison with other authors works some similarities can be established. Wang et al. [12] prepared Ti_3SiC_2 by reactive sintering with irregular porosity, the porous

Table 4
PEG and CAB removed after two-step debinding for feedstocks analysed.

vol%	49	50	51	52	53	54
Eliminated PEG (wt%)	92,6	91,7	92,3	90,4	91,1	91,4
Eliminated CAB (wt%)	96,5	97,9	98,5	97,2	97,1	96,6

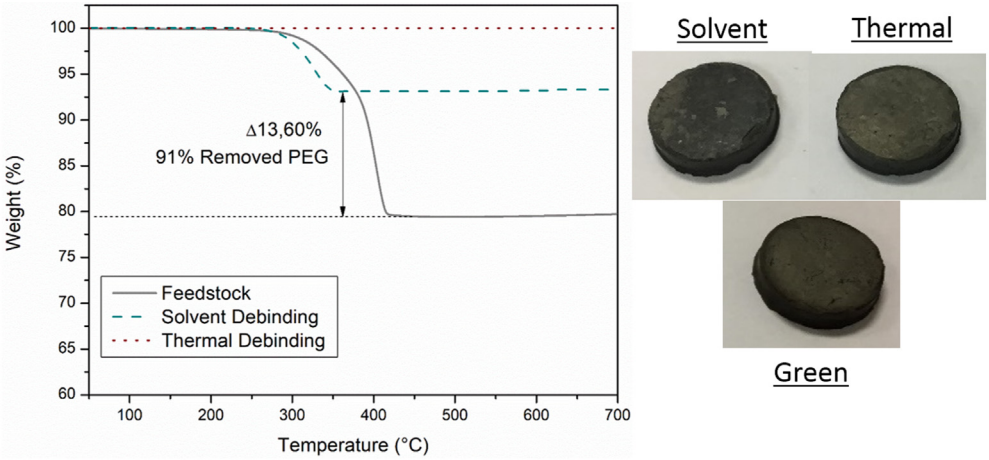

Fig. 11. TGA analysis of feedstock with a solid loading of 49 vol%, before and after the two-step debinding process.

morphology they obtained was similar to the one obtained in this work. However, reactive sintering is not a near-net shape method and does not give the possibility of generating complex shapes as does the PIM process.

In our work, macroporosity has not been achieved, nor intended. However, compared to space holder methods, the macroporosity in the samples can only be replicated with the use of sacrificial elements. Although this wide range-controlled porosity is not obtained, the

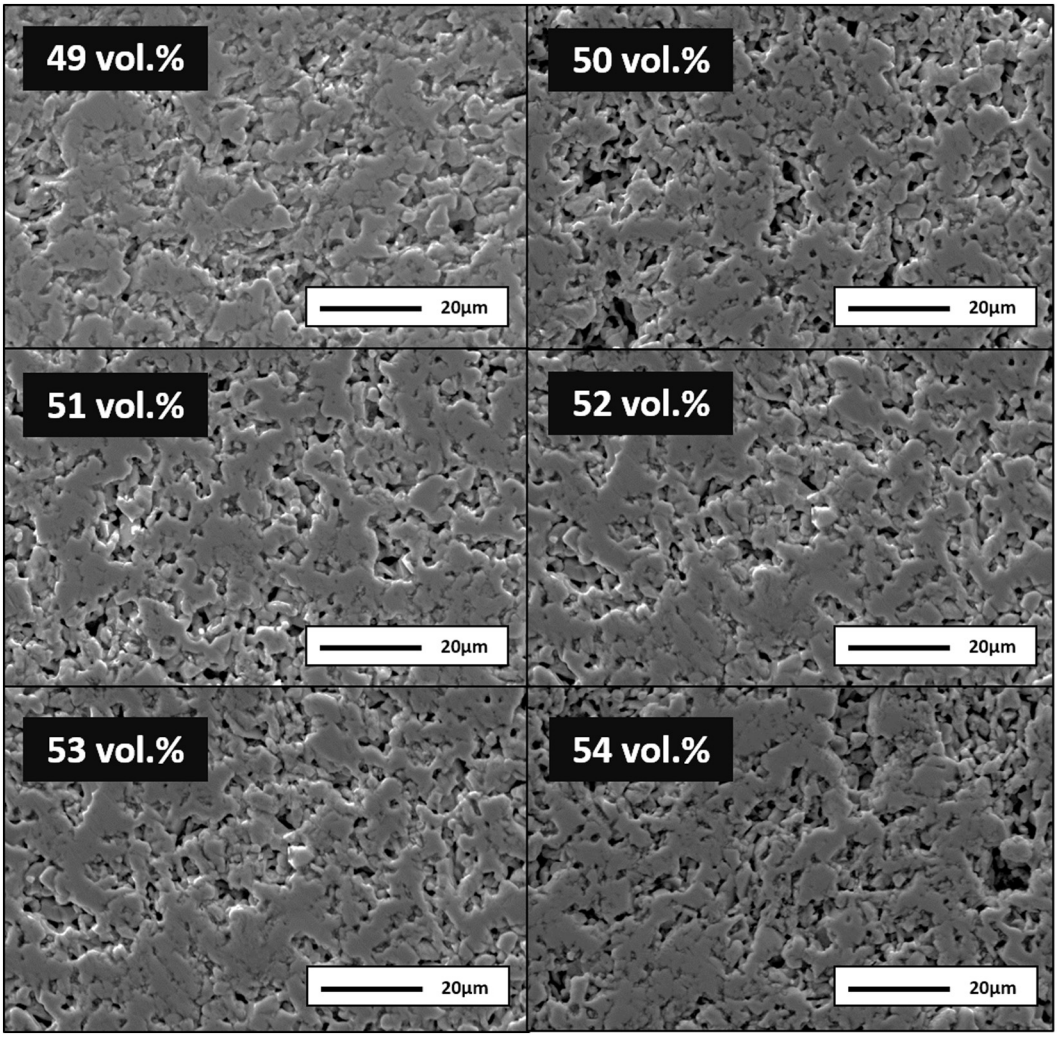

Fig. 12. SEM micrographs of sintered samples at 1300 °C with a solid loading of 49 to 54 vol%.

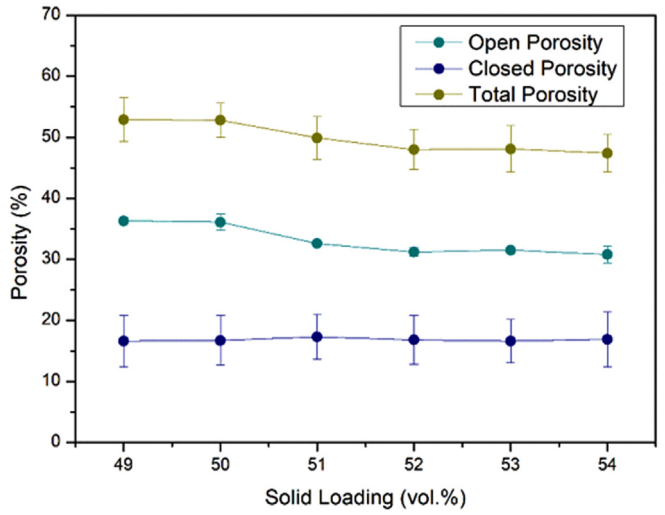

Fig. 13. Porosity measurements by vacuum infiltration of sintered samples with solid loadings of 49 to 54 vol%.

shape complexity that PIM offers could only be replicated with the use of near-net shape technologies or post machining of the samples.

In addition, compared to the PMMA addition strategy reported by Manonukul et al. [27], although the porosity morphology is better controlled using spherical PMMA particles, the use of the space holder added extra shrinkage to the samples. Moreover, the addition of PMMA does not give the effect of backbone usually used in PIM (CAB in this work), resulting in a highly controlled debinding to avoid the appearance of defects.

4. Conclusions

High quality porous Ti_3SiC_2 was produced by powder injection moulding for the first time without the need of a space holder or the addition of secondary-sacrificial binders. All stages of the PIM process were optimized. A critical solid loading was determined and a range of solid loadings were studied for the production of feedstocks using a multicomponent eco-friendly sustainable binder containing polyethylene glycol (PEG) and acetate butyrate cellulose (CAB) in a 70–30 vol% relation, respectively. All the mixtures produced showed good rheological behaviour: 1) low torque values of the feedstocks, 2) pseudoplastic behaviour of the mixtures, 3) homogenous mixing of the powder binder system and 4) viscosity values under the recommended for PIM allowing to increase or decrease the solid content in the feedstocks depending on the porosity desired. All feedstocks were suitable for the injection process, and an optimal solid loading was established with a 52 vol% of Ti_3SiC_2 powders in the mixture. Porous materials produced and the debinding cycle was optimized proposing a two-step process, first a solvent debinding in water for the elimination of polyethylene glycol (PEG) and a second stage to remove the acetate butyrate cellulose (CAB) remaining in the material. This two-step process guaranteed the structural integrity of all the materials produced with no presence of the polymeric binder after the sintering process. In addition, a high percentage of interconnected porosity can be obtained without the need of a space holder through PIM. The range of the irregular porosity obtained for all suited PIM feedstocks was between 47 and 53% and it was clearly related to the solid loading of each feedstock.

Supplementary data to this article can be found online at https://doi.org/10.1016/j.powtec.2020.11.022.

Declaration of Competing Interest

The authors declare that they have no known competing financial interests or personal relationships that could have appeared to influence the work reported in this paper.

Acknowledgements

The authors would like to thank the funding provided for this research by the Regional Government of Madrid (Dra. Gral. Universidades e Investigación) through the project (ADITIMAT-CM S2018/NMT-4411), the Spanish Government through the Ramón y Cajal contract RYC-2014-15014 and the Juan de la Cierva contract FJCI-2016-29004 and the project MAT2012-38650-C02-01.

References

[1] M. Barsoum, T. El-Raghy, The MAX Phases: Unique New Carbide and Nitride Materials, 2001https://doi.org/10.1511/2001.28.736.
[2] M.W. Barsoum, T. El-Raghy, Synthesis and characterization of a remarkable ceramic: Ti3SiC2, J. Am. Ceram. Soc. 79 (1996) 1953–1956, https://doi.org/10.1111/j.1151-2916.1996.tb08018.x.
[3] M.W. Barsoum, The Mn+1AXn phases: a new class of solids, Prog. Solid State Chem. 28 (2000) 201–281, https://doi.org/10.1016/S0079-6786(00)00006-6.
[4] M.W. Barsoum, M. Radovic, Elastic and mechanical properties of the MAX phases, Annu. Rev. Mater. Res. 41 (2011) 195–227, https://doi.org/10.1146/annurev-matsci-062910-100448.
[5] T. El-Raghy, M.W. Barsoum, Processing and mechanical properties of Ti3SiC2: I, reaction path and microstructure evolution, J. Am. Ceram. Soc. 82 (1999) 2849–2854, https://doi.org/10.1111/j.1151-2916.1999.tb02167.x.
[6] M.A. El Saeed, F.A. Deorsola, R.M. Rashad, Influence of SPS parameters on the density and mechanical properties of sintered Ti3SiC2 powders, Int. J. Refract. Met. Hard Mater. 41 (2013) 48–53, https://doi.org/10.1016/j.ijrmhm.2013.01.016.
[7] J.M. Córdoba, M.J. Sayagués, M.D. Alcalá, F.J. Gotor, Synthesis of Ti3SiC2 powders: reaction mechanism, J. Am. Ceram. Soc. 90 (2007) 825–830, https://doi.org/10.1111/j.1551-2916.2007.01501.x.
[8] J. Gonzalez-Julian, S. Onrubia, M. Bram, C. Broeckmann, R. Vassen, O. Guillon, High-temperature oxidation and compressive strength of Cr2AlC MAX phase foams with controlled porosity, J. Am. Ceram. Soc. 101 (2018) 542–552, https://doi.org/10.1111/jace.15224.
[9] B. Velasco, E. Gordo, S.A. Tsipas, MAX phase Ti2AlC foams using a leachable space-holder material, J. Alloys Compd. 646 (2015) 1036–1042, https://doi.org/10.1016/j.jallcom.2015.05.235.
[10] X. Liu, H. Zhang, Y. Jiang, Y. He, Characterization and application of porous Ti3SiC2 ceramic prepared through reactive synthesis, Mater. Des. (2015)https://doi.org/10.1016/j.matdes.2015.03.061.
[11] S. Ziqi, L. Ying, L. Meishuan, Z. Yanchun, Preparation of reticulated MAX-phase support with morphology-controllable nanostructured ceria coating for gas exhaust catalyst devices, J. Am. Ceram. Soc. 93 (2010) 2591–2597, https://doi.org/10.1111/j.1551-2916.2010.03776.x.
[12] Z. Wang, Y. Jiang, X. Liu, Y. He, Pore structure of reactively synthesized nanolaminate Ti3SiC2 alloyed with Al, Ceram. Int. 46 (2020) 576–583, https://doi.org/10.1016/j.ceramint.2019.09.005.
[13] J. Gonzalez-Julian, L. Classen, M. Bram, R. Vaßen, O. Guillon, Near net shaping of monolithic and composite MAX phases by injection molding, J. Am. Ceram. Soc. 99 (2016) 3210–3213, https://doi.org/10.1111/jace.14466.
[14] A. Dehghan-Manshadi, Y. Chen, Z. Shi, M. Bermingham, D. StJohn, M. Dargusch, M. Qian, Porous titanium scaffolds fabricated by metal injection Moulding for biomedical applications, Mater. (Basel) 11 (2018) 1573, https://doi.org/10.3390/ma11091573.
[15] G. Matula, J. Krzysteczko, Porous material produced by ceramic injection molding, J. Achieve. Mater. Manufactur. Eng. 71 (2015) 14–21.
[16] J.M. Contreras, A. Jiménez-Morales, J.M. Torralba, Influence of the Morphology and Particle Size on the Processing of Bronze 90/10 Powders by Metal Injection Moulding (MIM), 536, 2007 365–368, https://doi.org/10.4028/www.scientific.net/MSF.534-536.365.
[17] R.M. German, Prediction of Sintered Density for Bimodal Powder Mixtures, 2018https://doi.org/10.1007/BF02647329.
[18] E. Tabares, A. Jiménez-Morales, S.A. Tsipas, Study of the synthesis of MAX phase Ti 3 SiC 2 powders by pressureless sintering, Boletín La Soc. Española Cerámica y Vidr. (2020) 1–12, https://doi.org/10.1016/j.bsecv.2020.01.004.
[19] R.M. German, Injection Molding of Metals and Ceramics, Princeton New Jersey: Metal Powder Industries Federation, Princeton (New Jersey), 1997https://doi.org/10.4271/982417.
[20] J. Hidalgo, A. Jiménez-Morales, J.M. Torralba, Torque rheology of zircon feedstocks for powder injection moulding, J. Eur. Ceram. Soc. 32 (2012) 4063–4072, https://doi.org/10.1016/j.jeurceramsoc.2012.06.023.

[21] B. Hausnerova, B.N. Mukund, D. Sanetrnik, Rheological properties of gas and water atomized 17-4PH stainless steel MIM feedstocks: effect of powder shape and size, Powder Technol. 312 (2017) 152–158, https://doi.org/10.1016/j.powtec.2017.02.023.
[22] C. Abajo, J. Hidalgo, A. Jiménez-Morales, J.M. Torralba, Optimisation of eco-friendly binary binder system for powder injection moulding, Powder Metall. 57 (2014) 196–203.
[23] N.P. Cheremisinoff, Product Design and Testing of Polymeric Materials, Marcel Dekker, New York, USA, 1990https://doi.org/10.1002/pola.1991.080290918.
[24] A. de Waele, Viscosimetry and plastometry, J. Oil Colour Chem. Assoc. 6 (1923) 33–80.
[25] C. Abajo, A. Jiménez-Morales, J. Manuel, New processing route for ZrSiO 4 by powder injection moulding using an eco-friendly binder system ☆, Boletín La Soc. Española Cerámica y Vidr. 54 (2015) 93–100, https://doi.org/10.1016/j.bsecv.2015.05.003.
[26] B. Velasco, S. Tsipas, B. Ferrari, E. Gordo, MAX phase foams produced via powder metallurgy process using water soluble space holder, Powder Metall. 58 (2015) 95–99, https://doi.org/10.1179/0032589915Z.000000000226.
[27] A. Manonukul, N. Muenya, F. Léaux, S. Amaranan, Effects of replacing metal powder with powder space holder on metal foam produced by metal injection moulding, J. Mater. Process. Technol. 210 (2010) 529–535, https://doi.org/10.1016/j.jmatprotec.2009.10.016.

CHAPTER 7

CEM STUDY OF MAX PHASES FEEDSTOCKS

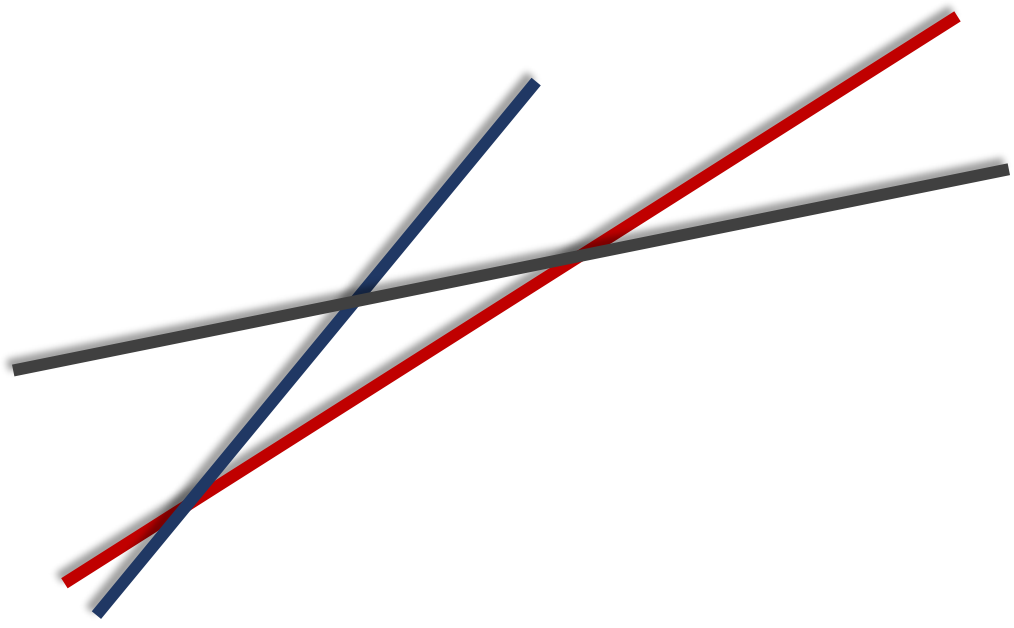

Contents

7.1 Extrusion-based additive manufacturing of Ti_3SiC_2 and Cr_2AlC MAX phases as candidates for high temperature heat exchangers 193

7.2 Mechanical properties of 3D printed MAX phases 205

7.1 Extrusion-based additive manufacturing of Ti_3SiC_2 and Cr_2AlC MAX phases as candidates for high temperature heat exchangers

Authors: Eduardo Tabares[a], Michael Kitzmantel[b], Erich Neubauer[b], Antonia Jiménez-Morales[a], Sophia A. Tsipas[a]

[a] Departamento de Ciencia e Ingeniería de Materiales e Ingeniería Química, IAAB, Universidad Carlos lll de Madrid, Avda. De la Universidad 30, 38911 Leganés, Spain

[b] RHP-Technology GmbH, Forschungs- und Technologiezentrum, A-2444 Seibersdorf, Austria

Journal: Journal of the European Ceramic Society
Publisher: ELSEVIER; ISSN: 0955-2219; Category: Materials Science, Ceramics
Position: 1 of 29 (Q1) IMPACT FACTOR: 5.302 (JCR 2020)

Scope of this paper:

Following the objectives of studying new sample production techniques, this scientific publication explores composite extrusion modelling (CEM) as another alternative processing route for MAX phases. In this case, Ti_3SiC_2 and Cr_2AlC feedstocks with PEG/CAB as a binder. The optimisation and selection of the optimal solid loading for Ti_3SiC_2 is shown previously in **Chapter 6,** whereas for Cr_2AlC is shown in this work. CEM offers the possibility of starting from the material in pellet form to be deposited directly layer-by-layer. In addition, all the printing parameters were optimised to control the correct deposition of the material, obtaining good quality samples with an appropriate filling, avoiding the generation of mayor defects during printing. Furthermore, the debinding process was adjusted to reduce the appearance of defects during this stage. Finally, a microstructural characterisation is performed to analyse the influence of this process on the consolidation of MAX phases. In this work, we have successfully transferred the developed PIM feedstocks to use as starting material in a new additive manufacturing route, achieving the 3D printing of good quality MAX phase samples.

Graphical Abstract:

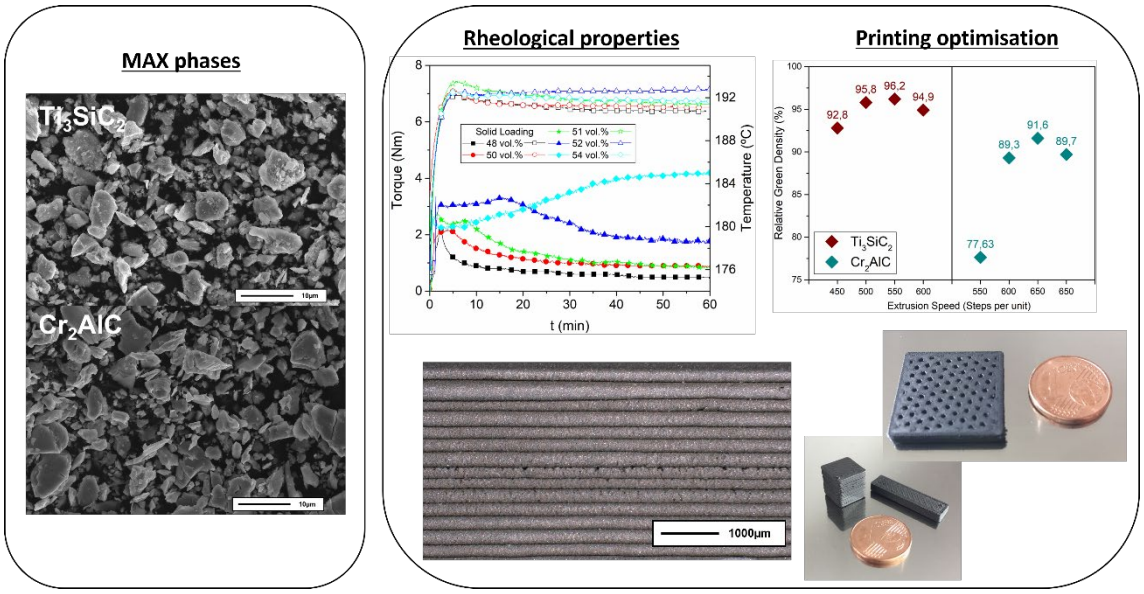

Journal of the European Ceramic Society 42 (2022) 841–849

Contents lists available at ScienceDirect

Journal of the European Ceramic Society

journal homepage: www.elsevier.com/locate/jeurceramsoc

Extrusion-based additive manufacturing of Ti_3SiC_2 and Cr_2AlC MAX phases as candidates for high temperature heat exchangers

Eduardo Tabares [a], Michael Kitzmantel [b], Erich Neubauer [b], Antonia Jimenez-Morales [a], Sophia A. Tsipas [a,*]

[a] Departamento de Ciencia e Ingeniería de Materiales e Ingeniería Química, IAAB, Universidad Carlos lll de Madrid, Avda. De La Universidad 30, 28911, Leganés, Spain
[b] RHP-Technology GmbH, Forschungs- Und Technologiezentrum, A-2444, Seibersdorf, Austria

ARTICLE INFO

Keywords:
Ti_3SiC_2
Cr_2AlC
MAX phase
Composite extrusion modelling (CEM)
Additive manufacturing
Pellet extrusion

ABSTRACT

High Temperature Heat Exchangers (HTHXs) are used in many industrial processes and are likely to become key components in green power generation. For the development of HTHXs, novel designs and new materials need to be explored. Additive manufacturing (AM) opens many possibilities for novel designs. Extrusion-based AM in general, and composite extrusion modelling (CEM) in particular, offers the opportunity of using new binder systems, that cannot be employed in other AM techniques. MAX phases, due to their ceramic-metallic properties combination, are great candidates for HTHXs. In this work, the printability of Ti_3SiC_2 and Cr_2AlC, through CEM with an innovative sustainable binder is explored. For this purpose, rheological properties of the feedstocks and the influence of the printing parameters are studied for each MAX phase feedstock. Microstructural analysis and final sample characterisation is performed, in order to determine the suitability of this technique to obtain near-net shape MAX phase parts.

1. Introduction

Additive Manufacturing (AM) has become one of the most promising production techniques in the last years due to the freedom of geometry design that this technology offers. Ceramic [1] and metal [2] 3D printing studies have noticeably increased in the last decade and new type of processing methodologies have been developed to adjust specific conditions for certain materials. Although AM of metallic or ceramic materials is currently focused on the prototyping of samples for a posterior production through other techniques, there are more and more areas where 3D printed samples are being used, from energy storage [3], aeronautics [4], medical [5] or environmental applications [6]. Most of the AM techniques require specific powder characteristics in order to obtain good quality printed parts [7,8]. Within the broad amount of Additive Manufacturing technologies, there are two main ways for classifing these techniques, depending on whether the part is obtained directly through the process or if a post processing process, such as debinding and sintering, is required to obtain the final part. A common direct AM process is Direct Energy Deposition, where the material is being deposited at the same time as appling energy for the conformation of the samples [9,10]. A laser or an electron beam is usually used as the energy source, and the depostion material is, typically, in wire or powder form. Powder Bed Fusion is another extended technique for metals and ceramics in powder form, where the energy is applied to a powder bed, melting or sintering the required shape in each layer, successively. After a layer is deposited, a new layer of fresh powder is spread in the bed, and energy is applied to the subsequent layer [11,12]. Another Direct AM technique is Sheet lamination; in this method the material is in a laminated form and is cut with the desired shape of the layer, and the next laminated sheet is sticked above [13,14]. Generally, Direct AM processing routes require specific processed raw-maerial bulk form (wire or sheet) or a specific powder morphology (spherical) to obtain the final sample, and the final component is prone to internal defects if the processing parameters are not optimized.

Indirect AM for metals and ceramics encompasses techniques such as VAT photopolymerization, Material Jetting, Binder jetting, fused filament fabrication (FFF) or fused deposition modelling (FDM) among others. In VAT photopolymerization; a resin or a slurry that contains the ceramic to be printed is polymerized layer by layer with an energy source, such as a laser, a projector or a LED light [15]. Material jetting also requires an energy source for the printing of the material but, in this case, the material that constitutes of a polymer with a ceramic charge, is

* Corresponding author.
E-mail addresses: etabares@ing.uc3m.es (E. Tabares), toni@ing.uc3m.es (A. Jimenez-Morales), stsipas@ing.uc3m.es (S.A. Tsipas).

https://doi.org/10.1016/j.jeurceramsoc.2021.10.042
Received 2 July 2021; Received in revised form 15 October 2021; Accepted 24 October 2021
Available online 29 October 2021

jetted during printing [16]. This same phenomenon happens for binder jetting, although, in this case, the binder is jetted into a ceramic or metallic powder bed, followed by a successive deposition of metallic or ceramic powder layers [17,18].

One the most widely used AM techniques is the material extrusion, usually referred to as fused filament fabrication (FFF) or fused deposition modelling (FDM). In this technology a filament that contains the metal or ceramic and a polymer binder is heated to acheive a specific viscosity in order to be deposited layer by layer. [1]. From this type of processing, a new way of extrusion technique appears, namely, composite extrusion modelling (CEM) also described as screw-based AM [19]. As for FDM, the material is extruded through a nozzle, but in this case the starting materials are pellets or granulates, commonly known as feedstocks. CEM presents some advantages compared to FDM in terms of avoiding difficult steps of filament production, since there is no need for a specific diameter tolerance to ensure the extrusion of the material. In addition, it is possible to increase the binder range used for 3D printing, since flexibility properties of the polymeric binder are no longer required. Moreover, reusability of the material is possible: if the printed temperatures are selected correctly and there is no polymer degradation during the printing, the feedstock can be pelletised and printed again [20]. With all this, CEM offers the possibility to print materials that do not comply with the required morphologies of the powder bed technologies or are not able to be produced as filaments or wires and allows to print highly charged feedstocks, using novel binder compositions [21].

HTHXs operate in more demanding conditions than other heat exchangers. They are exposed to temperatures above 750 °C and transfer fluids such as molten salts, liquid metals or hot gases [22]. Conventional materials used for lower temperature heat exchangers suffer from corrosion and oxidation at these temperatures [23]. Ceramic heat exchangers, that are more resistant to high temperatures and to oxidation and corrosion, exhibit low thermal shock resistance, are difficult to process and have lower than desired thermal conductivity [24–28]. HTHXs are used in gas turbine systems [29], high efficiency power plants [23,30], solar plants [31], hydrogen production [32], and high temperature fuel cell systems [33].

Additive manufacturing opens many possibilities for novel design of heat exchangers [34–36]. However, not all materials can be processed by additive manufacturing techniques, and each technique must be optimized for each given material, in order to avoid internal defects and ensure reproducibility.

With all these considerations, MAX phases stand as promising materials to be printed through CEM technology for their use as HTHXs. This family of ternary carbides and nitrides combine, in an excellent manner, properties of both ceramic and metallic materials [37]. They exhibit high stiffness, good oxidation and corrosion behaviour and good mechanical properties at high temperature combined with good electrical and thermal conductivity and easy machinability, within others. MAX phases have a nanolaminated structure, with a fixed stoichiometry and a general formula of $M_{n+1}AX_n$ where M is an early transition metal, A an element from groups IIIA and IVA of the periodic table and X either carbon or nitrogen [38]. In the recent years, MAX phases have been studied for high temperature applications [39,40] or nuclear power plants [41,42], amongst other applications. Additive manufacturing of MAX phases has been previously studied by W. Sun et al. [43] and Mylena M. M. Carrijo et al. [44] through rapid prototyping, an early stage of the binder-jetting technology. In their work, Ti_3SiC_2 samples were printed with densities of 90 %, studying the influence of the sprayed binder concentration and an intermediate step of cold isostatic pressing (CIP), prior to the sintering stage. B. Nan et al. [45] achieved synthesising Ti_3SiC_2-based materials starting from TiC:Si powders, combining 3D printing with liquid silicon infiltration (LSI). Direct ink writing was used by H. Elsayed et al. [46] to obtain Ti_2AlC porous structures, achieving a correct dispersion of the MAX phase powders in the ink and attaining a range of 44–63 vol.% of porosity in the printed samples. Other MAX phases, such as Cr_2AlC, has been studied by M. Belmonte et al. producing printable inks using aqueous-based dispersions. Cellular MAX phase structures were printed with 60 vol.% porosities with good thermal and electrical conductivities [47].

The aim of this work is to study AM pellet extrusion of Ti_3SiC_2 and Cr_2AlC MAX phases. For this purpose, both MAX phases were self-synthesised and powder production scaled-up for the production of high amount of powders. MAX phase feedstocks were produced using an innovative powder injection moulding (PIM) sustainable binder composition, based on polyethylene glycol (PEG) and cellulose acetate butyrate (CAB). The objective is to broaden the possible application fields of MAX phases as HTHXs by the production of complex shaped parts through additive manufacturing of pelletised feedstocks.

2. Material and methods

2.1. Initial materials characterisation

Ti_3SiC_2 and Cr_2AlC MAX phase powders were synthesised following a pressureless reactive sintering route. Although synthesis optimisation of the powders can be found elsewhere [48], a summary of the synthesis materials and procedure is detailed below. Firstly, high purity bulk MAX phases were obtained by mixing initial powders of Ti:SiC:C and Cr:Al:C with a molar ratio of 3:1,5:0,5 and 2:1,2:1, respectively, in a Turbula shaker mixer (WAB Group, Switzerland) for 1 h. Mixed powders were then cold isostatically pressed (EPSI Systems, Belgium) in cylindrical silicone moulds at 400 MPa. Pressed samples were synthesised by pressureless sintering under different conditions for each MAX phase. Ti_3SiC_2 was synthesised under vacuum atmosphere ($2{,}5 \times 10^{-5}$) in a tubular high vacuum furnace (HVT-15/50/450, Carbolite, UK) at 1300 °C for 6 h, with 5 °C/min as heating and cooling rates. On the other hand, Cr_2AlC was synthesised under protective argon atmosphere in a tubular furnace (STF-15/757450, Carbolite, UK) at 1300 °C for 4 h, with heating and cooling rates of 5 °C/min. In order to obtain MAX phases in powder form, synthesised samples were crushed in a planetary ball mill (Pulverisette 5/2, Fritsch, Germany) with a ball to powder ratio of 10:1 using isopropanol and argon atmosphere to ensure protective conditions. After drying the powders at 100 °C in air for 5 h, characterisation of the powders was performed, in order to study the purity and characteristics of the powders. Purity quantification of the powders was calculated by least-square procedure. For this purpose, integrated area of most intense peaks in the XRD patterns was measured and the powder composition was determined following Eq. 1 [49].

$$\%\ \text{Phase} = I_x / I_t \tag{1}$$

Where I_x corresponds to the integrated area of the most intense peak of the phase to be quantified and I_t is the summatory of the integrated areas of the most intense peaks of all present phases.

Particle size distribution of the powders was calculated by Dynamic Light Scattering (MasterSizer 2000, Malvern Instruments, UK), to study their suitability for CEM processes. Furthermore, Scanning Electron Microscopy (SEM, TENEO-FEI, Netherlands) coupled with energy-dispersive X-ray spectroscopy (EDS, DX-4-EDAX, USA) was performed to study the morphology of the synthesised powders. Density measurements of the powders was performed by Helium pycnometry (AccuPyc 1330, Micrometrics, US) and both tap and apparent density were calculated following the standards ASTM B527−20 and ASTM B212−17, respectively.

2.2. Feedstock optimisation

MAX phase feedstocks were produced using a multicomponent sustainable binder. This binder is composed by polyethylene-glycol (PEG), cellulose acetate butyrate (CAB), stearic acid (SA) and phenothiazine (PTZ); further information on the binder can be found elsewhere [50,

51]. The main purpose for this binder combination is to propose an environmentally friendly polymeric binder and to use a two-step debinding process, reducing the possibility of defects appearance during the binder removal. As a water-soluble polymer, PEG, avoids the use of organic solvents during its removal. CAB, in addition to as acting as a backbone to the mixture, is a promising polymer for extrusion-based technologies as a substitute of petroleum derivatives. In addition, PTZ is used as an antioxidant and SA as a surfactant to the mixture.

A rheological study of the feedstocks was performed by torque and capillary rheology measurement. Ti_3SiC_2 feedstock production has been previously reported [51] and optimised with a 52 vol.% of solid loading. Cr_2AlC feedstocks were mixed in a torque rheometer (Haake Polylab QC, Thermofisher, US) at 180 °C to study torque values for the different solid loadings prepared, with a fixed roller speed of 40 rpm for 1 h to analyse the mixture stabilisation with time. In addition, capillary rheology (Haake Rheocap S20, Thermofisher, US) was performed to study the viscosity of the feedstock prepared. Length-diameter ratio was 30:1 and test were performed at 180 °C varying the shear rates between 100 and 10.000 s^{-1}.

2.3. Additive manufacturing: composite extrusion modelling (CEM)

3D printing of the MAX phases was achieved through extrusion of the feedstocks in pellet form. A pellet extrusion head (V4 Pellet Extruder, Mahor-XYZ, Spain) installed in a FDM printer (TL-D3 Pro, Tenlog, China) was used for the CEM process. Printing parameters were varied in order to adjust the optimal printing conditions for each MAX phase, controlling both the external defects of the sample, and the correct filling of the internal zones. Some of the parameters that influence the most the pellet printing process are listed: temperature (extruder and bed), layer height, printing speed and extrusion speed. Although different nozzle diameters were used (0,2−0,8 mm), a 0,6 mm nozzle was selected for all the printing adjustments

As stated above, binder removal of the printed samples was achieved through a two-step debinding process. Firstly, samples were introduced in stirred water at 50 °C for the removal of PEG. After drying, samples were thermally debinded in a debinding furnace (GD-DC-50, Goceram, Sweden) under protective argon atmosphere, heating up to 500 °C, with heating and cooling rates of 0,5 °C/min and 1 °C/min, respectively, for both MAX phases. Sintering was performed under vacuum atmosphere at 1300 °C for 6 h, with heating and cooling rates of 5 °C/min. After each step of the debinding and sintering, samples were weighted in order to verify the amount of binder removed and the densities of the samples, considering that the material does not oxidize at these temperatures. In addition, Archimedes density was measured to compare and calculate the amount of porosity in the printed final parts. Furthermore, X-ray diffraction (XRD, Philips X'pert, Netherlands) analysis was performed to the printed parts with Cu Kα radiation at 40 kV and 40 mV, in order to study the possible decomposition of the MAX phases during the process.

3. Results and discussion

3.1. Feedstock optimisation and characterisation

High purity was achieved for the self-synthesised powders reaching 92 vol.% Ti_3SiC_2 MAX phase with $TiSi_2$ as the secondary phase. and a 96 vol.% purity of Cr_2AlC, having Cr_5C_3 as secondary phase. Powders have an irregular morphology (Fig. 1) and the particle size distribution of the produced powders is shown in Fig. 2. From the values in Table 1 the differences between the powders produced can be seen. Both MAX phase powders have a similar D_{90} particle size, 20 μm for Ti_3SiC_2 and 23 μm for Cr_2AlC. Although the morphology of the powders is not optimal for Additive Manufacturing, particle size distribution is in an optimum range for feedstock production [52]. There is a bigger difference between D_{10} and D_{50} values of Cr_2AlC powders and D_{90}, compared to those from Ti_3SiC_2; this could also can also be observed in Fig. 2 in terms of width and height of the curves, which can have an influence in feedstock fluidity [8]. In addition, tap and apparent density show a low packing behaviour of the powders; tap densities above 50 % are usually desired for feedstock production in powder injection moulding [53]. As it can be seen, tap density values of 39 and 45 % were measured for Ti_3SiC_2 and Cr_2AlC, respectively. These low values are expected since powders with irregular morphology have a lower packing behaviour than spherical powders. Furthermore, low packing values of the powders would suggest porous structures, although fully dense samples have been obtained with tap density values below that 50 % yield point [54].

Ti_3SiC_2 PEG/CAB feedstock characterisation and optimisation has been previously reported [51]. The optimal solid loading for this feedstock was 52 vol.% Multistep analysis of the Cr_2AlC PEG/CAB feedstocks shows the variation of the torque with the increase of solid loading in the mixture. Fig. 3a shows this multistep torque analysis, where the vertical lines represent an increase in the solid loading of the mixture by pouring powder inside the chamber. At low amounts of powders in the mixture,

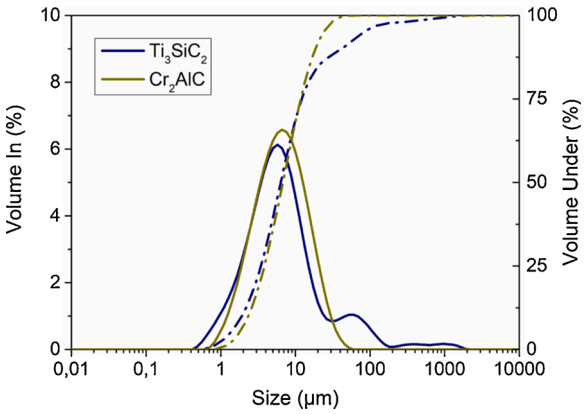

Fig. 2. Particle size distribution of self-synthesised Ti_3SiC_2 and Cr_2AlC MAX phases.

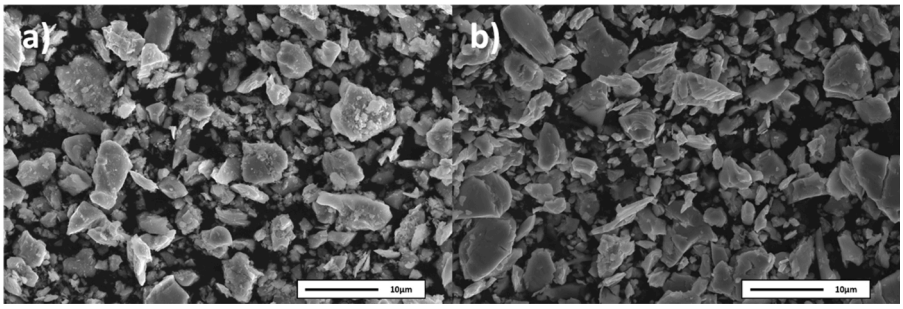

Fig. 1. SEM micrograph of self-synthesised powders of a) Ti_3SiC_2 and b) Cr_2AlC MAX phases.

Table 1
Ti_3SiC_2 and Cr_2AlC powder characteristics: particles size distribution, tap density and apparent density.

MAX Phase	D_{10}	D_{50}	D_{90}	ρ (g/cm^3)	Tap density (%)	App. Density (%)
Ti_3SiC_2	3	7	20	446	39	21
Cr_2AlC	2	6	23	520	45	38

torque response is consistent (45–51 vol.% in Fig. 3a), there is an increase of the torque value when the material is poured into the chamber, and a steady stabilisation while the powders are being mixed. At higher solid contents (51–56 vol.% in Fig. 3a), the final torque value after homogenisation increases noticeably; this effect can be better observed in Fig. 3b where final torque values are represented. In addition, with the increase of the solid content in the mixture, torque behaviour changes, there is a slight increase in the torque once the powder is introduced in the chamber, and the mixtures stabilises at higher torque values. This behaviour is due to fact that the amount of powder in the mixture is surpassing the optimal solid loading of the feedstock, thus the homogenisation of the feedstock is being deterred by the high amount of powder in the mixture. It is worth noting that, after surpassing the amount of solid content that the feedstocks is able to accept (56–62 vol.% in Fig. 3a), a continuous increase of the torque value would be expected. However, this effect is not seen due to the lubricant properties of the MAX phases, which show a graphitic-like behaviour, due to their nanolaminated structure [55]. Nevertheless, at this stage, the solid content of powder in the mixture has exceeded the amount of powder that the polymeric binder can accept and still remain homogenous. Once this lubricant effect is surpassed by the high solid content, the increase in the final torque values is more noticeable (62–65 vol.% in Fig. 3a). Final torque values are represented as a function of the solid loading in the chamber (Fig. 3b), in order to identify when a change on the rheological behaviour of the feedstocks occurs. A change in the slope of torque values during the increase of the solid content is an indicative of a change in the rheological behaviour. The aim of this representation is to establish an initial critical solid loading of the feedstocks and to study in-depth solid loadings close to that value.

Feedstocks with a solid loading between 48 and 54 vol.% were analysed by torque and capillary rheology, to determine the optimal solid loading and are represented in Fig. 4. From the torque rheology of the feedstocks (solid symbols in Fig. 4a) it is possible to see how the final torque value increases with the addition of solid content. Feedstock with a solid loading of 51 vol.% has almost the same final torque value compared to the feedstock with 50 vol.%, indicating a good behaviour with good homogenisation. At 52 vol.%, although there is a stabilisation of the torque with time, final torque values are higher compared to lower solid loadings, as expected. This effect is due to the excess of solid content in the mixture, hindering the homogenisation of the feedstock. Lastly, at 54 vol.% of solid loading there is no stabilisation of the feedstock, indicating a clear excess of powder in the mixture. Furthermore, internal temperature of the chamber (open symbols in Fig. 4a) is higher than the programmed (180 °C), due to the friction generated during the mixing of the powders and the binder system. Temperature-wise, there are no big differences that could illustrate a change of a rheological behaviour depending on the amount of solid loading in the feedstocks.

As a reference point for this work, in terms of rheological properties of the feedstocks, viscosity values of injection moulding feedstocks are the ones followed for the production of pellet extrusion-based AM

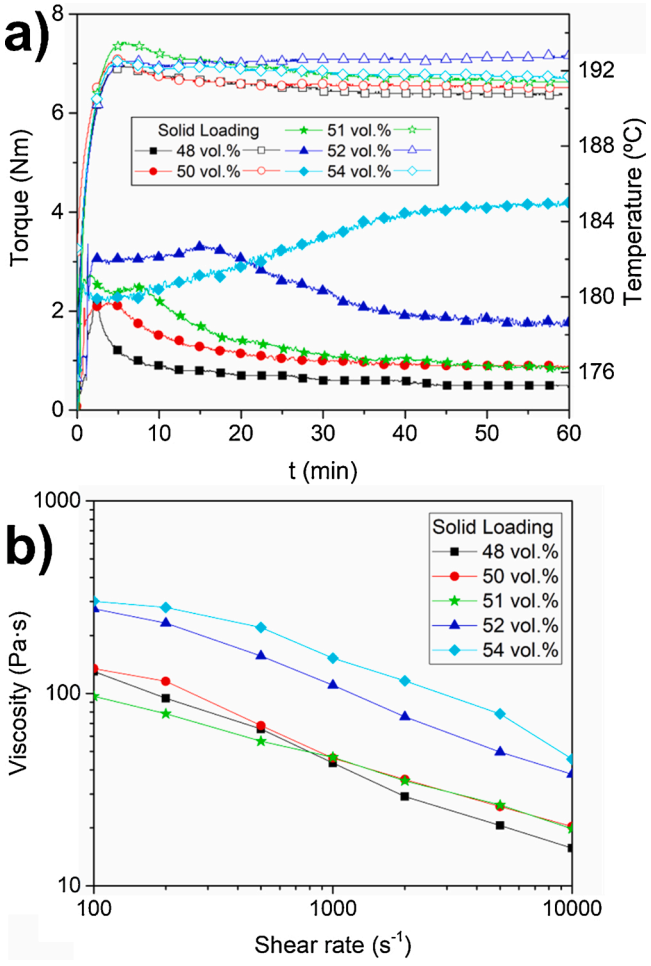

Fig. 4. a) Torque rheology (solid symbols correspond to torque values and open symbols to the registered temperatures) and b) Capillary rheology of Cr_2AlC PEG/CAB feedstocks with solid loading between 48 and 54 vol.%.

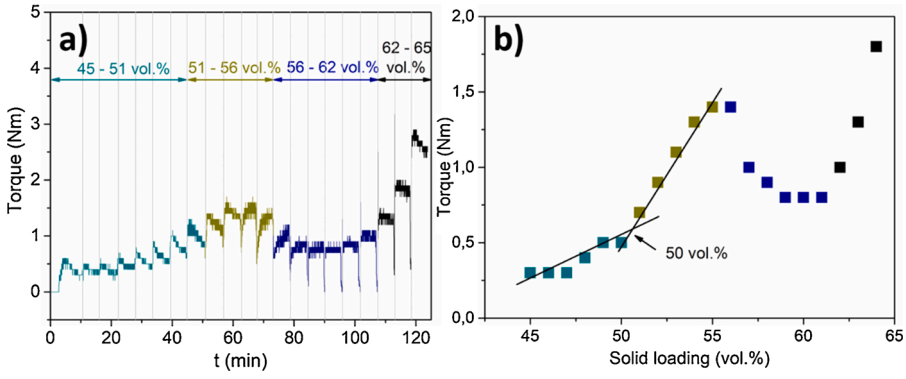

Fig. 3. a) Multistep torque analysis and b) final stabilised torque of Cr_2AlC PEG/CAB feedstocks with solid loading between 45 and 65 vol.%.

materials. As it can be seen in Fig. 4b, capillary rheology of the feedstocks exhibits a pseudoplastic behaviour, with a decrease of viscosity while increasing the shear rate for all solid loadings analysed. Generally, viscosity values under 1000 Pa·s are recommended for injection moulding materials [52], and this value is going to be taken as valid for pellet extrusion AM. From Fig. 4b, it can be seen how the viscosity of the feedstocks increases with the increase of solid loading, except for feedstock with 51 vol.%, that exhibits better rheology properties than feedstocks with higher powder filling. From all the rheological characterisation, 51 vol.% feedstock was selected as the optimal solid loading for the Cr_2AlC PEG/CAB system to be printed by extrusion-based AM.

3.2. CEM 3D printing of Ti_3SiC_2 and Cr_2AlC MAX phases

The first step for ensuring the correct flowability of the feedstocks through the nozzle is to select de adequate range of temperatures to extrude the material. For this, the material is heated at the selected temperatures inside the extrusion head, and the extruded material is analysed in order to identify incomplete extrusion of the material or defects, such as voids or bubbles in the extruded material prior to deposition. The range of temperatures was selected between 200 and 240 °C for both feedstocks. After this, material deposition in the printing bed (first layer) was optimised by varying various parameters such as the extrusion speed, printing speed and bed temperature, amongst other. Bed temperature was set at 50 °C for both MAX phases. Cross-section of the green printed samples during the process optimisation was analysed to study the internal defects produced during the printing of the materials (Fig. 5). As an example, in Fig. 5a the defects shown are common in high speed prints where the material is not correctly deposited. As it can be observed, the vertical gap throughout the sample corresponds to the separation between the wall and the infill of each deposition layer. Due to the high printing speed and low extrusion speed, the amount of material deposited is not enough to completely fill the sample. Controlling this layer-by-layer output during printing is of extreme importance, since these defects are going to be carried through all the consolidation steps, as it can be seen in the SEM image inset in Fig. 5a. Although this printing errors were solved by adjusting these parameters, it was observed that the layer thickness selected, depending on the width of the nozzle used, created this same gaps in the internal zone of the printed samples. With all this, a printing speed of 5 mm/s was selected for both MAX phases. Furthermore, by examining the cross-section, it is possible to see horizontal lines produced by the detachment of the printed layers, that occurs mainly due to high layer heights. Fig. 5b shows the longitudinal section of the printed samples, after the optimisation of the parameters. Layer-by-layer deposition should be thoughtfully analysed, since a small detachment of the layers, such as the ones showed in the SEM image inset in Fig. 5b, can cause the appearance of a bigger defect after the debinding and sintering processes (Fig. 5c). To avoid these defects, a reduction on the layer height, to 0,1 mm, was programmed to control layer deposition. In terms of the surface quality of the samples, layer height and line thickness have a great influence in the final part, and an example of the layer-by-layer deposition is shown in Fig. 6a. As a brief illustration of the visual aspect of the printed parts, Fig. 6b shows the different geometries produced in order to study the sinterability of the MAX phases through CEM and Fig. 6c is an example of a more complex geometry with high tolerances in the designed porous material, all of them with high surface quality. To better understand the effect of the printing parameter's and in addition to the visual inspection control of the samples, a green density analysis was performed on the printed samples, studying the influence of extrusion speed and printing speed on relative green density of the printed samples. As it can be observed in Fig. 7a, for both MAX phases feedstocks, initially, there is an increase in the relative green density with the increase of the extrusion speed. This is due to the increase in the amount of the material that is flowing through the nozzle and being deposited during the printing. For both feedstocks, it can be observed that a maximum relative green density value is reached (96,2 % for Ti_3SiC_2 and 91,6 % for Cr_2AlC), and after this, relative green density values decrease with further increase of the extrusion speed. This means that at higher extrusion speeds, once this maximum value is reached, there is more material deposited than it should, obtaining failed printed parts with inaccurate geometries. The selection of the extrusion speed was 550 steps per unit for Ti_3SiC_2 MAX phase feedstock and 650 steps per unit for Cr_2AlC, ensuring the correct deposition of the material, avoiding gaps during the printing and controlling the desired geometry of the samples. Comparing these values, it is noticeable that higher printing speeds are needed for the Cr_2AlC feedstock, compared to the Ti_3SiC_2. This effect is related to the rheological properties of the feedstocks, where Ti_3SiC_2 has a final torque value after torque stabilisation of 0,5 Nm [51] and whereas Cr_2AlC has a higher value of 1Nm (Fig. 4a). From the printing speed relative versus green density measurements shown in Fig. 7b, it can be seen how at lower printing speeds, the relative green density of the samples increases. As expected, the slower the printing speed, the better for the deposition of the material and the correct filling of the part. Although at 1 mm/sec slightly higher relative green densities are achieved than for a speed of 5 mm/sec, for both MAX phases, the printing time for this printing speed increases considerably, whereas only a small increase in the relative density is observed. Therefore, to achieve a compromise between sample quality and printing time, a printing speed of 5 mm/sec was chosen, for both feedstocks. It can also be observed how the printing speed has a higher influence on the relative green density for Cr_2AlC feedstocks, where a larger decrease in relative green density values at higher speeds is observed; that can also be associated to the rheological properties of this feedstock compared to Ti_3SiC_2.

Although reproducibility issues and geometry changes in the printed parts are other aspects to take into consideration, in terms of printing

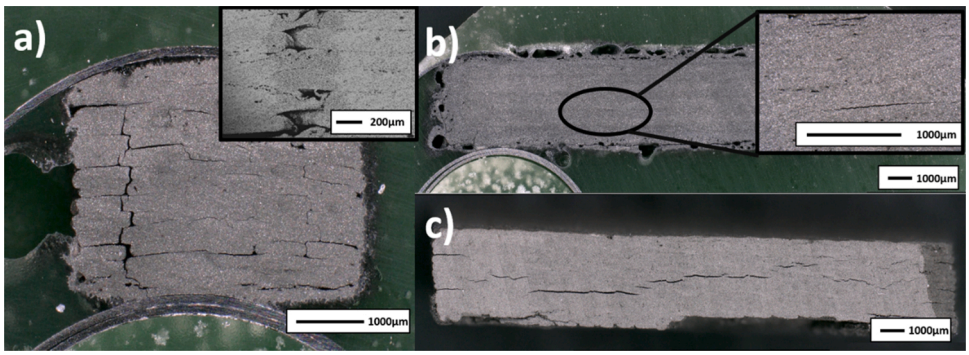

Fig. 5. a) Optical image of the cross-section of a green Ti_3SiC_2 part (inset: SEM micrograph of the sintered samples), b) optical image of the longitudinal section of a green Cr_2AlC part (inset: detailed optical image), c) optical image the sintered Cr_2AlC shown in b). (For interpretation of the references to colour in the Figure, the reader is referred to the web version of this article).

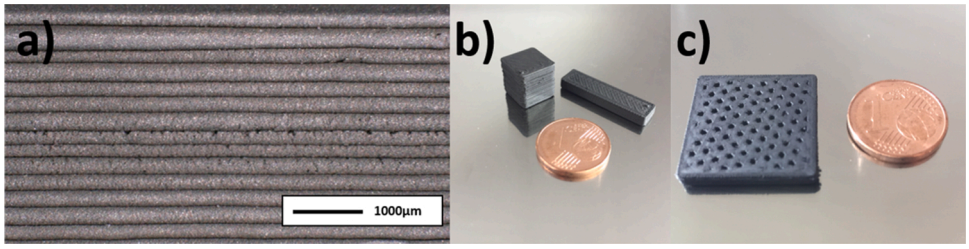

Fig. 6. a) Optical image of the layer deposition of a green Cr_2AlC part, b) example of different green geometries printed for a Ti_3SiC_2 (Left) and Cr_2AlC (Right) and c) porous green sample of Cr_2AlC. (For interpretation of the references to colour in the Figure, the reader is referred to the web version of this article).

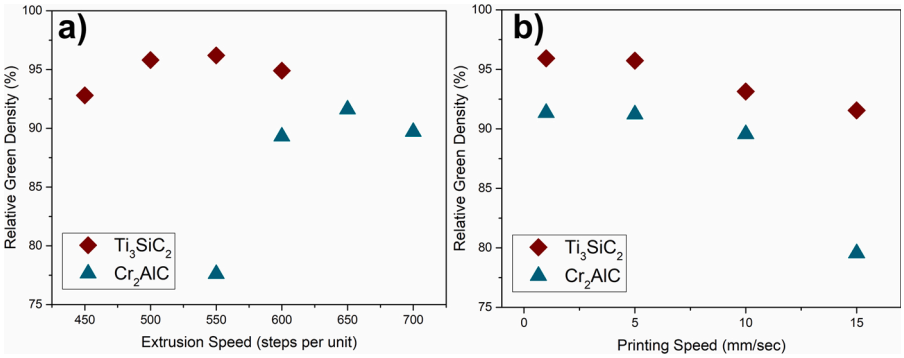

Fig. 7. Relative green densities of Ti_3SiC_2 and Cr_2AlC PEG/CAB feedstock at different a) extrusion speeds and b) printing speeds. (For interpretation of the references to colour in the Figure, the reader is referred to the web version of this article).

parameters adjustment, in all extrusion-based technologies, a summary of the final printing parameters used for defect-free MAX phase CEM samples are shown in Table 2.

Solvent debinding of the printed samples shows up to a 90 wt.% of the PEG was removed for both MAX phases, calculated by mass loss, with the remaining CAB acting as the backbone, ensuring the mechanical stability of the printed parts. After the second stage of the two-step debinding, mass loss indicates a binder removal of 99 wt.%, compared to the green sample, removing almost completely the CAB and the residual PEG by thermal debinding. Cross-sections of the brown parts were inspected in order to analyse possible defects produced by the debinding process. In spite that with the cutting process of binder-free samples it is possible to generate minor defects in the sample, due to the displacement of the powders during the process, it is still possible to disregard failed printed parts by the appearance of mayor cracks or defects. Through this two-step debinding process, brown parts maintained their structural integrity without the appearance of mayor defects in the internal or external zones of the samples.

First, sintering trials were performed on alumina plates. Most of the sintered samples exhibited warping effects produced by the internal stresses, typically generated during the printing process. This warping effect was different for each MAX phase. Ti_3SiC_2 exhibited low warping, but big internal cracks (Fig. 8a), generated due to delamination of the layers during sintering. On the other hand, Cr_2AlC showed higher warping angles but, in this case, instead of cracks, the microstructure shows high porous cavities in the cross-section (Fig. 8b). This difference defect appearance could be due to a better sintering behaviour of the MAX phase Cr_2AlC, that is also directly related to the higher shrinkage which will be discussed, for the final printed samples. In addition, the porosity seen in both MAX phases is expected, due to the sinterability properties of these materials, with a sintering behaviour characteristics of ceramics, combined with the use of a binder for the viscosity requirements of the CEM 3D printing [56]. This warping effect was solved by placing the brown printed samples in an alumina crucible and immersed in zirconia balls, and as a result the presence of cracks in the internal zones of the samples created by the detachment of the layers was prevented, along with achieving the desired geometries.

Table 2
Summary of the final printing parameters used for defect free MAX phase CEM samples.

Material	Ti_3SiC_2	Cr_2AlC
Nozzle Diameter (mm)	0,6	0,6
Extrusion speed (steps per unit)	550	650
Layer Height (mm)	0,1	0,1
Infill pattern	Rectilinear	Rectilinear
Infill percentage (%)	100	100
Infill Angles (°)	15/75/135	15/75/135
Extruder Temperature (°C)	210	230
Bed Temperature (°C)	50	50
Printing speed (mm/s)	5	5
Outline Under Speed (%)	80	80

3.3. Characterisation and microstructural analysis of printed samples

Density and shrinkage values of the final parts after CEM optimisation are shown in Table 3. In first place, Ti_3SiC_2 sintered samples show a relative density of 90 % and Cr_2AlC of up to 93 %. From this value, the better sinterability properties of the Cr_2AlC MAX phase powders compared to Ti_3SiC_2 can be observed; even though Cr_2AlC has a lower solid content (51 vol.% for Cr_2AlC and 52 vol.% for Ti_3SiC_2) this material shows lower porosities in the final parts. Comparing this values to previous works using the same Ti_3SiC_2 PEG/CAB feedstocks for injection moulding [51], porosities obtained by CEM are a 10 % lower than for PIM. This could be another effect of the internal stresses created during 3D printing, that might increase powder contact after debinding and favour the sinterability of the materials, in this case, the MAX phases. In terms of dimensional reduction of the printed samples, a higher shrinkage can be observed on the z axis than on the x and y axis, for both MAX phases. This effect has been previously reported [21], and could be due to the effect of the material deposition during the printing. Although the expected behaviour would be that as for the z axis the printing parameters are only affected by the layer height, in the x and y direction

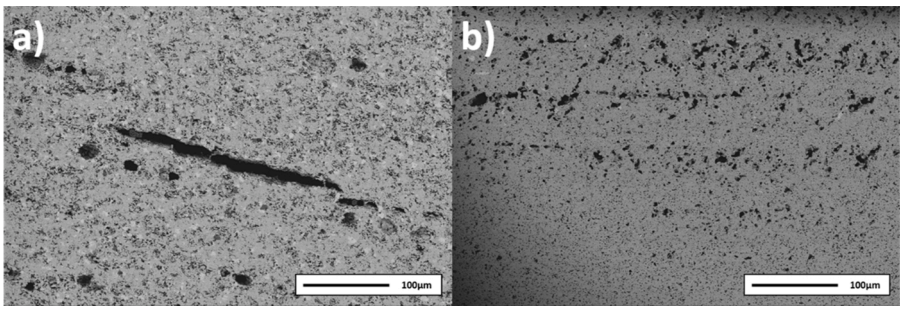

Fig. 8. SEM micrographs of defects found on sintered samples in a) Ti_3SiC_2 and b) Cr_2AlC MAX phases.

Table 3
Density and shrinkage measurements of Ti_3SiC_2 and Cr_2AlC printed samples.

Material	Relative density (%)	Shrinkage x–y (%)	Shrinkage z (%)
Ti_3SiC_2	90	8,63	10,39
Cr_2AlC	93	18,39	20,89

there are more variables in this deposition (i.e., wall thickness, infill angle) that are inevitably creating more spacing in the powder distribution; thus, shrinkage in this direction should be higher. What it seems to occur in this case is that the layer being deposited is cooling faster from layer to layer than in the x–y axis (the lines printed in each layer), reducing the contact point in the feedstock and creating a higher spacing. This effect can be controlled in the printing process by optimising the printing parameters and the infill pattern. Comparing the shrinkage values of both MAX phases, a difference of roughly 10 % between them can be observed, with Cr_2AlC showing higher shrinkage. This is directly related with the sinterability properties, discussed in terms of the relative density of the materials, that can be also seen in the SEM micrographs in Fig. 9. Micrograph Fig. 9b shows a lower porosity for the Cr_2AlC cross-section compared to the Ti_3SiC_2 sample (Fig. 9a). It is also possible to observe secondary phases (light grey areas in Fig. 9a) for Ti_3SiC_2, corresponding to an intermediate phase of $TiSi_2$ that, as mentioned earlier, is also present in the initial powders [48]. The presence of this secondary elements is confirmed by XRD analysis performed to the printed samples. Fig. 10 shows a comparison of the XRD patterns of the initial powders used for the production of MAX phase feedstocks and the final printed samples. As stated before, Ti_3SiC_2 exhibits a secondary phase, corresponding to $TiSi_2$, maintaining the initial purity of the samples (Fig. 10a). In the case of Cr_2AlC, there is a slight presence of an intermediate phase of Cr_5C_3, that is present in the initial powders (Fig. 10b). With this analysis it is possible to establish that decomposition of the MAX phases has not occured during the process and the possible presence of non-removed polymer after debinding has not affected the purity of the MAX phases after sintering.

It is important to note that the induced porosity may affect the properties of the MAX phase samples. Compared to the analysis made in Tsipas et al. work [40], analysing dense and porous Ti_3SiC_2 MAX phase samples obtained through a conventional powder metallurgy process of cold isostatic pressing and sintering, it can be noted that a high microporosity (31 vol.%) was obtained for the sample using commercially available powders. A decrease in thermal and electrical conductivity properties of Ti_3SiC_2 was observed with the increase of porosity in the samples. The thermal conductivity values for Ti_3SiC_2 porous samples varied from 6 W/m K to 23 W/mK, for porosity values from 66 vol% to 31 vol% respectively [40]. The reported thermal conductivity of bulk Cr_2AlC is 18 W/mK [57]. These are higher than thermal conductivities of other ceramic materials (such as SiC and Si_3N_4) with similar porosity. It would be expected that, for the CEM printed samples a near theoretical thermal and electrical conductivities are reached considering the relatively low porosity achieved in the process. Considering this behaviour for both MAX phases, with the designed open porosity as the printed sample exhibited in Fig. 6c suggests these materials could be great candidates for high temperature heat exchangers [58].

4. Conclusions

Ti_3SiC_2 and Cr_2AlC MAX phases have been successfully 3D printed by composite extrusion modelling (CEM). In this work the use of non-conventional powders for additive manufacturing processes, in terms of morphology, and a novel sustainable binder composition, has been explored. Rheological properties of the PEG/CAB system have been studied, producing feedstocks with optimal solid loading for the flowability and extrusion requirements of the CEM processing, starting from self-synthesised high purity Ti_3SiC_2 and Cr_2AlC MAX phase powders. Printing parameters have been optimised for the studied feedstocks, achieving good quality green samples. In addition, a two-step debinding process was successfully achieved, maintaining the structural integrity and desired geometry. Warping effect in the printed parts was avoided, obtaining good quality final samples. Moreover, densification of the samples is relatively high, considering the processing route studied (extrusion-based AM) and the sinterability properties of the MAX phases. All in all, a new processing route has been successfully developed for MAX phases giving a great added value to this material and expanding its possible applications as HTHXs.

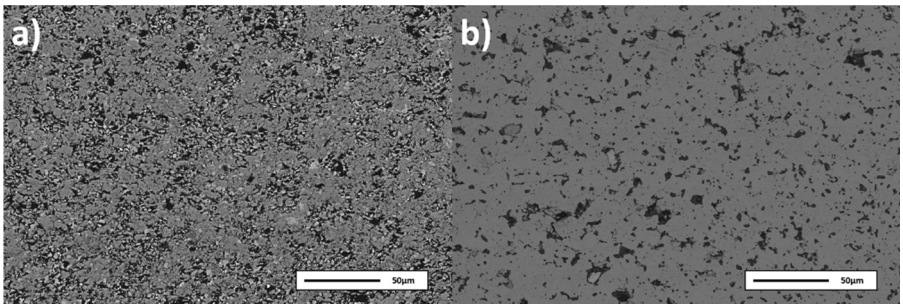

Fig. 9. SEM micrographs of printed a) Ti_3SiC_2 and b) Cr_2AlC MAX phases.

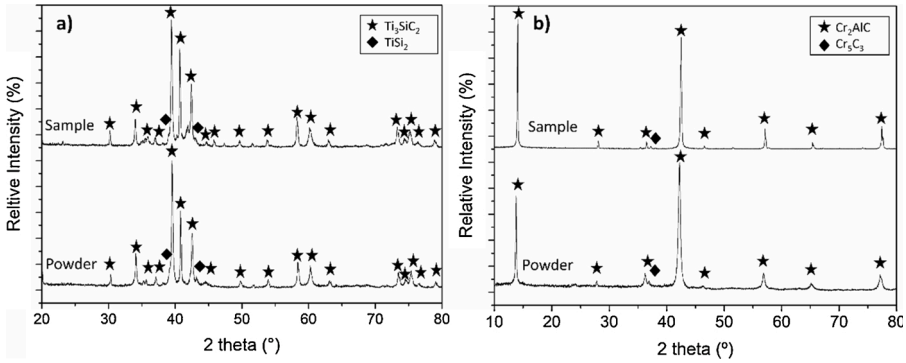

Fig. 10. Comparative x-ray diffraction pattern of the initial powders and printed samples of a) Ti_3SiC_2 and b) Cr_2AlC.

Declaration of Competing Interest

The authors declare that they have no known competing financial interests or personal relationships that could have appeared to influence the work reported in this paper.

Acknowledgements

The authors would like to thank the funding provided for this research by the Regional Government of Madrid (Dra. Gral. Universidades e Investigación) through the project P2018/NMT4411 (ADITIMAT-CM), and the Spanish Government through and the projects PID2019-106631GB-C43 and RTC2019-007049-4. The authors would also like to thank Lilla Valy, Fabian Czernilofsky and Tamas Lang for their help with the printing parameter optimisation.

References

[1] Z. Chen, Z. Li, J. Li, C. Liu, C. Lao, Y. Fu, C. Liu, Y. Li, P. Wang, Y. He, 3D printing of ceramics: a review, J. Eur. Ceram. Soc. 39 (2019) 661–687, https://doi.org/10.1016/j.jeurceramsoc.2018.11.013.
[2] B. Gadagi, R. Lekurwale, A review on advances in 3D metal printing, Mater. Today Proc. (2020), https://doi.org/10.1016/j.matpr.2020.10.436.
[3] L. Zeng, P. Li, Y. Yao, B. Niu, S. Niu, B. Xu, Recent progresses of 3D printing technologies for structural energy storage devices, Mater. Today Nano. 12 (2020) 1–13, https://doi.org/10.1016/j.mtnano.2020.100094.
[4] J.C. Najmon, S. Raeisi, A. Tovar, Review of Additive Manufacturing Technologies and Applications in the Aerospace Industry, Elsevier Inc., 2019, https://doi.org/10.1016/B978-0-12-814062-8.00002-9.
[5] R. Pugliese, B. Beltrami, S. Regondi, C. Lunetta, Polymeric biomaterials for 3D printing in medicine: an overview, Ann. 3D Print. Med. 2 (2021) 100011, https://doi.org/10.1016/j.stlm.2021.100011.
[6] M.N. Nadagouda, M. Ginn, V. Rastogi, A review of 3D printing techniques for environmental applications, Curr. Opin. Chem. Eng. 28 (2020) 173–178, https://doi.org/10.1016/j.coche.2020.08.002.
[7] A. Mussatto, R. Groarke, A. O'Neill, M.A. Obeidi, Y. Delaure, D. Brabazon, Influences of powder morphology and spreading parameters on the powder bed topography uniformity in powder bed fusion metal additive manufacturing, Addit. Manuf. 38 (2021) 101807, https://doi.org/10.1016/j.addma.2020.101807.
[8] J.H. Tan, W.L.E. Wong, K.W. Dalgarno, An overview of powder granulometry on feedstock and part performance in the selective laser melting process, Addit. Manuf. 18 (2017) 228–255, https://doi.org/10.1016/j.addma.2017.10.011.
[9] M. Ansari, E. Jabari, E. Toyserkani, Opportunities and challenges in additive manufacturing of functionally graded metallic materials via powder-fed laser directed energy deposition: a review, J. Mater. Process. Technol. 294 (2021) 117117, https://doi.org/10.1016/j.jmatprotec.2021.117117.
[10] A. Singh, S. Kapil, M. Das, A comprehensive review of the methods and mechanisms for powder feedstock handling in directed energy deposition, Addit. Manuf. 35 (2020) 101388, https://doi.org/10.1016/j.addma.2020.101388.
[11] J. Wilkes, Y.C. Hagedorn, W. Meiners, K. Wissenbach, Additive manufacturing of ZrO2-Al2O3 ceramic components by selective laser melting, Rapid Prototyp. J. 19 (2013) 51–57, https://doi.org/10.1108/13552541311292736.
[12] N.T. Aboulkhair, M. Simonelli, L. Parry, I. Ashcroft, C. Tuck, R. Hague, 3D printing of Aluminium alloys: additive Manufacturing of Aluminium alloys using selective laser melting, Prog. Mater. Sci. 106 (2019) 100578, https://doi.org/10.1016/j.pmatsci.2019.100578.
[13] D.A. Klosterman, R.P. Chartoff, N.R. Osborne, G.A. Graves, S. Rodrigues, Development of a curved layer LOM process for monolithic ceramics and ceramic matrix composites, Rapid Prototyp. J. 5 (1999) 61–71.
[14] S. Yi, F. Liu, J. Zhang, S. Xiong, Study of the key technologies of LOM for functional metal parts, J. Mater. Process. Technol. 150 (2004) 175–181, https://doi.org/10.1016/j.jmatprotec.2004.01.035.
[15] G.Miao Diptanshu, C. Ma, Vat photopolymerization 3D printing of ceramics: effects of fine powder, Manuf. Lett. 21 (2019) 20–23, https://doi.org/10.1016/j.mfglet.2019.07.001.
[16] E. Willems, M. Turon-Vinas, B.C. dos Santos, B. Van Hooreweder, F. Zhang, B. Van Meerbeek, J. Vleugels, Additive manufacturing of zirconia ceramics by material jetting, J. Eur. Ceram. Soc. 41 (2021) 5292–5306, https://doi.org/10.1016/j.jeurceramsoc.2021.04.018.
[17] X. Lv, F. Ye, L. Cheng, S. Fan, Y. Liu, Binder jetting of ceramics: powders, binders, printing parameters, equipment, and post-treatment, Ceram. Int. 45 (2019) 12609–12624, https://doi.org/10.1016/j.ceramint.2019.04.012.
[18] M. Ziaee, N.B. Crane, Binder jetting: a review of process, materials, and methods, Addit. Manuf. 28 (2019) 781–801, https://doi.org/10.1016/j.addma.2019.05.031.
[19] J. Gonzalez-Gutierrez, S. Cano, S. Schuschnigg, C. Kukla, J. Sapkota, C. Holzer, Additive manufacturing of metallic and ceramic components by the material extrusion of highly-filled polymers: a review and future perspectives, Materials (Basel). 11 (2018), https://doi.org/10.3390/ma11050840.
[20] A.I. Nurhudan, S. Supriadi, Y. Whulanza, A.S. Saragih, Additive manufacturing of metallic based on extrusion process: a review, J. Manuf. Process. 66 (2021) 228–237, https://doi.org/10.1016/j.jmapro.2021.04.018.
[21] W. Lengauer, I. Duretek, M. Fürst, V. Schwarz, J. Gonzalez-Gutierrez, S. Schuschnigg, C. Kukla, M. Kitzmantel, E. Neubauer, C. Lieberwirth, V. Morrison, Fabrication and properties of extrusion-based 3D-printed hardmetal and cermet components, Int. J. Refract. Met. Hard Mater. 82 (2019) 141–149, https://doi.org/10.1016/j.ijrmhm.2019.04.011.
[22] X. Zhang, H. Keramati, M. Arie, F. Singer, R. Tiwari, A. Shooshtari, M. Ohadi, Recent developments in high temperature heat exchangers: a review, Front. Heat Mass Transf. 11 (2018), https://doi.org/10.5098/hmt.11.18.
[23] D. Aquaro, M. Pieve, High temperature heat exchangers for power plants: performance of advanced metallic recuperators, Appl. Therm. Eng. 27 (2007) 389–400, https://doi.org/10.1016/j.applthermaleng.2006.07.030.
[24] C.A. Lewinsohn, M.A. Wilson, J.R. Fellows, H.S. Anderson, Fabrication and joining of ceramic compact heat exchangers for process integration, Int. J. Appl. Ceram. Technol. 9 (2012) 700–711, https://doi.org/10.1111/j.1744-7402.2012.02788.x.
[25] J. Schmidt, M. Scheiffele, M. Crippa, P.F. Peterson, E. Urquiza, K. Sridharan, L. C. Olson, M.H. Anderson, T.R. Allen, Y. Chen, Design, fabrication, and testing of ceramic plate-type heat exchangers with integrated flow channel design, Int. J. Appl. Ceram. Technol. 8 (2011) 1073–1086, https://doi.org/10.1111/j.1744-7402.2010.02573.x.
[26] C. Schmitt, D.W. Agar, F. Platte, S. Buijssen, B. Pawlowski, M. Duisberg, Ceramic plate heat exchanger for heterogeneous gas-phase reactions, Chem. Eng. Technol. 28 (2005) 337–343, https://doi.org/10.1002/ceat.200407119.
[27] J. Schulte-Fischedick, V. Dreißigacker, R. Tamme, An innovative ceramic high temperature plate-fin heat exchanger for EFCC processes, Appl. Therm. Eng. 27 (2007) 1285–1294, https://doi.org/10.1016/j.applthermaleng.2006.11.007.
[28] H.J. Strumpf, D.M. Kotchick, M.G. Coombs, High-temperature ceramic heat exchanger element for a solar thermal receiver, JPL Publ. 104 (1982) 233–246.
[29] K.A. Al-attab, Z.A. Zainal, Performance of high-temperature heat exchangers in biomass fuel powered externally fired gas turbine systems, Renew. Energy 35 (2010) 913–920, https://doi.org/10.1016/j.renene.2009.11.038.
[30] C. Luzzatto, A. Morgana, S. Chaudourne, G. Sorbieg, A new concept composite heat exchanger to be applied in high-temperature industrial processes, Science (80-.). 17 (1997) 789–797.
[31] Q. Li, G. Flamant, X. Yuan, P. Neveu, L. Luo, Compact heat exchangers: a review and future applications for a new generation of high temperature solar receivers, Renewable Sustainable Energy Rev. 15 (2011) 4855–4875, https://doi.org/10.1016/j.rser.2011.07.066.
[32] C. Mansilla, J. Sigurvinsson, A. Bontemps, A. Maréchal, F. Werkoff, Heat management for hydrogen production by high temperature steam electrolysis, Energy 32 (2007) 423–430, https://doi.org/10.1016/j.energy.2006.07.033.
[33] L. Magistri, A. Traverso, A.F. Massardo, R.K. Shah, Heat exchangers for fuel cell and hybrid system applications, J. Fuel Cell Sci. Technol. 3 (2006) 111–118, https://doi.org/10.1115/1.2173665.

[34] W.D. Gerstler, D. Erno, Introduction of an additively manufactured multi-furcating heat exchanger, Proc. 16th Intersoc. Conf. Therm. Thermomechanical Phenom. Electron. Syst. ITherm 2017 (2017) 624–633, https://doi.org/10.1109/ITHERM.2017.7992545.
[35] M.A. Arie, A.H. Shooshtari, M.M. Ohadi, Experimental characterization of an additively manufactured heat exchanger for dry cooling of power plants, Appl. Therm. Eng. 129 (2018) 187–198, https://doi.org/10.1016/j.applthermaleng.2017.09.140.
[36] M.A. Arie, A.H. Shooshtari, V.V. Rao, S.V. Dessiatoun, M.M. Ohadi, Air-side heat transfer enhancement utilizing design optimization and an additive manufacturing technique, J. Heat Transfer 139 (2017), https://doi.org/10.1115/1.4035068.
[37] M. Barsoum, T. El-Raghy, The MAX Phases: Unique New Carbide and Nitride Materials, 2001, https://doi.org/10.1511/2001.28.736.
[38] M.W. Barsoum, The Mn+1AXn phases: a new class of solids, Prog. Solid State Chem. 28 (2000) 201–281, https://doi.org/10.1016/S0079-6786(00)00006-6.
[39] J. Gonzalez-Julian, T. Go, D.E. Mack, R. Vaßen, Thermal cycling testing of TBCs on Cr2AlC MAX phase substrates, Surf. Coatings Technol. 340 (2018) 17–24, https://doi.org/10.1016/j.surfcoat.2018.02.035.
[40] S.A. Tsipas, E. Tabares, T. Weissgaerber, T. Hutsch, F. Sket, B. Velasco, Thermophysical properties of porous Ti2AlC and Ti3SiC2 produced by powder metallurgy, J. Alloys. Compd. 857 (2021) 158145, https://doi.org/10.1016/j.jallcom.2020.158145.
[41] J. Ward, S. Middleburgh, M. Topping, A. Garner, D. Stewart, M.W. Barsoum, M. Preuss, P. Frankel, Crystallographic evolution of MAX phases in proton irradiating environments, J. Nucl. Mater. 502 (2018) 220–227, https://doi.org/10.1016/j.jnucmat.2018.02.008.
[42] H.H. Qarra, K.M. Knowles, M.E. Vickers, S. Akhmadaliev, K. Lambrinou, Heavy ion irradiation damage in Zr2AlC MAX phase, J. Nucl. Mater. 523 (2019) 1–9, https://doi.org/10.1016/j.jnucmat.2019.05.034.
[43] W. Sun, D.J. Dcosta, F. Lin, T. El-Raghy, Freeform fabrication of Ti3SiC2 powder-based structures: part I - Integrated fabrication process, J. Mater. Process. Technol. 127 (2002) 343–351, https://doi.org/10.1016/S0924-0136(02)00284-4.
[44] M.M.M. Carrijo, H. Lorenz, I. Filbert-Demut, G.M. De Oliveira Barra, D. Hotza, X. Yin, P. Greil, N. Travitzky, Fabrication of Ti3SiC2-based composites via three-dimensional printing: influence of processing on the final properties, Ceram. Int. 42 (2016) 9557–9564, https://doi.org/10.1016/j.ceramint.2016.03.036.
[45] B. Nan, X. Yin, L. Zhang, L. Cheng, Three-dimensional printing of Ti3SiC2-based ceramics, J. Am. Ceram. Soc. 94 (2011) 969–972, https://doi.org/10.1111/j.1551-2916.2010.04257.x.
[46] H. Elsayed, A. Chmielarz, M. Potoczek, T. Fey, P. Colombo, Direct ink writing of three dimensional Ti2AlC porous structures, Addit. Manuf. 28 (2019) 365–372, https://doi.org/10.1016/j.addma.2019.05.018.
[47] M. Belmonte, M. Koller, J.J. Moyano, H. Seiner, P. Miranzo, M.I. Osendi, J. González-Julián, Multifunctional 3D-Printed cellular MAX-Phase architectures, Adv. Mater. Technol. 4 (2019) 1–8, https://doi.org/10.1002/admt.201900375.
[48] E. Tabares, A. Jiménez-Morales, S.A. Tsipas, Study of the synthesis of MAX phase Ti3SiC2 powders by pressureless sintering, Bol. La Soc. Esp. Ceram. y Vidr. (2020), https://doi.org/10.1016/j.bsecv.2020.01.004.
[49] J.M. Córdoba, M.J. Sayagués, M.D. Alcalá, F.J. Gotor, Synthesis of Ti3SiC2 powders: reaction mechanism, J. Am. Ceram. Soc. 90 (2007) 825–830, https://doi.org/10.1111/j.1551-2916.2007.01501.x.
[50] J. Hidalgo, A. Jiménez-Morales, J.M. Torralba, Torque rheology of zircon feedstocks for powder injection moulding, J. Eur. Ceram. Soc. 32 (2012) 4063–4072, https://doi.org/10.1016/j.jeurceramsoc.2012.06.023.
[51] E. Tabares, S.C. Cifuentes, A. Jiménez-Morales, S.A. Tsipas, Injection moulding of porous MAX phase Ti3SiC2 without using space-holder, Powder Technol. 380 (2021) 96–105, https://doi.org/10.1016/j.powtec.2020.11.022.
[52] R.M. German, Injection molding of metals and ceramics, Princeton New Jersey: metal powder industries federation, Princeton (New Jersey) (1997), https://doi.org/10.4271/982417.
[53] R.M. German, Powder Injection Molding, Metal Powder Industries Federation, 1990.
[54] C. Abajo, J. Hidalgo, A. Jiménez-Morales, J.M. Torralba, Optimisation of eco-friendly binary binder system for powder injection moulding, Powder Metall. 57 (2014) 196–203.
[55] M.W. Barsoum, T. El-Raghy, Synthesis and characterization of a remarkable ceramic: Ti3SiC2, J.Am.Ceram.Soc. 79 (1996) 1953–1956, https://doi.org/10.1111/j.1151-2916.1996.tb08018.x.
[56] B. Velasco, E. Gordo, L. Hu, M. Radovic, S.A. Tsipas, Influence of porosity on elastic properties of Ti2AlC and Ti3SiC2 MAX phase foams, J. Alloys. Compd. 764 (2018) 24–35, https://doi.org/10.1016/j.jallcom.2018.06.027.
[57] M. Barsoum, MAX Phases: Properties of Machinable Ternary Carbides and Nitrides, John Wiley & Sons, 2013, https://doi.org/10.1002/9783527654581.
[58] M. Ozturk, B. Dogan, Enhancement of heat exchangers with metal foams, World J. Environ. Res. 9 (2019) 15–28, https://doi.org/10.18844/wjer.v9i1.4555.

7.2 Mechanical properties of 3D printed MAX phases

Authors: Eduardo Tabares[a], Gabriel Mazón-Ortíz[a], S.C. Cifuentes[b], Michael Kitzmantel[c], Erich Neubauer[c], Antonia Jiménez-Morales[a], Sophia A. Tsipas[a]

[a] Departamento de Ciencia e Ingeniería de Materiales e Ingeniería Química, IAAB, Universidad Carlos lll de Madrid, Avda. De la Universidad 30, 38911 Leganés, Spain

[b] Área de Ciencia e Ingeniería de Materiales, ESCET, Universidad Rey Juan Carlos, C/Tulipán s/n, 28933 Móstoles, Madrid, Spain

[c] RHP-Technology GmbH, Forschungs- und Technologiezentrum, A-2444 Seibersdorf, Austria

Journal: Proceedings of the Euro PM 2021 Congress and Exhibition (Conference Paper), Euro PM 2021, On-line,18-22 October 2021

Scope of this paper:

As a complementary study of the scientific publication shown in **Section 7.1**, this congress paper exhibits the characterisation of the initial materials used in this work and the rheological properties of both Ti_3SiC_2 and Cr_2AlC feedstock. In addition to this, mechanical properties of the printed samples were evaluated in terms of hardness, plastic and elastic work and elastic modulus. The values obtained were compared to those obtained to the hot-pressed samples showed in **Chapter 5, Section 5.1**, in order to understand the effect of the porosity and most importantly the accumulation in certain zones corresponding to the 3D printing process. From this work, the influence of the porosity and localised porosity produced through the CEM process has been analysed. The effect of the added porosity to the samples lowers the mechanical behaviour of the 3D printed samples, as expected, but this decrease is relatively low, resulting in an attractive processing for the production complicated shaped MAX phase sample.

Graphical Abstract:

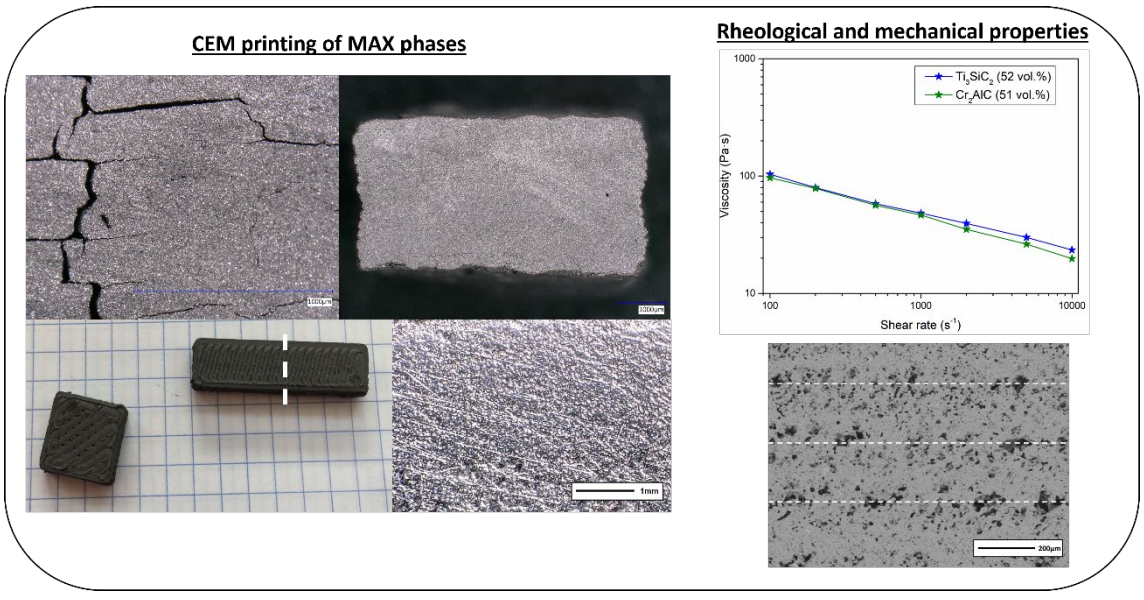

Manuscript refereed by Christian Kukla (University of Leoben, Austria)

Mechanical properties of 3D printed MAX Phases

E. Tabares (etabares@ing.uc3m.es)[a], G. Mazón-Ortíz (100399389@alumnos.uc3m.es)[a], S.C. Cifuentes (sandra.cifuentes@urjc.es)[b], M. Kitzmantel (m.ki@rhp.at)[c], E. Neubauer (e.ne@rhp.at)[c], S.A. Tsipas (stsipas@ing.uc3m.es)[a], A. Jimenez-Morales (toni@ing.uc3m.es)[a]

[a] Departamento de Ciencia e Ingeniería de Materiales e Ingeniería Química, IAAB, Universidad Carlos III de Madrid, Avda. De la Universidad 30, 38911 Leganes, Spain

[b] Área de Ciencia e Ingeniería de Materiales, ESCET, Universidad Rey Juan Carlos, C/Tulipán s/n, 28933 Móstoles, Madrid, Spain

[c] RHP-Technology GmbH, Forschungs- und Technologiezentrum, A-2444 Seibersdorf, Austria

Abstract

MAX phases are a group of ternary carbides and nitrides with a fixed stoichiometry and nanolaminated structure that combine some of the most interesting metallic and ceramic properties, with good electrical and thermal conductivity and good mechanical properties at high temperature. In terms of Additive Manufacturing technologies, Composite Extrusion Modelling (CEM) stands as a promising alternative for printing materials that are not suited for other Additive Manufacturing techniques. In this processing route, feedstocks in pellet or granulate form are extruded, avoiding difficult steps of filament production and widening the selection of polymeric binder compositions, since filament flexibility and uniformity is not required for the pellet materials. In this work, two MAX phases (Ti_3SiC_2 and Cr_2AlC) have been printed through CEM using a multicomponent binder (PEG/CAB) for the feedstock production. Mechanical properties of the printed samples with the desired geometry were analysed after debinding and sintering.

Keywords: MAX phases, Ti_3SiC_2, Cr_2AlC, CEM, Additive Manufacturing, mechanical properties

Innovative aspects

- **Composite Extrusion Modelling of MAX phases**
- **Optimization of feedstocks for sinter-based Additive Manufacturing**
- **Use of a novel multicomponent binder**

Introduction

Additive Manufacturing (AM) has attracted the attention of the research community as an alternative processing route for a wide range of materials and as a new way to manufacture shapes and geometries not feasible by other processing techniques. Within the vast number of technologies that AM comprehends, extrusion-based processing where feedstocks are used, stands as a promising route due to its similarities with injection moulding. Although not every material that can be injected can also be printed. The first step is to study the rheological behaviour of the feedstock. Extrusion-based AM widens the possible applications of many “known” materials, but also increases the possible use of new materials through a cost efficient production route [1].

One of the new materials that can be used through extrusion-based production route is MAX phases. They are ternary nitrides or carbides compounds with a general formula of $M_{n+1}AX_n$, where M is a transition metal, A is an element form groups IIIA or IVA, generally, from the periodic table and X either C or N, with n being a value between 1 and 3. MAX phases combine, in an unusual way, some of the best properties of ceramic (high rigidity, good mechanical properties at high temperatures, high resistance to corrosion and oxidation) and metallic materials (good thermal and electrical conductivity, machinability) [2]. Their nanolaminated structure, were layers of the elements M and X are combined with layers of the element A, is what gives MAX phases these excellent properties. In addition, they present good mechanical damping behaviour due to this nanolaminated nature [3].

The polymeric binders usually used in extrusion-based additive manufacturing are thermoplastics with adequate viscosity such as high performance thermoplastic elastomers [1]. In the last years there have been some studies using different AM techniques to produce MAX phases [4, 5]. In this work two MAX phases, Ti_3SiC_2 and Cr_2AlC were printed using CEM technique that uses feedstock pellets as raw materials. A multicomponent binder was used for the feedstock that combined typical polymers used in feedstocks suitable for additive manufacturing techniques with water soluble polymers in order to reduce the carbon footprint.

Experimental procedure

MAX phase powders were self-synthesised in large scale for the optimization and production of the printable feedstocks. Ti_3SiC_2 synthesis has been studied previously obtaining a 92 vol.% purity starting from Ti:SiC:C as raw powders with a molar ratio of 3:1,5:0,5 [6]. In addition, feedstock production of the Ti_3SiC_2 MAX phase has been optimised and rheologically characterized in a previous work [7].

Cr_2AlC powders were obtained varying parameters from previously reported high purity synthesis [8]. This synthesis starts from elemental powders of Cr, Al and C with a molar ratio of 2:1,2:1 and mixed in a Turbula shaker mixer for 1 hour. Mixed powders were introduced in silicone moulds and cold isostatically pressed at 4000 bar (EPSI systems, Belgium). Pressed samples were then sintered under protective argon atmosphere at 1300 ºC for 4 hours (Carbolite STF15/75/450, UK) and milled in a planetary ball mill (Pulverisette 5/2, Fritsch; Germany), controlling the milling parameters to obtain the desired particle size distribution with a ball to powder ratio of 5:1. Milling of the pellets was performed using isopropanol to avoid excessive temperatures during the process and under argon to control oxidation of the powders. Lastly, powders were then dried in air at 90 ºC for 6 hours and sieved to obtain the final MAX phase Cr_2AlC powders with a purity of 96 vol.%. Particle size distribution analysis of the powders was performed by laser diffraction (MasterSizer2000, Malvern Instruments, UK). Tap density and apparent density was also calculated for the MAX phase powders following standards ASTM B527 – 15 and ASTM B417 – 18 respectively. These density measurements are directly related to the powder rheological behaviour. Micrographs of the powders shows the irregular morphology of the self-synthesized powders, characteristic of the MAX phases (Figure 1). Relative, apparent and tap density of the produced powders are shown in Table 1 in addition to particle size distribution.

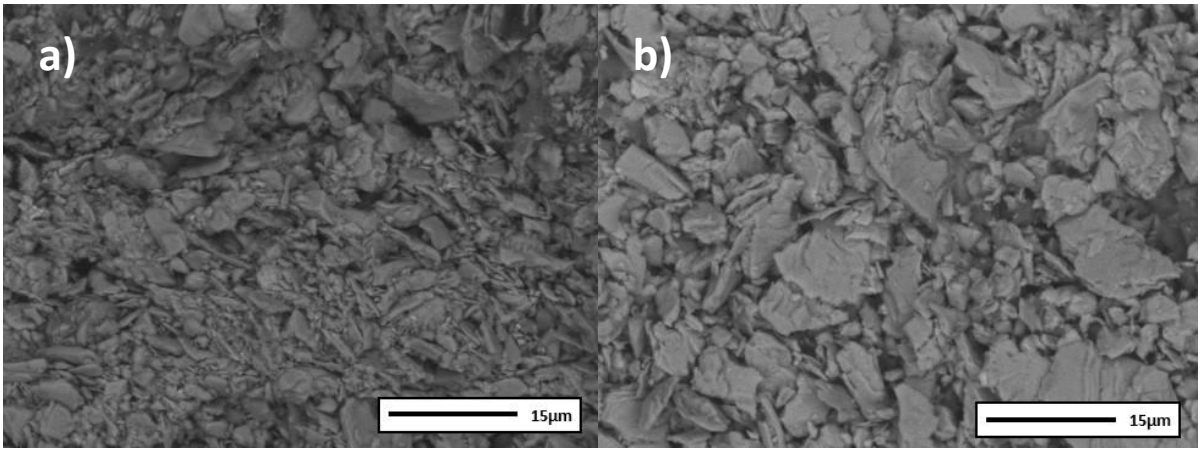

Figure 1. SEM micrographs of self-synthesized powders of a) Ti_3SiC_2 and b) Cr_2AlC

Table 1. Particle size distribution and densities of the self-synthesized Ti_3SiC_2 and Cr_2AlC MAX phase powders.

	D(90) µm	Relative Density (g/cm^3)	Apparent Density (%)	Tap density (%)
Ti_3SiC_2	20	4,46	21	39
Cr_2AlC	23	5,20	38	45

The same multicomponent binder described in [7] was employed for both feedstocks, using a mixture of polyethylene glycol (PEG) due to its solubility in water, cellulose acetate butyrate (CAB) acting as the back-bone and stearic acid as a surfactant. Feedstocks were produced in a blade mixing equipment (Haake Polylab QC, Thermofisher, US) for 1 hour at 180 ºC controlling the torque produced during the mixture. After pelletizing the feedstocks, rheological properties were studied by capillary rheology (Haake Rheocap S20, Thermofisher, US) obtaining viscosity properties of the mixtures at a set temperature of 180 ºC with a relation between length and diameter of the die 30:1.

MAX phases feedstocks were printed in a pellet extruder head (V4 Pellet Extruder, Mahor-XYZ, Spain) mounted in a regular FDM 3D printer (TL-D3 Pro, Tenlog, China). Simple geometries, rectangular (25x7x4 mm) and square shapes (10x10x4), were printed in order to optimise the printing parameters. Binder removal from the printed samples was achieved by a two-step debinding process. Firstly, samples were solvent debound in stirred distilled water at 50 ºC for 5 hours to remove the PEG. In a second stage, samples were thermally debinded for the degradation of the CAB at 450 ºC for 1 hour with heating and cooling rates of 0,5 ºC/min, accomplishing a 99 vol.% binder removal. Samples were then sintered under high vacuum (2×10^{-5} bar) at 1300 ºC for 6 hours, with heating and cooling rates of 5 ºC/min (HVT-15/50/450, Carbolite, UK). To control the properties of the printed samples, Archimedes

density was measured to calculate the relative density and porosity produced throughout the printing process.

Vickers hardness measurements were performed in a Zwick Roell Z 2.5 tester with a force of 10 N. Hardness values of the printed samples were compared with hot-pressed MAX phase samples in order to have a better understanding of the printed mechanical properties. In addition, with the surface indentation, Young's modulus and elastic and plastic work was measured with a speed for load application of 1 mm/min and a speed of 2 mm/min for load removal.

Results and discussion

Rheological behaviour, in terms of viscosity, of the MAX phase feedstocks produced determined by capillary rheology it is shown in Figure 2. A pseudoplastic behaviour of the feedstocks can be observed as the shear rate increases from 100 to 10000 s^{-1}. This behaviour is what it is expected for a feedstock that it is going to be extruded, for example for powder injection moulding (PIM), or similarly in this case, for extrusion-based Additive Manufacturing. Viscosity values under 1000 Pa·s are recommended for PIM [9] processing to ensure an optimal injection of the material. Although there is not an ideal value set for AM processing of feedstocks, considering the material is being extruded through a nozzle, it can be assumed that this limit value is valid for extrusion-based AM. Both MAX phases exhibit lower values than this recommended value for all shear rates.

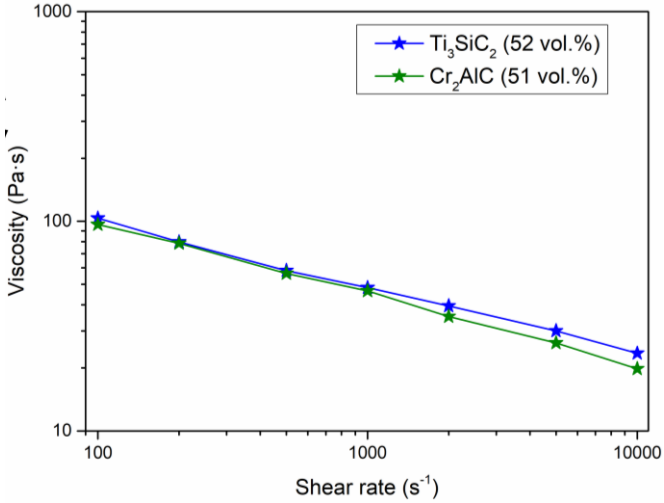

Figure 2. Apparent viscosity values obtained by capillary rheology at 180 ºC for Ti_3SiC_2 and Cr_2AlC feedstocks with a solid loading of 52 vol.% and 51 vol.% respectively and PEG/CAB as binder.

Table 2. Printing parameters of Ti_3SiC_2 and Cr_2AlC MAX phase feedstocks.

Material	Ti_3SiC_2	Cr_2AlC
Nozzle Diameter (mm)	0,6	0,6
Extrusion speed (steps per unit)	550	650
Layer Height (mm)	0,1	0,1
Infill Angles (º)	15/75/135	15/75/135
Extruder Temperature (ºC)	210	230
Bed Temperature (ºC)	50	50
Printing speed (mm/s)	5	5

A summary of the printing parameters of the MAX phase feedstocks is shown in Table 2. It can be seen that the printing temperature is higher than the one used for studying the rheological properties. This selected temperature is directly related to the nozzle diameter used during the printing, as the material needs higher flowability for lower extrusion diameters. Nozzle diameters used during the optimization of the feedstocks were varied from 0,4 to 0,8 mm, settling finally with a 0,6 mm nozzle, which gives the best relation between surface quality and extrusion filling of the printed samples. Extrusion speed, as revolutions of the screw, can also be adjusted and plays a key factor as a parameter to control to ensure the correct deposition of the material layer by layer. Layer height was also varied to improve the quality of the samples and was set to 0,1 mm. In addition, Figure 3 summarises the optimization of the printing process. In first place, Figure 3 a) shows the optical imagine of the cross-section corresponding to a

green printed sample with a lack of material during the deposition. In this figure, it can be seen that material deposition is not optimal since there are big gaps between the wall and the infill and in-between each deposited layer. These defects could increase after the debinding process resulting in a defective part. In Figure 3 b) shows the cross-section of a sample with optimal printing parameters. As it can be seen, a good layer by layer deposition was achieved with no gaps in-between layers. In addition, there is no delamination between the printed wall and the internal filling of the printed sample, obtaining no mayor defects in the green state. In addition, Figure 3 c) shows green extrusion-based printed samples with different geometries.

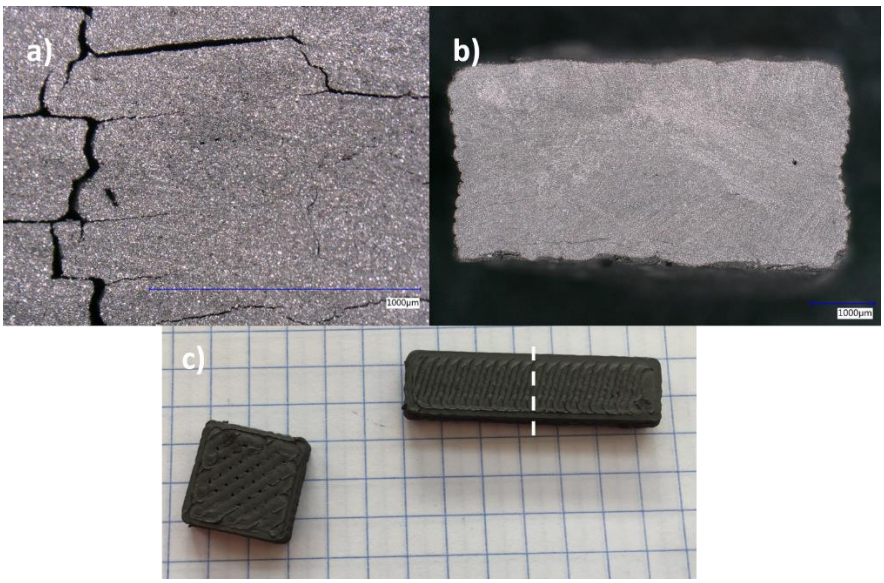

Figure 3. Ti_3SiC_2-PEG/CAB a) cross-section of non-optimise printed part b) cross-section of optimised printed sample and c) printed geometries.

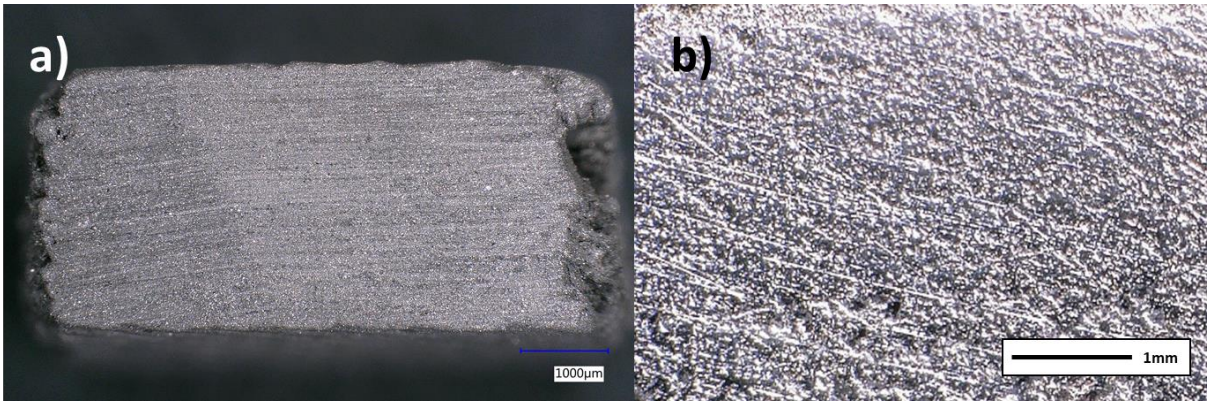

Figure 4. Printed Cr_2AlC a) brown part (after solvent and thermal debinding) and b) sintered cross-section.

After two-step debinding of the printed samples, 99 vol.% of the binder was removed maintaining the structural integrity of the samples. No mayor defects were found on the brown samples, as it is shown in Figure 4 a). After sintering, cross-section of the samples was analysed in order to see if delamination was produced. Optical image of the cross-section (place and direction of the cross-section cut marked as a dash line in Figure 3-c) of the printed samples is shown in Figure 4 b) where it is clear that no big defects are found after printing. From this optical image the appearance of some micro porosity can be noted. To better understand the mechanical properties of the printed MAX phases, this porosity was determined. In addition, shrinkage of the samples after debinding and sintering was calculated. These values are summarised in Table 3. In terms of relative density, the printed samples show a porosity of 11% for the Ti_3SiC_2 sample and 9% for Cr_2AlC printed MAX phase. This porosity is strictly related to two factors: first, the sinterability of the MAX phase that behaves in this sense as a ceramic material, with lack of high relative density through pressureless sintering methods. Secondly, the porosity introduced into the sample due to the layer-by-layer deposition of the printing process. Nevertheless, these porosity values of the printed samples are lower than the ones expected for the composite extrusion modelling technique. The relative low porosity of the samples could be due to the internal residual stresses produced during the printing stage. It is known that in Material Extrusion with filaments and CEM

processes this kind of stress produces warping of the samples not only for metal or ceramic printing but also for polymers. In this case, the sinterability of the MAX phases could by enhanced by this stress accumulation during the material deposition. This effect could also be explained by the high shrinkage values of the samples, that show a 47 vol.% size reduction for the Ti_3SiC_2 and up to a 52 vol.% in the case of the Cr_2AlC MAX phase, respectively, presenting anisotropy between x-y and z direction.

Table 3. Mean relative density and shrinkage values of the CEM printed MAX phases.

	Theoretical density (g/cm^3)	Relative density (%)	Shrinkage (vol.%)
Ti_3SiC_2	4,52	89	47
Cr_2AlC	5.20	91	52

Hardness, elastic and plastic work, recovery index and Elastic modulus of the printed parts are summarized in Table 4. Values have been obtained by performing measurements in different areas of the samples in order to be able to differentiate if there is any variation in properties between the cross-section and the surface of the samples. Measurements were done after metallographic preparation to avoid errors caused by the surface roughness. In addition, measurements for hot-pressed (HP) samples of the same self-synthesized powders for both MAX phases are shown for comparative purposes. These HP samples have a relative density of 95 and 98% for Ti_3SiC_2 and Cr_2AlC, respectively.

Firstly, analysing the different areas of the printed Ti_3SiC_2 MAX phase it can be observed that there is a difference between the surface and the cross-section of the sample for all the values. This indicates some anisotropy in the printed samples, due to the printing pattern. Plastic work is higher than the elastic work, both on cross section and in the surface, as expected for a ceramic-like material in terms of mechanical properties. Recovery index is lower than for the hot-pressed sample and this could be due to the effect of localised porosity in the boundaries between each layer (Figure 5), hindering the recovery of the material after the plastic deformation. This porosity effect is also noticeable in the hardness values of the printed samples that show lower values (92 HV10 in cross section and 94 HV10 in surface) than the HP samples (322 HV10). Young´s modulus values are slightly higher for the printed samples (52 kN/mm^2 in cross section and 57 kN/mm^2 on the surface) than for the HP samples (43 kN/mm^2), but much lower than the reported value for dense Ti_3SiC_2 samples, 343 kN/mm^2 [10], most probably due to the presence of porosity.

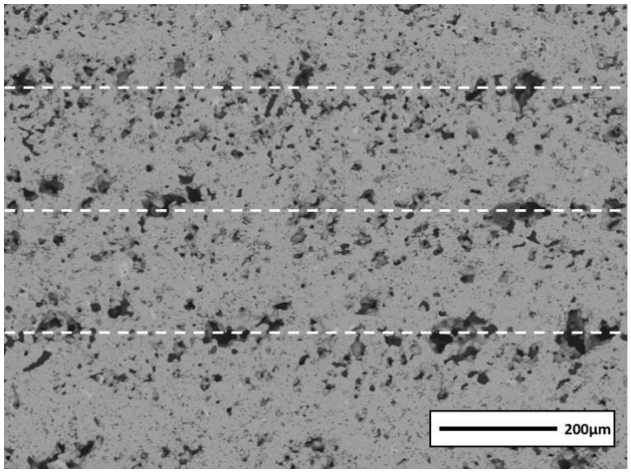

Figure 5. SEM micrographs of Cr_2AlC printed MAX phase exhibiting the porosity accumulation between the layers marked in with dash lines.

Secondly, analysing hardness values of both the surface and cross-section of the Cr_2AlC printed samples it can be seen that there is also some anisotropy in hardness value, with higher hardness in the cross section (424 HV10 in the surface and 448 HV10 in the cross section). This could also be related to the porosity accumulation within the different layers. Once the indentation is made, the porosity accumulation will affect in a higher way the hardness of the surface measurements than the cross-section because the indentation is being made perpendicular to the deposited layers through the surface. These hardness values, although closer, are still lower than the hot-pressed sample mainly due to the relative density difference between both processing techniques. Recovery index and both elastic and plastic work are similar for the different areas of the printed samples and comparable to the HP samples. Regarding, the elastic modulus, in this case we are able to observe a lower value for the printed samples (150 kN/mm^2 in cross section and 173 kN/mm^2 on the surface) than the HP sample (225 kN/mm^2), this could also be due to the higher porosity of the printed samples. For comparison, the Young's modulus for completely dense samples is 245 kN/mm^2 for Cr_2AlC MAX phase [10].

Table 4. Mechanical properties for Ti_3SiC_2 and Cr_2AlC MAX phases of different zones of the printed samples and properties of hot-pressed samples. W_{elast} and W_{plast}, stand for the elastic and plastic work during the indentation and μ_{IT} the recovery index after releasing the indentation.

Material	Zone	Hardness (HV10)	W_{elast} (Nmm)	W_{plast} (Nmm)	μ_{IT} (%)	E modulus (kN/mm^2)
Ti_3SiC_2	Surface	92	0,010±0,001	0,067±0,003	12,5±0,3	52±5,32
	Cross-section	94	0,009±0,001	0,069±0,008	11,3±1,1	57±7,21
	HP	322	0,021±0,004	0,040±0,004	34,2±4,5	43±10,81
Cr_2AlC	Surface	424	0,009±0,001	0,028±0,003	23,7±1,1	150±18,57
	Cross-section	448	0,008±0,001	0,026±0,002	22,5±1,6	173±16,20
	HP	535	0,017±0,001	0,024±0,001	24,7±2,5	225±15,34

Conclusions

Self-synthesised Ti_3SiC_2 and Cr_2AlC have been successfully printed through a new processing route. This is composite extrusion modelling (CEM) using an alternative sustainable binder composed by polyethylene-glycol and cellulose acetate butyrate. Printing parameters have been optimised in order to obtain samples with no mayor internal defects and with a good surface quality. Binders from the printed samples were removed in a two-step debinding process solvent debinding of PEG in water, avoiding the use of organic solvents, and degradation of the back-bone (CAB) by thermal debinding. Sintering of the samples was achieved obtaining 89 and 91 % density for Ti_3SiC_2 and Cr_2AlC, respectively. Mechanical properties of the printed samples were measured, and samples show a similar behaviour as those produced by conventional processing routes such as hot pressing. Young´s modulus and recovery index of the printed samples are similar than those HP. On the other hand, hardness measurement show lower values for both MAX phases compared to the hot-pressed ones, with Ti_3SiC_2 MAX phase showing a higher difference. This effect is directly related to the layer-by-layer production and the porosity accumulation produced within the layers, characteristic of the Material Extrusion with filaments and CEM processing, besides the particle morphology of the MAX phase used and the solid loading of the feedstocks.

Acknowledgements

The authors would like to thank the funding provided for this research by the Regional Government of Madrid (Dra. Gral. Universidades e Investigación) through the project P2018/NMT4411 (ADITIMAT-CM), and the Spanish Government through and the projects PID2019-106631GB-C43 and RTC2019-007049-4.

References

[1] W. Lengauer *et al.*, “Fabrication and properties of extrusion-based 3D-printed hardmetal and cermet components,” *Int. J. Refract. Met. Hard Mater.*, vol. 82, no. February, pp. 141–149, 2019, doi: 10.1016/j.ijrmhm.2019.04.011.

[2] M. W. Barsoum and M. Radovic, “Elastic and Mechanical Properties of the MAX Phases,” *Annu. Rev. Mater. Res.*, vol. 41, no. 1, pp. 195–227, 2011, doi: 10.1146/annurev-matsci-062910-100448.

[3] M. Barsoum and T. El-Raghy, *The MAX phases: unique new carbide and nitride materials*, vol. 89. 2001.

[4] M. Belmonte *et al.*, “Multifunctional 3D-Printed Cellular MAX-Phase Architectures,” *Adv. Mater. Technol.*, vol. 4, no. 9, pp. 1–8, 2019, doi: 10.1002/admt.201900375.

[5] D. J. Dcosta, W. Sun, F. Lin, and T. Ei-Raghy, “Freeform fabrication of Ti3SiC2 powder-based structures: Part II - Characterization and microstructure evaluation,” *J. Mater. Process. Technol.*, vol. 127, no. 3, pp. 352–360, 2002, doi: 10.1016/S0924-0136(02)00320-5.

[6] E. Tabares, A. Jiménez-Morales, and S. A. Tsipas, “Study of the synthesis of MAX phase Ti3SiC2 powders by pressureless sintering,” *Bol. la Soc. Esp. Ceram. y Vidr.*, 2020, doi: 10.1016/j.bsecv.2020.01.004.

[7] E. Tabares, S. C. Cifuentes, A. Jiménez-Morales, and S. A. Tsipas, “Injection moulding of porous MAX phase Ti3SiC2 without using space-holder,” *Powder Technol.*, vol. 380, pp. 96–105, 2021, doi: 10.1016/j.powtec.2020.11.022.

[8] J. Gonzalez-Julian, S. Onrubia, M. Bram, and O. Guillon, “Effect of sintering method on the microstructure of pure Cr2AlC MAX phase ceramics,” *J. Ceram. Soc. Japan*, vol. 124, no. 4, pp. 415–420, 2016, doi: 10.2109/jcersj2.15263.

[9] R. M. German, *Powder Injection Molding*. Metal Powder Industries Federation, 1990.

[10] M. Barsoum, *MAX phases: Properties of machinable ternary carbides and nitrides*. 2013.

CHAPTER 8

CONCLUSIONS

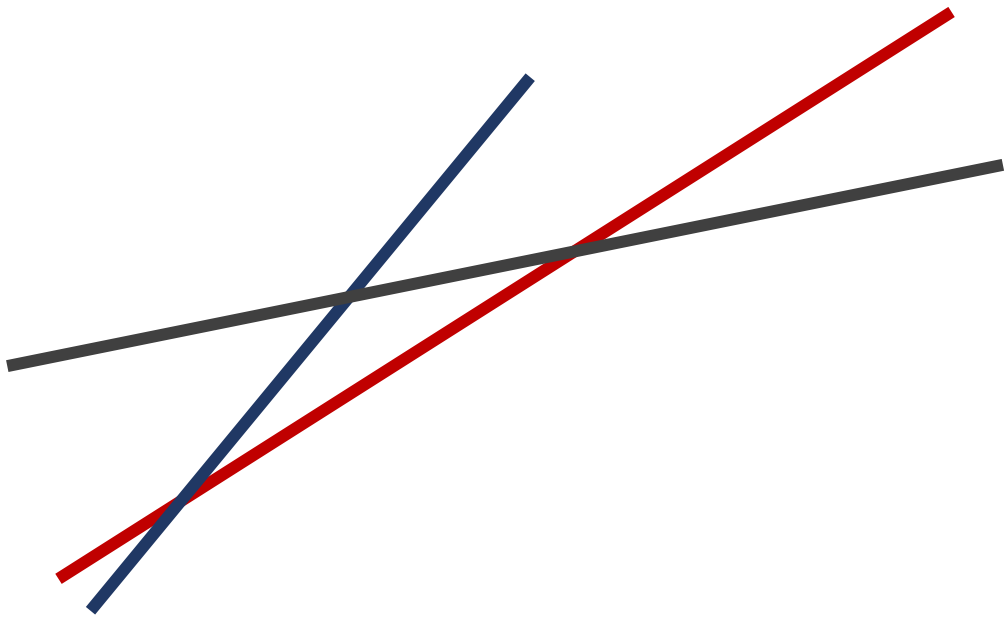

8. Conclusions

The main conclusions obtained throughout this work are directly related to the main goals and objectives proposed for this PhD thesis. Thus, partial conclusions obtained during this work, for each main objective, are displayed in this chapter:

MAX phase synthesis

- Different MAX phases powders have been successfully synthesised, obtaining high purity levels, through pressureless sintering. Ti_3SiC_2 was synthesised starting from Ti, SiC and C with a molar ratio of 3:1.5:0.5 reaching 94% of purity after a heat treatment of 1300 ºC for 6 h under vacuum conditions. Regarding Cr_2AlC, the synthesis was performed starting from elemental powders of Cr, Al and C with a molar ratio at 2:1.2:1 with a purity of 98% after a heat treatment at 1300 ºC for 6 h under protective argon atmosphere. In addition, Ti_2AlC/Ti_3AlC_2 composite MAX phase was also synthesised starting from Ti, Al and TiC with a molar ratio of 1:1:0.75 after a heat treatment at 1400 ºC for 4 h under protective argon atmosphere. It can be stated that, the synthesis procedure that is followed for MAX phases is influenced by the starting powders and the initial molar ratios. In essence, the starting material should be carefully selected depending on the synthesis route that is going to be followed. The synthesis methods developed were simple, reproducible, scalable and produced high purity MAX phase powder with controlled powder size distribution.

- Furthermore, thermodynamic calculations were performed to establish the synthesis mechanism of the MAX phases. Albeit they are theoretical calculations, the proposed synthesis reactions give step-by-step description of how the synthesis is achieved and explain the different secondary phases found in the final products. Nevertheless, the particle size of the materials used for the synthesis have an effect on the final synthesis and the initial composition should also be carefully selected.

- Ti_3SiC_2 and Cr_2AlC MAX phases were selected for the study of new processing routes and, for this purpose, the scalability of the powder production was successfully achieved obtaining purities of 92% and 96%, respectively. The scale-up process of the powder production was accomplished with the compaction of the powders by cold isostatic pressing (CIP). Although final purity of the powders was reduced by a 2% for both MAX phases, the amount of material obtained after this synthesis methods was increased by a 5000%.

Conventional powder metallurgy consolidation

- Validation of the synthesised powders was performed by the consolidation of Ti_3SiC_2 and Cr_2AlC by uniaxial pressing and sintering, cold isostatic pressing and sintering and hot pressing. A lack of densification of the samples can be observed, compared to other authors' work, and this is mainly due to the densification of already-synthesised MAX phase powders instead of an in-situ synthesis of the MAX phases while the consolidation technique is applied. Nevertheless, and although some decomposition of the Ti_3SiC_2 powders was observed for hot-pressed samples above 1300 ºC, consolidated samples by all techniques showed good phase stability demonstrating the quality of the synthesised powders. Different densification values were obtained for the different techniques used achieving the best values for cold isostatic pressed and sintered Ti_3SiC_2 and hot-pressed Cr_2AlC samples reaching 83% and 96% of relative density respectively.

- Mechanical properties of the samples showed a close dependence to the porosity values. Elastic modulus of the Ti_3SiC_2 samples processed displayed lower values (83 kN/mm^2) than those reported in the literature, due to the low densifications obtained. On the other hand, Cr_2AlC sample exhibited similar elastic modulus to those in the literature, due to the high densification attained in these samples (225 kN/mm^2). In addition, cyclic compressive strength showed no hysteresis, with no noticeable difference between the cold isostatic press and sintered and hot-pressed samples.

- In terms of wear behaviour, the self-lubricating effect characteristic of MAX phases was observed for all samples analysed. From these tests, a dependence on the porosity was also observed. Cold isostatic pressed and sintered Ti_3SiC_2 and Cr_2AlC exhibited different wear properties that were not only affected by the difference in the porosity of the samples but on the different wear mechanisms of each material. Although both materials presented a combination of abrasive and adhesive wear, the abrasive effect was more noticeable for Ti_3SiC_2. On the other hand, hot-pressed samples exhibited a similar wear rate for all loads studied (5 and 10 N). This effect seems to be a combination of the lubricating effect of the material and the small grain size obtained after the process, resulting in a lower amount of generated debris during the tests. The wear mechanism of the MAX phases analysed can be distinguished by a quasi-plastic deformation combining abrasive and adhesive mechanism for Ti_3SiC_2 and a predominant adhesive behaviour for Cr_2AlC.

Powder injection moulding

- MAX phase feedstocks were produced and rheologically characterised. Two different multicomponent binders were used for the feedstocks production, both using PEG as a filler and CAB and PP as backbones. From torque rheology, capillary rheology and homogeneity characterisation, the solid loadings selected as optimal were: 52 vol.% for Ti_3SiC_2/PEG-CAB, 51 vol% for Cr_2AlC/PEG-CAB, 49 vol.% for Ti_3SiC_2/PEG-PP and 51 vol.% for Cr_2AlC/PEG-PP. When optimal solid loading was surpassed, MAX phase feedstock showed a decrease in the viscosity, this behaviour has not been previously observed and was attributed to the lubricating nature of MAX phases. However, these solid loading were not appropriate for PIM. All feedstocks exhibited a pseudoplastic behaviour with viscosities below those recommended for PIM (1000 s^{-1}). Torque rheology showed a complete stabilisation of the mixtures after 30 min and final torque values for the PEG/PP feedstocks were higher (2-4 Nm) compared to PEG/CAB system (0,2-1 Nm).

- PEG/CAB and PEG/PP feedstocks were able to be injected by low pressure injection moulding (LPIM), obtaining good quality green parts with no mayor defects in the surface of the samples and a good filling of the mould. The optimal injection temperatures were 200 ºC for Ti_3SiC_2 feedstocks and 220 ºC for Cr_2AlC for the PEG/CAB binder and 250 ºC and 270 ºC for the PEG/PP binder, respectively. This difference in temperature goes in concordance with the rheological measurement analysed.

- The binder removal was performed in a two-step debinding process. First, PEG was removed by solvent debinding in distilled water at 60 ºC for 5 h. Up to a 91-95 wt.% of the PEG was removed in this process avoiding internal defects in the samples and creating the open porosity needed for the later backbone removal. These steps allow the use of a green solvent, compared to the typically organic solvents used for solvent debinding, having a lower environmental impact of the process. CAB was removed by thermal debinding at 300 ºC for 1 h under argon with a heating and cooling rate of 2 ºC/min maintaining the structural integrity of the samples and removing a 99 wt.% of the remaining binders.

- Porous Ti_3SiC_2 MAX phase samples were obtained after sintering process. Porosity could be tailored controlling the amount of solid loading used in the feedstocks, without using any space-holder in the mixtures and achieving up to a 53% of porosity. This porosity is interconnected and mainly open, ideal for filter or catalytic applications.

Composite extrusion modelling

- Ti_3SiC_2 and Cr_2AlC MAX phases feedstocks using a PEG/CAB as a binder were pelletised and printed through composite extrusion modelling (CEM). Several printing parameters were adjusted for the successful printing of the MAX phases, i.e.: extrusion temperature, bed temperature, layer height, layer thickness, extrusion speed and printing speed, amongst others. This last two parameters had a great effect on the quality of the final samples. Analysing the relative density of the printed parts under different conditions, it was possible to see that by increasing the extrusion speed the sample's relative density increased due to the increase in the amount of material that was extruded. Once a certain speed is surpassed, the quality of the sample is lost by the excess of material being deposited. In the case of the printing speed, the quality of the samples improved with the reduction of the speed, achieving increasingly less quality improvement when further reducing the speed. This suggests a compromise between the improvement on the quality, related to the relative density, and the printing time of the parts. Best conditions were selected at an extrusion temperature of 210 ºC, printing speed of 5 mm/s and an extrusion speed of 550 steps per unit for Ti_3SiC_2 and a temperature of 230 ºC, a printing speed of 5 mm/s and an extrusion speed of 650 steps per unit for Cr_2AlC.

- Due to some difficulties with the complete elimination of the polymers, thermal debinding process was adjusted to ensure the correct degradation of the binders compared to the injected moulded parts. Temperature was set at 500 ºC for 1 h and a heating and cooling rate of 0,5 ºC/min. With this modification the amount of polymer removed after the process was of 99%, avoiding the appearance of cracks and the warping of the sample due to internal stresses generated during printing.

- Brown parts were immersed in zirconia balls during the sintering steep to control the warping of the samples. Sintering conditions were optimised at 1300 ºC for 6 hours with heating and cooling rates of 5 ºC/min. Samples exhibited a final relative density of 90% and 93% for Ti_3SiC_2 and Cr_2AlC, respectively. Moreover, the volumetric shrinkage obtained for the samples was 10% for Ti_3SiC_2 and 21% for Cr_2AlC, densifications relatively high considering the porosity of injected samples. This confirms the correct deposition of the layers achieved and optimum selection of the printing parameters, that resulted in control of the contraction generated by the internal stresses produced during the 3D printing process. All this, while controlling any cross contamination of the MAX phase powders due to a reaction with remaining binder and avoiding the decomposition of this materials.

In brief and as a general conclusion, MAX phase powders have been synthesised, scaling-up the process maintaining high purity levels of the powders. The powder quality was validated by conventional MAX phase processing analysing the mechanical properties and wear behaviour of the consolidated porous samples. Two routes were explored for the processing of near-net-shaped samples, powder injection moulding and additive manufacturing, using sustainable polymeric binders. Powder characterisation was performed to study the suitability for the feedstocks production and, in addition, an optimal solid loading was selected for each feedstock analysing and studying the rheological behaviour. Moreover, injected MAX phase samples were produced with tailored porosity without the use of space-holders. Lastly, these produced binders were processed by composite extrusion modelling to obtain 3D printed MAX phase samples. This process allowed the possibility of printing powders not commonly suited for additive manufacturing process and staring from feedstock pellet raw material. 3D printed MAX phases exhibited a good geometrical quality and relatively high densification. All this establishes porous and dense MAX phases produced by PIM or CEM routes, for applications such as, catalytic devices, filters or as high temperature heat exchangers.

CHAPTER 9

FUTURE LINES AND PERSPECTIVES

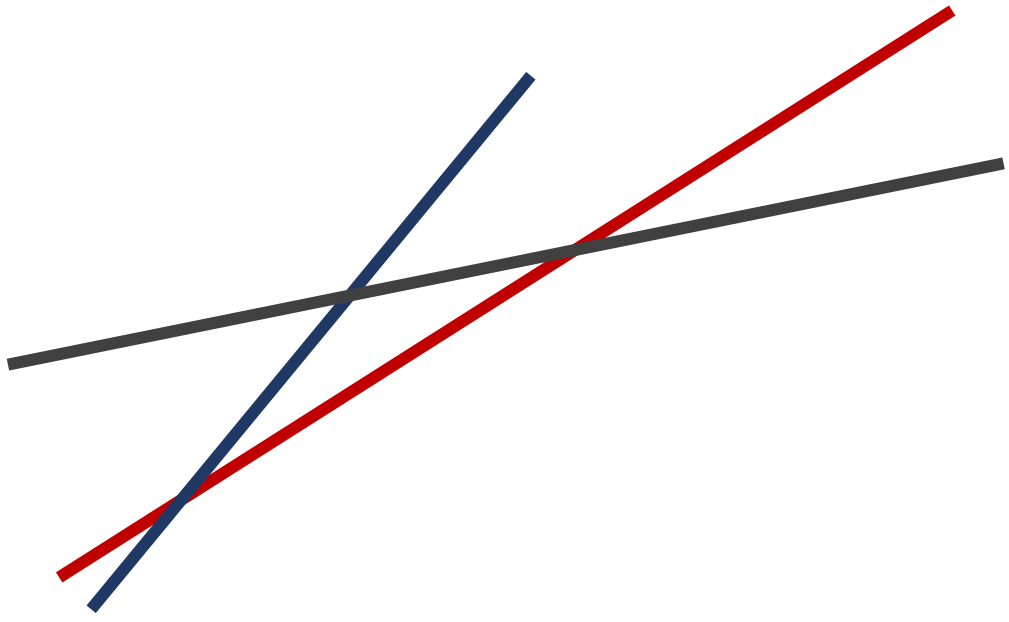

9. Future lines and perspectives

Based on the results obtained from this work, there are some steps that need to be optimised and further investigated.

- Explore further consolidation techniques for MAX phase powders for the production of dense and porous materials. Although the aim of the use of conventional powder metallurgy processing in this work was to corroborate the quality and processability of the powders, more effective techniques could be explored, such as Spark Plasma Sintering (SPS), in order to obtain both porous and dense MAX phases samples.
- Detailed characterisation of the porosity of the samples obtained after the PIM process. A tomography study would allow to measure the size, distribution and shape of the pores. This would lead to a better evaluation of injected MAX phase samples for their potential application as high temperature heat exchangers.
- Optimisation of the PEG/PP-based MAX phase feedstocks for composite extrusion modelling. This feedstocks presented a reproducibility problem during the printing step. Therefore, optimisation of the binder composition would be necessary with an addition of surfactant additive or by exploring other thermoplastic backbones in order to improve the printing reproducibility.

In addition, several studies can emerge from the basis of the feedstock-based processing techniques developed in this thesis:

- Cyclic oxidation tests should be performed to both injected and printed samples to identify and study how the processing routes affect the oxidation and thermal shock resistance of the samples. Furthermore, and related to the properties of MAX phases at high temperature, flame tests could be performed to macroporous printed samples (as the demonstrator shown in Chapter 3) in order to confirm the possible applicability of these materials as hydrogen burner components.
- Application of other additive manufacturing technologies. There are many in-direct AM techniques that could be explored for the production of complex-shaped MAX phase components. As an example, lithography-based technology is an interesting alternative, due to the high-quality samples and small sizes that can be obtained with this technique. A preliminary study was done to print MAX through this technology in collaboration with Incus Technology GmbH, which is not included in this work. Although the characteristics of the powders developed in this work were not suited for the photopolymerization of the feedstocks with UV, a laser polymerisation could be performed in order to obtain good quality samples.
- In-situ synthesis of MAX phases, after the injection or printing process. A study on the viability of obtaining the MAX phase in-situ, during the sintering step should be carried

out, since, if successful, this could enhance the amount of solid loading of the feedstocks as well as making the process more efficient. Nevertheless, a strict control of the powder size distribution, morphology and molar ratios would be necessary in order to ensure the correct synthesis of the MAX phases.